Characterization of the subunits of the γ-secretase complex

Inaugural-Dissertation

zur Erlangung des Doktorgrades
der Mathematisch-Naturwissenschaftlichen Fakultät

der Heinrich-Heine-Universität Düsseldorf

vorgelegt von

Kun Yu

aus Liaoning, China

Hamburg, November 2016

aus dem Institut für Physikalische Biologie

der Heinrich-Heine-Universität Düsseldorf

Gedruckt mit der Genehmigung der
Mathematisch-Naturwissenschaftlichen Fakultät der

Heinrich-Heine-Universität Düsseldorf

Referent: Prof. Dr. Jörg Labahn

Korreferent: Prof. Dr. Henrike Heise

Tag der mündlichen Prüfung: 15.11.2016

Table of Contents

List of Figures

List of Tables

1 Introduction

1.1 The background of Alzheimer's disease

The Alzheimer's disease (AD) is an irreversible, progressive, neurodegenerative brain disease. It was named after a German psychiatrist Alois Alzheimer who described the first case of AD in 1906 [1]. Patients with AD usually gradually lose their ability to live independently. Their brain functions are found to be severely impaired until death. The Alzheimer's disease has been reported as the 4th leading cause of death in developed countries with an estimated number of 47.5 million people suffering worldwide [2]. It is predicted to affect 1 in 85 people worldwide by 2050 [3]. Due to the lack of effective drugs, AD not only causes great suffering to patients and their families, but also brings a heavy burden on society.

Most AD cases are diagnosed at an elderly age and termed as late-onset AD (LOAD). There are approximately 5% of AD cases that are diagnosed before the age of 65 and termed as early-onset (EOAD) [4]. Typically, LOAD and EOAD appear as isolated cases. Environmental factors and genetic variations (e.g., apolipoprotein E (APOE) gene) may act as risk factors. However, there are approximately 13% of the EOAD cases that showed an autosomal-dominant inheritance, which is referred to as familial Alzheimer's disease (FAD) [5]. Three genes have been identified in this autosomal-dominant form of the early-onset FAD (eFAD): APP on chromosome 21, PSEN-1 on chromosome 14, and PSEN-2 on chromosome 1 [6].

The occurrence of the Alzheimer's disease is closely related to the formation of two abnormal structures in the brain. One is the insoluble amyloid plaques formed by β-amyloid (Aβ) located outside the neurones. The other one is the neurofibrillary tangles which are twisted fibres of tau proteins inside the cells (Figure 1.1). Both of them may cause neuronal stress, lead to loss of connections between neurons and subsequent shrinkage of the AD brains. Based on these two hallmarks of AD, two preeminent hypotheses of AD were proposed. The tau hypothesis of Alzheimer's disease suggests that anomalous signalling cascades promote the abnormal hyperphosphorylation of tau proteins which cause the formation of paired helical filament (PHF) and the long-term production of neurofibrillary tangles (NFTs) in AD brains [7]. These tau proteins belong to the microtubule-associated protein family, which are nervous system specific and essential for microtubule assembly [8,9]. There are six isoforms of tau proteins. All of them can be incorporated upon assembly of the PHFs [9,10]. Under AD-related pathological conditions, tau proteins were found to be extensively modified [11,12], the self-aggregated tau proteins depolymerise microtubules, interfere with axonal transport and lead to neuronal death [13].

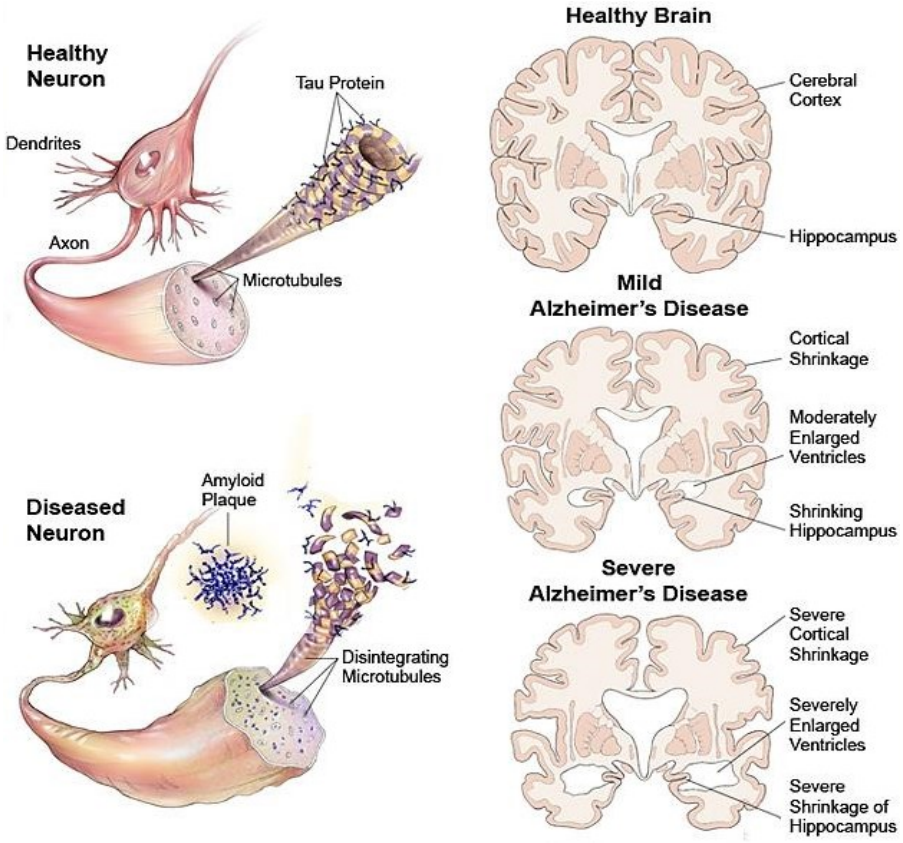

Figure 1.1 Amyloid plaques, neurofibrillary tangles, and the AD brain.
The formation of amyloid plaques and neurofibrillary tangles contribute to the loss of connections between neurons in the brain and the subsequent symptoms of AD. (Resource: American Health Assistance Foundation)

The amyloid (or Aβ) cascade hypothesis initially proposes that the polymerization of Aβ peptides into protease-resistant fibres and deposition of the Aβ peptides are the crucial steps in the pathogenesis of Alzheimer's disease; changes in tau and subsequent formation of NFTs are triggered by toxic concentrations of Aβ [14,15]. As the knowledge of Alzheimer's disease increased, the concept of the amyloid cascade hypothesis has been developed: The central factor in AD is an imbalance between production and clearance of $A\beta_{42}$ and related Aβ peptides (Figure 1.2) [16]. Furthermore, an improved amyloid hypothesis includes an effect of tau onto the neurotoxicity of Aβ [17,18].

The central factor of AD, Aβ, is actually a group of small peptides of 30 to 51 amino acids [19]. The most common isoforms are $A\beta_{40}$ and $A\beta_{42}$ with the latter one being more fibrillogenic. The Aβ peptides are derived from the amyloid precursor protein (APP) through the proteolytic processing by β- and γ-secretase enzymes [20]. Several alternatively spliced transcripts of APP have been discovered in humans, among them, three major isoforms of APP (APP_{695}, APP_{751}, and APP_{770}) were identified [21–24]. Alternative cleavage of APP at the cell surface within the Aβ

sequence is executed by α-secretase, thereby precluding Aβ formation [25]. The APP processing by α-, β- and γ-secretase is shown in Figure 1.3: α- or β-secretase cleave APP in its extracellular domain, releasing the amino-terminal fragment called secreted APP (sAPP) α or β and the carboxyl-terminal fragment CTF83 (α) or 99 (β), respectively. The membrane-anchored CTFs are successively cleaved by γ-secretase at the ε-cleavage site generating the APP intracellular domain (AICD). This is rapidly followed by ζ-cleavage and γ-cleavage generating p3 (from CTFα) or Aβ (from CTFβ) [26,27]. Mutations in or around the Aβ cleavage region of APP were reported to be responsible to the eFAD by altering the production of Aβ or its aggregation property [16]. It was also found that an APP mutation near the β-secretase cleavage site led to a reduced Aβ production and therefore showed a protective effect with regard to Alzheimer's disease [28]. In the last decades, the Aβs and γ-secretase were extensively studied to find an efficient treatment for Alzheimer's disease.

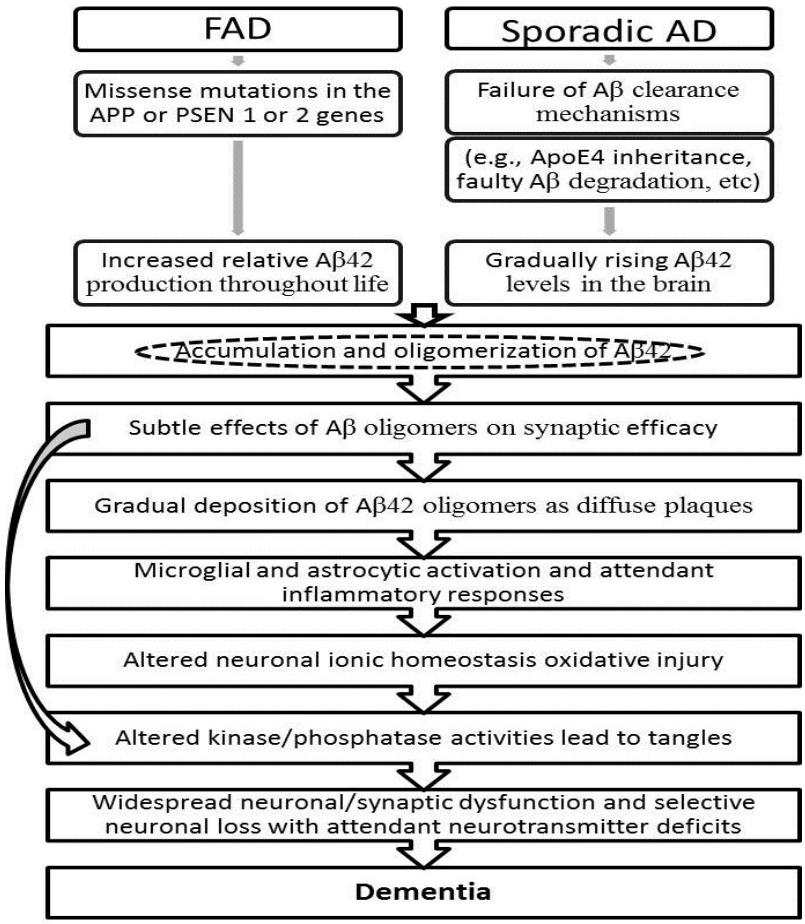

Figure 1.2 The amyloid cascade hypothesis (adapt from [16]).

In the amyloid cascade hypothesis, the central factor in AD relies on an imbalance between production and clearance of $A\beta_{42}$ and related Aβ peptides (dashed circle). The polymerization and deposition of the protease-resistant Aβ peptides are the crucial steps in the pathogenesis of Alzheimer's disease; changes in tau and subsequent formation of NFTs are triggered by the toxic concentrations of Aβ.

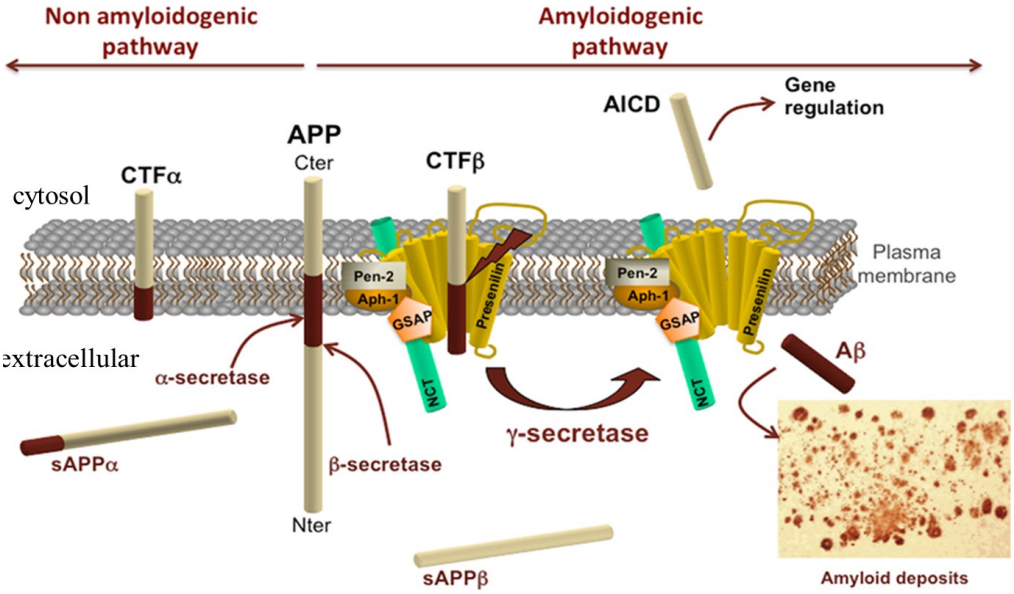

Figure 1.3 APP processing by α-, β- and γ-secretase (adapt from [29]).

APP processing by secretase activities is divided into the non-amyloidogenic pathway on the left and the amyloid genic pathway on the right. The α- or β-secretase cleaves APP in its extracellular domain releasing the amino-terminal fragment called secreted APP (sAPP) α or β and the carboxyl-terminal fragment CTFα or β, respectively. In the amyloidogenic pathway, the membrane-anchored CTF β is successively cleaved by γ-secretase generating the APP intracellular domain (AICD) and Aβ.

1.2 Functional studies of γ-secretase and its subunits

The γ-secretase is a multi-subunit protease complex. It acts as an integral membrane protease cleaving single path transmembrane proteins inside the membrane. Besides the generation of apoptotic intracellular peptides from APP, γ-secretase also plays important roles in the processing of over 90 reported type I transmembrane protein substrates [30]. Ligand-induced cleavage of the receptor protein Notch is mediated by γ-secretase which indicates a crucial role of γ-secretase in the cell-fate decisions during development [31,32]. Other substrates of γ-secretase, such as ErbB-4 [33], E-cadherin (Wnt signalling pathway) [34], CD44 [35], etc., suggest that γ-secretase also functions in the signalling pathways which are important for cell proliferation and differentiation.

There are four protein components of γ-secretase: presenilin (PS), nicastrin (NCT), anterior pharynx-defective 1 (APH-1) and presenilin enhancer 2 (PEN-2) [36–38]. Presenilins are nine-transmembrane proteins with the amino-terminus in the cytosol and the carboxyl-terminus exposing to the extracellular space [39,40]. There are two homologues of presenilin proteins, PS1 and PS2, existed in human brains [41–43]. In γ-secretase, the full-length presenilins undergo heterogeneous endoproteolysis in the large loop segment between TM 6 and TM 7 to produce a 28-34 kDa N-terminal fragment (NTF) and a 14-26 kDa C-terminal fragment (CTF) [44]. The PS NTF and CTF fragments remain associated with each other and appear in a high-molecular-

weight complex from both *in vivo* and detergent solubilized *in vitro* system [44–47]. Knockdown of PS1 reduces γ-secretase activity, while elimination of PS1 and PS2 abolish γ-secretase activity completely [48–51]. Two highly conserved aspartate residues residing in TM 6 (Asp^{257} for PS1 and Asp^{263} for PS2) and TM 7 (Asp^{385} for PS1 and Asp^{366} for PS2) have been demonstrated to be proteolytically active [52–55]. It has been proven that the heterodimers of NTF and CTF together, but not the full-length presenilin proteins, form the catalysis subunit of the γ-secretase complex and function as an aspartyl protease [44,52,53,56]. There are over hundreds amino acid mutations in presenilins identified to be associated with familial AD by changing the $A\beta_{42}/A\beta_{40}$ ratio [57,58]. Apart from the γ-secretase related functions, presenilins were also found to be involved in other cellular regulations such as acting as passive Calcium leak channels [59–61].

Nicastrin is a 709-residues, type I transmembrane glycoprotein with a single transmembrane domain which was initially identified from immunoaffinity purification with PS antibodies [62]. The transmembrane domain of nicastrin directly interacts with APH-1, while a α-helix and its surrounding loops in the extracellular domain (ECD) of nicastrin has been found to interact with the C-terminal of PEN-2 [40,63]. Nicastrin, the largest component of γ-secretase, has approximately 16 predicted N-glycosylation sites, with an additional molecular weight of 30 to 70 kDa depending on the expression cell type and constructions [64]. This extensive glycosylation is tightly regulated. It protects of the protein against degradation by trypsin but is not essential for the γ-secretase activity [65–68]. The role of nicastrin in the γ-secretase complex is controversial. Evidence showed biologically interactions among presenilin, nicastrin and the APP C83 or C99 substrates [62,69]. The large extracellular domain of nicastrin has been initially characterised as the substrate recognition executor by binding to the free amino terminus from the ectodomain of γ-secretase substrates [70]. Particularly the Glu^{333} and its nearby residues in the DAP domain (the DYIGS motif and peptidase homologous region) has been proven to be important for the substrate recognition [70,71]. Antibodies generated against the ECD of nicastrin have been found to be capable of inhibiting γ-secretase activity [72,73]. However, in a more recent study, researchers showed that both acetylated and unacetylated Notch substrates could be processed by γ-secretase with equal efficiency, indicating that the requirement of a free N-terminus as mentioned in Shah, et al.'s study is not essential for nicastrin-induced recognition. Furthermore, remarkable conformation changes of nicastrin ECD in γ-secretase upon inhibitor/substrate binding have been initially speculated [65,74,75]. A closing-opening working model of nicastrin ECD as a substrate receptor has been proposed based on the structure of the protein as well [40,76]. However, other studies indicated that instead of contributing to the γ-secretase enzymatic activity, nicastrin is involved in the complex maturation (stabilisation) [67,77]. Rather than

actively recruiting the substrates, a novel steric block mechanism has been proposed based on these results which give nicastrin the role of a gatekeeper in the γ-secretase complex [78,79].

APH-1 is identified as a ~ 30 kDa seven transmembrane protein which is required for the proper cell surface localisation of the Notch pathway component APH-2/nicastrin in *C. elegans* embryo [79]. Two isoforms of APH-1 are found in humans, APH-1a and APH-1b, respectively [79,80]. APH-1a exists in two alternative splice forms with identical N-termini but the different length of C-termini, namely APH-1aS (247-amino acid splice variant) and APH-1aL (265-amino acid splice variant) [80,81]. It has been proven that both the splice variants APH-1a as well as APH-1b are components of distinct PS1 or PS2- γ-secretase complexes, thus possibly at least six distinct γ-secretase complexes are existing with different tissue- or cell- specificity [82]. APH-1 is considered as the major stabiliser of the γ-secretase complex [83]. It directly interacts with mature and immature nicastrin and CTF of Presenilins inside the membrane and serves as a structural scaffold [40,81,84,85]. Studies pointed out that certain mutations of the conserved glycine residues in the GXXXG motifs in APH-1 TM 4 abolished the formation of γ-secretase complex [86–88]. Two highly conserved His^{171} and His^{197} in TM 5 and TM 6 of APH-1 have been identified to be important for APH-1 binding in γ-secretase and the γ-secretase activity [89]. These two residues were also found to involve in the APH-1 mediated γ-secretase substrate binding process [90]. However, apart from roles in the stabilisation and trafficking of γ-secretase, whether APH-1 is involved in other enzymatic activities of γ-secretase is still unclear. In a more recent research, γ-secretase-related proteolytic processing on APP CTFα or Notch ΔE was not effected within APH-1-knockout cells, which suggests that APH-1 is dispensable for processing these two γ-secretase substrates [91].

PEN-2 is the smallest component of the γ-secretase complex, which has only 101 amino acids. It was firstly identified by genetic screening in *C. elegans* and found to be broadly expressed and localised in the intracellular membrane compartments [80]. Co-immunoprecipitation and knockdown experiments further confirmed the incorporation of PEN-2 in the γ-secretase complex [92]. The interaction partner of PEN-2 inside γ-secretase complex has been identified as PS1-NTF upon detergent-mediated dissociation [85]. Chimeric replacement and triple mutations further suggest that the sites involved in binding of PS1 and PEN-2 are located in the first third of TM 4 in PS1 [93]. The role of PEN-2 in the γ-secretase complex has been investigated extensively in its facilitation of Presenilins endoproteolysis. Knockdown of PEN-2 expression by RNA interference leads to a significant accumulation of full-length PS1 together with a reduced level of PS1 fragments [83,94]. Expression of PEN-2 wildtype or C-terminally truncated

proteins in the PEN-2 knockdown cells recovers the PS1 endoproteolysis [95,96]. In one study which introduced chimeric PEN-2 molecules with exchanged TMDs, it revealed that residues 18 to 31 of PEN-2 were functional important for the generation of PS1 fragments [97]. More recently, by proteoliposome reconstitution, PEN-2 was proved to be necessary and sufficient to induce PS endoproteolysis and activity in an *in vitro* system [98]. However, studies involving the proteasome inhibitors in either PEN-2 knockdown or knockout cell lines suggested that rather than initializing the PS endoproteolytic processing, PEN-2 stabilised the endoproteolytic products [99,100]. It has been reported that PEN-2 is crucial for the NCT maturation, PS NTF-CTF heterodimer stabilisation and even the activity of γ-secretase [92,95,101]. In the absence of PEN-2 or in the presence of truncated PEN-2, either PS fragments or PEN-2 undergoes rapid proteasomal degradation [96]. Shortening or elongation of the C-terminus of PEN-2 promoted endoproteolysis of PS1, but failed in the stabilisation of the N- and C-terminal fragments, furthermore it failed to facilitate the maturation of NCT [96,97]. An enhanced γ-secretase activity was induced by PEN-2 after PS NTF/CTF heterodimer formation [102]. Deletion of PEN-2 in the mouse embryo led to a Notch-deficiency phenotype and PEN-2 $^{-/-}$ fibroblasts abolished the Aβ and NICD production [101]. Additionally, through regulation of a novel interaction partner of PEN-2, ferritin light chain, expression levels of PEN-2 and PS1 NTF were changed which could further affect the γ-secretase-mediated Aβ and NICD generation [103]. However, a more detailed mechanism is still not available. Mutations in different regions of PEN-2 showed diverse influence on γ-secretase maturation and activity indicating different roles of PEN-2 in the γ-secretase function [96,100,101,104].

As mentioned above, the acquiring of each component of γ-secretase complex is cooperatively regulated by the proteins in the existing subcomplex. The assembly order of the proteins of the γ-secretase complex has been elucidated based on experiments results from co-expression, RNA interference and detergent-induced dissociation. The assembly process initiates shortly after translation and membrane insertion of each component in the endoplasmic reticulum (ER). The immature nicastrin and APH-1 firstly assemble into an intermediate complex. This subcomplex has been reported to be maintained in the detergent-induced dissociation of γ-secretase [84,85] and could form in the absence of PEN-2 and presenilin [105]. The following step is unclear: Whether presenilin is firstly recruited by this iNCT/APH1 subcomplex or if it forms another subcomplex with PEN-2 [106]. However, evidence from co-expression of nicastrin, APH-1, and PS, as well as knockdown of PEN-2 suggested a stable trimeric complex formation of iNCT, APH-1, and presenilin holoprotein [83,94,107]. It is more likely that the iNCT/APH-1 subcomplex serves as a scaffold for presenilin proteins. PEN-2 then incorporates into the

trimeric subcomplex to facilitate the endoproteolysis of presenilin and stabilise the PS subunits. As shown in Figure 1.4, the complete assembly of all four components leads to the maturation of nicastrin, and this complex is exported from the ER through the Golgi via post-Golgi vesicles to the plasma membrane [37,108–110].

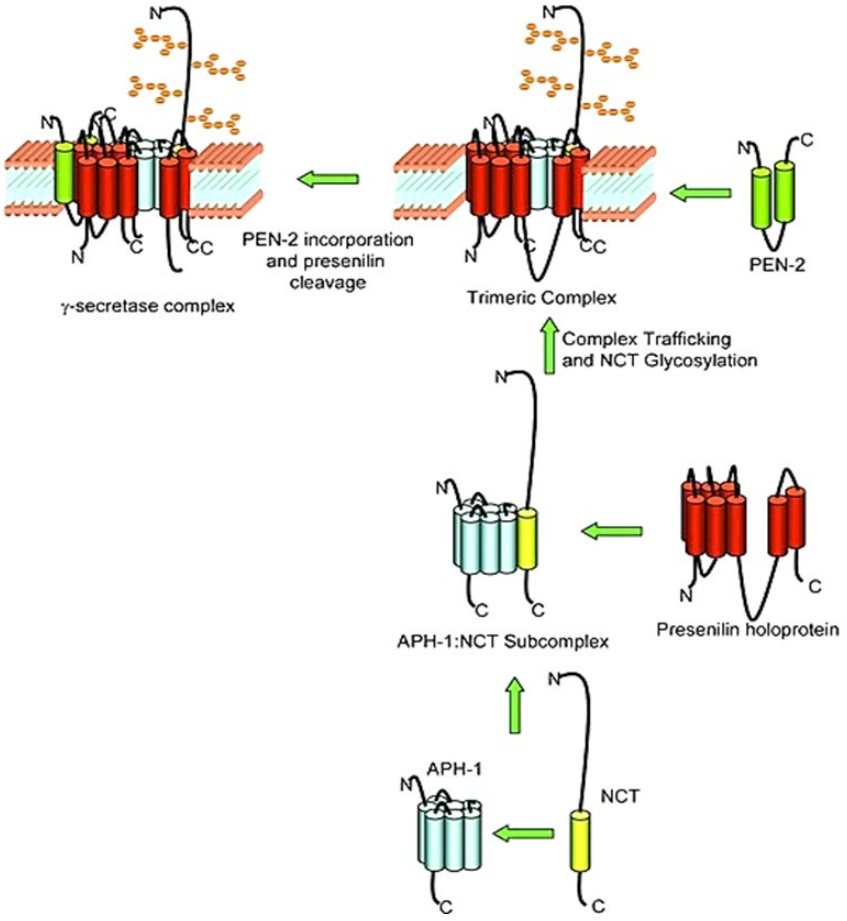

Figure 1.4 Assembly of the γ-secretase complex (adapt from [109]).
The assembly of γ-secretase initiated shortly after translation and membrane insertion of each component in the ER. The immature nicastrin and APH-1 firstly assembled into an intermediate complex. The following step might involve the formation of a stable trimeric complex of iNCT, APH-1 and presenilin holoprotein, and the exportation of this trimeric subcomplex accompany with the maturation of nicastrin. PEN-2, then finally incorporated into the trimeric subcomplex to facilitate the endoproteolysis of presenilin and stabilise the PS subunits.

1.3 Structural studies of γ-secretase and its single component

The progress of γ-secretase structural studies was limited initially to only interactions between different components and topologies of each component were proposed. It has been speculated that presenilins may form a homodimer within the γ-secretase complex to execute different enzymatic activities [111,112]. The initial substrate binding site and the active site of presenilins have been suggested to be different [113]. The last 7 amino acids at the C-terminus of presenilin have been reported to be essential for the binding with nicastrin [114]. A PAL motif

(Pro^{433}Ala^{434}Leu^{435}) in the TM 9 of presenilin CTF has been proved to be crucial for the γ-secretase activity [114–116]. And a hydrophilic cavity in the catalytic core of presenilin is found to be formed by the PAL motif, TM 9 and TM 1 of presenilin 1 [117–120].

The first two reconstructed EM structures of the γ-secretase complex from mammalian cells were released in 2006: They showed a spherical shape of the complex with visible pores at the top and bottom [121,122]. An improved cryo-EM structure with 12 Å resolution was published 3 years later giving an average molecular mass of the purified γ-secretase of ~230 kDa, which supported the 1:1:1:1 stoichiometry of the four components [123]. Consistent with the previous result from the negative staining EM [121], this new cryo-EM structure presented a globular shape of the γ-secretase complex with a height of ~ 85 Å and a top-view dimension of ~ 80 × 90 Å which is slightly larger than the required area for harbouring the complex [123]. Similar dimensions (100 × 70 × 105 Å) of the γ-secretase complex have been reported for an 18 Å cryo-EM structure [124]. The authors [124] also tried to distinguish the γ-secretase complex and a trimeric γ-secretase subcomplex consisting of nicastrin, APH-1 and presenilin. However, their results suggested that there is no significant conformational change upon PEN-2 binding [124]. During the same period, a structure of the C-terminal fragment of human Presenilin 1 has been determined by NMR using detergent-free cell-free expression and solubilization in SDS micelles [125]. In the NMR structure, six α-helical regions were identified, including two typical soluble helices named helix α and β in the N-terminal loop region, a short transmembrane helix (TM 7 with the catalytic aspartate at its amino terminus), a full membrane spanning helix (TM 8), and two shorter helices (helix 9a and 9b from TM 9) [125]. Comparisons were made between the PS1-CTF NMR structure and an atomic model of human PS1 derived from the crystal structure of an archaeal presenilin homologue [126]. This archaeon *Methanoculleus marisnigri* JR1 (MCMJR1) protein used shares 19.3% primary sequence identity and 52.8% similarity with human PS1, and has been reported to be a primitive GXGD-type di-aspartyl intramembrane protease which exhibited proteolytic activity against APP-derived substrates [127,128]. When comparing the NMR structure and the EM structure, the Asp^{385} in the TM 6 is oriented in an opposite directions [126]. This archaeon protein formed a tetrameric complex in the crystal, which raised again the hypothesis that the presenilins and other components in the γ-secretase might not follow the 1:1:1:1 stoichiometry.

Nevertheless, these single component structures and the development of the experimental techniques lead to a breakthrough in the structural studies of the γ-secretase complex. The alignment of 3D reconstructed EM structures between compound E-bound and unbound γ-

secretase complexes revealed a significant domain rotation and density shifts on the external surface which resulted in the closure of a lateral cleft and a lower pore of the central channel [74]. This dynamic conformational change was further attributed to the highly mobile NCT ECD [75]. The authors [75] pointed out that at least three distinct, dynamically equilibrated conformations (compact, intermediate and extended) existed in wild-type γ-secretase complexes. Inhibitors binding enriched a compact conformation, in which the NCT ECD adopted a closer distance to the membrane core, while incorporating the mutated Presenilin 1 (ΔE9) to the complex caused a transition from intermediate to extended conformations. A more detailed cryo-EM structure identified 19 TMs of γ-secretase at 4.5 Å [129]. From the reconstructions, the TMs of the γ-secretase complex were arranged into a horseshoe shape. Well-defined densities which outside the membrane-spanning region was assigned to the extracellular domain of nicastrin [129]. At the same year, a crystal structure of nicastrin ECD from *Dictyostelium purpureum* (sharing 23% identity and 40% similarity with the human nicastrin) was resolved at 1.95 Å resolution [76]. In this structure, the ECD of DpNCT is divided into a large lobe on the top and a small lobe at the bottom with an extended loop from the small lobe forming a lid cover over part of the large lobe [76]. Comparison with its structural homolog, a bacterial aminopeptidase (BAP), suggested a putative substrate-binding pocket which includes the previously reported substrates-recognition-related residues locating under the lid [70,71,76]. The assignment of all 20 TMs to each component (3 TMs for PEN-2 instead of 2 TMs) in the densities was achieved by the utilisation of an additional T4-lysozyme fused at the amino terminus of presenilin 1 [130]. In the 4.32 Å cryo-EM structure, the ECD of nicastrin sits right on top of TM horseshoe centre with a α-helix closely approaching the C-terminus of PEN-2. In this study, a novel conformation of PEN-2 with 3 TMs was found with the amino terminus of PEN-2 located on the cytoplasmic side and the carboxyl terminus facing the extracellular side. More recently, a near-complete atomic model of γ-secretase was built based on an improved 3.4 Å cryo-EM analysis [40]. The densities of TM 2 in presenilin 1 were further improved by binding to a di-peptidic inhibitor DAPT [131]. Additionally, an NMR structure of the transmembrane domain of NCT in SDS and DPC was released [132]. This NMR structure showed an attachment to the membrane via a region formed by residues Val^{697}-Ala^{702} in the C-terminus of nicastrin which might be involved in the γ-secretase complex formation [132]. Detailed features of the γ-secretase complex have been illuminated from the obtained structures, such as interacting amino acids between each component, the catalytic interface between TM 6 and TM 7 of presenilin, alignment of disease-related mutations.

1.4 Aim of this study

As an unconventional aspartyl protease with a broad range of substrates, structural information of the γ-secretase and its components would contribute to understanding not only of its physiological function, but also of pathogenic mechanism which may guide an efficient development of pharmaceuticals. The recent high-resolution cryo-EM structures reduced the urgent need to obtain structures for the four γ-secretase components. Still many important facts about this system are to be investigated, specifically the details of the assembly of the γ-secretase complex and its rearrangements during the processing of substrates.

This project aimed mainly at the production and characterization of γ-secretase proteins for crystallisation and structural analysis. Another focus of this work was the substrate containing initiation complex of γ-secretase.

The following objectives were defined for the initial research plan:

- **Establish expression and purification protocols for the γ-secretase proteins**

  Recombinant expression of individual subunits of the γ-secretase complex was planned to be investigated in the cell-free and the *E.coli* expression system. Detergent screening for optimal solubilization independence of protein stability was considered to be of highest importance to obtain functional proteins. As membrane proteins are known to pose a difficult purification problem, it was planned to use purification by affinity tags.

- **Biophysical characterization of the γ-secretase proteins**

  Identification of the target proteins by mass spectrometry was planned. CD-spectroscopy was employed to provide information of the secondary and tertiary structure of the isolated proteins. The stability of the human membrane proteins was expected to be monitored by thermal denaturation experiments. When the work started, no structural information for γ-secretase was available, therefore it was planned to subject the isolated proteins to crystallisation experiments.

- **Assembly of γ-secretase complexes and their interaction with substrate**

  The isolated proteins should be used for experiments on the assembly of γ-secretase, respectively, the sub-complexes that are relevant for the mechanism of this proteolytic enzyme. APPC100 was planned to be produced for further investigation of the mechanism of substrates processing.

2 Materials and methods

2.1 Instruments and Materials

2.1.1 Instruments and Consumables

Instruments	Company
Micro-Centrifuge	Sigma
Mixing Block	BIOER(MB-102)
Thermal Cycler	BIO-RAD (T100)
Refrigerated Incubator Shaker	INNOVA (423L)
Incubator Shaker	INFORS Unitron
Cell disruptor (EmulsiFlex-C3)	Avestin
Sigma 1-14K	SIGMA
Ultracentrifuge (SORVAL LYNX 6000)	Thermo Scientific
Benchtop centrifuge (HERMLE Z 233 M-2)	Thermo Scientific
Akta Explorer	GE Healthcare Life Science
T80/T80+ UV-VIS Spectrophotometer	PG INSTRUMENTS
ChemiDoc XRS Gel Documentation Systems	Bio-Rad
Trans-Blot® SD Semi-Dry Electrophoretic Transfer Cell	Bio-Rad
AVIV Model CD 425	AVIV
Mosquito LCP	TTP LABTECH LTD

Consumables	Company
EasyXpress Protein Synthesis Kit	Qiagen
RTS™ 500 ProteoMaster™ *E. coli* HY Kit	5PRIME
Rapid Ligation Kit	ThermoScientific
Plasmid Mini/Midi kit	Qiagen
Gel Extraction Kit	Qiagen
MassRuler™ DNA Ladder (Low/Middle/High Range)	ThermoScientific
Restriction enzymes	ThermoScientific
Antarctic Phosphatase	ThermoScientific
Phusion Hot Start DNA-polymerase	ThermoScientific

Ni-NTA/Ni-IDA resin	Qiagen
Monoclonal Anti-polyHistidine−Peroxidase	Sigma
PureCube Rho1D4 Agarose, peptide, antibodies	Cube Biotech
Flag resin	GeneScript
OctA-Probe, Presenilin 1 (D-10) Antibody, secondary antibodies	Santa Cruz biotechnology
Prestained Protein Marker	Jena Bioscience
BenchMarker™ Protein Ladder	Invitrogen
PD-10 empty column and desalting column	GE Healthcare Life Science
Complete EDTA-free Protease Inhibitor	Roche Applied Science
Lipids (PC, PE, Brain Total extract, Brain Polar lipids extract, Egg PC)	Avanti Polar Lipids, Inc.
Detergents (Fos-12, 14, 16)	Cube Biotech
Detergents (CHAPSO, CYMAL-6, DDM, DM, etc.)	Anatrace
Dialysis tubing Spectra/Por® 7	Spectrumlabs

2.1.2 Bacterial cultivation related materials

Table 2.1 Bacterial strains and genotypes.

E. coli strain (manufacturer, Purpose)	Genotype
Top 10 (Invitrogen, plasmid amplification)	F^- mcr A Δ (mrr-hsd RMS-mcr BC) φ 80lac ZΔ M15 Δlac X74 rec A1 ara D139 Δ (araleu) 7697 gal U gal K rps L (StrR) end A1 nup G
C41(DE3) (Lucigen, Protein Expression)	F^- ompT hsdSB (rB^- mB^-) gal dcm (DE3)
C43(DE3) (Lucigen, Protein Expression)	F^- ompT hsdSB (rB^- mB^-) gal dcm (DE3)
BL21(DE3) (Invitrogen, Protein Expression)	F^- ompT hsdSB (rB^- mB^-) gal dcm rne131 (DE3)

Table 2.2 Vectors for Expression.

Vector (manufacturer, purpose)	Antibiotic Resistance
pQE-2 (Qiagen, Protein Expression)	Kanamycin
pET 15b (Invitrogen, Protein Expression)	Ampicillin
pET 27b (Invitrogen, Protein Expression)	Kanamycin
pET-Duet (Invitrogen, Protein Expression)	Ampicillin

Table 2.3 Bacterial cultivation medium

	Composition (per liter)
LB	10 g Tryptone, 5 g Yeast Extract, 10 g NaCl
DYT	16 g Tryptone, 10 g Yeast Extract, 5 g NaCl
SOB	20 g Tryptone, 5 g Yeast Extract, 0.5 g NaCl, 2.5 mM KCl, 10 mM $MgCl_2$, 10 mM $MgSO_4$
TB	12 g Tryptone, 24 g Yeast Extract, 4 mL Glycerol
Phosphate Buffer for TB medium	0.17 M KH_2PO_4,0.72 M K_2HPO_4

All media components are weighted and dissolved in Milli-Q water and autoclaved at 121°C for 20 minutes. For TB medium, 100 mL of sterilised phosphate buffer was added to 900 mL TB medium before usage.

Table 2.4 Antibiotics and stock solutions used in cell cultivation.

Stock solutions	Concentration
Ampicillin sodium salt	200 mg/mL
Kanamycin sulfate	50 mg/mL
IPTG	0.2 M
Glucose	40% (w/v)

2.1.3 Gel Electrophoresis, Purification and Assay Buffers

Table 2.5 Gel electrophoresis buffer

Buffer	Composition
Agarose gel	
TAE	40 mM Tris, 1 mM EDTA, pH 8.0
SDS-PAGE	
SDS-Sample buffer	62 mM Tris, 2 % (w/v) SDS, 5 % (v/v) β-Mercaptoethanol, 20%(w/v) Glycerol, 0.2 % (w/v) Bromophenol blue
Running buffer	25 mM Tris, 192 mM Glycine, 0.1 % (w/v) SDS
MES running buffer	50mM MES, 50mM Tris-Base, 0.1% SDS, 1mM EDTA, pH7.3
Blue silver staining solution (1L)	10% Phosphoric acid, 10% Ammonium sulphate, 1.2g Coomassie G-250, 200 mL Methanol

Western Blot	
Transfer Buffer	39 mM Glycine, 48 mM Tris base, 20% Methanol
TBS/TBS-T buffer	20 mM Tris base pH 7.6, 137 mM NaCl, w/o 0.1% Tween 20
Blocking buffer	TBS-T buffer + 5% non-fat milk powder

Table 2.6 Composition of SDS-PAGE

Home-Made SDS-PAGE Solution components	5 % Stacking gel (10 mL)	12 % Resolving gel (25 mL)	15 % Resolving gel (25 mL)
H_2O	6.8	8.2	5,7
30 % Acrylamide	1.7	10.0	12.5
1.M Tris, pH8.8		6.3	6.3
1.0 M Tris, pH 6.8	1.25		
10 % SDS	0.1	0.25	0.25
10 % ammonium persulfate	0.1	0.25	0.25
TEMED	0.01	0.01	0.01

Table 2.7 Composition of purification buffers

Buffer	Composition
Cell- Free expression	
Wash Buffer	20 mM Tris-HCl, pH 8.0, 300 mM NaCl, 2 mM β-ME, 10% Glycerol
Pellet Solubilization Buffer	20 mM Tris-HCl, pH 8.0, 2 mM β-ME, 10% Glycerol, 6 M Urea, 1% SDS
Osmotic shock	
Sucrose Buffer	50 mM HEPES, 20% Sucrose, 1 mM EDTA, pH 7.9.
$MgSO_4$ Buffer	5 mM $MgSO_4$
Lysis Buffer	20 mM HEPES, 10% Glycerol, pH 7.4, add fresh 1 mM PMSF, Protease Inhibitor, Lysozyme (10 mg/g cell), DNase (5 mg/g cell)
Lipids Hydration Buffer	20 mM HEPES, 150 mM NaCl, 5% Glycerol, pH 7
Activity Buffer	50 mM HEPES, pH 7.4, 5 mM $MgCl_2$, 5 mM $CaCl_2$, 150 mM NaCl, 0.25% CHAPSO
Sucrose Gradient Buffer	20 mM HEPES, 150 mM NaCl, pH 7.4, supplemented with different sucrose gradient

2.2 Cloning

Cloning is a molecular biology method for the faithful reproduction of DNA molecular which contains the sequence of interest. After the transformation of the target genes from one organism into another suitable host organism, normally, limitless amounts of this molecular can be produced, which thus enable the further study of the target gene or its protein product [133].

In this work, oligonucleotides of Presenilins, PEN-2, APH-1 and NCT were ordered from Eurofins MWG, Ebersberg, Germany (see Appendix I: DNA and protein sequences). In the N-terminal of the target sequence, a deca-histidine tag and a Factor Xa Cleaving site were introduced. The forward and reverse primers were designed containing desired restriction sites (see Appendix II: Primers). For Rho-tag constructs, the Rho1D4 tag was introduced by primers. All the primers were synthesised from BioTeZ Berlin Buch GmbH, Germany. The PCR reactions were set up as following: (20 µL for testing condition)

Table 2.8 PCR reactions setting.

Component	20 µL reaction	50 µL reaction	Final conc.
Autoclaved milli-Q H2O	add to 20 µL	add to 50 µL	
5x Phusion HF Buffer	4 µL	10 µL	1x
10 mM dNTPs	0.4 µL	1 µL	200 µM each
Primer A	0.4 µL	1 µL	2 µM
Primer B	0.4 µL	1 µL	2 µM
Template DNA	0.4 µL	1 µL	1 pg –10 ng per 50 µL
DMSO 100 %	1 µL	2.5 µL	5 %
Phusion Hot Start DNA Polymerase (2 U/ µL)	0.2 µL	0.5 µL	0.02 U/ µL

The preliminary experiment conditions were set based on the polymerase and the length of the primers (Table 2.9). Basically, for primers > 20 nt, annealing step was performed for 10 – 30 s at aT_m + 3 °C of the lower T_m primer. For primers ⩽ 20 nt, a temperature equal to the T_m of the lower T_m primer was used in the PCRs.

Table 2.9 The cycling conditions for Phusion High- Fidelity DNA Polymerase.

Steps	3 steps	2 steps	No. Of Cycles
Initial denaturation	98 °C, 30 s		1
Denaturation	98 °C, 5-10 s		25-35
Annealing	64 °C-69°C, 10 s	72 °C, X s	
Extension	72 °C, X s		
Final extension	72 °C, 5 min, 4 °C Hold		1

The PCR product was further purified by agarose gel electrophoresis. The band corresponding to the respective product was extracted using Gel Extraction Kit. The purified PCR product was then digested with restriction enzymes. The double digested insert and vector are ligated using rapid ligation kit. The ligation mixture was transformed into Top 10 competent cell by heat-shock transformation for amplification. Positive colonies are used for further ligation into expression vectors. The purified plasmid was subjected to restriction enzyme digestion and sequencing for confirmation of the desired insert.

2.3 Cell-free expression

The *in vitro* expression system, also called cell-free expression system, has been developed in the past decades. It has been emphasised as a powerful system in the production of membrane proteins, which offers an opportunity to synthesise membrane proteins directly in the hydrophobic environment by the addition of hydrophobic compartments[134]. The production of membrane protein is always a challenging task in the *in vivo* expression system because of the highly hydrophobic nature of membrane proteins and their specific requirements in the living cells like translocation, post-translational modification, and toxicity upon the insertion into the host cell membrane. Comparing to the well developed and commonly used *in vivo* expression system, the *in vitro* expression system has certain exceptional advantages. The *in vitro* expression method is based on cellular crude extract containing all the biomolecular components required for translation. It tremendously reduces the complexity and therefore eliminates most of the problems mentioned above. The *in vitro* expression system is stable and compatible with different kinds of additives like certain detergents, lipids, cofactors and substrates [135]. These additives can be helpful to solubilize or stabilise the synthesised membrane protein. Another advantage is that the reactions of *in vitro* expression system are efficient. Instead of cell culture, harvesting and opening cells, the *in vitro* produced protein can be ready for further purification procedure in 2 to 24 hours, which substantially shortens the operating time.

Different modes have been reported to synthesise membrane protein in the *in vitro* expression system[134,136]. Basically, in the precipitate-based *in vitro* expression, membrane proteins are synthesised in the absence of an artificial hydrophobic environment and precipitated after translation. This type of expression provides an efficient way to quantify the total yield of a designed reaction and these precipitated membrane proteins can be solubilized later by

detergents. The other way is to synthesise membrane proteins in the presence of membrane mimicking compartments such as detergents, liposomes or nanodiscs. There are different tolerances of the *in vitro* expression system to the different kinds and concentrations of detergents, as a few harsh detergents appear to severely inhibit the expression machinery of cell extracts. The Brij derivatives are usually the first considered detergents in the initial detergent screen as they showed excellent compatibility to the *in vitro* expression system. Instead of adding detergents, adding liposomes to the reaction can bring membrane proteins into suspension. Considering the natural environment, defined liposome additives might offer an excellent opportunity for analysis of membrane proteins, especially the membrane protein complexes. The Nanodiscs are self-assembled discoidal particles composed of a phospholipid membrane bilayer surrounded by an apolipoprotein ring (scaffold protein) [137]. It is a recently developed tool for investigating the membrane protein reconstitution and can be used to produce soluble, functional and homogeneous membrane proteins for further analysis [138].

2.3.1 Plasmid preparation for *in vitro* translation

All the plasmids were prepared in a concentration range between 300-400 ng/μL. In general, plasmids were transferred into Top10 competent cells and cultivated in 25-50 mL SOB medium for amplifying. Plasmid extraction was performed using standard commercial kit. An additional ethanol precipitation step was introduced for further concentrating the plasmids.

2.3.2 Nanodiscs preparation

Buffers for Nanodiscs preparation are listed as below:

Table 2.10 Nanodiscs preparation buffer

Buffer	Composition	Note
Lipids Buffer	20 mM Tris-HCl, pH 7.4, 100 mM Na Cholate	
Dialysis Buffer	20 mM Tris-HCl, pH 7.4, 100 mM NaCl	5 L each time, use filtered stock, equilibrate at 4 °C before use
SEC Buffer	10 mM Na_2HPO_4, 150 mM NaCl, pH 7.4	filter and de-gas

For Nanodiscs assembly, 11 mg MSP1D1 or MSP1D1ΔH5 protein powder was resuspended in 5.5 mL MiliQ to achieve a final concentration of 2.2 mg/mL. An MSP protein to lipids mole ratio of 1:70 was chosen for reconstitution. DMPC lipids were equilibrated to room temperature before use (-20 °C in store). A 50 mM working solution of lipids was prepared in lipids buffer and incubated at 37 °C for 20 min to complete dissolution. Lipids and MSP protein were mixed

in a 15 mL falcon tube and alternately incubated at 4 and 37 °C for 3 times (each incubation lasts 20 mins). Dialysis was performed in the cold room using an MWCO 1000 Da membrane. Fresh dialysis buffer was exchanged twice a day. This procedure lasts for 3-4 days. The dialysed sample was then loaded to HiLoad Superdex 200 column with 2 mL injection volume. The elution fractions were collected and concentrated to 15 mg/mL for further use.

2.3.3 *In vitro* reaction set-up and analysis

In general, *in vitro* expression reactions were performed with 500 rpm shaking at 30°C for 2 hours. The reaction mixtures were centrifuged at 20,000 ×g for at least 1 hour to separate the soluble and the insoluble fractions. The supernatant and the pellet fractions were collected separately. The pellets were washed with Wash Buffer and solubilized in Pellet Solubilization Buffer. The samples were heated at 46 °C, 10 mins before loading to SDS-PAGE. Each fraction was analysed by SDS-PAGE and subsequent staining or western blot transfer and immobilised detection. For small scale *in vitro* expression, the reactions were set up as follow:

Table 2.11 *In vitro* expression reaction set up (25 µL)

Reaction Components	Volume	Note
E. coli extract	8.5 µL	
Reaction Buffer	10 µL	Mix before use (ATP inside)
IPTG (50 mM stock)	0.5 µL	50 times dilute
RNase-free water	Add up to 25 µL	
DNA plasmid	2 µL	0.5-1 µg. For negative control, 2 µL of RNase-free water was added instead.
Additives (detergents, nanodiscs, etc.)	X	Protease inhibitor was introduced into the reaction mixture to prevent the degradation of the membrane proteins.
Total	25 µL	

2.4 *In vivo* membrane protein expression and purification

2.4.1 Expression, cell opening and detergent screening

The transformation procedure was performed as described in section 2.1. The prepared plasmid was transferred into *E. coli* BL21 (DE3), or C41/C43 (DE3) competent cells for the expression of the respective protein. To set up the primary cell culture, the colonies were picked from agar plates and inoculate into TB medium with respective antibiotic and 2% (w/v) glucose. The primary cultures were incubated at 30 °C overnight with a shaking speed of 150 rpm. For the

main cultures, 175 mL of TB medium with antibiotic were aliquoted into 2L baffled flasks. The primary cultures were added to reach an initial OD_{600} above 0.2. The cells were grown at 30 °C with shaking at 100 rpm to an OD_{600} in the range of 0.8-1.3 and induced with 0.4 mM IPTG at 16 °C for 16-20 hours (1mM IPTG at 30 °C for 4 hours for the expression of APPC100 protein). The cells were then harvested by centrifugation at 5000 rpm for 30 min.

To remove the periplasmic fractions, cell pellets were resuspended in sucrose buffer with a ratio of 5 mL per gram cell pellet and homogenised by glass Porter before pelleting down at 7,000 ×g for 30 min at 4 °C. The supernatant was discarded and the pellet was re-suspended in 5 mM $MgSO_4$. The mixture was then incubated on ice for 10 min and centrifuged at 4500 ×g for 20 min at 4 °C.

Lysis buffer was added with a ratio of 8 mL per gram cell pellet after osmotic shock treatment. EDTA-free protease inhibitor (Roche) 1 tablet/50 mL buffer, 1 mM PMSF, 1 mg/mL Lysozyme and 5 mg/50 g cell pellet DNaseI were added to the lysis buffer freshly. The suspension was incubated in the cold room with stirring for 1 hour before passing through the cell disruptor. The final lysate was obtained by passing the material through the cell disruptor for 3-8 times with pressure between 10,000-20,000 psi and centrifugation at 900 ×g for 30 min to exclude unopened cells. Centrifugation at 9,000 ×g for 30 min was performed to pellet down inclusion bodies and cell debris. The supernatant was then subjected to ultracentrifugation at 100,000 ×g for 1 hour to harvest the membrane. All centrifugation steps were performed at 4 °C. The cell membranes were resuspended and homogenised in lysis buffer to make a stock solution. Membrane stocks were flash frozen in liquid nitrogen and stored at -80 °C until further use. SDS-PAGE samples from each step were normalised to the input cell pellet weight and stored for further analysis.

Detergents used in solubilization screening are listed in Table 2.12. For detergent screening, membrane stocks were diluted into different solubilization buffers with a ratio of 8mL solubilization buffer per gram cell pellets and incubated overnight at 4 °C with gentle agitation. The mixture was then subjected to ultracentrifugation at 100,000 ×g for 1 hour. Samples of supernatant and pellet were made by adding 5×Loading Buffer and incubate at 46 °C for 10 min before SDS-PAGE and western blot analysis.

2.4.2 Affinity chromatography

In this work, proteins were purified under the protocol for respective tags: polyhistidine (His), Rho1D4 (Rho) or Flag affinity tags.

Table 2.12 Properties of detergents used in solubilization screen.

Detergent used for solubilization	Abbr.	Type	CMC (% W/V)	CMC (mM)	Formula Weight (g/mol)	Micelle Size (kDa)
n-Octyl-ß-D-glucopyranoside	OG	N	0.53	18	292.4	23
n-Nonyl-ß-D-glucopyranoside	NG	N	0.20	6.5	306.4	41
n-Decyl-ß-D-maltopyranoside	DM	N	0.087	1.8	482.6	33
n-Dodecyl-ß-D-maltoside	DDM	N	0.0087	0.17	510.6	40 - 76
n-Octyl-ß-D-Thioglucopyranoside	OTG	N	0.28	9	308.4	58
N,N-Dimethyl-dodecylamine-N-oxide	LDAO	Z	0.023	2	229.4	76
CYMAL-6	Cy 6	N	0.028	0.56	508.5	46
FOS-choline-12	FOS-12	Z	0.047	1,5	351.5	18 - 21
FOS-choline-14	FOS-14	Z	0.0049	1,2	379.5	47
FOS-choline-16	FOS-16	Z	0.00053	0.013	407.5	72
N-Lauroylsarcosine sodium salt	NLS	A	0.42	13.7	293.7	
CHAPSO	CHAPSO	Z	0.5	8	630.9	7
Nonidet P40	NP40	N	0,05 - 0,3	50	603	60 - 95

2.4.2.1 IMAC

In general, solubilized fractions will be mixed with Ni-NTA or Ni-IDA resin and incubate in the cold room for 3 hours in a batch mode. Washing away of the impurities will be done in 3 steps: higher concentration of detergent (20 CMC), a higher concentration of sodium chloride (500 mM) and a slightly increased concentration of imidazole (25-30 mM). In total, 20-30 column volumes (CV) of washing buffer are needed. The target protein will be eluted in 5 × 1 CV elution buffer with 250-300 mM imidazole.

2.4.2.2 Rho AC

Rho1D4 refers to 9 amino acids (T-E-T-S-Q-V-A-P-A) on the C-terminal of bovine rhodopsin [139]. It has shown several advantages in membrane protein purification including high specificity of the antibody-epitope binding, high yield of the target protein and no interruption to functional studies [140,141].

The Rho1D4 affinity resin from Cube Biotech has a binding capacity up to 3-4 mg protein per mL resin. To perform Rho purification, an adequate amount of PureCube Rho1D4 Agarose was

equilibrated with equilibration buffer. The sufficient binding of target protein to the resin was achieved by incubating the solubilized fractions and agarose mixture at 4˚C overnight on an end-over-end shaker. The binding suspension was then transferred to a disposable gravity flow column. Flow-through was collected and the column was washed with at least 10 × 1 CV buffer. To elute the rho1D4-tagged protein, 1 CV of Elution Buffer (with 200 µM peptide) was added and incubated with rotation for 1 hour at 4 °C. This step was repeated at least 5 times to achieve a sufficient elution.

2.4.2.3 Flag AC

The FLAG™ peptide is a short and hydrophilic peptide with 8 amino acids (DYKDDDDK). It is widely used in protein expression and purification without interfering with protein folding or function [142,143].

The Anti-DYKDDDDK G1 Affinity Resin has a binding capacity of approximately 1 mg protein per mL settled resin. A batch binding format was applied for an efficient purification. The equilibrated resin was incubated with solubilized fractions overnight at 4 °C with end-to-end rotation. The suspension was loaded onto an empty PD-10 column to collect the resin. The resin was washed with 10-20 CV of wash buffer to remove any non-specific binding. After the column drained completely, the target protein was eluted with 6 × 1 CV of acid elution buffer (0.1 M glycine HCl, pH 3.5 with detergent) into Eppendorf tubes containing 1/20 CV of 1 M HEPES, pH 9.0. It is not recommendable to leave the column in the acid elution buffer for more than 15 minutes. The column was re-equilibrated immediately after elution.

2.4.3 Size exclusion chromatography

Size exclusion chromatography (SEC), also known as gel filtration separates proteins depending on the differences in molecular size. It is commonly used as the polishing steps in a purification procedure. In this work, Superose 6 10/300 GL, Superdex 200 10/300 GL and HiLoad 16/600 Superdex 200 pg columns were used for the investigation of the homogeneity and stability of purified proteins. Different columns were used based on their different properties. According to the manufacturer, Superose 6 10/300 GL has a broad fractionation range from 5×10^3–5×10^6 Da, while the Superdex 200 column has a high resolution within a fractionation range from 1×10^4–6×10^5 Da. Compare to analytical columns, the prep grade column has a better resolution at the disadvantage of increased run time.

Column equilibration was performed in SEC buffer. Elution Fractions containing the target protein from affinity chromatography were pooled and concentrated using a suitable cut-off concentrator to the desired volume (0.5 mL for analytical columns and 1-2 mL for prep grade

column).The samples were filtrated through a 0.22 μm filter before loading to the column. The apparent molecular weight of detergent-protein complex was calculated based on the calibration curve of the respective column. The protein concentration of the elution fractions from SEC was determined by measuring A_{280} using a UV-VIS spectrophotometer.

2.5 Protein Identification and Characterization

2.5.1 Circular dichroism spectroscopy

Circular dichroism (CD) has been extensively used for the investigation of protein structure and folding properties. It is based on the differential absorption of left-handed and right-handed circularly polarised light by chromophores [144]. In proteins, different structural elements have characteristic CD spectra in different UV ranges (Figure 2.2 and Figure 2.3). Typically, the peptide bonds are the main absorption group in the far UV range. CD spectra in this range are widely investigated to obtain the secondary structural compositions of protein.

In the near UV range (320 to 260 nm) the absorptions from aromatic side chains and disulphide bonds contribute to the CD spectra. A proper signal from near UV CD indicates the presence of tertiary structure in the proteins under investigation.

The CD measurements were conducted using an Aviv CD425 spectrometer. The approximate protein amount which is needed for measurements in the far UV region is 30 μg (300 μL of ~0.1 mg/mL protein in a 0.1 cm pathlength cuvette), and for a near UV CD measurement it is 1.7-3 mg (minimum 2.5 mL of 0.7-1 mg/mL protein in a 1 cm path length cuvette). It is essential to determinate an accurate concentration of the protein for a CD measurement. Usually, CD spectra are normalised using the following equation to the mean residue ellipticity for comparison [145],

$$[\theta]_{mrw,\lambda} = \frac{MRW \times \theta}{10d \times c}$$

where $[\theta]_{mrw,\lambda}$ is the mean residue ellipticity in units of deg×cm^2×dmol^{-1}, MRW is the mean residue weight of the protein (the molecular weight divided by N - 1, where N is the number of amino acids in the polypeptide chain), θ is the observed ellipticity (degrees), d is the path length (cm) and c is the protein concentration (g/mL).

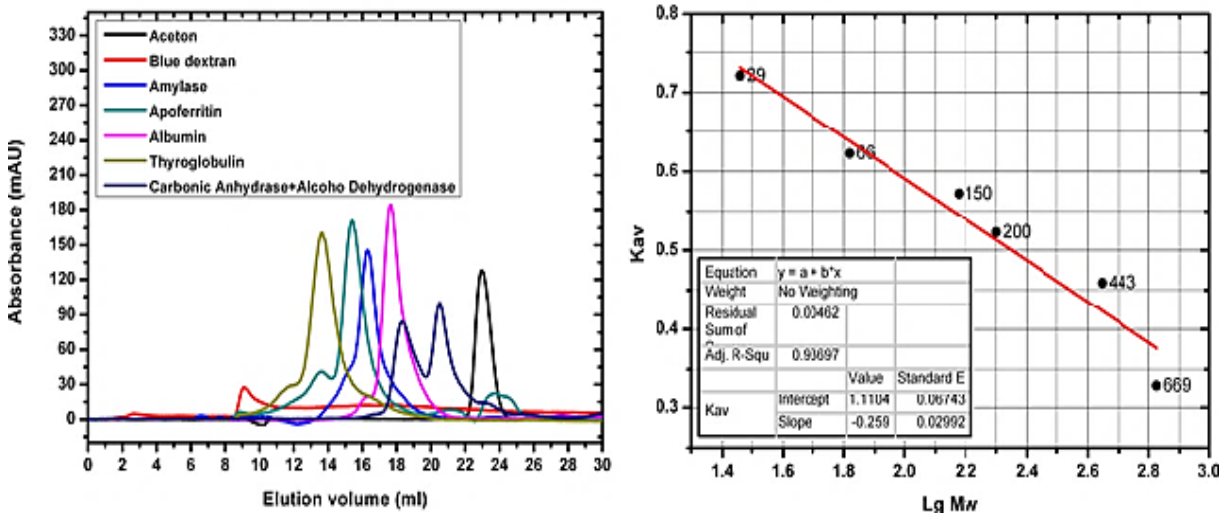

Figure 2.1 Calibration curve of Superose 6 10/300 GL.

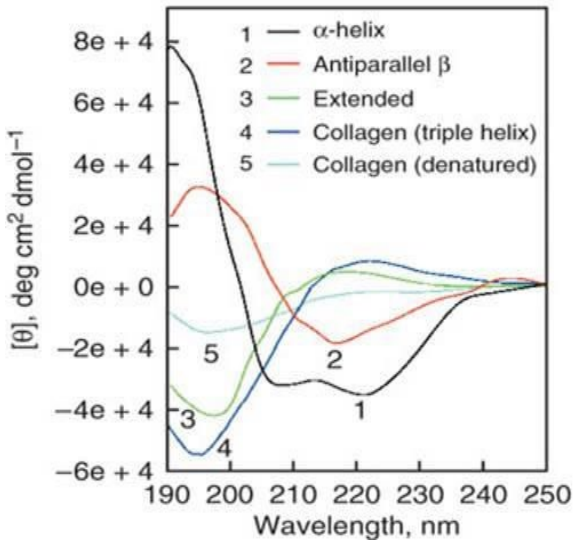

Figure 2.2 CD spectra for polypeptides in far UV range (adapt from [146]).

100% α-helix (1) shows two negative bands at 222 nm and 208 nm, 100% β-sheets (2) have a negative band at 218 nm, and the random coil spectrum (3) has a positive peak in the range between 210 – 220 nm and a negative peak at 195 nm. And placental collagen in its (4, blue) native triple-helical and (5, cyan) denatured forms from [146].

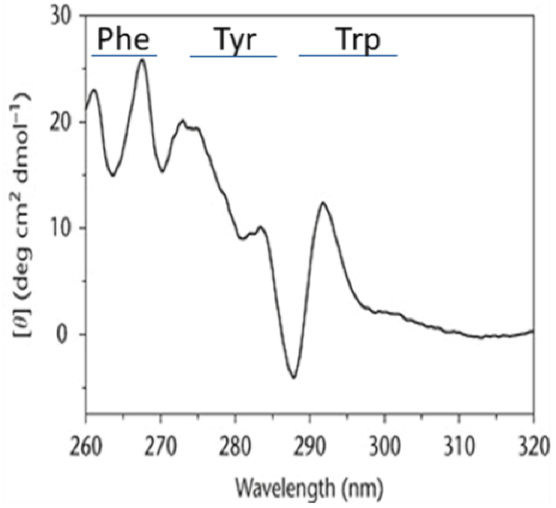

Figure 2.3 CD spectra for type II dehydroquinase (*Streptomyces coelicolor*) in near UV range (adapt from [144]).

Tryptophan shows an emission peak between 290 nm and 305 nm; Tyrosine has a peak range between 275 and 282 nm with a shoulder at longer wavelength may overlap with Trp peak; Phenylalanine shows weaker but sharper peaks between 255 and 270 nm [144].

For the CD measurements, purified protein samples were exchanged to their CD buffers by passing through a PD-10 desalting column, and the protein concentrations were determined with a UV spectrometer in the fresh CD buffer. A concentrating step might be involved to reach a desired concentration of proteins. In this case, a buffer control with the same treatment

was performed for an accurate concentration determination of proteins purified in detergents and proper baseline correction of CD-spectra. Buffer compositions are also crucial for far-UV CD measurements. There are many components show high absorption in this range. Commonly used buffers and reagents have been extensively studied [144,146]. In this work, 10 mM NaH_2PO_4 supplemented with detergents were used as standard CD buffer. All far UV and near UV CD spectra measurements were performed at 4 °C. Temperature scans (from 4 °C to 98 °C) were performed at a heating rate of 2 ºC per minute with an averaging time of 3 seconds.

Deconvolutions of obtained CD data are performed on online server DichroWeb with the CDSSTR analysis program using Reference set SMP180.

2.5.2 Fluorescence spectroscopy

Fluorescence is generated by a 3-step process which is illustrated by Jablonski diagram (Figure 2.4): Molecules are excited upon absorbing photons; then, non-radiative transition between different vibrational states in the excited electronic state (S_1) occur through conformational changes, collisional quenching and other processes; and finally, fluorescence emission returns the system to the electronic ground state (S_0). For proteins studied by fluorescence, either an intrinsic fluorophore or an extrinsic fluorochrome can be used for the investigation of protein folding properties. There are three aromatic amino acids in proteins which contribute to the fluorescence spectra: Phenylalanine, tyrosine and tryptophan (Figure 2.5). Compare to the other two amino acids, tryptophan dominates the emission of the proteins due to its high absorptivity and quantum yield. In principle, tryptophan emission spectra reflect the environment of the tryptophan residues. Denaturation and unfolding of the protein change the microenvironment of Trp, therefore, leading to a decrease of quantum yield (fluorescence intensity) and sometimes, a red shift of the emission spectra. The stability curve and its midpoint value (melting temperature, T_m) could then be obtained by gradually increasing the temperature to unfold the protein and the measured fluorescence intensity at each temperature step.

The fluorescence spectroscopy experiments were performed with AVIV Model 425 spectrometer. An excitation wavelength of 295 nm was used to selectively excite Trp only. Emission spectra were collected from 450 nm to 300 nm. Thermal denaturation experiments were performed from 4 °C to 98 °C with a heating rate of 2 ºC per minute and an averaging time of 1 second.

Proteostat dye (EnzoLife Sciences) and SYPRO Orange dye (Invitrogen) were employed as extrinsic fluorochrome in ThermalFluor experiments. Proteostat dye is a molecular rotor-type fluorophore, which releases an increasing fluorescence upon the constraint of the fluorophore

rotation. It has been widely used to study protein aggregation [147]. And for SYPRO Orange dye, it binds to hydrophobic surfaces based on the protein unfolds and results in an increase in fluorescence signal [148]. The temperature-induced unfolding of the proteins was then monitored by the fluorescence signal change and this signal change was used for determining the melting temperature.

In ThermalFluor experiments, protein within a concentration range of 0.3 mg/mL to 1.8 mg/mL was added to sample buffer supplied with 2 µL of fluorescence dye solution in a total volume of 25 µL. The measurements were performed in a temperature range from 25-95 °C using 1 °C per minute gradient, with 5 minutes equilibration time at the initial step. Sample buffer (20 mM HEPES, 200 mM NaCl, 10% Glycerol, 3 CMC FOS-14, 1 mM TCEP) was used as control. Experiments were carried out using Bio-Rad MyIQ system at SPF EMBL, Hamburg.

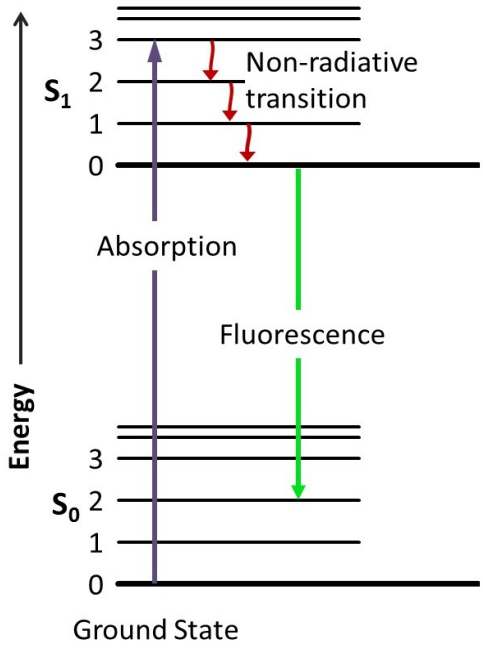

Figure 2.4 Jablonski diagram (adapt from [149]).
The electronic states of a molecule and the transitions between them were shown. The states are arranged vertically by energy. Non-radiative transitions are indicated by red arrows and radiative transition, i.e., fluorescence is indicated by the green arrow.

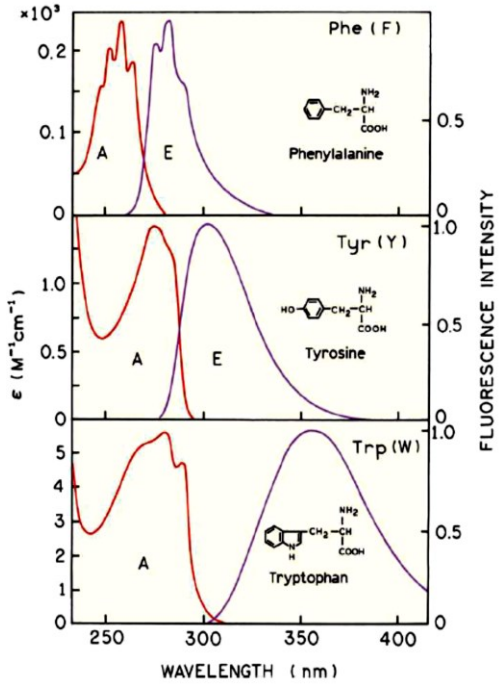

Figure 2.5 The absorption and emission spectra of Phe, Tyr and Trp (adapt from [150]).
The absorption spectra of Phe, Tyr and Trp are shown in red curves and the emission spectra are purple. Absorption and emission spectra of the aromatic amino acids were obtained in pH 7 aqueous solution.

2.5.3 Microscale thermophoresis

Microscale thermophoresis (MST) is a recently developed technique to characterise protein-

ligand, protein-DNA, or protein-protein interactions (Figure 2.6) [151]. The measurement reflects the movement of particles in a temperature gradient. The depletion of the solvated molecules in the heated area could be described by:

$$\frac{C_{hot}}{C_{cold}} = \exp(-S_T \times \Delta T)$$

Where the C_{cold} and C_{hot} are the molecule concentrations in the cold and hot area, ΔT is the temperature difference, S_T is the Soret coefficient which is a measure of the strength of the thermophoretic molecule flow compared with ordinary diffusion[152]. The measured thermophoresis signal F_{norm} corresponds to S_T and probes the change of molecular size, charge, and hydrophobicity, etc.al upon binding [151].

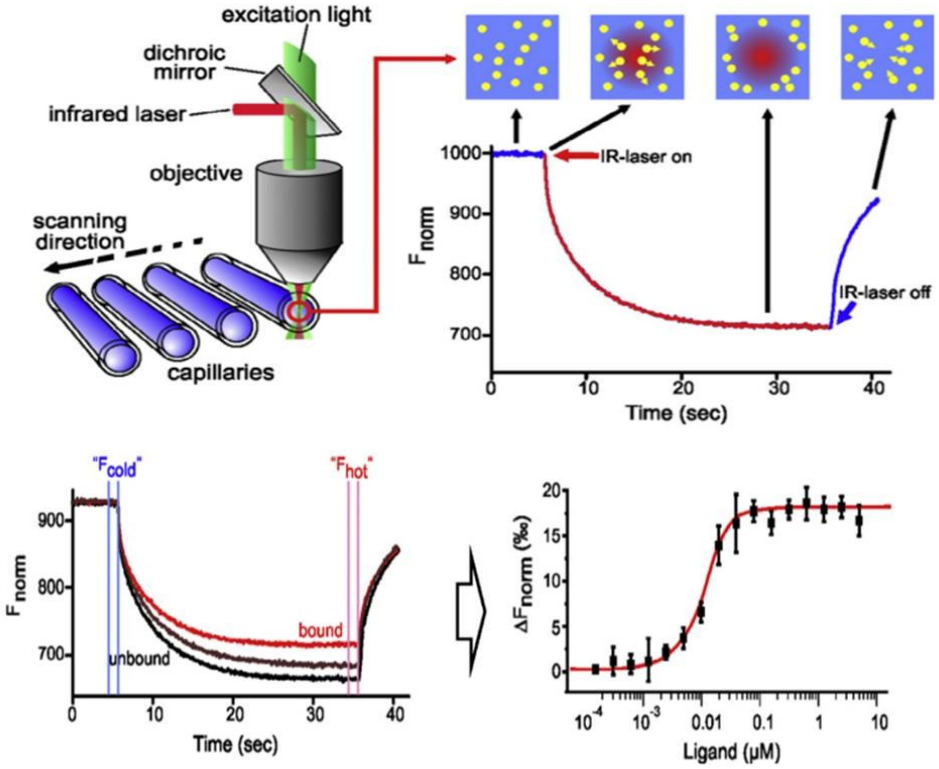

Figure 2.6 MST setup and experiments [153].

Upper panel: A schematic representation of MST optics. The fluorescence within the capillary is excited and detected. The temperature gradient is created by a focused infrared (IR) laser. Thermophoresis of fluorescent molecules is recorded as follows: a constant ‘‘initial fluorescence’’ as the molecules are homogeneously distributed before the laser is switched on; within the first second after switching on the IR laser, the temperature jump is observed; following by a diffusion-limited thermophoretic movement of the fluorescently labeled molecules towards steady; and after switching off the laser, an inverse T-Jump followed by the ‘‘back diffusion’’ of molecules. Lower panel: A typical binding experiment. The thermophoresis of a fluorescent molecule (black, unbound) changes upon binding to a non-fluorescent ligand (red, bound), resulting in different MST time traces. The normalised fluorescence (F_{norm}) is defined as F_{hot}/F_{cold}. Titration of the non-fluorescent ligand results in a gradual change in thermophoresis, which is plotted as ΔF_{norm} to yield a binding curve, which can be fitted to derive the binding constants [153]

MST analysis was performed using NanoTemper Monolith NT.115 (NanoTemper, GmbH). Purified hNCT or APPC100 were fluorescently labelled using the NanoTemper protein labelling kit RED-NHS. The labelling procedure was performed at 4 °C overnight. 20 nM of NT647-labeled hNCT was incubated with different concentrations of APPC100 (from 1 nM to 40 μM) and loaded into Monolith NT Capillaries. In the reverse experiments, 40 nM of NT647-labeled APPC100 was titrated by 0.2 nM to 10 μM of hNCT. Measurements were performed at 20 °C by using 40% LED power and 40% IR-laser power.

2.5.4 Other methods

Dynamic light scattering (DLS) is a technique to determine the size distribution profile of particles in solution. In DLS experiments, scattered light from particles in solution at 90° is detected and analysed with autocorrelation function [154]. Protein samples were filtered prior DLS measurements using a 0.22 μm centrifugal filter unit at 9000 rpm for 5 minutes. Wyatt disposable cuvette was used with a loading volume of 4 μL. All measurements were performed at 25 °C using DynaPro Nanostar (serial no. 323-DPN, Wyatt Technology Corporation). Data have been processed using Dynamics v.7 software.

Protein identification was performed by mass spectrometric analysis. Tryptic peptides were generated by proteolytic digestion (by trypsin) of the protein in the SDS-PAGE band. Protein bands in the blue silver stained SDS-PAGE was submitted for mass spectrometry (LC-MS/MS) at the Core Facility Mass Spectrometric Proteomics of the UKE.

2.6 Macromolecular crystallization

The methodologies of membrane protein crystallisation can be divided into 2 major groups: *in surfo* and the bilayer methods [155]. The *in surfo* method is using detergent solubilized protein directly in crystallisation screens, while the bilayer method involves different lipids to provide a host matrix for membrane protein crystals to grow.

The Crystallization Screen Kits used are listed as follow:

Kit	Company
JCSG Core suites I- IV, JCSG +	Qiagen
The MbClass suite	Qiagen
The PEGs II suite	Qiagen
The pHclear suite	Qiagen
The CubicPhase I and II suites	Qiagen

MRC 2-well Crystallization Plates from Jena Bioscience were used for crystallisation trials performed using *in surfo* method in vapour diffusion form, and the bilayer methods in bicelle form and traditional *in meso* (lipidic cubic phase, LCP) form. NeXtal CubicPhase MO Plates were used for crystallisation performed in controlled *in meso* phase crystallisation (CIMP) method [156]. In both of the plates, a volume of 65 µL undiluted screen solution was added into reservoir wells.

To set up crystallisation screens based on *in surfo* method, proteins with purity over 95% were first concentrated to a desired concentration (5-10 mg/mL) and then dispensed into protein wells of the plates with a volume of 100-200 nL using a Mosquito Robot. The protein drops were covered by an equal volume of screening solution and stored in 16 °C incubator to allow crystal growth.

Lipid bicelles are formed by long-chain phospholipids and either detergent or short-chain lipids or detergents, which will provide membrane proteins with a native-like bilayer environment for crystallization[157,158]. In solutions, the long-chain phospholipids are arranged in a central planar bilayer with the hydrophobic tails shielded by a bunch of short-chain phospholipids or detergents [159]. The diameter of the bicelles is controlled by the long-chain to short-chain lipids ratio [158]. In the experiment, bicelle lipids are prepared in a final concentration of 40% with a DMPC: CHAPSO molar ratio of 2.6, 2.8 and 3. Several cycles of freezing and heating (40 °C-50 °C) were performed to transfer the lipids into more organised phases, such as the perforated lamellar phase [158]. The well-prepared bicelle lipids will form a clear gel phase at room temperature. To reconstitute membrane protein into bicelles, the detergent-purified protein with a concentration of 15 mg/mL was added to the bicelle solution in a 1:4 (V/V) ratio which gives a final bicelle concentration of 8%. The mixture was incubated on ice for about 30 min to complete the reconstitution. The crystallisation plates were set up as described above.

Crystallisation of membrane proteins in LCP was first introduced in 1996 [160]. There are two major advantages of this method: firstly, it provides a more native-like environment for membrane proteins comparing to detergent micelles; secondly, crystals obtained in LCP showed a lower solvent content and better ordering in LCP [161]. In a traditional LCP crystallisation trail, protein was firstly mixed with monoolein at room temperature using the syringe mixing device at a ratio of 2:3 (w/w) before applying to the crystallisation plates. In a controlled in meso phase crystallisation (CIMP), the crystallisation plates are pre-coated with monoolein in the protein wells. Detergent-purified proteins were dispensed directly into these

wells. The plates were then sealed and incubated at 22 °C for 3 hours or overnight. After the incubation, an additional diluted screening solution (Figure 2.7) was added to the experimental well and 65 µL of undiluted screening solution is transferred to the reservoir wells. The resealed plate is incubated at 22 °C and monitored for crystals growth.

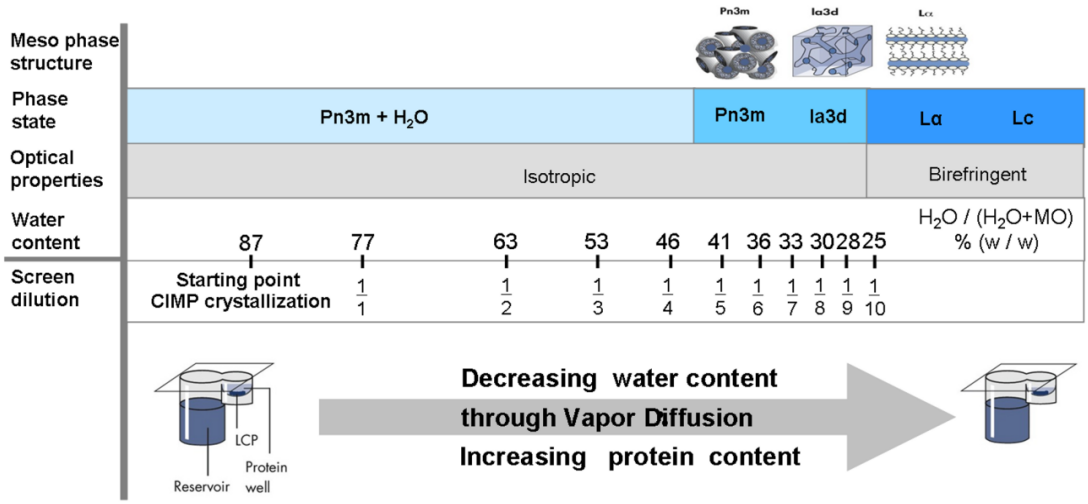

Figure 2.7 Simplified phase diagram of monoolein/water at room temperature (adapt from [156]).

2.7 Protein reconstitution and activity assay

A native-like lipids environment is important for membrane proteins, not only for structural determination but also for proper functions. Proteoliposomes which are formed by detergent-purified membrane proteins integrated into phospholipid vesicles have been applied to a very diverse range of membrane functions [162–165]. In this study, it has been used as a tool to study the protein complex formation and activity assay.

2.7.1 Liposome preparation

To prepare liposome, lipids were dissolved and mixed in organic solvents (here we used chloroform or chloroform: methanol mixtures) at a concentration of 10-20 mg/mL. The organic solvent was then removed under a nitrogen stream and the sample thoroughly dried by placing the vials in a vacuum device pumping overnight. The dried lipid film was suspended in lipid hydration buffer to a final concentration of 20 mg/mL. Sonication was performed to generate small unilamellar vesicles. The flash-freezing and thawing procedure was repeated to fuse the SUVs to large multilamellar vesicles (LMVs). The LMV suspension was passed 11 times through a 100 nm polycarbonate filter to form vesicles (liposomes) with a uniform size. The extrusion was performed at 50-60 °C. The prepared liposome was then diluted to 4 mg/mL and

solubilized using 5% CHAPSO slightly over the concentration at which the liposome was saturated (R_{sat}). The detergent-liposome mixtures were incubated at room temperature or in the cold room for at least 1 hour to reach equilibrium.

2.7.2 Reconstitution of proteins into detergent destabilised liposomes

The Protein of interest was added to detergent-destabilized liposomes at ratios from 1:50 to 1:100 (w/w). The mixture was incubated with end-over-end rolling in the cold room for 2 hours. The detergent removal was achieved by successive additions of SM_2-Biobeads (to a total amount of 25 × lipids weight), which allows a slow process. After the final step of detergent removal, biobeads were separated by passing the protein-liposome-biobeads suspension through an empty PD-10 column. The reconstituted proteoliposomes were collected and pelleted down by ultra-centrifugation at 100 000 ×g for 1 hour.

2.7.3 Sucrose floating assay

Sucrose gradient centrifugation was performed to separate unintegrated protein and proteoliposomes. Different sucrose gradient solutions were prepared at following concentrations (w/v): 80%, 37%, 32.5%, 29.5%, 21%, 17.2%, 13.4%, 9% [98]. Reconstituted proteoliposome samples were mixed with 80% sucrose buffer at 1:1 ratio (v/v) and layered at the bottom of a Thinwall Ultra-Clear™ 38.5 mL Tube (Beckman Coulter). 5 mL of each sucrose gradient solution were layered into the tubes from high concentration to low concentration. The centrifugation was performed in Avanti J-30i centrifuge with a JS-24.38 rotor at 20 000 rpm (72 000 ×g) for 16 hours at 4 °C. The fractions with turbidity were collected and analysed by SDS-PAGE and western blot.

2.7.4 Dialysis

To remove the excess sucrose, dialysis was performed for the fractions containing the target proteins using a 15 kDa cut-off dialysis tubing (Spectra Por 7, from Spectrumlabs). A 100 × sample volume of dialysis buffer (20 mM HEPES, 150 mM NaCl, 5 mM $CaCl_2$, 5 mM $MgCl_2$, pH 7.4) was prepared. Dialysis was completed by stirring in the cold room for 23 hours, with 3 exchange of buffer.

2.7.5 Activity assay

Different fractions were examined (membrane fractions, detergent-purified proteins, reconstituted proteoliposomes) for their proteolytic activity on the well-known γ-secretase substrate APP-C100. The APP-C100 substrate was expressed in *E. coli* BL21 (DE3) strain as

described in section 2.4.1. Purification of APP-C100 was performed in different detergents (FOS-14, Triton X-100 or NP-40) as described in 2.4.2.3. The purified substrate was treated with 0.5% SDS by heating at 65 °C for 5 min and centrifuged for 1 min at 13000 rpm to remove the precipitate. 1-3 µL of supernatant was added to each activity reaction. PE (3-sn-Phosphatidylethanolamine from Santa Cruz biotechnology) and 16:0-18:1 PC (PC, 1-palmitoyl-2-oleoyl-sn-glycero-3-phosphocholine from Avanti) lipids mixture (with 1:9 or 1:4 weight ratio) were added to the reactions to a final concentration of PC in the range between 0.1 - 0.2%. Alternatively, egg PC (Avanti) was used as a substitute for POPC. Reactions were incubated for 4-20 hours at 37 °C or 42 °C on a heating block with gentle agitation and stopped by adding 12 µL SDS-sample buffer. For the reactions involving the γ-secretase inhibitor, 1 mg of $L_{685,458}$ (672.8 g/mol) was dissolved in 148.6 µL DMSO to make a 10 mM stock solution. The working concentration of the inhibitor was 1 µM. The results were analysed on 15% SDS-PAGE or 4-12% NuPAGE® (Novex) gels.

3 Results

3.1 Cell-free expression of different components of γ-secretase

In this work, an *E. coli* based *in vitro* translation system was used to investigate the expression of each component or co-expression of the γ-secretase sub-complex. For the interaction study, a second affinity tag was introduced by PCR to facilitate the pull-down experiments and the detection procedure. All constructs involved in the experiments are listed in Table 3.1, and their behaviour in the cell-free expression system is described as follow.

Table 3.1 Constructs of Proteins

Abbr.	Protein	Vector	Constructs
A1	APH-1	pQE2	N10×His+Factor Xa+protein
A3	APH-1	pET27b	Protein+C-HSV+C6×His
A7	APH-1	pET27b	Protein+C-Rho-tag
N1	Nicastrin	pQE2	N10×His+Factor Xa+protein
N2	Nicastrin	pET27b	Protein+ C6×His
P1	PEN-2	pQE2	N10×His+Factor Xa+protein
P3	PEN-2	pET27b	Protein+C-HSV+C6×His
P7	PEN-2	pET27b	Protein+C-Rho-tag
PS1-22b	Full-length Presenilin 1	pET22b	
H1	Full-length Presenilin 1	pET15b	N6×His+Thrombin+protein
H1N	Presenilin 1 N-terminal fragment	pET15b	N6×His+Thrombin+protein
H1C	Presenilin1 C-terminal fragment	pET15b	N6×His+Thrombin+protein
1NR	Presenilin 1 N-terminal fragment	pET27b	Protein+C-Rho-tag
1CR	Presenilin1 C-terminal fragment	pQE2	Protein+C-Rho-tag
PS2N	Presenilin2 N-terminal fragment	pQE2	
PS2CTF	Presenilin2 C-terminal fragment	pQE2	
2R	Full-length Presenilin 2	pQE2	Protein+C-Rho-tag
2NR	Presenilin 2 N-terminal fragment	pET27b	Protein+C-Rho-tag

3.1.1 Cell-free expression in precipitation mode

A detergent-free expression was initially employed to confirm the expression of target proteins

in the *E. coli* based *in vitro* translation system. For the membrane proteins expression, an advantage of this mode is that less impurity is incorporated into the pellet fractions after centrifugation. As shown in Figure 3.1A, dominating bands of target proteins were clearly visible in the pellet fractions on the blue-stained SDS-PAGE without further purification. Most of the constructs could be expressed in the *in vitro* system under a standard condition (Figure 3.1 and Figure 3.2). APH-1 with a C-terminal His tag (A3 in Figure 3.1) and nicastrin with a C-terminal His tag (N2 in Figure 3.2) did not show strong signals on the PAGE indicating low expression levels of these two constructs.

After confirming the expression of the target proteins, two types of detergents were selected to solubilize the expressed membrane proteins from the pellet: DDM (n-Dodecyl β-D-maltoside), a mild non-ionic detergent which has been wildly used for the stabilisation and activation of membrane proteins, and zwitterionic phosphocholine (FOS) detergents. As shown in Figure 3.3, FOS-12 (n-Dodecylphosphocholine) and FOS-16 (n-Hexadecylphosphocholine) successfully solubilized both nicastrin and PEN-2 proteins from the pellet, while DDM worked poorly in both cases. This difference in the solubilization efficiency was also observed in the membrane solubilization experiments which is described in chapter 3.2.2.

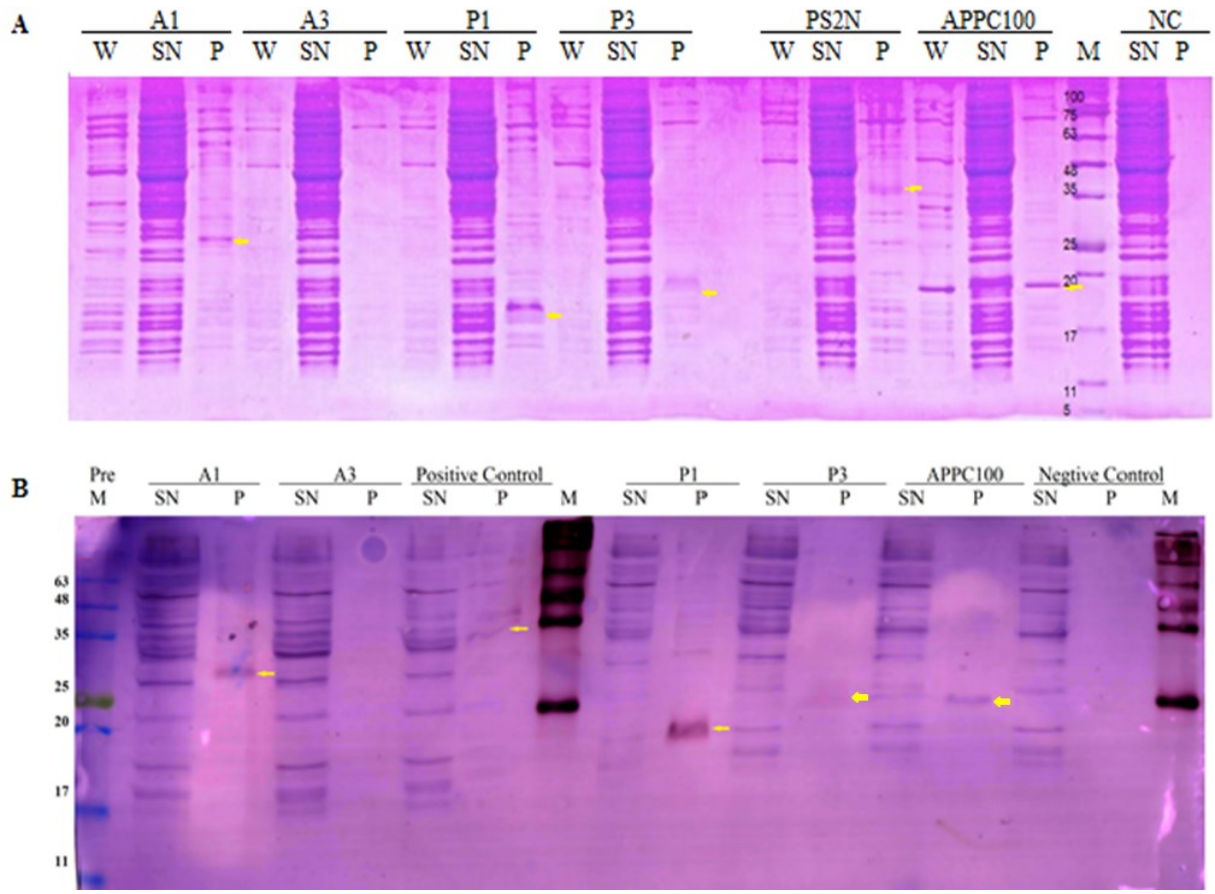

Figure 3.1 SDS-PAGE of cell-free expressed proteins in the precipitation mode.

Detergent free in-vitro expression reactions were performed at 30 °C for 2 hours. Samples were made as described in section 2.3.3. A: Blue-stained SDS-PAGE. B: Anti-His western blot. W: samples from the washing step; SN: supernatant samples after centrifugation; P: pellet after centrifugation; NC: negative control samples (reaction without adding plasmid). PS2N was used as a positive control. Yellow arrows indicate the expected target proteins. Protein abbreviations were listed in Table 3.1. His-tagged APH-1 (A3) did not show a positive signal indicating a low expression level of this protein in the current system.

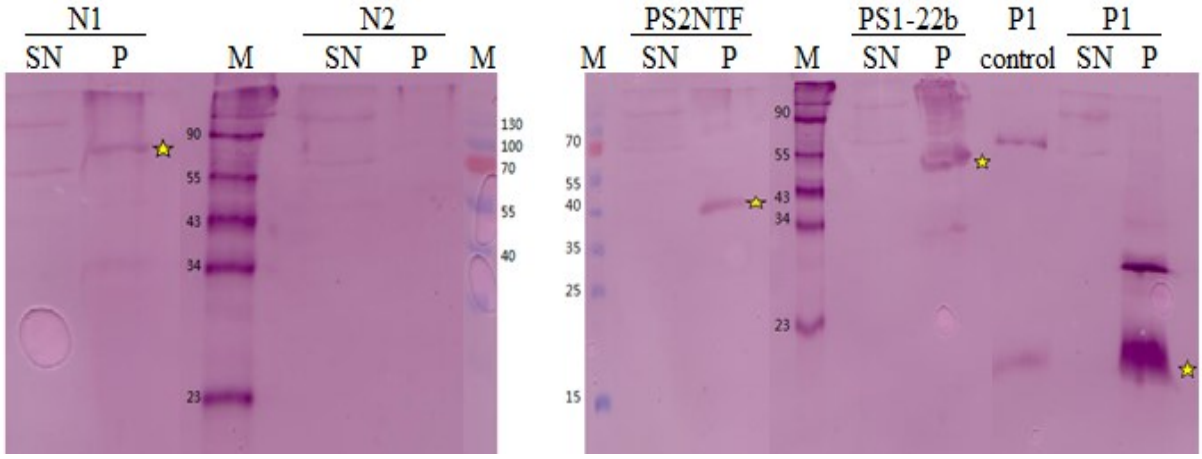

Figure 3.2 Anti-His western blot of proteins expressed from precipitation-mode cell-free expression.

All reactions were performed at 30°C for 2 hours. Pellets were washed 3 times before making samples for SDS-PAGE. Yellow stars indicate the expected target proteins. Protein abbreviations were listed in Table 3.1. N2 (nicastrin) did not show strong signals at the expected molecular weight indicating a low expression level of this construct.

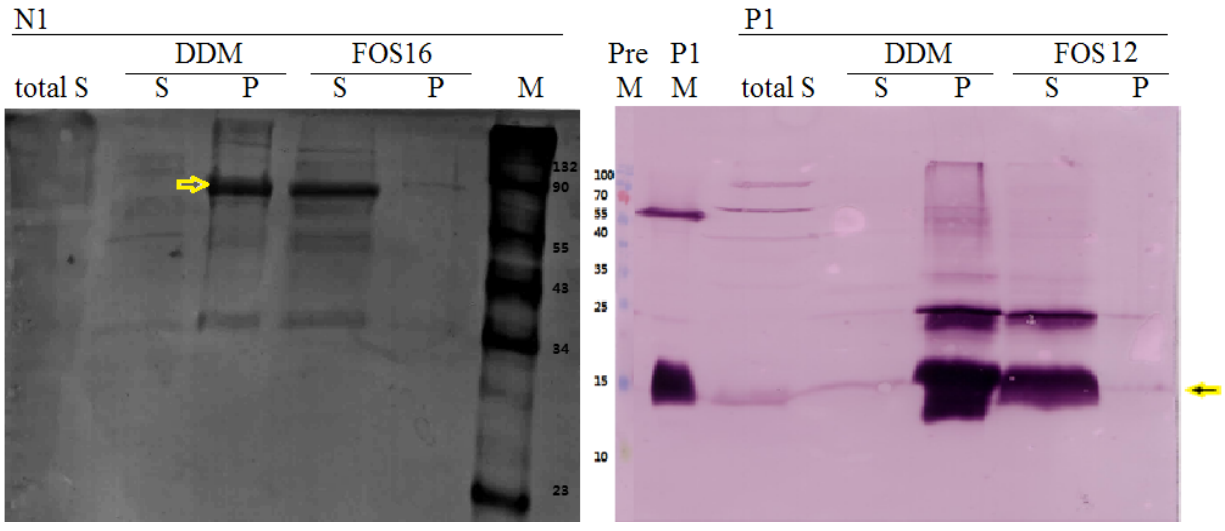

Figure 3.3 Solubilization of NCT and PEN-2 from *in vitro* expressed pellet.

25 µL of in vitro expression reactions were performed at 30 °C for 2 hours. The pellets were solubilized with 1% DDM, 1% FOS-12 or 1% FOS-16. Total S: the supernatant after reaction; S and P indicate the supernatant and the pellet after detergent solubilization. Yellow arrows indicate the monomeric form of expected target proteins. For both nicastrin and PEN-2, FOS-cholines showed better solubilization ability than DDM.

3.1.2 Cell-free expression with solubilization

Simultaneously, detergents and nanodiscs were introduced into reactions to solubilize the synthesised target proteins directly after expression.

First of all, different kinds and concentrations of detergents or nanodiscs were screened for an optimal yield or an optimal integration of protein into nanodiscs. As expected, additives introduced to the *in vitro* reactions showed an inhibition effect on the expression of target proteins. Harsh detergents impaired the *in vitro* expression system significantly (Figure 3.4). Brij derivatives (Brij 58 and Brij 98) showed the best compatibility with the expression system (Figure 3.4). For most of the constructs, the target proteins were produced in the soluble state in the presence of Brij 35 (Figure 3.5).

Alternatively, the insertion of proteins into nanodiscs was confirmed by utilisation of Rho-tagged proteins and His-tagged nanodiscs after affinity purification (Figure 3.6). The Rho-tagged proteins were captured by the Rho1D4 resin, but not the empty nanodiscs. Both of proteins and nanodiscs were detected in the elution fractions. The signal intensity from His-tagged nanodiscs correlated with the signal intensity of Rho-tagged proteins, which indicated a successful insertion. Two different nanodiscs with different diameters were tested for PEN-2 insertion. Both of them could partially bring PEN-2 into a soluble state without a significant difference in the insertion ratio of the target protein (Figure 3.9).

Moreover, different compatibility of different additives or reaction conditions was evaluated. Initially, for nicastrin, neither detergents nor nanodiscs could efficiently bring the protein to the supernatant in the reactions performed at 30 °C (Figure 3.7). Upon optimisation, a lower temperature (20 °C) combine with a longer reaction time (16 hours) successfully increased the nicastrin protein fractions in the supernatant with Brij 35 addition (Figure 3.8). Nevertheless, nanodiscs still showed low solubilization efficiency for this 77 kDa protein under the optimised condition (Figure 3.8).

The yield of APH-1 was significantly improved with the Rho-tag construct. The total yields of the target protein were similar from the 20 °C overnight reaction and the 30 °C 2 hours reaction (Figure 3.10). However, a distinct fragmentation band was observed in the protein samples obtained from higher temperature reactions. Therefore, the lower temperature reaction condition was selected to avoid the protein degradation.

Based on these results, the constructs and reaction conditions of each component of the γ-secretase complex were selected for further upscale purification and characterization (Table 3.2).

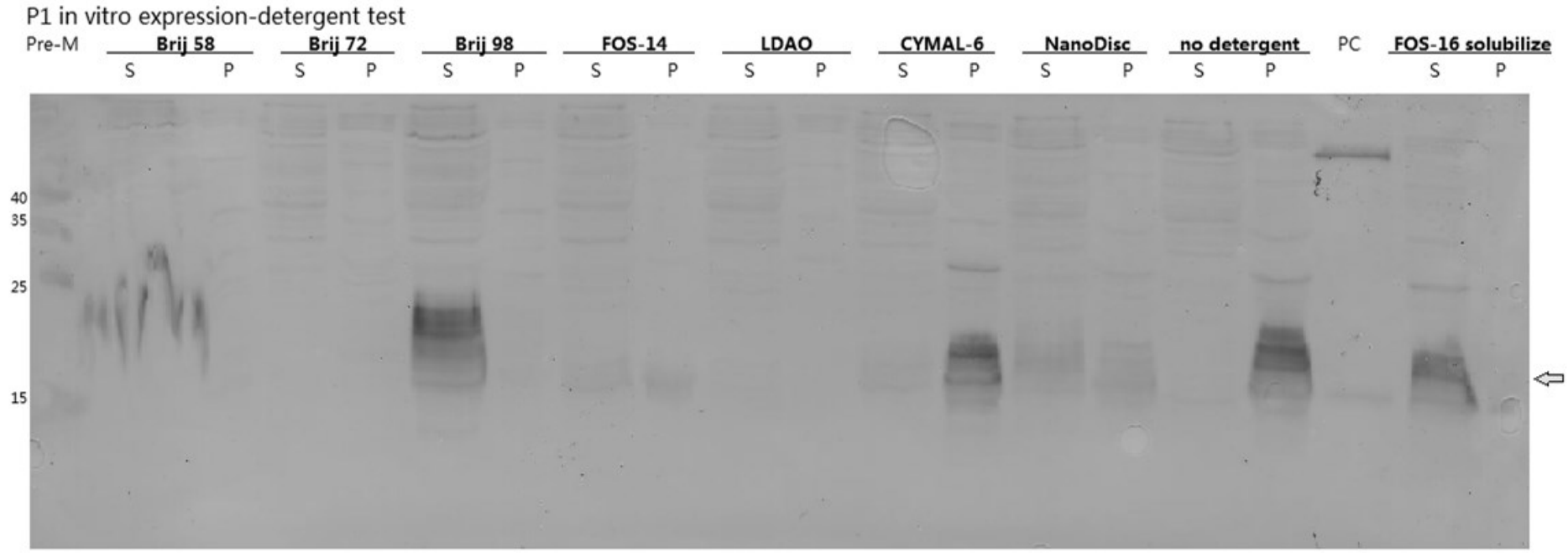

Figure 3.4 PEN-2 *in vitro* expression detergent test.

Reactions were performed at 30 °C for 2 hours. Detergents working concentration in the reactions were 1.5% Brij 58, 0.2% Brij 72, 0.2% Brij 98, 0.8 mg/mL Nanodiscs, 0.0138% FOS-14, 0.092% LDAO, 0.112% CYMAL-6. Re-solubilization of the precipitation mode expressed PEN-2 was performed with 1% FOS-16 solubilization buffer at 4 °C overnight. FOS-14: n-tetradecyl phosphocholine. LDAO: N,N-Dimethyldodecylamine N-oxide. CYMAL-6: 6-Cyclohexyl-1-Hexyl-β-D-Maltoside. PC: positive control of PEN-2. The arrow indicates the expected position of the target protein. Harsh detergents impair the in vitro expression system significantly, while Brij derivatives (Brij 58 and Brij 98, but not Brij 72) showed a much better compatibility. CYMAL-6 did not suppress the expression system but exhibited poor solubilization efficiency of the expressed membrane protein.

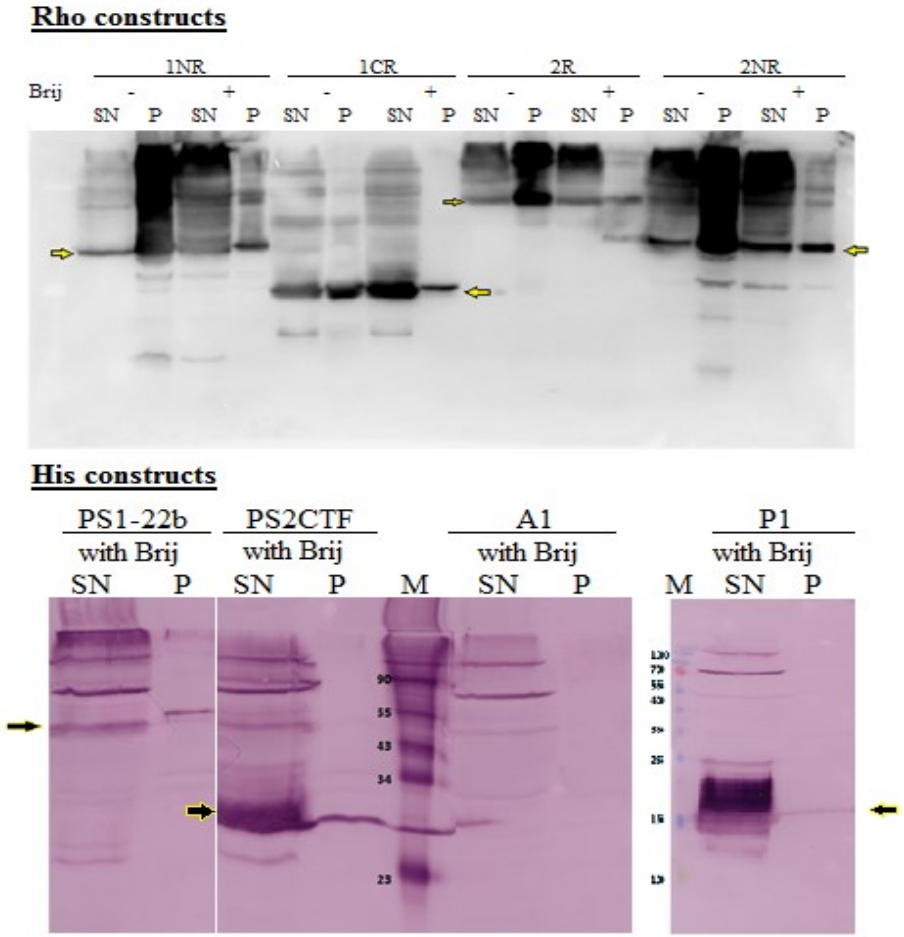

Figure 3.5 *In vitro* expression of different constructs with Brij35.
Reactions were performed at 30 °C for 2 hours. 0.2% Brij35 was added to the detergent-mode reactions. Upper panel: anti-Rho western blot of Rho-tagged proteins expressed with and without Brij 35. "-" are the reactions without Brij 35 addition, "+" are the reactions with Brij 35. Lower panel: anti-His western blot of His-tagged proteins in the presence of Brij 35. The yellow arrow indicates the expected target proteins.

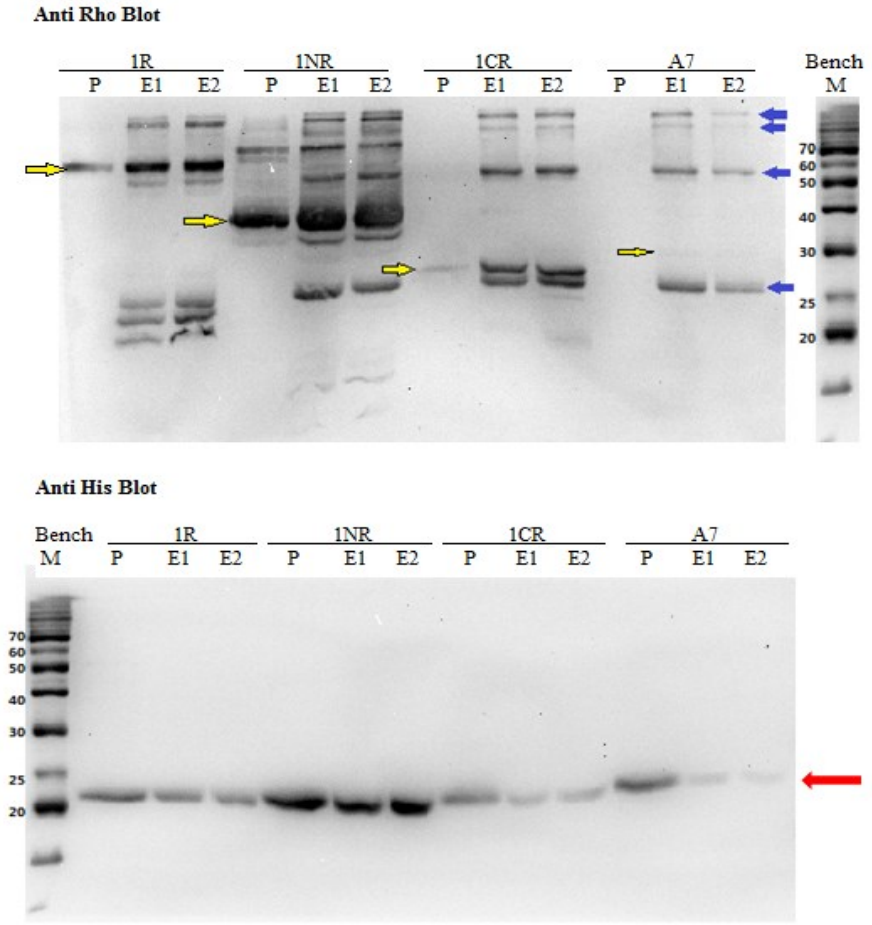

Figure 3.6 *In vitro* expression and purification of Rho-tagged proteins with Nanodiscs.
Reactions were performed at 30 °C for 2 hours. 1.5 mg/mL Nanodiscs was added to the reactions. P: pellet after reaction; E1, E2: Elute fraction 1 and 2 from the Rho affinity purification; Yellow arrow: target proteins; Blue arrow: signals from rho-resin; Red arrow: MSP delta H5. The insertion of the target proteins into nanodiscs was confirmed by the presence of both in the elution fractions.

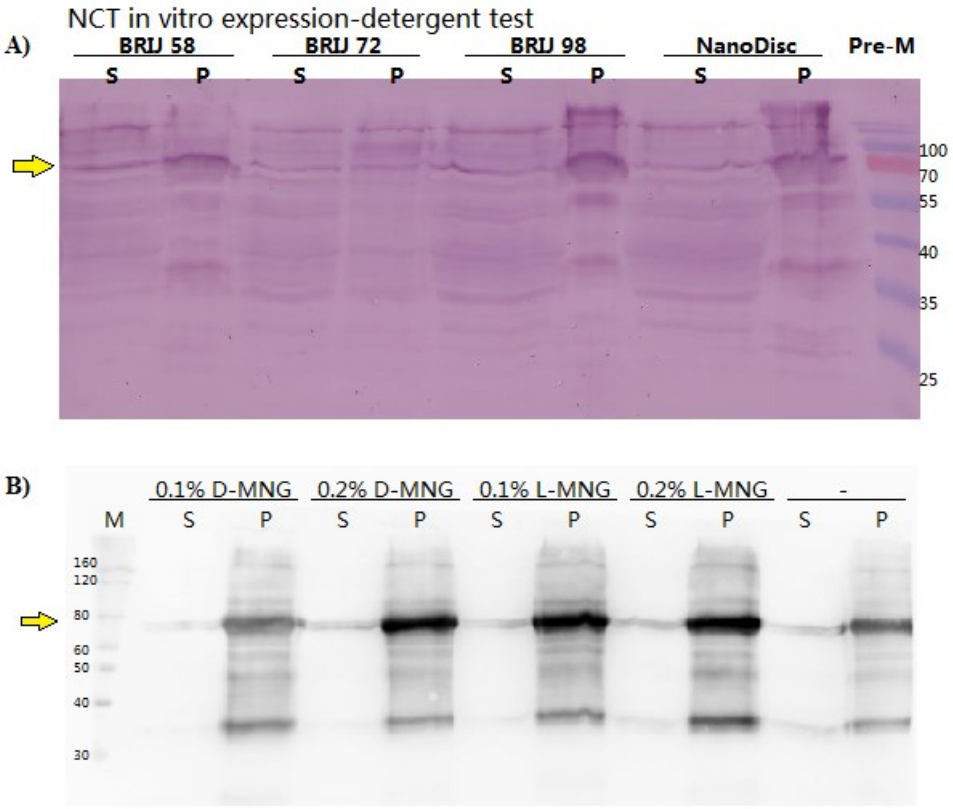

Figure 3.7 *In vitro* expression of NCT in presence of different detergents.

Reactions were performed at 30 °C for 2 hours. Detergents working concentration were used as follow: 1.5% Brij58, 0.2% Brij72, 0.2% Brij98, 0.8 mg/mL Nanodiscs. B: double chain detergents test. D-MNG: Decyl Maltose Neopentyl Glycerol, L-MNG: Lauryl Maltose Neopentyl Glycerol. The yellow arrow indicates the expected position of target proteins.

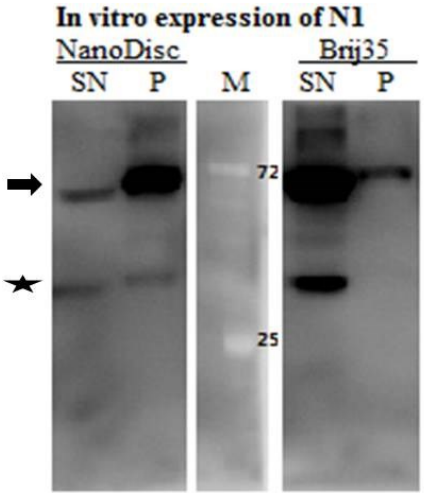

Figure 3.8 *In vitro* expression of NCT at 20 °C.

Reactions were performed at 20 °C overnight (15 hours). 3 mg/mL nanodiscs and 0.2% Brij 35 were added to the reactions, respectively. NCT is indicated in arrow, the star indicates a degradation fragment of NCT.

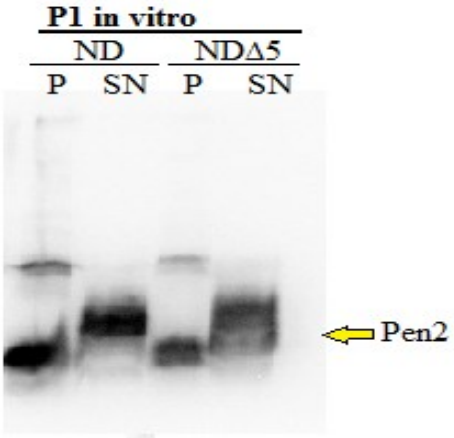

Figure 3.9 PEN-2 in vitro expression with different Nanodiscs.

Reactions were performed at 30 °C for 2 hours. 1.5 mg/mL Nanodiscs was added to the reactions. The arrow indicates the expected target protein. Proteins in the supernatant migrated differently from the samples made from pellet which might be due to the different buffer composition and pH of these two fractions.

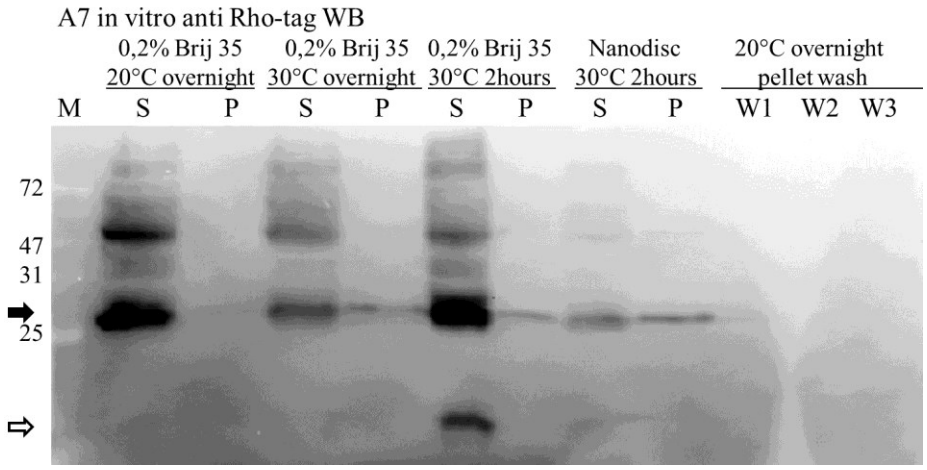

Figure 3.10 Effect of temperature and duration on the expression of APH-1.
Reactions were performed at different temperatures and time durations as indicated in the headline. 0.2% Brij35 or 1.5 mg/mL Nanodiscs was added to the reaction mixtures. Rho-tagged APH-1 monomer showed an apparent molecular weight of 30 kDa with a dimer band around 60 kDa. The lower signal represented the degradation fragment of APH-1 was observed in the 30 °C, 2 hours-sample. APH-1 is indicated in solid black arrow, a degradation fragment is indicated by the open arrow.

3.1.3 Purification and characterization of cell-free expressed proteins

For homogeneity analysis of the *in vitro* expressed membrane proteins, upscale reactions with 150 µL to 1 mL reaction volume were set up. The supernatants after centrifugation, which contained the target membrane proteins, were incubated with affinity resins for the first step purification. The elution fractions from the affinity column were collected and protein yields were estimated (Table 3.2). Size exclusion chromatography (SEC) was performed for an oligomerization state estimation and homogeneity analysis.

Table 3.2 Expression Condition and Yield of each component

Abbr.	Protein	Expression condition	Yield
1NR	Presenilin 1 N-terminal	0.2% Brij35 at 20 °C overnight	~ 115 µg/200 µL (Elute fraction in 200 mM Peptide)
1CR	Presenilin1 C-terminal	0.2% Brij35 at 20 °C overnight	~ 87 µg/200 µl (Elute fraction in 200 mM Peptide)
A7	APH-1	0.2% Brij35 at 20 °C overnight	~ 75 µg protein /200 µL reaction (Elute fraction in 200 mM Peptide)
N1	nicastrin	0.2% Brij35 at 20 °C overnight	~36.8 µg/200 µL reaction (Elute fraction in 300 mM Imidazole)
P1	PEN-2	0.1%Brij, 30 °C, 2 hours	~ 175-200 µg /mL (Batch), ~ 285µg/mL (Continuously) (Elute Fraction in 300 mM Imidazole)

For Presenilin Rho-tagged constructs, the existence of target proteins in the elution fractions from affinity chromatography was proved by both western blot and coomassie blue stain of

SDS-PAGE (Figure 3.11). A significant loss of protein was observed during SEC. There is one homogenous peak at 20.25 mL from the purification using a Superdex200 10/300 GL column for PS1 NTF, which corresponds to an apparent molecular weight of ca. 31 kDa (Figure 3.12 A). The existence of the target protein in this peak fraction was confirmed by both western blot and blue silver-stained SDS-PAGE (Figure 3.11, sample I). However, this apparent molecular weight was much lower than the expected size of a detergent-protein complex (approximately 54 kDa, 19 kDa for FOS-12 micelles and 35 kDa for PS1 NTF). For PS1CTF, two peaks were collected from Superdex200 10/300 GL column (Peak I and II in Figure 3.12 B) and analysed by SDS-PAGE. A minor amount of the target protein was detected by western blot in Peak II (Figure 3.11, sample II). This peak shared a nearly identical elution volume with the Rho-tagged PS1 NTF. The unexpected apparent sizes of both PS1 NTF and PS1 CTF eluted from SEC and the severe loss of the target proteins upon SEC experiments suggested that the proteins did not form a proper complex with the detergent micelles. These purified proteins were probably unfolded and precipitated on the column.

The SEC profile of Rho-tagged APH-1 showed five different fractions and protein signals appeared only in fraction III (Figure 3.13). CD spectra of this *in vitro* expressed A7 showed a negative peak around 195 nm, which corresponded to the characteristic shape of the random coil, indicating an unfolded state of the obtained materials (Figure 3.14).

For nicastrin, there were 3 peaks from SEC (Figure 3.15). Protein signals were shown in Peak II at 10.5 mL and Peak III at 15 mL, which are corresponding to an approximate molecular weight of 1440 kDa and 246 kDa, respectively. An amount of 3-µg nicastrin protein was obtained after SEC from a 200-µL reaction.

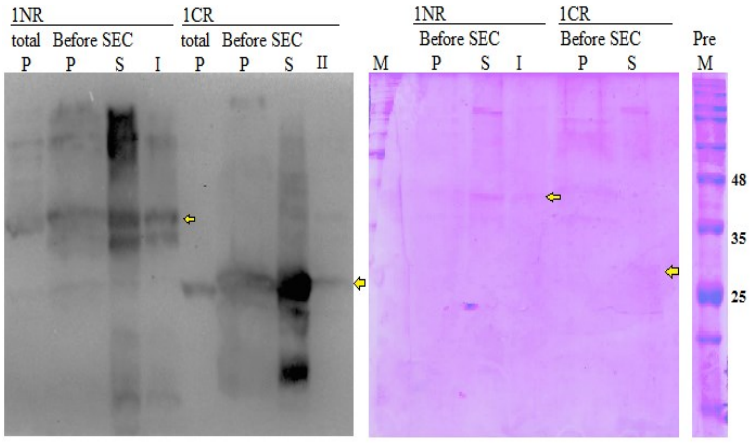

Figure 3.11 SDS-PAGE of *in vitro* expressed PS 1 fragments. 200 µL reactions performed at 20 °C overnight with 0.2% Brij 35. SEC buffer: 20 mM Tris-HCl, 150 mM NaCl, 3CMC FOS-12. P: pellet, S: supernatant, I: protein samples from the peak fractions in SEC. Yellow arrows indicate the target proteins. 1NR: C-terminal Rho-tagged Presenilin 1 NTF; 1CR: C-terminal Rho-tagged Presenilin 1 CTF.

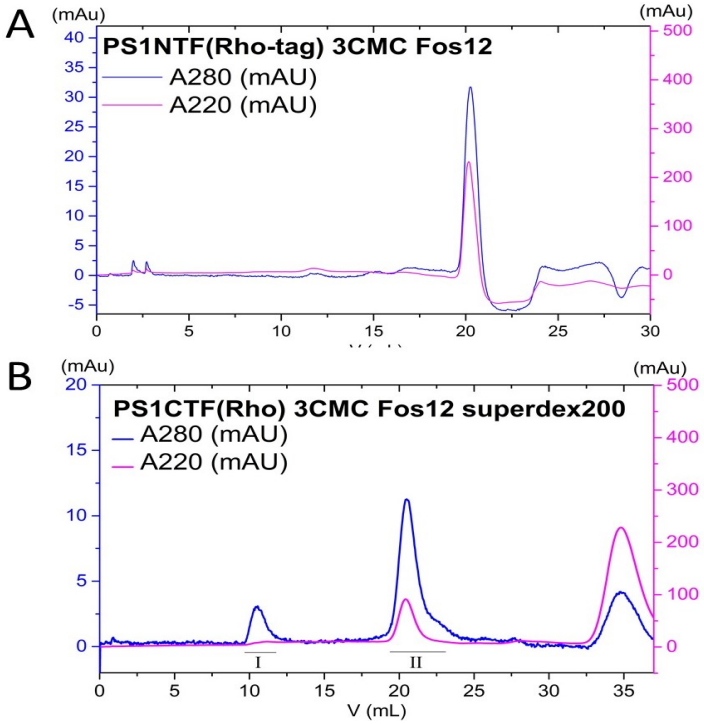

Figure 3.12 SEC of Presenilin 1 NTF and CTF in FOS-12.
Proteins were prepared from in vitro expression with Brij 35 and purified through Rho1D4 resin in the presence of FOS-12. Superdex 200 10/300 GL column was equilibrated in 20 mM Tris-HCl, 150 mM NaCl, 10% Glycerol, 3 CMC FOS-12. Samples were loaded and eluted at a flow rate of 0.5 mL/min. A: SEC of C-terminal Rho-tagged Presenilin 1 NTF; B: SEC of C-terminal Rho-tagged Presenilin 1 CTF. The absorption at 220 nm was monitored as an indication of protein, as well as the Rho peptide used in the elution buffer from the affinity purification.

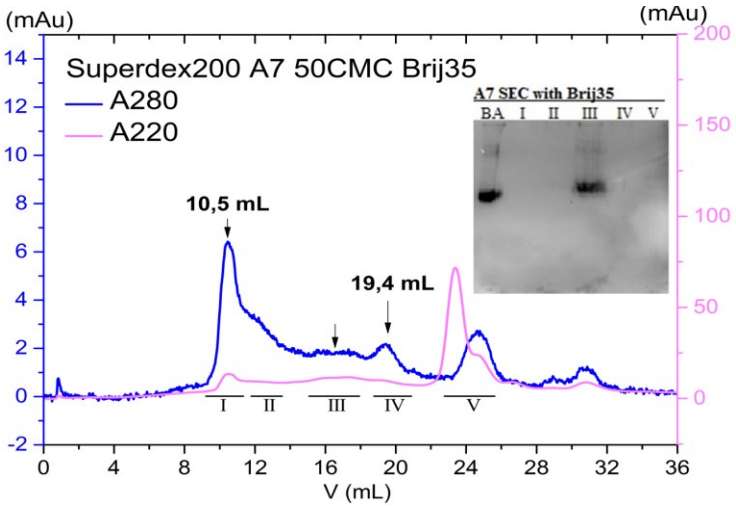

Figure 3.13 Purification of *in vitro* expressed APH-1 by SEC.
The reaction was performed in 200 µL at 20 °C overnight with Brij 35. Rho-affinity purification was carried out in Buffer A (20 mM Tris-HCl, 150 mM NaCl, 10% Glycerol, 0.5% Brij 35) at 4°C. Superdex 200 10/300 GL was equilibrated in Buffer A. Fractions from SEC were collected and concentrated before loading to SDS-PAGE.

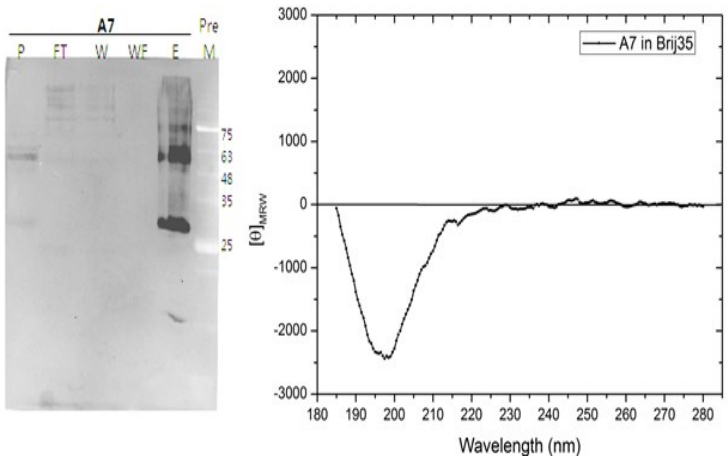

Figure 3.14 Far UV CD spectra of *in vitro* expressed APH-1 in Brij35.
200 µL *in-vitro* reaction was performed with 0.1% Brij35 at 20 °C overnight. Elution fractions from Rho1D4 resin were pooled and exchanged buffer through a PD-10 desalting column. CD buffer: 10 mM Na_2HPO_4, pH 7.4, 2 CMC Brij 35. The CD measurement was performed by JASCO J-810 spectropolarimeter at 4°C.

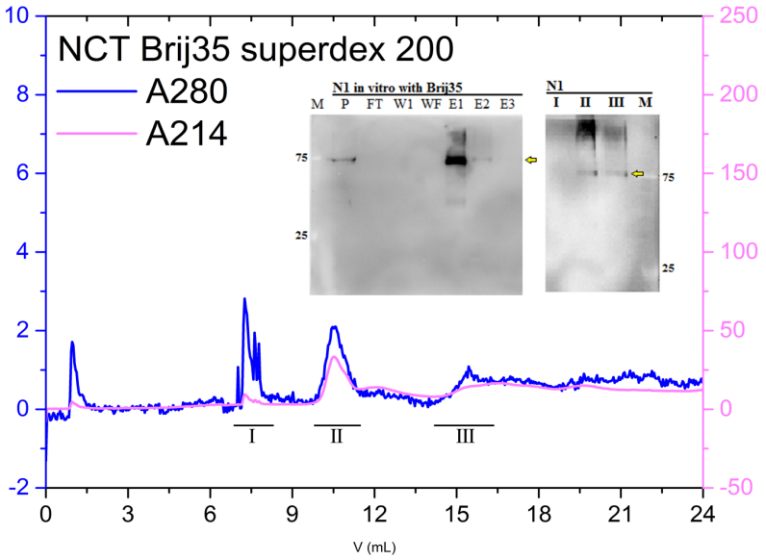

Figure 3.15 Purification of *in vitro* expression obtained NCT by SEC.
200 µL in-vitro reaction was performed with 0.1% Brij 35 at 20 °C overnight. Ni-NTA affinity purification was carried out in Buffer A (20 mM Tris-HCl, 150 mM NaCl, 10% Glycerol, 0.5% Brij 35) at 4°C. Superdex 200 10/300 GL was equilibrated in Buffer A. Fractions from SEC were collected and concentrated before loading to SDS-PAGE. The Y-axis shown here are with a unit of mAu.

PEN-2 showed the highest yield and the best quality among all the protein constructs (Figure 3.16). A homogenous peak was obtained from SEC in the presence of Brij 35 (Figure 3.17, black curve). This peak contained the major amount of the target protein with an apparent molecular weight of 192 kDa (Figure 3.17, inset). Instability of the protein upon storage was observed (Figure 3.17, orange curve). A serial detergent screening was performed to select a suitable condition which maintained a homogenous protein sample with a low oligomerization state (Table 3.4). PEN-2 showed different states of oligomerisation in the FOS-choline group detergent micelles. The addition of reducing reagent (1 mM TCEP) helped to break oligomers of the protein to a smaller size: trimer in Brij35 purification or dimer in FOS-12 purification. PEN-2 purified in DM showed an apparent molecular weight from SEC even smaller than the size of DM micelles. This is probably due to either a misfolding of the protein or an unusually low ability of the protein to bind detergent. A device for continuous *in vitro* expression was further tested for the PEN-2 protein expression. After the screening and optimisation of the expression and purification conditions, PEN-2 reached a yield of ~150 µg purified homogenous protein per mL reaction volume.

CD spectrum of *in vitro* expressed PEN-2 showed a positive peak around 195 nm and two negative peaks at 208 nm and 222 nm, which matched to a typical α-helical structural protein (Figure 3.18). Deconvolution showed a secondary structure content of 32% helix and 20% strands, which is close to the prediction results from SOPMA web server (36.21% α-helix, 18.1% extended strand), but lower than the content calculated based on the cryo-EM structure (5FN2, 68 residues for helix, 58.6%).

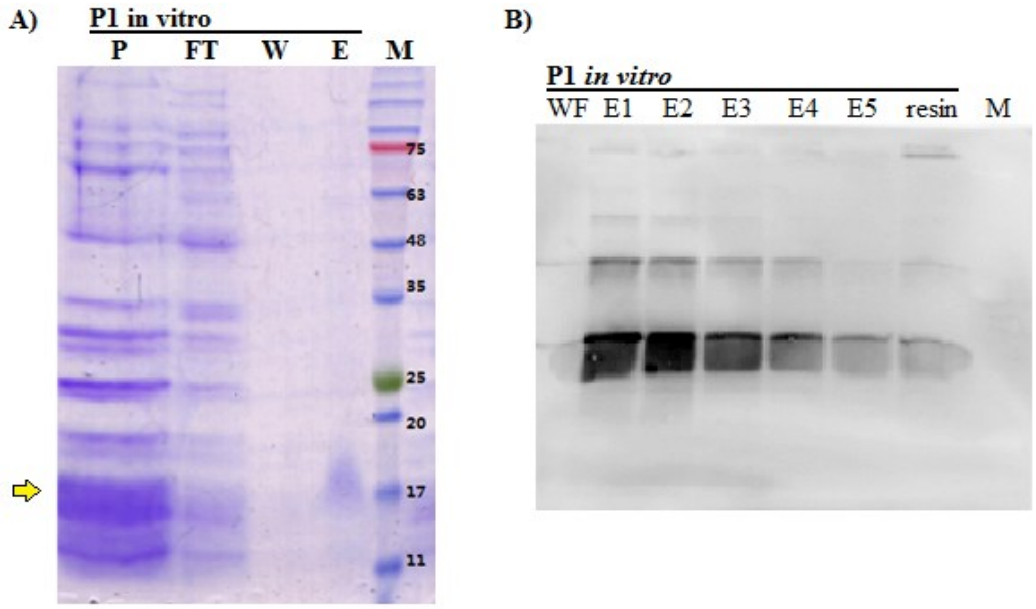

Figure 3.16 Affinity purification of *in vitro* expressed PEN-2.

300 µL in-vitro reaction was performed with 0.2% Brij 35 at 30 °C for 3 hours. Affinity purification was carried out using Ni-NTA resin (Qiagen). A: SDS-PAGE stained with coomassie brilliant blue. B: Western blot (anti-His tag). The yellow arrow indicates the expected position of the target protein. P: pellet after reaction; FT: flow through from the affinity purification; W: sample from the washing step; WF: sample from the last washing fraction; E: elution fractions.

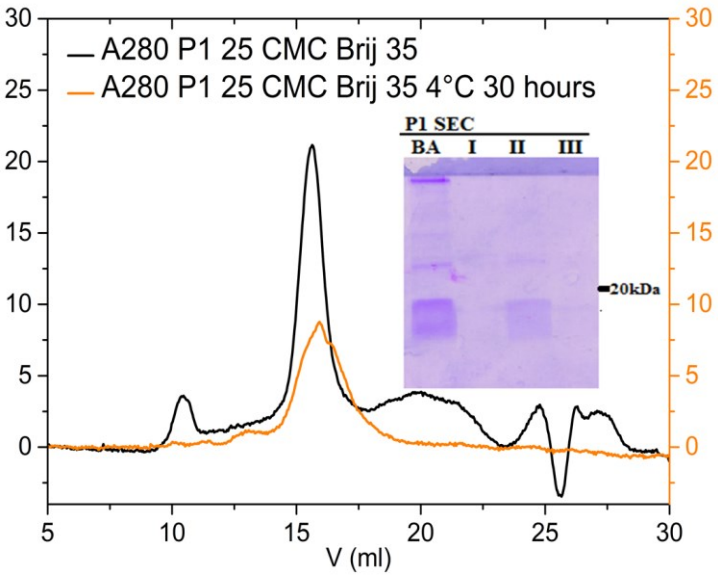

Figure 3.17 Stability of *in vitro* expressed PEN-2 in Brij35 upon storage.

300 µL in-vitro reaction of PEN-2 with 0.2% Brij 35 at 30 °C for 3 hours. Elution fractions from affinity purification were concentrated to 0.5 mL. Superdex 200 10/300 GL column was equilibrated in 20 mM Tris pH 7.4, 150 mM NaCl, 5% Glycerol, 25 CMC Brij 35. Black curve: samples applied immediately after affinity purification. Orange curve: samples stored at 4 °C for 30 hours. Instability of the protein upon storage was observed. The Y-axis shown here are with a unit of mAu.

Table 3.3 Deconvolution of CD data from Brij35 purified PEN-2

Helix 1	Helix 2	Strand 1	Strand 2	Turns	Unordered	Total
0.18	0.14	0.12	0.08	0.19	0.29	1

Solutions from the CDSSTR method using reference database 7
NRMSD: 0.014 (DichrWeb)

Table 3.4 Size estimation based on SEC of different detergents purified PEN-2

Detergent	Micelle Size (kDa)	Elution Volume (mL)	Cal. MW (kDa)	Oligomer State
Brij35	49	15.6	192	10
Brij35+TCEP		14 17.5	345 95	21 3
FOS-12	18,981	18,6	60,3	3
FOS-12+TCEP		19,43	43	2
FOS-14	40,98	15,4	200	10
FOS-16	72,53	16	164	6
DM (+TCEP)	33,3	20,43	29	smaller than a monomer

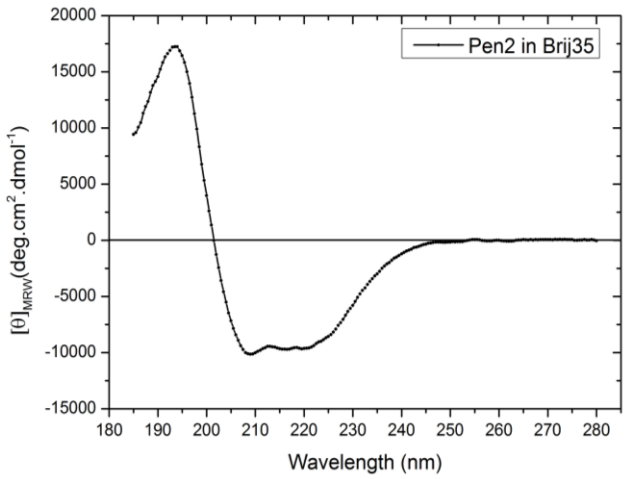

Figure 3.18 Far UV CD spectra of *in vitro* expressed PEN-2 in Brij 35.
200 µL in vitro reaction was performed with 0.1% Brij35 at 30 °C for 3 hours. Elution fractions from Ni-NTA resin were pooled and exchanged buffer through a PD-10 desalting column. CD buffer: 10 mM Na_2HPO_4, pH 7.4, 2 CMC Brij35. The CD measurement was performed by JASCO J-810 spectropolarimeter at 4 °C.

3.1.4 Investigation of sub-complex formation in cell-free expression system

Co-immunoprecipitations and co-expression of different components of the γ-secretase were performed to investigate the interaction between *in vitro* expressed proteins. For the co-expressions, two plasmids of different subunits with different tags were added to the same reaction mixture in the presence of Brij 35 or nanodiscs. The products were further purified through affinity columns against different tags, samples of each step were analysed with western blot.

Nicastrin has been proposed to be the substrate recognizer in the γ-secretase[70,166,167]. Therefore, a co-expression of APPC100 and nicastrin was performed in the presence of Brij35 (Figure 3.19). Both of the proteins were presented in the supernatant after the reaction. The co-elution of APPC100 and NCT from the Ni-NTA resin indicated a physical association between these two proteins.

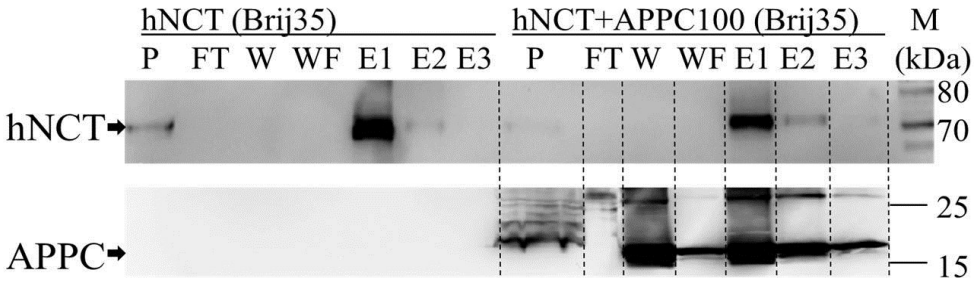

Figure 3.19 Western blot analysis of NCT and co-expressed NCT+APPC100 in Brij 35.
In vitro reactions performed at 20 °C overnight with 0.2% Brij 35. The supernatants were incubated with 50 µL Ni-NTA resin (100%) at 4°C for 3.5 hours. 30 × CV of washing buffer (containing 20mM Imidazole and 2CMC Brij35) were applied to exclude unspecific binding. Elution Buffer contains 300 mM Imidazole and 2CMC Brij 35. Upper panel: anti-His western blot for His-tagged NCT. Lower panel: anti-flag western blot for Flag-tagged APPC100. The weak signal from APPC100 in the last washing step might be due to an unspecific binding of APPC100 to the Ni-NTA resin.

The interaction between Presenilin NTF and CTF, Presenilin and PEN-2 were investigated by pull-down assays using individually expressed protein or co-immunoprecipitations using co-expressed two proteins with nanodiscs. Rho-tagged proteins were used as the 'bait' proteins immobilised on the Rho1D4 resin, while His-tagged proteins were used as the prey proteins (Figure 3.20). Pull down assays did not show co-elution of NTF and CTF, nor NTF and PEN-2. This indicated the absence of the sub-complexes formation in the presence of Brij35.

For the reactions performed with nanodiscs, co-immunoprecipitation method was employed to investigate the protein-protein interaction. Proteins with different affinity tags were expressed in the presence of nanodiscs. Purification was performed through Rho1D4 resin (Figure 3.21). The signal of PS1 (right half of the anti-His blot) and PEN-2 (left half of the anti-His blot) in the elution fractions proved a successful insertion of both proteins into the same nanodiscs. A two-step affinity purification was applied for PS2 NTF and PS2 CTF co-expressed with nanodiscs (Figure 3.22). Both proteins gave signals in the final elution fractions which further confirmed the presence of both proteins in the same nanodiscs.

As mentioned above, both NTF and CTF of Presenilins could successfully insert into the same nanodiscs upon *in vitro* co-expression. Substrates and inhibitors were then added to the *in vitro* reactions to test the activities of theses co-expressed fragments. Anti-His and anti-Rho western blot proved the existence of both components in the reactions. Anti-flag blot showed signal from *in-vitro* expressed APPC100. However, there is no observation of the expected product signal from the western blot (Figure 3.23) indicating the NTFs and CTFs although were retained by the same nanodiscs but probably did not form the correct interaction sub-complex.

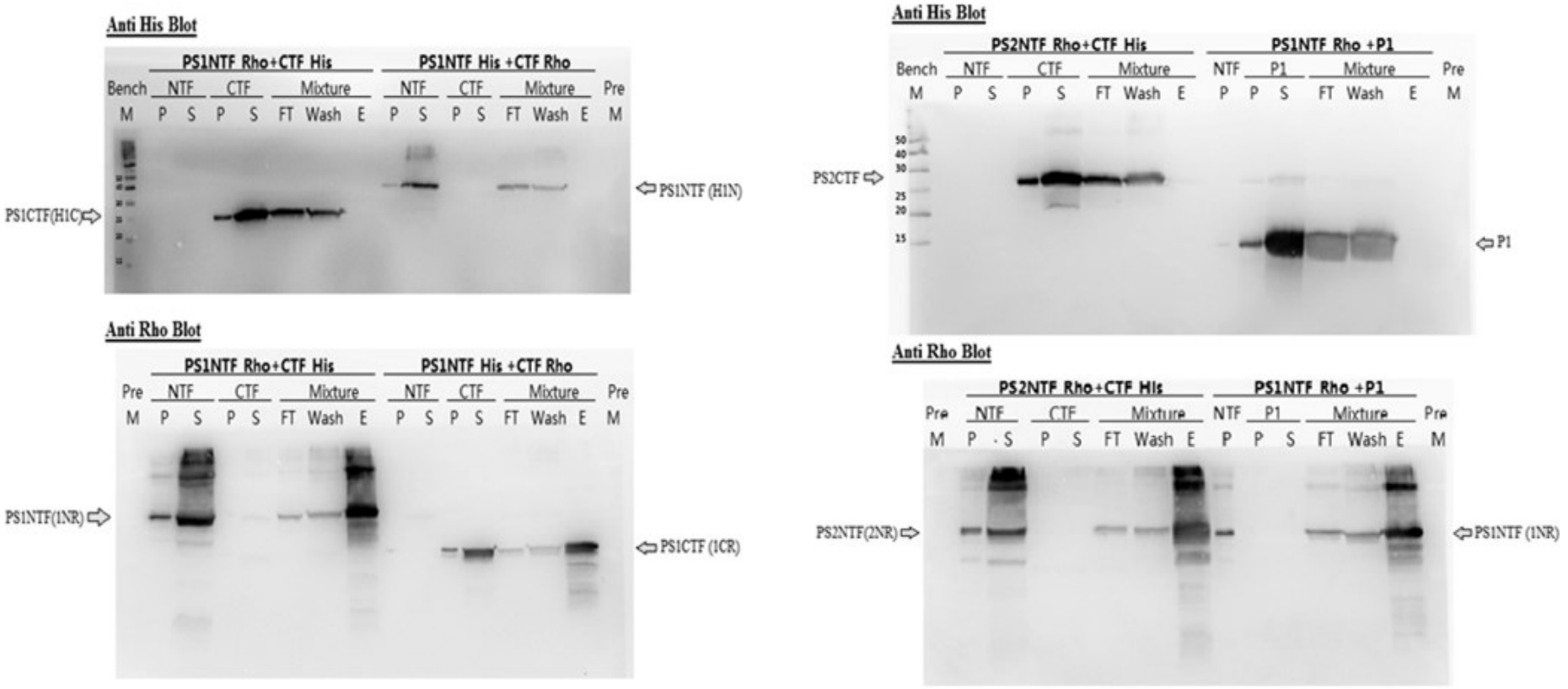

Figure 3.20 Pull-down experiment of *in vitro* expressed NTF+CTF and PS1NTF+PEN-2.

50 µL *in vitro* reactions were performed at 25 °C overnight (15 hours) with 0.2% Brij 35 for respective construct. Reactions were terminated by centrifugation at 15 000 rpm for 1 hour. 5 µL of the supernatant was taken for the samples of reaction supernatant. Pellet samples were made by adding 40 µL Loading Buffer to dissolve the pellets. Two fractions containing potential interaction proteins were pooled (NTF and CTF, NTF and PEN-2) and incubated at 4 °C with 600 rpm shaking for 8 hours with the addition of 900 µL 0.25% Brij 35 buffer (1 mM TCEP, Protease Inhibitor). Affinity purification was performed with 200 µL 50% Rho-resin. Incubation of the protein mixture and resin were carried out at 4 °C overnight with shaking. Left panel two western blots were the anti-His (upper) and anti-Rho (lower) western blot analysis of Presenilin 1 NTF and CTF. Right panel two western blots were the anti-His (upper) and anti-Rho (lower) western blot analysis of Presenilin 2 NTF and CTF, as well as Presenilin 1 NTF with PEN-2. The existence of the Rho-tagged proteins in the elution fractions was confirmed. However, no His-tagged proteins were pulled down by its potential partner in the presence of Brij 35.

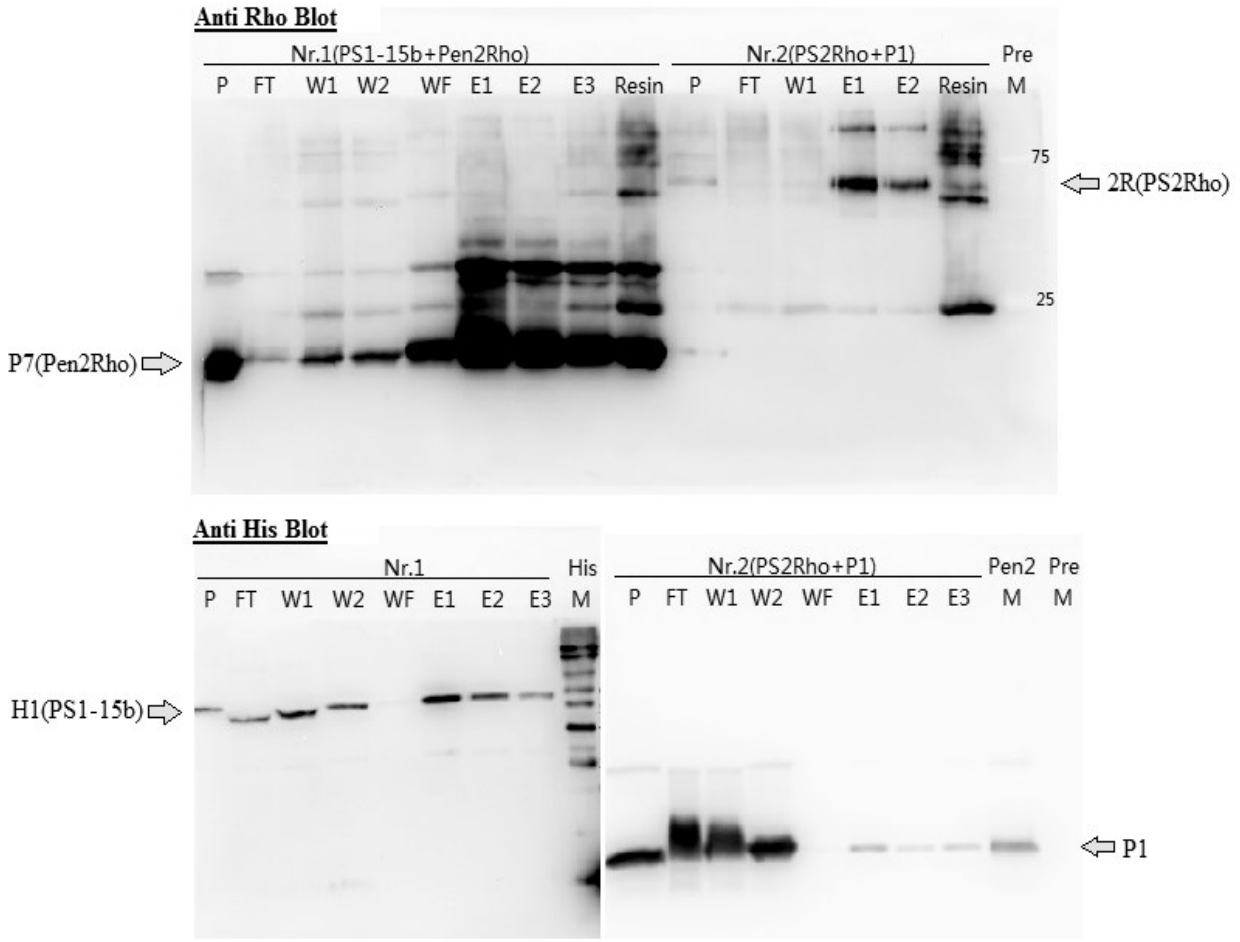

Figure 3.21 *In vitro* co-expression of PS1+PEN-2, PS2+PEN-2 in nanodiscs.

In vitro reactions were performed at 30 °C for 2 hours with 3 mg/mL Nanodiscs. Reaction mixtures were centrifuged at 15000 rpm for 1 hour. The supernatant was incubated with 50 µL (50%) Rho1D4 resin at 4 °C overnight. 20 × CV washing buffer was applied. Elution was performed in the presence of 800 µM peptide. 2 × CV of elution buffer was applied for each elution fraction with shaking at 1000 rpm for 2.5 hours before collection. Reaction Nr.1: co-expression of His-tagged Presenilin 1 with Rho-tagged PEN-2; Reaction Nr.2: co-expression of Rho-tagged Presenilin 2 with His-tagged PEN-2. Western blot signals of Presenilin and PEN-2 were observed in the elution fractions from Rho1D4 resin which indicates the presence of both proteins in the same nanodiscs. Arrows indicate the expected position of the target proteins. P1: His-tagged PEN-2.

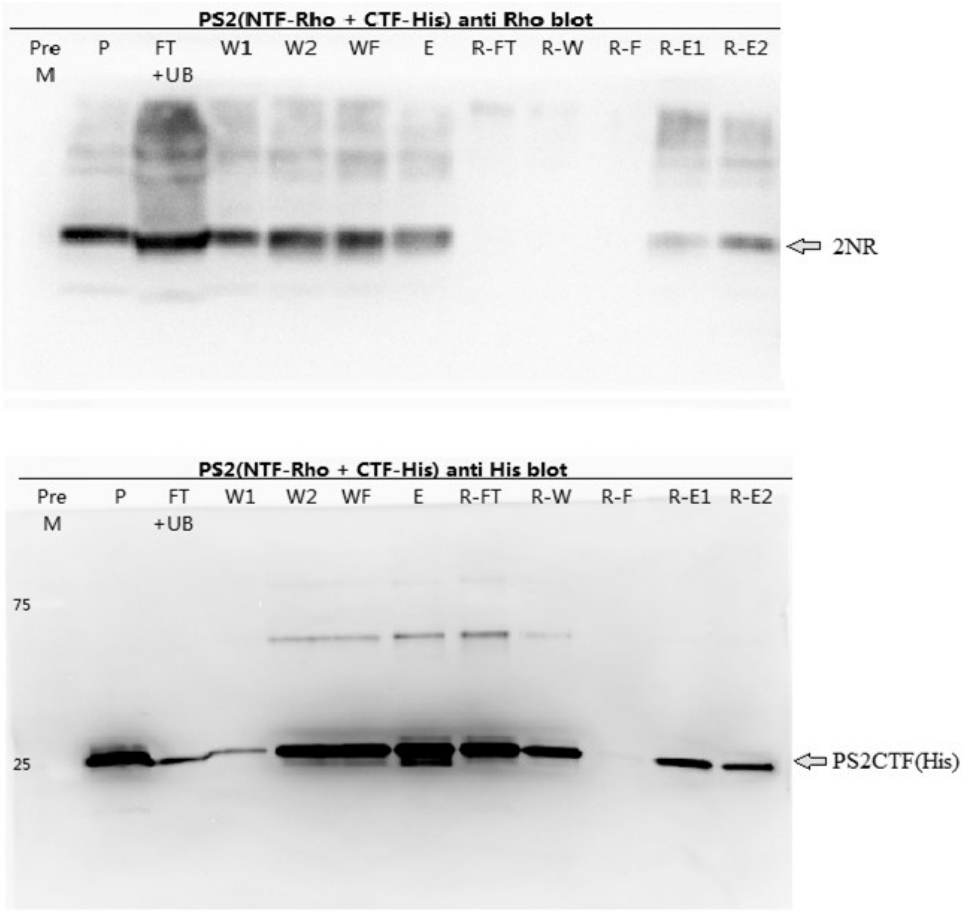

Figure 3.22 *In vitro* co-expression of PS2NTF+ PS2CTF in nanodiscs.

In vitro reactions were performed at 27 °C for 2 hours with 2.5 mg/mL Nanodiscs. The supernatant was incubated firstly with Ni-NTA resin in the cold room for 1.5 hours, W1 was performed with 10mM Imidazole Buffer, W2 was performed with 20mM Imidazole Buffer, each washing step used 10 × CV washing buffer. The elution fractions from Ni-NTA resin were then incubated with 50 µL (50%) Rho1D4 resin at 4 °C overnight. 20×CV washing buffer was applied to exclude unspecific binding. Elution was performed with 800 µM peptide buffer. 2NR represents Rho-tagged PS2NTF. Western blot signals from both Presenilin 2 NTF and CTF were observed in the final elution fractions after two-step affinity chromatography which confirmed the insertion of both proteins into the same nanodiscs.

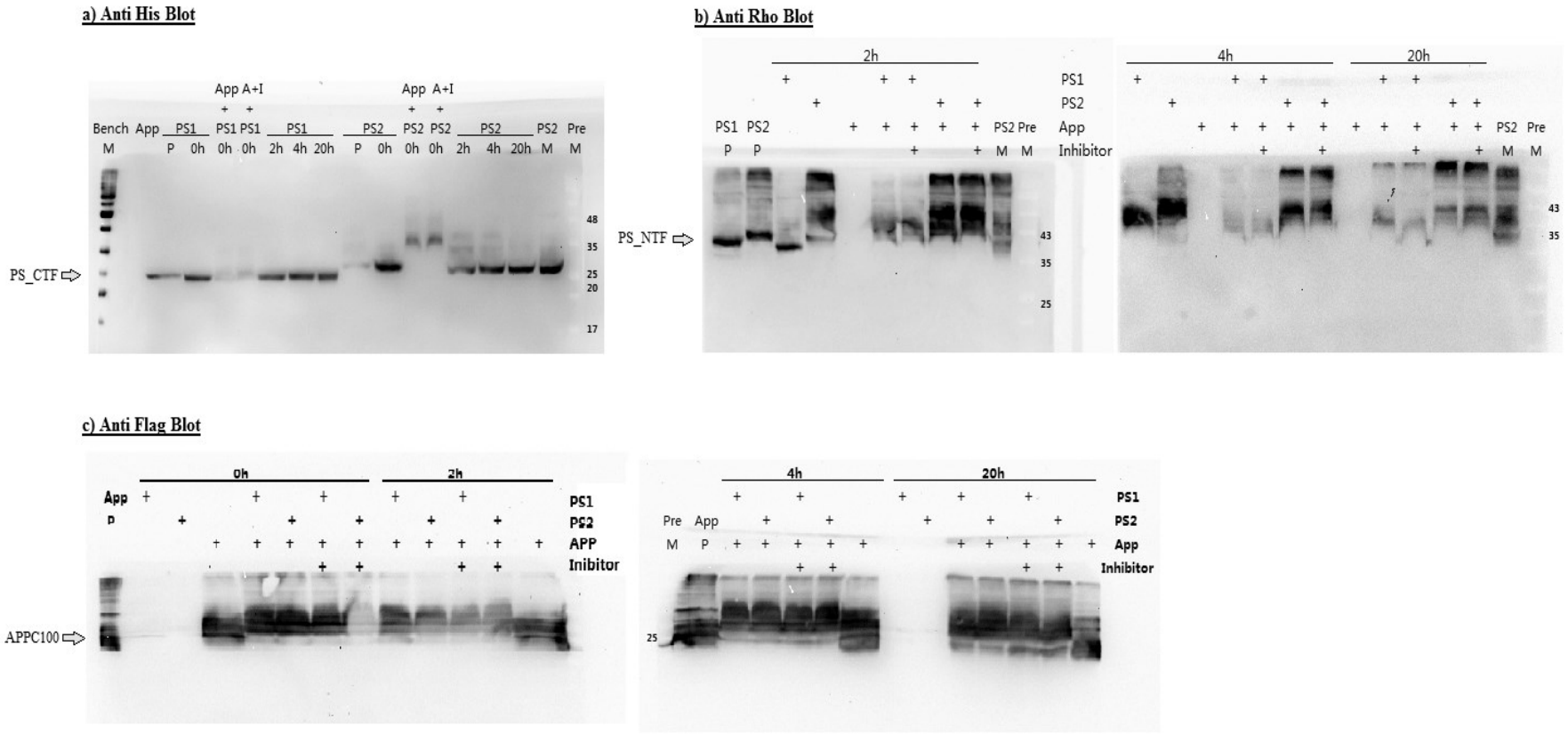

Figure 3.23 Activity assay using *in vitro* obtained sub-complexes.

PS1NTF+CTF, PS2NTF+CTF and APPC100 were expressed from *in vitro* reactions performed with 3 mg/mL Nanodiscs (at 28 °C for 3 hours). The supernatants were diluted to 200 µL using reaction buffer (20 mM Tris, 150 mM NaCl, pH7.4+Protease Inhibitor). The γ-secretase inhibitor L685,458 was added as a negative control. 60 µL PS fragments+60 µL APPC100 or 60 µL PS+ 60 µL AppC100+1 µM L685,485 samples were prepared for the activity assays. Activity assay was performed at 37 °C. The same sample volume (15 µL for a single protein and 30 µL for mixture) was taken for SDS-PAGE analysis at 0 hour, 2 hours, 4 hours and 20 hours, respectively. a) anti-His tag western blot of PS CTFs; b) anti-Rho western blot of PS NTFs; c) anti-Flag western blot to detect APPC100 substrates and the cleavage products. However, there is no signal from the products obtained here.

3.2 Overexpression of different components of γ-secretase in *E. coli*

To obtain each component of the γ secretase of sufficient quality and quantities, up-scaled expressions of the proteins were performed in *E. coli in vivo* expression system.

3.2.1 Cell growth curves and protein distribution of different components

The productions of each individual protein by *E. coli* cells were investigated in the following three steps: Firstly, growth curves for uninduced and induced cells were constructed to test different cell strains carrying different plasmids; secondly, cell cultures were induced at three OD_{600} steps (0.6, 0.9 and 1.2) to investigate the influence on the final cell biomass and protein production; thirdly, cells were harvested at different time points to analyse the total protein expression amount after induction.

In the first step, among all the samples tested, C43 strains reached a higher cell density (an average final OD_{600} above 10) comparing to BL21 cells (a final OD_{600} between 4 and 8). From the second step of the investigation, an increase of final protein yield was observed correlating with the OD_{600} at induction. An OD_{600} at induction between 1 and 1.5 was chosen for the different constructs. A severe suppression of cell growth was observed in PEN-2 BL21 strains comparing to other constructs (pink curve in Figure 3.24). In the third step, cell samples were taken at different time points after induction and normalised to the cell pellet weight before applying to the SDS-PAGE. As shown in Figure 3.25, nicastrin showed the highest amount of protein production after 16 hours induction in BL21 strains, while there was only a weak signal from C43 cells (top panel). PS1 CTF showed a much lower total yield even in BL21 strains (middle panel). PEN-2 expressed in BL21 strains gave the most intensive signal at 24 hours induced cell pellets (Figure 3.25, bottom panel). For APH-1, weak signals were obtained only in the gel pockets which indicated large aggregations (data not shown). PS1 NTF protein production was not affected much by different harvesting points. A degradation band was observed from the western blot. The distributions of target proteins were investigated next. For Aph1, there was no signal detected by western blot (Figure 3.26) indicating low expression of the protein. A different system might be necessary for this seven transmembrane protein expression. PEN-2 was distributed in both membrane and supernatant fractions after ultracentrifugation. A large amount of protein was observed in the inclusion body fraction for nicastrin. For PS1CTF, although the total yield was higher in BL21 strains, a certain amount of proteins was found in the inclusion body fractions. There is not much difference in the protein amount in the membrane fraction comparing the BL21 and C43 strains.

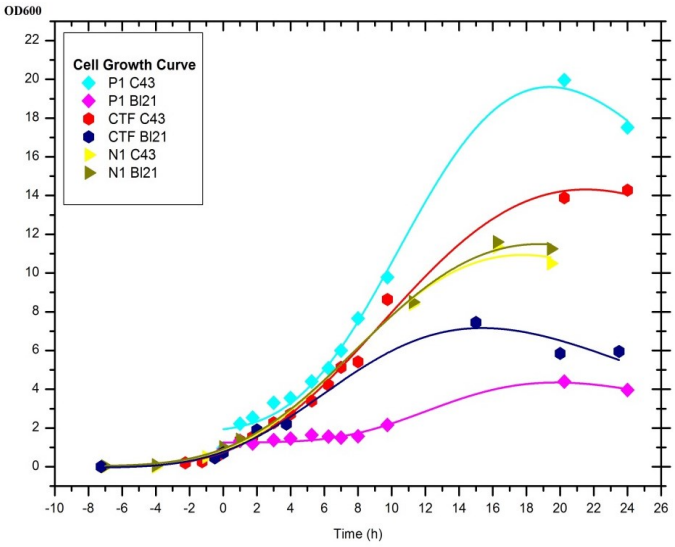

Figure 3.24 Cell growth curves of different proteins in different bacteria strains.

The cell growth curves of PEN-2 (P1), PS1CTF and NCT (N1) were compared between *E.coli* BL21 (DE3) and C43 strains. The optical densities of cell cultures were monitored at different time points. The growth curves of the two cell strains expressing hNCT did not show a significant difference, while both PEN-2 (magenta) and Presenilin 1 CTF (dark blue) showed a severe suppression on the BL21 (DE3) cells growth, but not to the C43 cells.

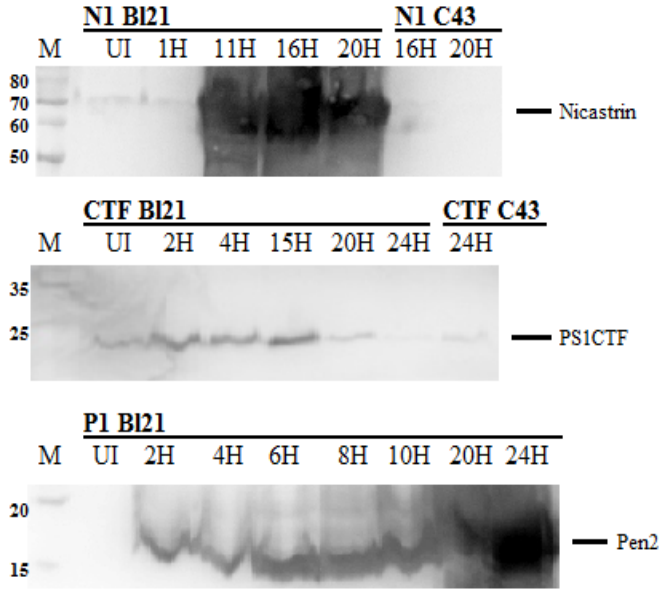

Figure 3.25 Effect of inducing length on the protein expression.

Western blotting of NCT, PS1CTF and PEN-2 by a monoclonal anti-polyhistidine antibody. Cell cultures were taken after certain hours as labelled after induction (at 16 °C). UI: un-induced cells. All samples were normalised to the cell pellet weight. NCT and PS1CTF reached a yield maximum at 15-16 hours in the BL21 (DE3) strain. The expression level of NCT and PS1CTF was much lower in C43 (DE3) strain comparing to the BL21 (DE3) strain. PEN-2 expression was continuously increasing with the time course.

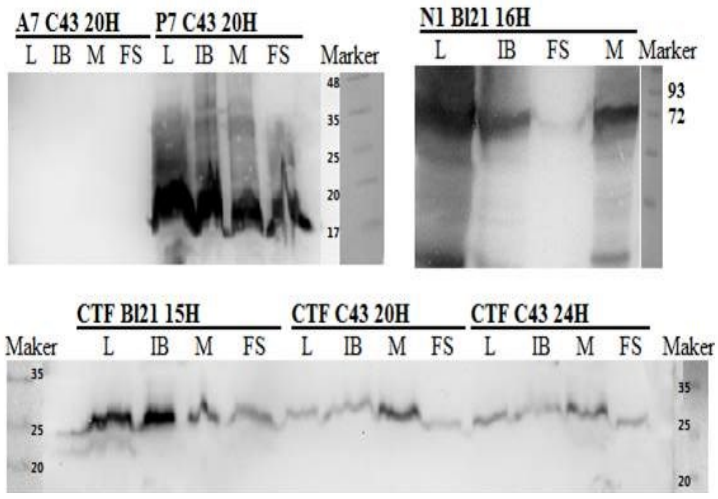

Figure 3.26 Protein distributions in different fractions.

Protein distributions of APH-1, PEN-2, NCT and PS1CTF are presented. Sonication was performed to open the cells. Inclusion body samples were made after centrifuging at 7000 g for 30 min at 4 °C. Membrane fraction samples were made from the pellet after centrifugation at 15000 rpm for 90 min at 4°C. All pellets were solubilized using 6 M Urea +10% SDS buffer. L: Lysate; IB: Inclusion body; FS: supernatant after 15000 rpm centrifugation; M: Membrane fractions.

3.2.2 Screening of detergent for solubilization of each component

To obtain a water-soluble protein–detergent–lipid complex, detergent screening was carried out. For each well-expressed component, a suitable solubilization/detergent was to be selected (the method is described in section 2.4.1). The properties of the detergents used in the solubilization screens are listed in Table 2.12. N-Lauroylsarcosine sodium salt (NLS) was used here as a positive control. Detergents, such as maltosides, glucosides and LDAO were tested because of their high contribution to the record counts in the membrane protein data bank [168,169]. CHAPSO was chosen because it was extensively used in γ-secretase complex purification and activity assays [170,171].

As shown in Figure 3.28, for all four proteins presented here, phosphocholine group detergents (FOS-12, FOS-14 and FOS-16) showed similar solubilization efficiency compared to the positive control (NLS). Glucosides group detergents (NG, OG and OTG) and CHAPSO were poor solubilizers for the proteins investigated here. Other detergents exhibited different solubilization abilities for different proteins. For Presenilin 1 full-length protein, LDAO showed a better solubility than CYMAL-6, DDM and CHAPSO (Figure 3.28 b). Maltosides detergents (DM and DDM), LDAO and CYMAL-6 could partially solubilize PEN-2 protein (less than 50%, Figure 3.28 c). Nicastrin exhibited a high instability in most detergents, as SDS-resistant aggregations were observed on the top of the gels in the solubilized membrane samples (Figure 3.28 d). Based on these results, detergents were selected for further purifications for each protein in the next step.

3.2.3 Yield and oligomerization state of each component

The yield of purified protein was estimated from the UV absorption of SEC elution fractions and the oligomerization state of each component was determined from the SEC profiles. The yield and homogeneity of each component were compared between different *E. coli* strains (BL21 and C43) and different constructs (Rho-tag and His-tag recombinant proteins). The quantity and quality of the samples varied dramatically depending on *E. coli* strains and detergents. Consisted with the cell growth curve results described in section 3.2.1, *E. coli* C43 cell strains gave a high final cell quantity for most constructs (shown in the fourth column of Table 3.5). However, regarding the protein yields, BL21 strains showed a promising advantage.

The His-tagged constructs of Presenilin (H1), Presenilin NTF (H1N) and PEN-2 (P1) expressed in *E. coli* BL21 (DE3) strains showed the highest yields with a value between 3.6 to 4.8 mg purified proteins per liter cell culture. Nicastrin (N1) has a yield of over 1 mg per liter cell culture. One Rho construct of PEN-2 (P7) was expressed in *E. coli* C43 (DE3) strain which

could yield around 0.7 mg purified protein liter cell culture. These constructs were used for the further investigation of the properties of the purified proteins.

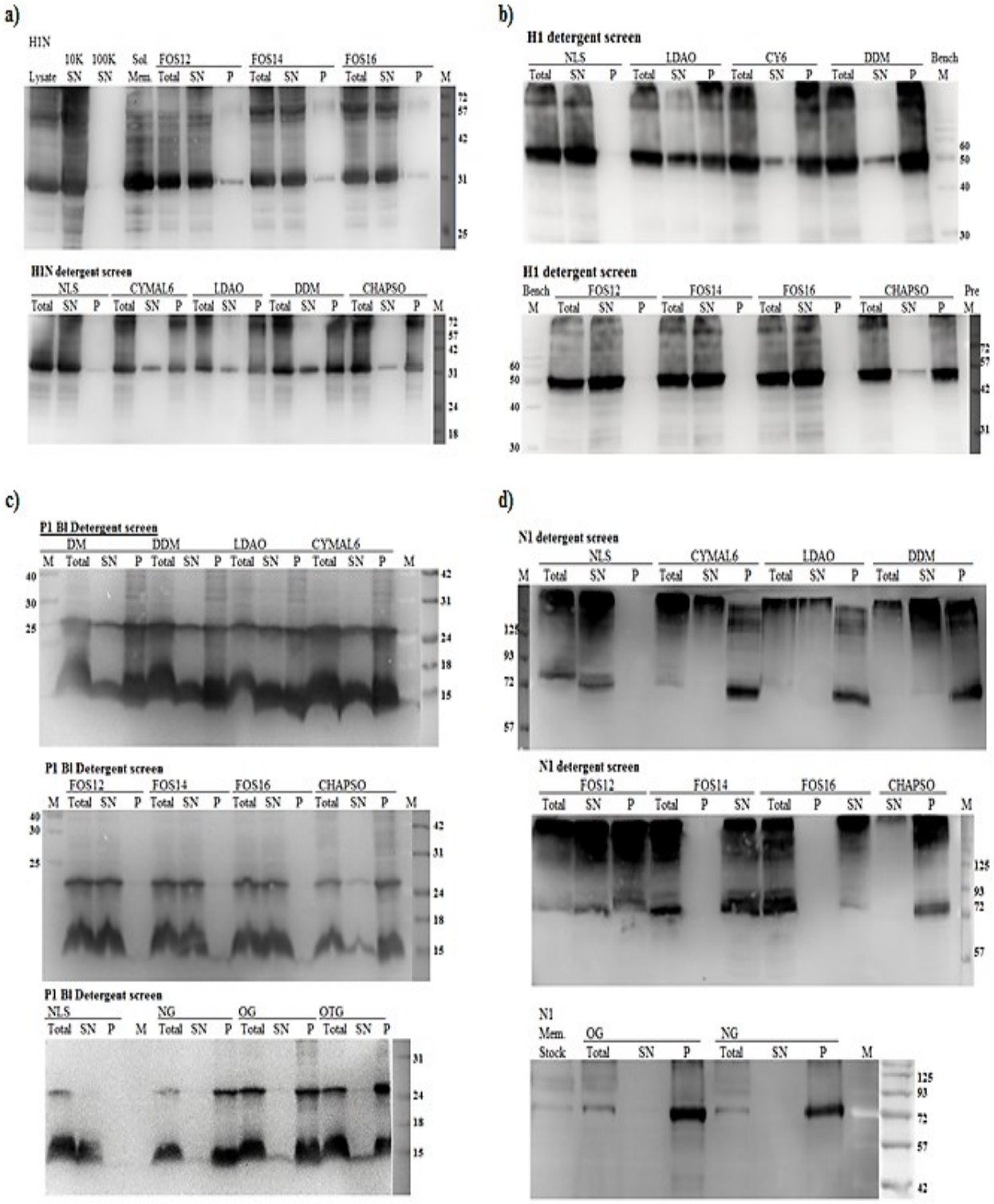

Figure 3.27 Detergent screening for different proteins.

Aliquots of membrane fractions were solubilized with 8-12 different detergents and analysed via SDS--PAGE and Western blot. 2% NG, OG, OTG and CHAPSO were used in the solubilization buffer; other detergents were used with 1% concentration (w/v). a) Presenilin 1 NTF protein (H1N); b) Presenilin 1 full length protein (H1); c) PEN-2 protein (P1); d) Nicastrin protein (N1). Total: solubilized membrane before centrifugation; SN: supernatant after solubilization; P: pellet after solubilization.

Table 3.5 The yields and expression levels of different proteins.

Protein	Constructs	Cell strain	Average cell pellets weight per culture (g/L)	Approximate protein amount per gram cell pellet (mg/g)	Protein amount per liter culture (mg/L)
Nicastrin	N1	C43(DE3)	21	0.012	0.25
		BL21(DE3)	24.5	0.05	1.2
PEN-2	P1	C43(DE3)	25.5	0.03	0.76
		BL21(DE3)	9	0.48	4.3
	P7	C43(DE3)	30	0.023	0.69
		BL21(DE3)	8.5	0.026	0.22
Presenilin 1	H1	BL21(DE3)	12	0.4	4.8
	H1N	BL21(DE3)	18	0.2	3.6
	1NR	BL21(DE3)	11	0.04	0.44
Presenilin 2	2R	BL21(DE3)	11	0.013	0.14
	2NR	C43(DE3)	14	0.015	0.21
		BL21(DE3)	9	0.05	0.45

To determine the oligomer state of each protein, size exclusion chromatography (SEC) was applied after affinity purification. The detailed results are described in accordance with the respective proteins as following.

3.2.3.1 Nicastrin

The N1 construct used of the nicastrin protein encodes 692 amino acids with an approximate molecular weight of 77 kDa and theoretical pI of 5.94. A considerable amount of the target proteins were found in the inclusion bodies which indicating incorrect folding (data not shown). Lowering the induction temperature facilitated the protein folding and brought over 50% of the target protein into the supernatant. Nicastrin has one transmembrane region and a large extracellular domain. In the experiment, unexpectedly, most of the target proteins were found in the membrane fraction which indicates a high insertion efficiency of the proteins into the cell membrane.

As shown in Figure 3.28, both the *E. coli* BL21 and C43 strain expressed nicastrin proteins that showed broad and asymmetric SEC peaks in the presence of N-Lauroylsarcosine sodium salt (NLS). This indicates multiple oligomeric states and therefore low protein quality. The presence of the target proteins was confirmed by both blue stain SDS-PAGE and anti-His tag western blot (Figure 3.28). N1 showed an apparent molecular weight around 75 kDa on the SDS-PAGE. C43 strain expressed nicastrin showed a lower yield compared to expression in the BL21 (DE3) strain. Degradation was observed for both proteins.

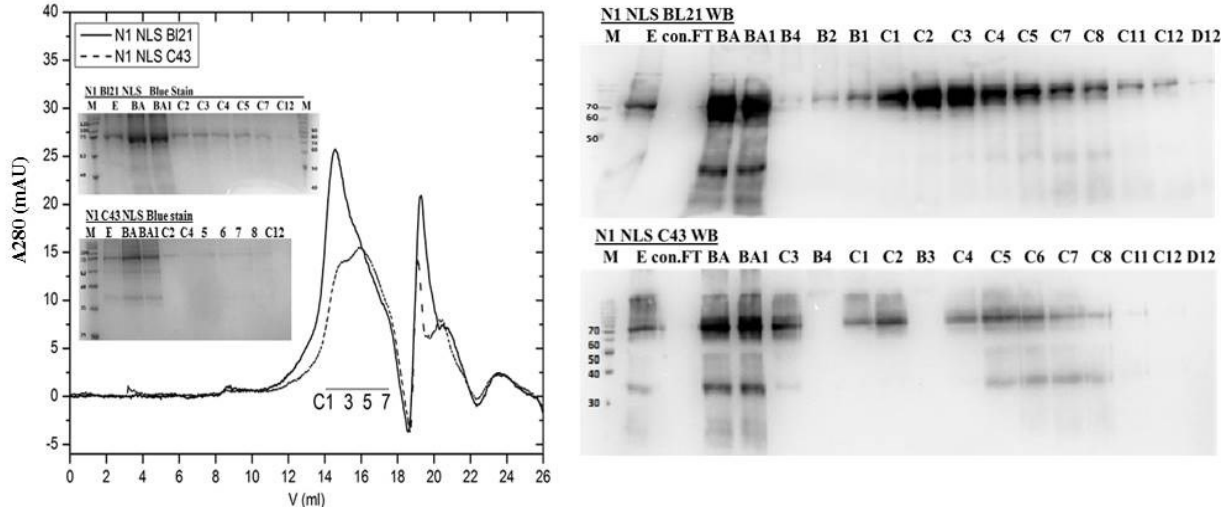

Figure 3.28 SEC and SDS-PAGE of NLS purified nicastrin proteins.

Superose 6 10/300GL column was used in the experiment. SEC buffer: 0.4% NLS, 300 mM NaCl, 20 mM Tris pH 7.4, 10% Glycerol. E: elution fraction from Ni-NTA. BA: samples taken after concentration before applied to Akta. BA1: samples taken from BA samples after 1-day storage in the cold room. Left panel: SEC and blue stained SDS-PAGE of NLS purified NCT. Right panel: Western blot of SEC fractions.

Although solubilization with DDM did not work well in the detergent screens (Figure 3.27 d), DDM is still one of the favourable detergents in conventional membrane protein purification and crystallisation. The partial extraction of nicastrin from cell membranes was achieved by using a 2% DDM in the solubilization buffer. The SEC profile and SDS-PAGE of DDM purified nicastrin proteins indicated unstable, multiple oligomeric species existing in the samples (Figure 3.30). For FOS-14 purified nicastrin, four to five peaks/shoulders were observed initially in the SEC profiles, representing aggregates, target proteins and degradation fragments, respectively (Figure 3.29). One dominating peak contains the target proteins (Peak II in Figure 3.29 a and Peak III in Figure 3.29 b). The degradation fragments were eluted after the full-length target protein on the SEC column and therefore can be separated. The elution volumes of the main peak for BL21 and C43 strains expressed proteins overlaid well with each

other. Both have the calculated molecular weight of 455 kDa which indicated a hexamer of nicastrin plus a detergent micelle.

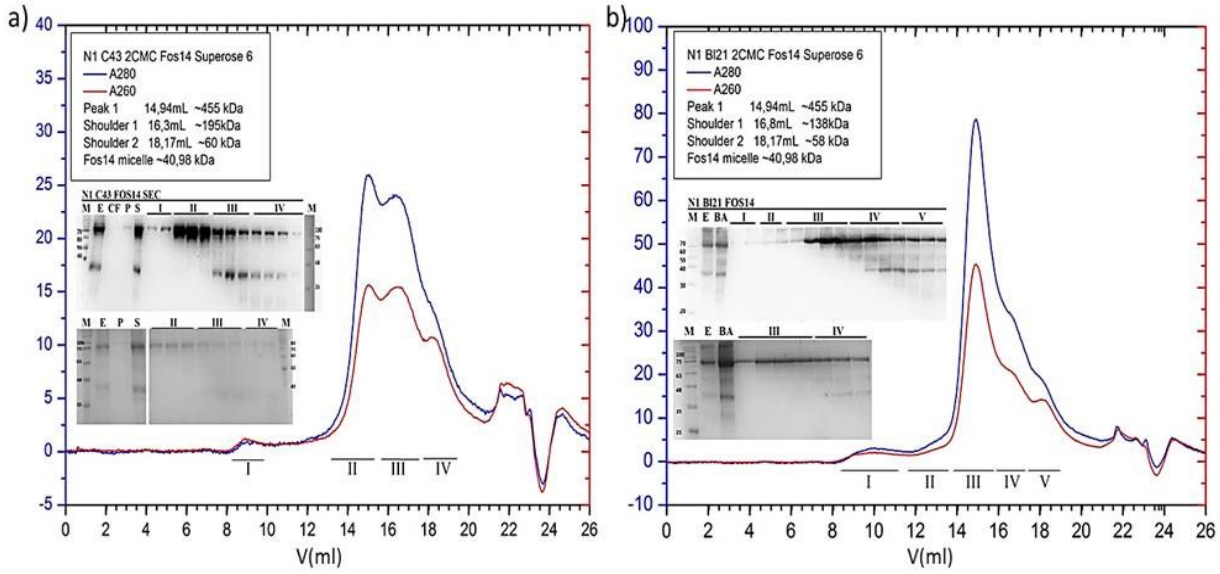

Figure 3.29 SEC and SDS-PAGE of FOS-14 purified nicastrin proteins.

a) SEC profile of C43 expressed NCT in FOS-14; b) SEC profile of BL21 expressed NCT in FOS-14. Superose 6 10/300GL column was used in the experiment. SEC buffer : 2 CMC FOS-14, 300 mM NaCl, 20 mM Tris pH7.4, 1 mM TCEP, 10% Glycerol. The Y-axis shown here has a unit of mAu. E: elution fraction from Ni-NTA. CF: samples taken from concentrating flow through. P: pellet from concentrated protein before loading. S: supernatant from concentrated protein before loading. Inset: anti-his western blot of the SEC fractions (Upper); blue stained SDS-PAGE (Lower).

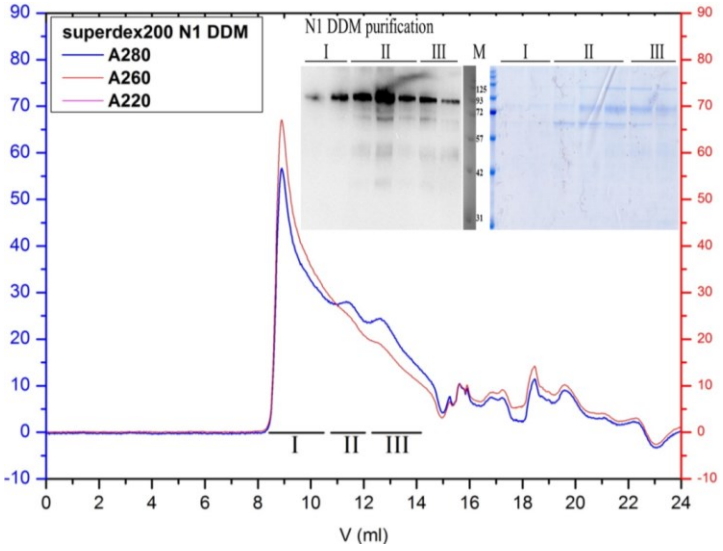

Figure 3.30 DDM purification of nicastrin.

Superdex 200 10/300GL column chromatography with. SEC buffer: 2 CMC DDM, 200 mM NaCl, 20 mM HEPES pH7.4, 1mM TCEP, 10% Glycerol. The Absorption is given in units of mAu. The second and third peaks contained both impurities and degradation fragments. The apparent molecular weights of proteins in peak fractions were 440kDa and 220kDa, respectively.

Insets: anti-his western blot (left); blue stained SDS-PAGE (right).

To remove the impurities, ion exchange chromatography (IEX) and a second affinity chromatography were used. As shown in Figure 3.31, the target protein was eluted from the

HiTrap Q column at conductivity around 17 mS/cm. However, the purity of the protein was not improved. There was still a higher molecular weight band between 93 and 125 kDa and an additional lower molecular band between 31 and 42 kDa co-eluted with the target protein. A severe loss of the protein amount was observed during the IEX purification. These observations indicated IEX was not a suitable purification step for final purification of the nicastrin protein sample. A significant improvement of the purity of the target protein was achieved by a second Ni-NTA affinity chromatography (Figure 3.31).

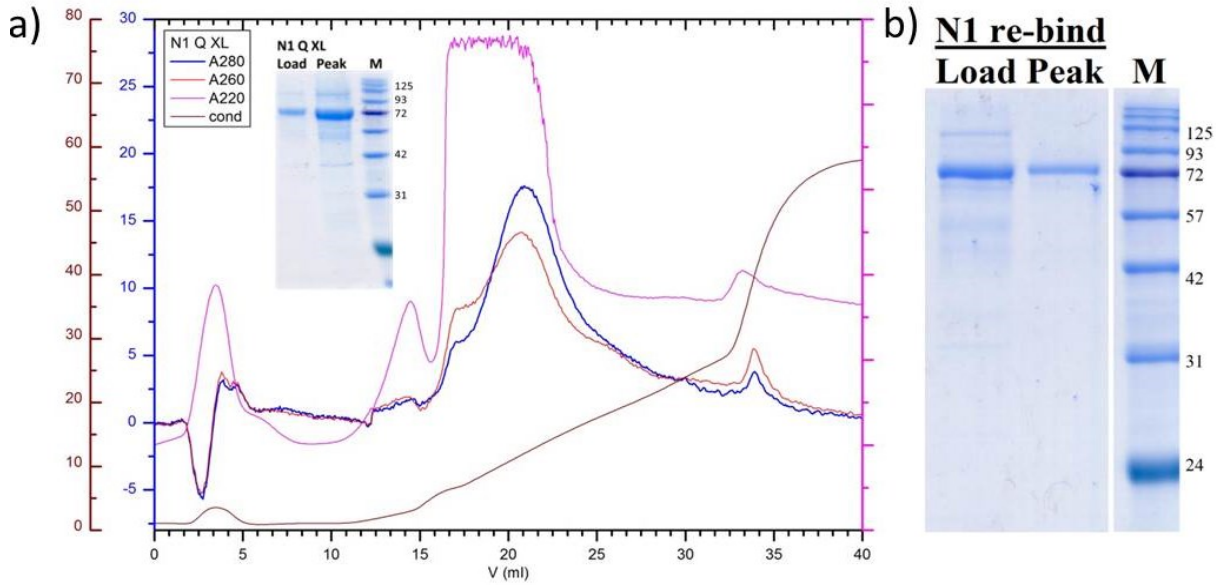

Figure 3.31 IEX and second affinity purification of FOS-14 purified nicastrin.
a) IEX of FOS-14 purified nicastrin. HiTrap Q XL column (GE, Healthcare) was used. IEX Buffer A: 20 mM HEPES, pH 7.4, 10% Glycerol, 2 mM TCEP, 2 CMC FOS-14; Buffer B: 20 mM HEPES, pH 7.4, 10% Glycerol, 1 M NaCl, 2 mM TCEP, 2 CMC FOS-14. The Absorption is given in units of mAu. The dark red Y-axis shows the scale of conductivity with the unit of mS/cm. b) Purification of nicastrin by re-binding to Ni-NTA shows a substantial improvement of purity.

There are 11 cysteines in the amino acid sequence of nicastrin protein. For reduction of oligomerization of nicastrin, the purification protocol of nicastrin was optimised by using higher ratios of solubilization buffer to cell pellet (4-8 mL pre 1 gram) and the addition of reducing reagent immediately after elution from the Ni-NTA affinity purification. To achieve a better separation, HiLoad Superdex 200 prep grade column was applied (Figure 3.32). A sharper and more symmetrical SEC peak was obtained at elution volume around 60 mL, and two smaller peaks which contained the degraded fragments were separated successfully from the main peak. From the calibration curve, the detergent-protein complexes eluted in the main peak showed an apparent molecular weight of 362 kDa indicating a tetrameric nicastrin. The

elution fractions from the main peak were pooled and concentrated to 5-10 mg/mL and showed over 95% purity on the blue stained SDS-PAGE. The dominating band from Figure 3.32 was analysed by mass spectrometry (LC-MS/MS) at the Core Facility Mass Spectrometric Proteomics of the UKE. The entire sequence of nicastrin with matched peptides was shown in Figure 3.33 with 58% coverage and a score of 480.36 (Sequest HT). The detected peptides included the C-terminal end of the protein. This, together with the presence of N-terminal His-tag as detected by western blot, proves the isolate to be the full-length protein.

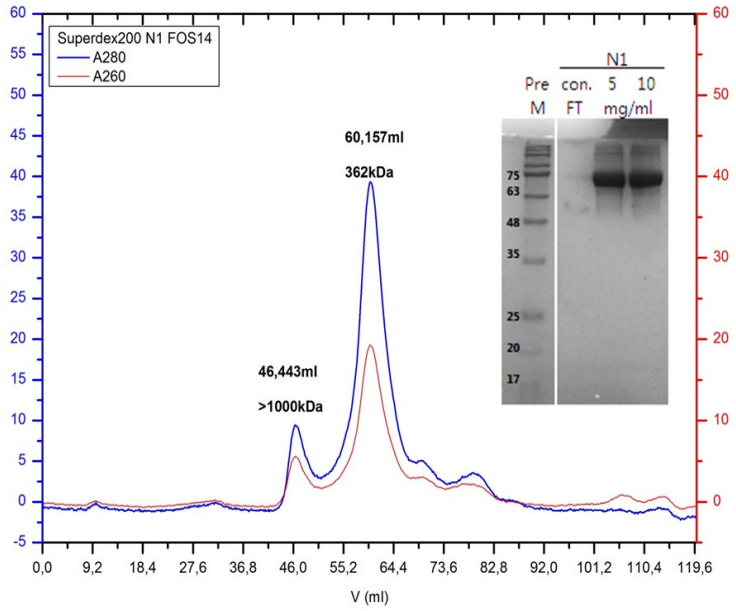

Figure 3.32 SEC of FOS-14 purified nicastrin proteins (*E. coli* BL21strains expression). Superdex 200 PG column with SEC buffer: 20 mM HEPES pH 7.4, 2 CMC FOS-14, 300 mM NaCl, 1 mM TCEP, 10% Glycerol. The Absorption is given in units of mAu. Con.FT: Samples taken from concentrated flow through of pooled SEC fractions.

1 MHHHHHHHHHHAIEGRNSVERKIYIPLNKTAPCVRLLNATHQIGCQSSISGDTGVIHVVE
61 KEEDLQWVLTDGPNPPYMVLLESKHFTRDLMEKLKGRTSRIAGLAVSLTKPSPASGFSPS
121 VQCPNDGFGVYSNSYGPEFAHCREIQWNSLGNGLAYEDFSFPIFLLEDENETKVIKQCYQ
181 DHNLSQNGSAPTFPLCAMQLFSHMHAVISTATCMRRSSIQSTFSINPEIVCDPLSDYNVW
241 SMLKPINTTGTLKPDDRVVVAATRLDSRSFFWNVAPGAESAVASFVTQLAAAEALQKAPD
301 VTTLPRNVMFVFFQGETFDYIGSSRMVYDMEKGKFPVQLENVDSFVELGQVALRTSLELW
361 MHTDPVSQKNESVRNQVEDLLATLEKSGAGVPAVILRRPNQSQPLPPSSLQRFLRARNIS
421 GVVLADHSGAFHNKYYQSIYDTAENINVSYPEWLSPEEDLNFVTDTAKALADVATVLGRA
481 LYELAGGTNFSDTVQADPQTVTRLLYGFLIKANNSWFQSILRQDLRSYLGDGPLQHYIAV
541 SSPTNTTYVVQYALANLTGTVVNLTREQCQDPSKVPSENKDLYEYSWVQGPLHSNETDRL
601 PRCVRSTARLARALSPAFELSQWSSTEYSTWTESRWKDIRARIFLIASKELELITLTVGF
621 GILIFSLIVTYCINAKADVLFIAPREPGAVSY

Figure 3.33 Peptides identified by LC-MS/MS analysis of nicastrin.
Matched peptides are shown in bold red. The transmembrane region identified from EM structure 5FN2 [40] is underlined.

3.2.3.2 PEN-2

For PEN-2, the study was focused on two constructs, namely P1 with N-terminal His-tag and

P7 with C-terminal Rho-tag.

3.2.3.2.1 P1

The P1 construct of PEN-2 encodes 116 amino acids with a predicted molecular weight of 13.9 kDa and a theoretical pI of 9.25. The isolated protein showed a strong monomer band around 18 kDa and a dimer band between 24 to 31 kDa on a 15% SDS-PAGE (Figure 3.34).

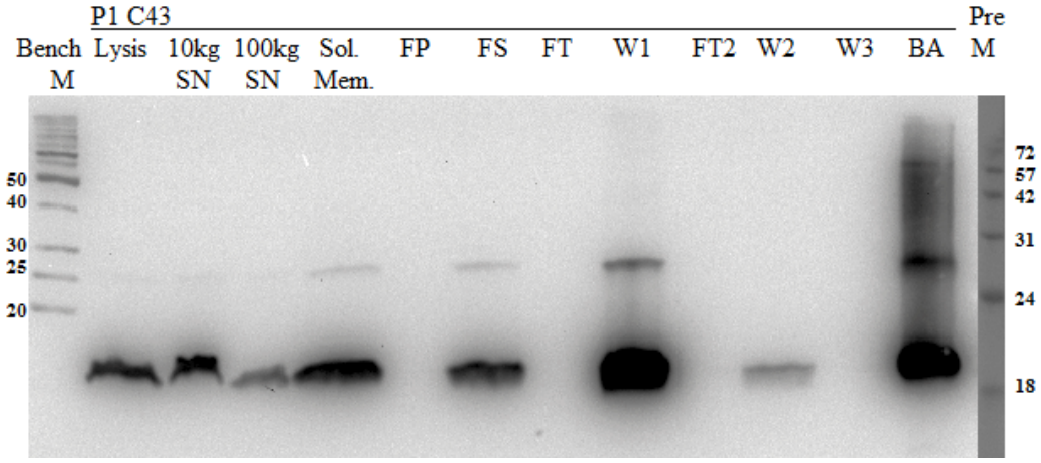

Figure 3.34 Purification of *E. coli* C43 strains expressed PEN-2 proteins.
10kgSN: sample from the supernatant after 10 000 g centrifugation; 100kgSN: sample from the supernatant after 100 000 g centrifugation; FP: final pellet after solubilization with 1% FOS-14; FS: final supernatant after solubilization; FT: Flow through from Ni-NTA column; W1: eluted fractions with 250 mM imidazole concentration; FT2: Flow through from the re-loading to the Ni-NTA column; W2 and W3: different washing steps with increasing imidazole concentration; BA: concentrated elution fractions before loading to SEC.

Comparing DDM and FOS-14 purification of PEN-2, DDM purified proteins exhibited a lower purity on the blue stained SDS-PAGE, as well as asymmetric peaks from SEC profiles (Figure 3.35 a). The overall distribution of PEN-2 proteins in the DDM SEC fractions was confirmed by western blot. The total protein yield determined after SEC was much lower from DDM purifications than the FOS-14 purifications (here shown by different peak heights from SEC in Figure 3.35). A possible explanation for this could be a lower stability of PEN-2 in the presence of DDM which would cause losses by protein aggregations. In the FOS-14 purification, PEN-2 showed one dominant, well-defined, symmetric peak with a small leading peak (Figure 3.35 b). The first peak contains proteins with higher oligomerization (~231 kDa) and the second peak contains proteins with a size corresponding to a PEN-2 protein dimer with a FOS-14 detergent micelle (~68 kDa, Figure 3.35 b). The same dimer peak was obtained for BL21 strains expressing PEN-2 proteins.

Although solubilization of PEN-2 did not work well with LDAO and CHAPSO as shown in Figure 3.27 c, efforts were made to bring the proteins into these two detergents for the crystallisation or activity assay purpose. FOS-14 purified PEN-2 proteins with different oligomerization states (Peak I and II fractions, Figure 3.35 b) were applied to Ni-NTA column separately, and the on-column detergent exchange was performed. However, most of the protein was precipitated on the resin (Figure 3.36, left panel). In addition to the low recovery rate, protein tended to be highly aggregated in the new detergent which was observed from the high elution volume (at exclusion volume) of the SEC column (Figure 3.36, right panel).

To investigate whether the formation of the first peak from the SEC profile of FOS-14 purified PEN-2 was caused by the equilibrium between the low and high oligomeric PEN-2, the two peaks were collected separately and re-loaded to the SEC column. As shown in Figure 3.37, there is a clear transition from the first peak (high oligomeric PEN-2) to the second peak (the dimeric PEN-2). Therefore the formation of the first peak of PEN-2 was mainly caused by concentration-dependent oligomerization.

FOS-14 purified PEN-2 proteins with different purities and oligomer states distributed into three peaks on Superdex 200 PG columns (Figure 3.39). There was a difference of the calculated molecular weights between this column and Superose 6 column eluted proteins which could be caused by the different behaviours of membrane proteins on different columns/matrix. The monomer band from PEN-2 on the blue stained SDS-PAGE was submitted for mass spectrometry (LC-MS/MS). The entire sequence of PEN-2 (P1 construct) with identified peptides with 15% coverage and a score of 77 (Sequest HT) is shown in Figure 3.38. This low coverage was relatively typical for the membrane proteins as a consequence of the low accessibility of the transmembrane domains to trypsin digestion[172].

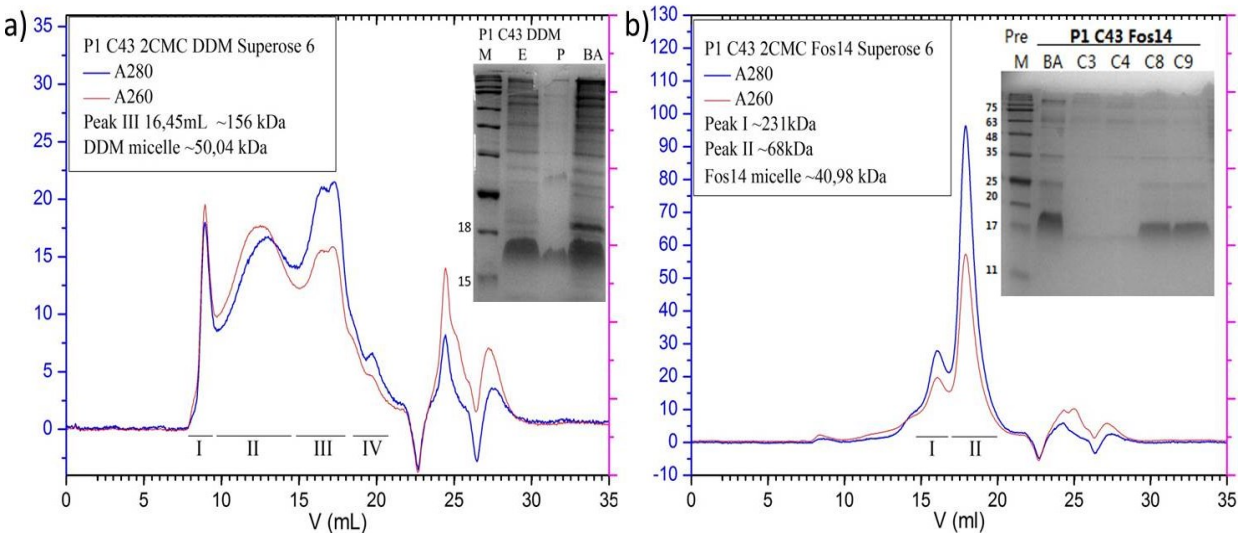

Figure 3.35 SEC and blue stain of DDM and FOS-14 purified PEN-2 (*E. coli* C43 strains expression).

Superose 6 10/300GL column with SEC buffer: 2 CMC DDM or FOS-14, 300 mM NaCl, 20 mM Tris pH 7.4, 1 mM TCEP, 5% Glycerol. Equal amounts of cell membranes were used in the solubilization step for a. and b.. The Absorption is given in units of mAu.

Insets: blue stained SDS-PAGE. a) DDM purification of PEN-2. E: elution fraction from Ni-NTA. P: pellet from concentrated protein before loading to Akta. BA: samples taken from concentrated proteins before loading to Akta. b) FOS-14 purification of PEN-2. Fraction C3 and 4 belong to Peak I; Fraction C8 and 9 belong to Peak II.

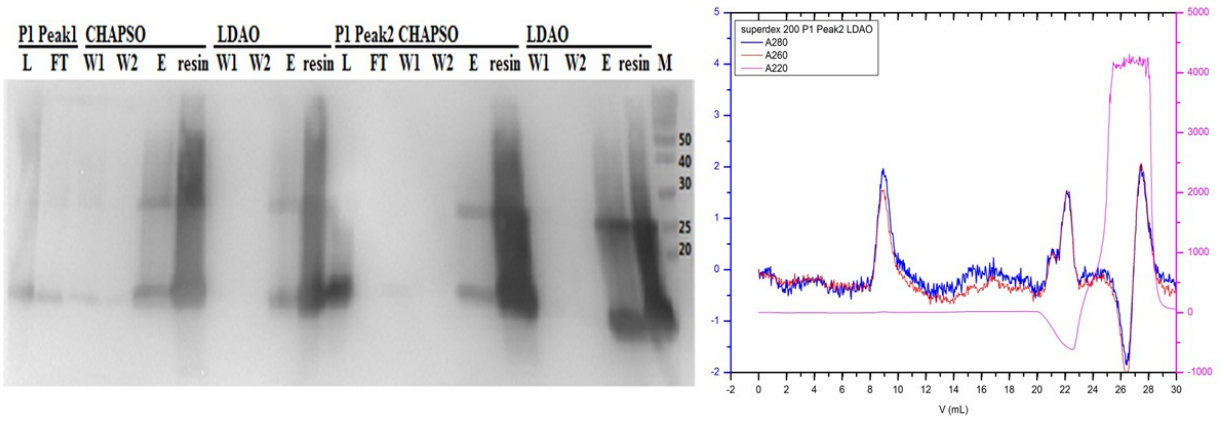

Figure 3.36 PEN-2 on-column exchange detergents.

FOS-14 solubilized PEN-2 was bound to Ni-NTA resin. On-column detergent exchange was performed by extensively washing the protein-bound resin with the buffer containing new detergent. Left panel: anti-his western blot of samples from on-column exchange detergents. Most of the proteins were found to be retained on the resin upon buffer exchange. Right panel: SEC profile of LDAO eluted PEN-2. LDAO eluted PEN-2 proteins from Ni-NTA resin were concentrated to 0.5 mL and loaded to Superdex 200 10/300GL column. The Y-axis shown here has a unit of mAu. The elution volume shifted to the void volume of the column indicating aggregation of PEN-2 in the presence of LDAO.

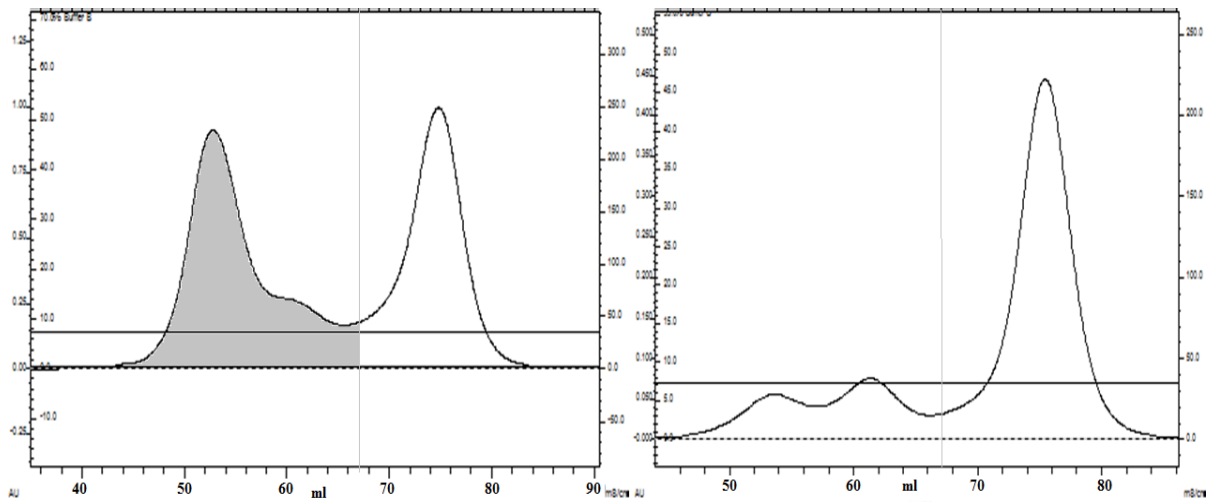

Figure 3.37 Transitions between the two peaks of FOS-14 purified PEN-2 proteins.
SEC buffer (Superdex 200 PG column): 20 mM Tris, pH 7.4, 2 CMC FOS-14, 200 mM NaCl, 2 mM TCEP, 10% Glycerol. Left panel: SEC profile of FOS-14 purified PEN-2 proteins; Right panel: re-load the fractions from the gray area (left) to SEC.

1 MHHHHHHHHHHAIEGRNLERVSNEEKLNLCRKYYLGGFAFLPFLWLVNIFWFFREAFLVP
61 AYTEQSQIKGYVWRSAVGFLFWVIVLTSWITIFQIYRPRWGALGDYLSFTIPLGTP

Figure 3.38 Peptides identified by LC-MS/MS analysis of PEN-2.
Matched peptides are shown in bold red. The transmembrane region identified from EM structure 5FN2 [40] is underlined.

It has been reported that active γ-secretase complexes are largely localised within lipid rafts which are the cellular membrane microdomains enriched with cholesterol [173–175]. Evidence showed that cholesterol is important for the association of each component of the γ-secretase to lipid rafts [176–178]. To evaluate the effect of cholesterol, solubilization and purification of PEN-2 were also carried out in detergents supplemented with cholesterol (Cholesterol Hemisuccinate Tris salt, CH210, Anatrace). There was no significant difference in the purity of the target proteins purified with or without cholesterol (Figure 3.40). However, a shift in the retention time of the eluted proteins is observed on SEC. The FOS-14-CHS purified PEN-2 showed a higher apparent molecular weight comparing to the proteins obtained without cholesterol addition (Figure 3.40 and Figure 3.41). These results indicated the integration of cholesterol into the detergent-protein complexes which caused a size increase of the protein-detergent complex (ca. 40 kDa for the dimer fraction).

The four components of the γ-secretase complex showed again a stoichiometry ratio of 1:1:1:1 in the recent cryo-EM structure [40]. Here, PEN-2 formed a dimer in the FOS-14 micelles which might prevent the sub-complex formation in the downstream experiments. Efforts were made to

break down these oligomers by using phosphocholine detergent with longer aliphatic chains, e.g. FOS-16. Compared to the FOS-14 detergent, FOS-16 has a larger micellar size with an approximately molecular weight of 72 kDa. As shown in Figure 3.42, the calculated molecular weight of PEN-2 proteins inside FOS-16 micelles is approximate 100 kDa which corresponds to a dimer as well. Thus, this longer chain detergent did not help in breaking up the PEN-2 homo-oligomers.

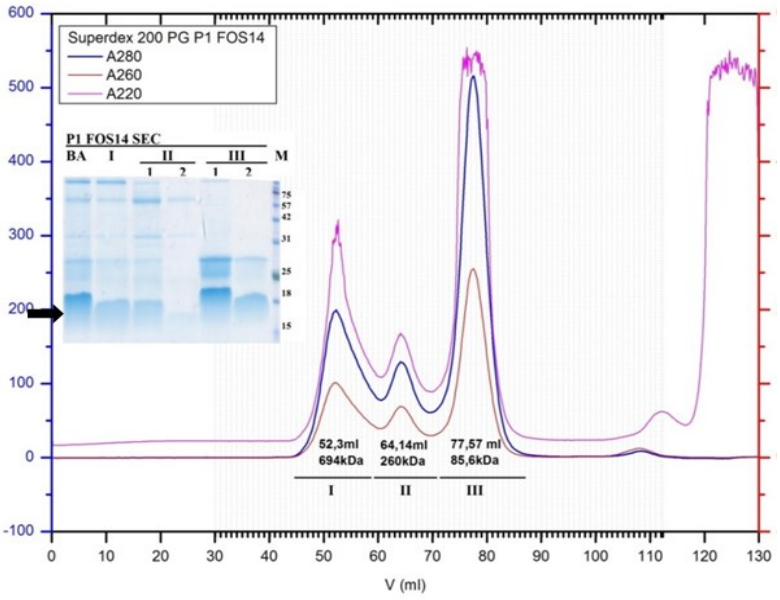

Figure 3.39 SEC of FOS-14 purified PEN-2 proteins (*E. coli* BL21 strains expression). Superdex 200PG column with SEC buffer: 2 CMC FOS-14, 150 mM NaCl, 20 mM HEPES pH 7.4, 2 mM TCEP, 10% Glycerol. Absorption in units of mAu. Inset: blue stained SDS-PAGE. 1: pooled and concentrated peak fractions; 2: the peak fraction samples. Black arrow indicates PEN-2 monomer.

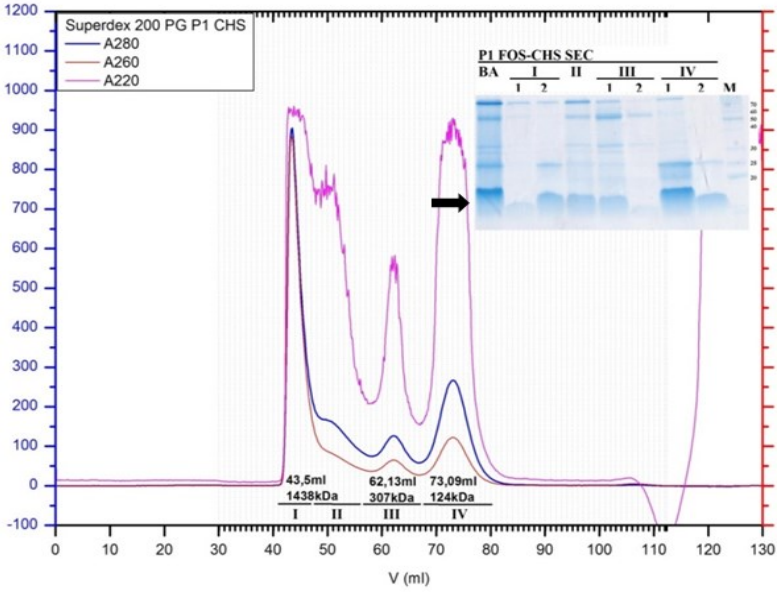

Figure 3.40 SEC of FOS-14-CHS purified PEN-2 proteins (*E. coli* BL21 strains expression). Superdex 200PG column with SEC buffer: 2 CMC FOS-14+CHS, 150 mM NaCl, 20 mM HEPES pH7.4, 2 mM TCEP, 10% Glycerol. Absorption in units of mAu.
Inset: blue stained SDS-PAGE. 1: concentrated pooled peak samples; 2: peak fraction samples. Black arrow indicates PEN-2 monomer.

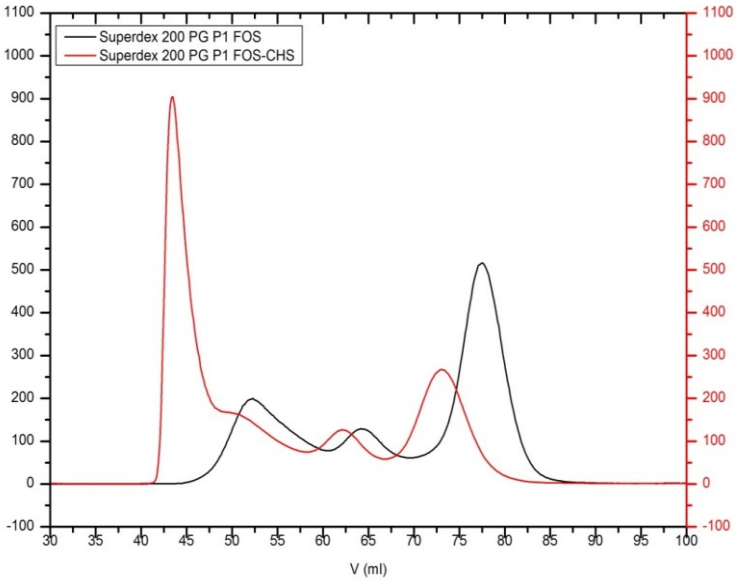

Figure 3.41 Comparison of the SEC profiles of FOS-14 and FOS-14-CHS purified PEN-2.

A shift in the retention volume of the eluted proteins is observed. The FOS-14-CHS purified PEN-2 (red) showed a higher apparent molecular weight from the SEC comparing to the proteins obtained without cholesterol addition (black). Absorption in units of mAu.

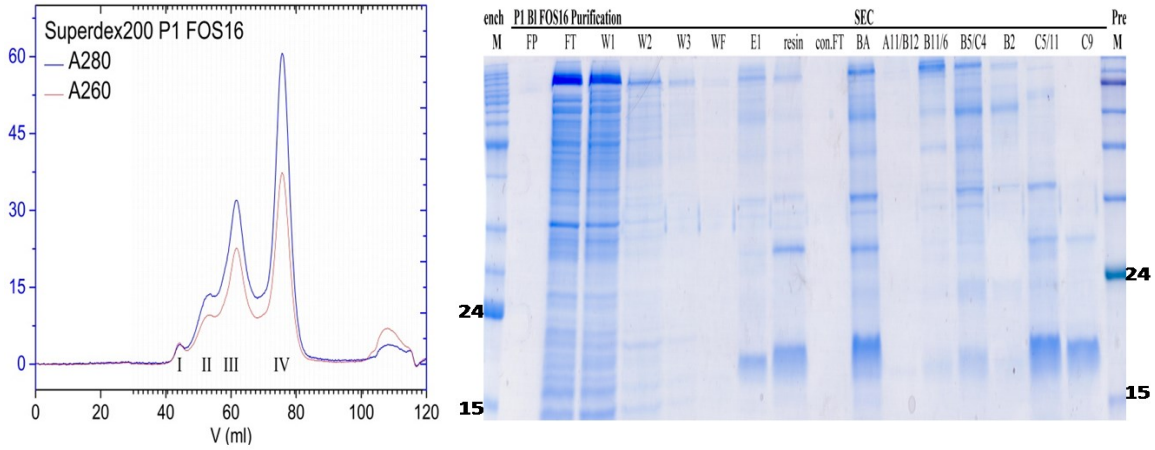

Figure 3.42 SEC of FOS-16 purified PEN-2 Proteins (*E. coli* BL21 strains expression).
Superdex 200PG column with SEC buffer: 2 CMC FOS-16, 150 mM NaCl, 20 mM HEPES pH 7.4, 2 mM TCEP. Absorption in units of mAu. Right: blue stained SDS-PAGE of PEN-2 samples from affinity purification and SEC.

3.2.3.2.2 P7

The P7 construct of PEN-2 has a C-terminal Rho tag which was designed to facilitate the study of the interaction between the His-tagged Presenilin and PEN-2. Theoretically, this Rho-tagged PEN-2 protein has a molecular weight of 13.2 kDa and a pI of 8.85.

As shown in Figure 3.43, Rho-tagged PEN-2 proteins migrated to the same level as His-tagged PEN-2 proteins on the SDS-PAGE at around 18 kDa. Both *E. coli* BL21 and C43 strains expressed Rho-tagged PEN-2 eluted at the same volume in FOS-14 detergent from SEC. The elution volume referred to a protein-detergent complex with an apparent molecular weight of approximate 107 kDa which indicated a tetrameric oligomer. This purified Rho-tagged PEN-2 protein was further utilised in the interaction assays and biophysical characterization.

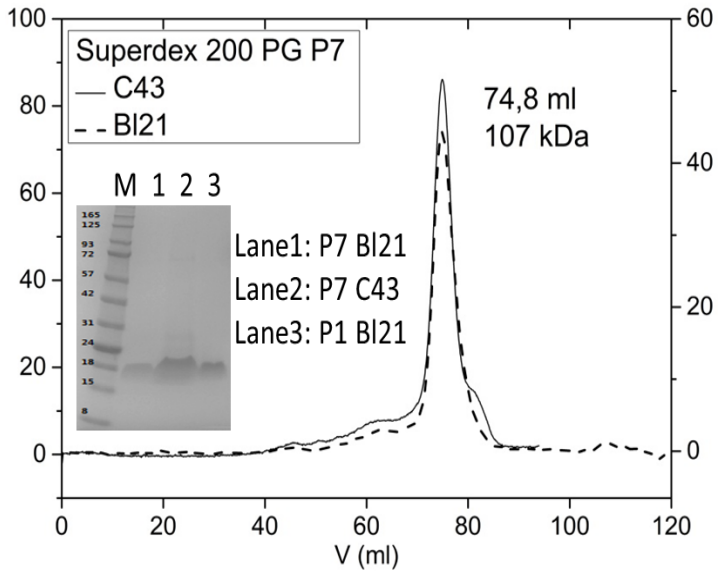

Figure 3.43 SEC profiles of FOS-14 purified Rho-tagged PEN-2 proteins.
Superdex 200PG column with SEC buffer: 20 mM HEPES pH 7.4, 200 mM NaCl, 2 CMC FOS-14, 10% Glycerol, 2 mM TCEP. Absorption in units of mAu.
Inset: Blue stained SDS-PAGE of FOS-14 purified Rho-tagged PEN-2 (P7) and His-tagged PEN-2 (P1). Both BL21 and C43 strains expressed Rho-tagged PEN-2 showed a homogenous peak with an apparent molecular weight around 107 kDa.

3.2.3.3 Presenilin

Presenilin recombinant proteins were produced in different constructs: full-length protein, N-terminal fragment, C-terminal fragment and mutated proteins.

3.2.3.3.1 Presenilin 1 Full-length protein

Presenilin 1 full-length protein, *E. coli.* BL21 expressed H1 construct (with N-terminal His tag, a predicted molecular weight of 54.8 kDa and theoretical pI of 5.64), gave a better yield than any other of the combinations of different constructs and bacteria strains screened for expression and purification. A high purity could already be achieved by the first step of affinity chromatography (Figure 3.44). An intensive signal of the target protein was observed in the flow through fractions from the affinity purification. Considering there was always enough resin used in each experiment, this western blot signal might come from the incorrectly folded proteins or the proteins with the affinity tags which were not accessible.

As shown in Figure 3.45 (left panel), the SEC purification of Presenilin 1 in FOS-14 revealed at least two different oligomer states of the proteins existed in the detergent micelles. The leading peak eluted at around 59 mL corresponds to an apparent molecular weight of 389 kDa (hexamer), while the following peak with a calculated molecular weight of 191 kDa contained trimeric Presenilin 1 in FOS-14 micelles. Comparing to the FOS-14 purified proteins, the two peaks of FOS-16 purified Presenilin 1 eluted earlier from the SEC column (Figure 3.45, right panel). The second peak showed a calculated molecular weight of 210 kDa, which was 2.5 times the sum of the molecular weights of a Presenilin monomer and a FOS-16 micelle. It is likely that the FOS-16 purified Presenilin 1 still forming a trimer in the protein-detergent

complex, but in a more compact form compared to the FOS-14 purified proteins. Protein identification of Presenilin 1 was performed via tandem mass spectrometry (LC-MS/MS). The full-length band showed coverage of 36.4% and a score of 368 (Sequest HT) (Figure 3.46).

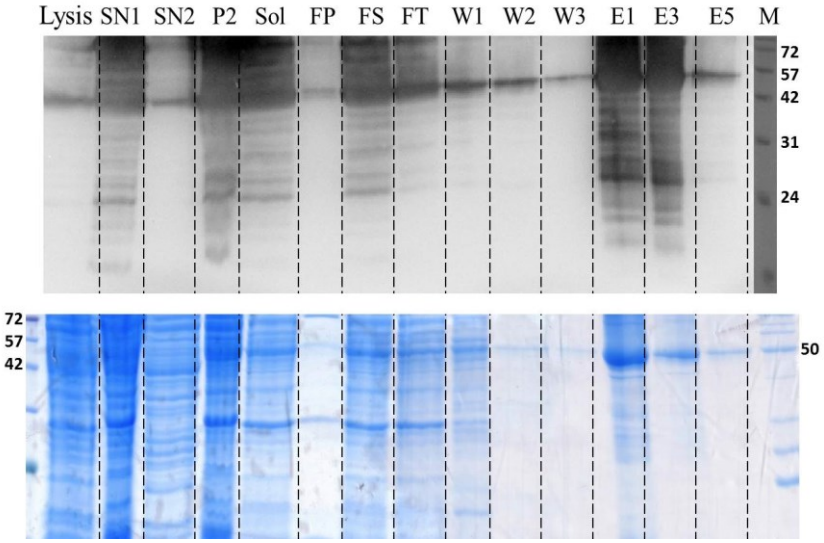

Figure 3.44 Purification of Presenilin 1 wildtype full-length protein.
Western blot (upper panel) and blue stained SDS-PAGE (lower panel) of PS1 protein samples from lysate and affinity purification. Most proteins were found in the membrane fraction (mem. stock). FOS-14 were used for the solubilization. Proteins were eluted in five fractions (E1, E3 and E5).

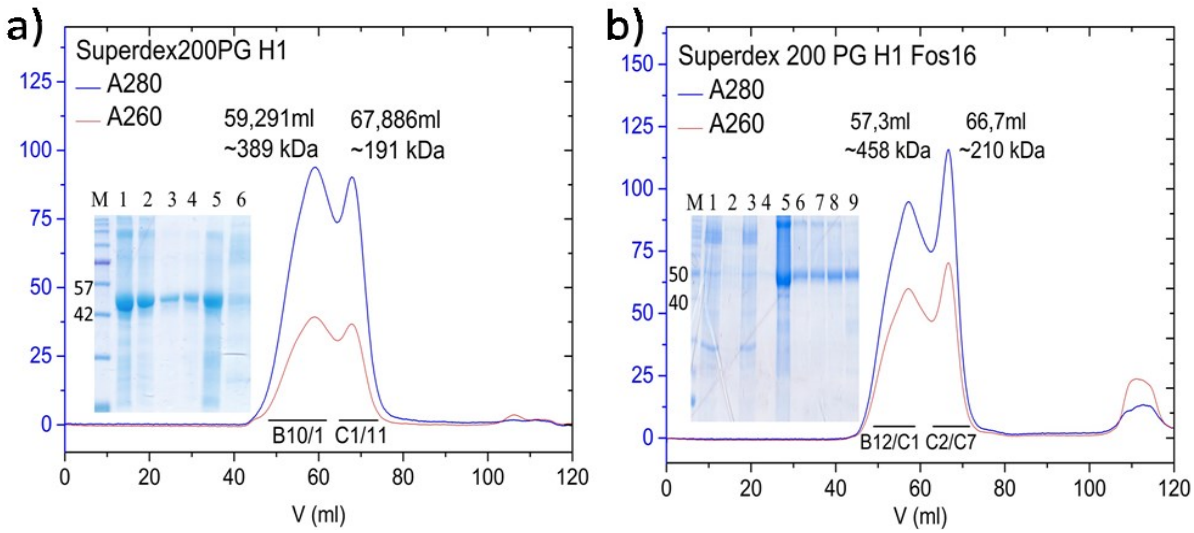

Figure 3.45 SEC of FOS-14 and FOS-16 purified Presenilin 1 (*E. coli* BL21 strains expression).
Superdex 200PG column with SEC buffer: 2 CMC FOS-14 (left) or FOS-16 (right), 150 mM NaCl, 20 mM HEPES pH7.4, 2 mM TCEP. Absorption in units of mAu. (a) Insert: lane1-concentrated protein sample before SEC; 2-SEC fraction B10/1; 3-SEC fraction C1; 4-SEC fraction C3; 5-SEC fraction C1/11; 6-solubilized membrane. (b) Insert: 1-4: affinity purification FT, W1, W2, W3; 5: concentrated protein sample before SEC; 6-SEC fraction B5; 7-SEC fraction B4; 8-SEC fraction C2; 9-SEC fraction C5/7

1 MGSSHHHHHHSSGLVPRGSHMTELPAPLSYFQNAQMSEDNHLSNTVRSQNDNRERQEHND
61 RRSLGHPEPLSNGRPQGNSRQVVEQDEEEDEELTLKYGAKHVIMLFVPVTLCMVVVVATI
121 KSVSFYTRKDGQLIYTPFTEDTETVGQRALHSILNAAIMISVIVVMTILLVVLYKYRCYK
181 VIHAWLIISSLLLLFFFSFIYLGEVFKTYNVAVDYITVALLIWNFGVVGMISIHWKGPLR
241 LQQAYLIMISALMALVFIKYLPEWTAWLILAVISVYDLVAVLCPKGPLRMLVETAQERNE
301 TLFPALIYSSTMVWLVNMAEGDPEAQRRVSKNSKYNAESTERESQDTVAENDDGGFSEEW
361 EAQRDSHLGPHRSTPESRAAVQELSSSILAGEDPEERGVKLGLGDFIFYSVLVGKASATA
421 SGDWNTTIACFVAILIGLCLTLLLLAIFKKALPALPISITFGLVFYFATDYLVQPFMDQL
481 AFHQFYI

Figure 3.46 Peptides identified by LC-MS/MS analysis of Presenilin 1.
Identified peptides are shown in bold red. Transmembrane regions identified from EM structure 5A63 [40] and 5FN2 [131] are underlined.

Besides purification performed at pH 7.4, a pH 8 buffer was also adapted from its homolog's protocol to test the pH influence on the protein. Increasing salt concentration was tested to reduce the strength of column binding of impurities. Different reducing reagents (TCEP, DTT and β-ME) were introduced after the affinity purifications to analyse the influence on the protein oligomeric states. These changes in the purification condition did not show significant influence on the on-column behaviour of Presenilin 1, except for proteins purified with 10 mM β-ME. The elution volume was dramatically reduced for the protein purified with 10 mM β-ME (at 75 mL, with a calculated molecular weight of 100 kDa), which indicated a denaturation effect of this high amount of reducing reagent on the protein. Similar to PEN-2, the FOS-14-CHS purified Presenilin 1 showed a higher apparent molecular weight from the SEC comparing to the proteins obtained without cholesterol addition (Figure 3.47) indicating a formation of cholesterol-detergent-protein complexes.

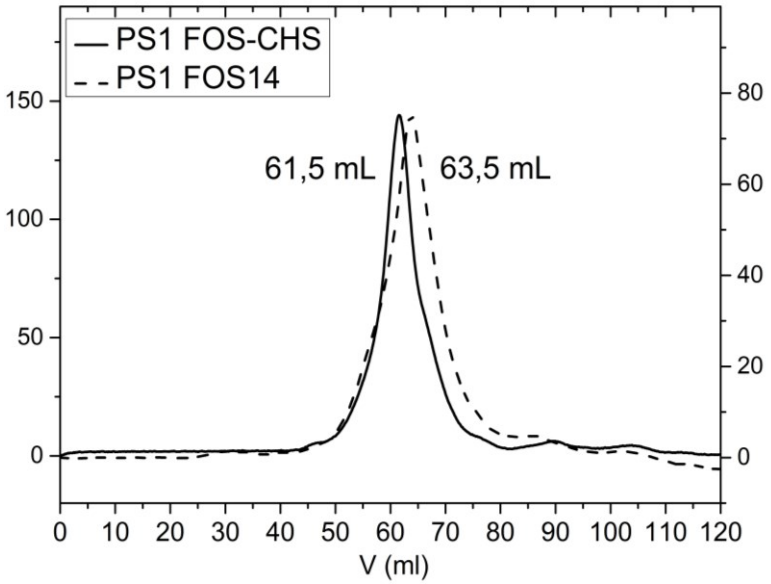

Figure 3.47 Comparison of the SEC profiles of FOS-14 and FOS-14-CHS purified Presenilin 1.
A shift in the retention volume of the eluted proteins was observed. The FOS-14-CHS purified PS1 (solid) showed a higher apparent molecular weight from the SEC comparing to the proteins obtained without cholesterol addition (dash). Absorption in units of mAu.

3.2.3.3.2 Presenilin 1 N-terminal fragment

Presenilin 1 N-terminal fragment was built in two constructs: H1N with N-terminal His tag and 1NR with C-terminal Rho tag. For both constructs, the expression of the target protein was detectable. Both proteins could be solubilized by FOS-14 and purified using the appropriate affinity resin. However, the protein quality (purity and homogeneity) from 1NR construct was poor (data not shown). Thus, the purification of Presenilin 1 N-terminal fragment was mainly focused on the H1N construct (calculated molecular weight of 35.4 kDa, theoretical pI of 6.53).

As shown in Figure 3.48, multiple peaks were eluted from SEC purification performed in FOS-14 which indicated the existence of at least three different oligomeric species in the sample (Figure 3.48). Fractions from different peaks were collected separately and additional SEC (4 to 5 times) were performed to separate a more homogenous peak with a lower oligomer state. Purification of Presenilin 1 N-terminal fragment was also performed in FOS-12. There was no significant difference in the purity of these two detergent purified proteins (left and right PAGEs in Figure 3.49). The leading peaks in the two SEC profiles contained proteins with the calculated molecular weight of 240 kDa and 206 kDa, respectively. Both of them correspond to a hexametric Presenilin 1 NTF. The calculated molecular weight of the FOS-14 purified Presenilin 1 NTF in the second peak is 188 kDa which indicated a tetramer, while proteins from the FOS-12 purified second peak showed an apparent molecular weight of 124 kDa which corresponded to a trimer.

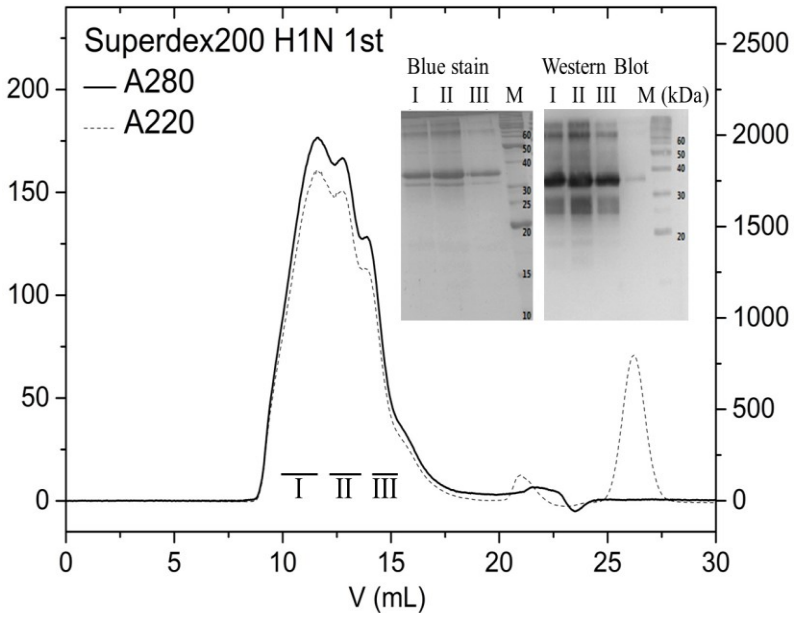

Figure 3.48 SEC of FOS-14 purified Presenilin 1 NTF proteins (*E. coli* BL21 strains expression).
Superdex 200 10/300GL column with SEC buffer: 3 CMC FOS-14, 200 mM NaCl, 20mM HEPES pH 7.4, 1 mM TCEP, 10% Glycerol. Absorption in units of mAu. The target proteins were eluted in all three peaks from the SEC as observed from both blue stain SDS-PAGE and western blot (insets).

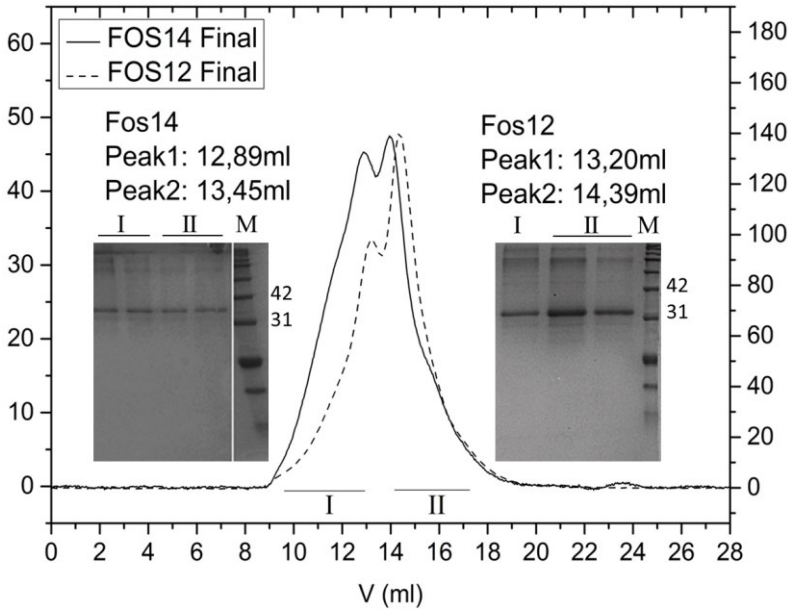

Figure 3.49 Comparison of the SEC profiles of FOS-14 and FOS-12 purified PS1 NTF.
Superdex 200 10/300GL column with SEC buffer: 2 CMC FOS-14 (black curve) or 2 CMC FOS-12 (red curve), 200 mM NaCl, 20 mM HEPES pH 7.4, 1 mM TCEP, 10% Glycerol. Inset: blue stained SDS-PAGE of the peak fractions obtained from FOS-14 purification (left) and the peak fractions purified from FOS-12 (right). Absorption in units of mAu.

3.2.3.3.3 Presenilin 1 C-terminal fragment

Presenilin 1 C-terminal fragment (PS1CTF) was expressed in a C-terminal Rho-tagged construct with a theoretical molecular weight of 20.6 kDa and pI of 4.55. As shown in Section 3.2.1, Presenilin 1 CTF construct showed a low yield in the preliminary expression experiments. *E.coli.* BL21 (DE3) strains were chosen for the up-scaled expression and purification because of its relatively higher productivity. Consistent with former results (Figure 3.26), more than 50% of the target proteins remained in the supernatant after a 100 000 g centrifugation step (Figure 3.50, left panel). The failure of insertion of Presenilin 1 CTF into the cell membranes might be probably due to a misfolding of the protein. Solubilization and affinity purification of the membrane attached Presenilin 1 CTF proteins were performed in FOS-14 or N-Lauroylsarcosine sodium salt (NLS). Approximately 85% of the FOS-14 solubilized Presenilin 1 CTF protein could be eluted from Rho1D4 resin in four to five fractions, while NLS, which is known to be a harsh detergent, showed denaturation effect on the Rho1D4 resin: Both the target protein and the antibodies bound to the matrix were eluted in this detergent (Figure 3.50, right panel). From western blot, Presenilin 1 CTF showed a signal right below the 25 kDa marker (Figure 3.50). However, there is no visible band observed in this range from the silver blue stained SDS-PAGE. Comparing the western blot signal from the *in-vitro* expressed and the *in vivo* expressed Presenilin 1 CTF in Figure 3.50, it might be possible to obtain a larger amount of this protein for downstream applications using a continuous *in-vitro* expression system.

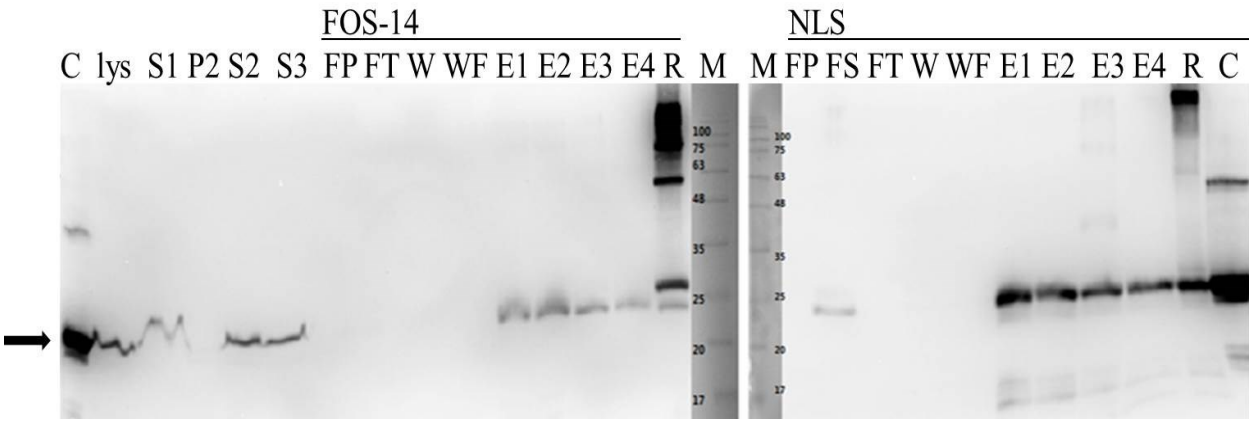

Figure 3.50 Purification of Presenilin C-terminal fragment.

Western blot of PS1 CTF protein samples from opening cell process and affinity purification. C: PS1 CTF control from in-vitro expression. Centrifugation was performed at 900 g (S1), 10 000 g (P2, S2) and 100 000 ×g (S3). Most proteins were found in the supernatant after ultracentrifugation (S3). FOS-14 and NLS were tested for the solubilization. R: resin sample after elution. Black arrow indicates PS1 CTF.

3.3 Overexpression of APH-1 in insect cells

The fourth component of γ-secretase, APH-1, showed a poor expression level in the bacterial expression system. New constructs of APH-1 for the insect expression system were designed (as shown in Figure 3.51). The insect expression construct of APH-1 employed double tags at the C-terminus separated by different enzymatic cleavage sites to facilitate the identification and purification procedure. A signal peptide was introduced to the N-terminus of APH-1 to facilitate the target protein expression [179]. Double-tagged APH-1 (with or without signal peptide) was cloned into two different vectors, pOET2 and pOET4 (Oxford Expression Technologies). The major difference between these two vectors is the promoters utilised for the expression of foreign genes. In the pOET2 vector, an AcMNPV polyhedrin promoter is employed, while the pOET4 vector is using a late AcMNPV basic (p6.9) promoter which provides an earlier expression. The expression levels of four different constructs of APH-1 were investigated in the preliminary experiments by Cube-Biotech, Monheim. According to the pre-test results, the APH-1 construct without the signal peptide in the pOET2 vector at MOI 2 was chosen.

Similarly to other components, detergent screening was firstly performed for APH-1 expressed from insect cells (Figure 3.52). The new construct of APH-1 has a calculated molecular weight of 32.4 kDa and a theoretical pI of 7.16. The protein signals were obtained between 24 kDa and 31 kDa on western blot. A band with higher molecular weight (at around 57 kDa) was also observed which might refer to a dimer of the target protein. Only FOS-12 and FOS-14 exhibited successful solubilization of the target proteins with anti-His tag blotting (Figure 3.52

a), while signals were obtained with CHAPSO and NLS solubilization as well from anti-Rho tag blotting (Figure 3.52 b). The signal intensity difference could be due to the different accessibility of the two tags.

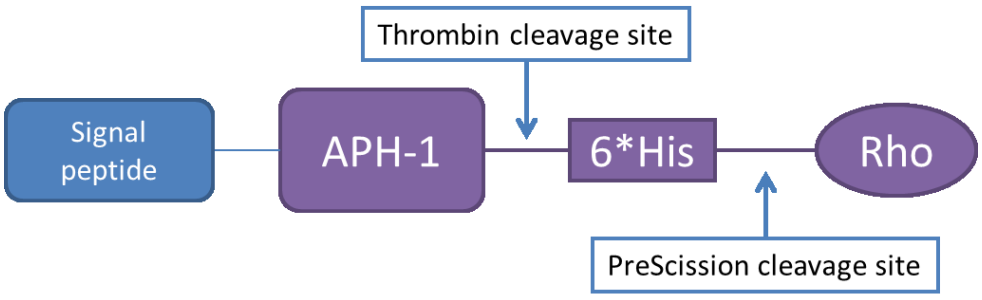

Figure 3.51 Construct design of APH-1 for insect cell expression.
A 6×histine tag following by a Rho tag was introduced to the C-terminus of APH-1 for the insect expression. Thrombin cleavage site and PreScission cleavage site were included between the protein and the tags as indicated by the arrow. A signal peptide was introduced to the N-terminal of APH-1 to facilitate the target protein expression.

Purification of the insect cell expressed APH-1 was further carried out in FOS-14. To reduce the duration of experiments, the target proteins were first applied to Ni-NTA resin. Although the His tag was located between AHP-1 and the Rho tag, the recombinant protein showed a good binding affinity to the resin (Figure 3.53 a). Besides the monomer and dimer bands, there were also aggregates detected in the Ni-NTA elution fractions. The eluted fractions were concentrated and subjected to a Superose 6 column. Three peaks were eluted from the SEC including a dominating peak with an elution volume of 15.9 mL (Figure 3.53 b). It corresponded to an apparent molecular weight of 243 kDa, which indicated a hexametric APH-1. However, the blue stain of the SEC fractions showed a low purity of the loaded sample (Figure 3.54 a). The high apparent molecular weight from SEC could be also attributed to these co-purified impurities. To achieve a higher purity of the target protein, a second Rho affinity purification was performed. A degradation fragment appeared in the elution fractions from Rho affinity column after a one-day purification step (Figure 3.54 b). This severe degradation indicated a low stability of this detergent purified protein. The purification of APH-1 was further performed in a combination of Rho affinity purification and SEC using a Superdex 200 column. This protocol yielded two major species in the elution fractions (Figure 3.55). The leading peak contained protein-detergent complexes with an apparent molecular weight of 255 kDa, while the second peak contained smaller complexes of 147 kDa (trimer). The concentrated protein sample showed a weak but similar pattern on both blue stained SDS-

PAGE and western blot which containing both monomer and dimer bands (Figure 3.55). This purification procedure yielded a total purified protein amount of 80 μg per gram insect cell pellet.

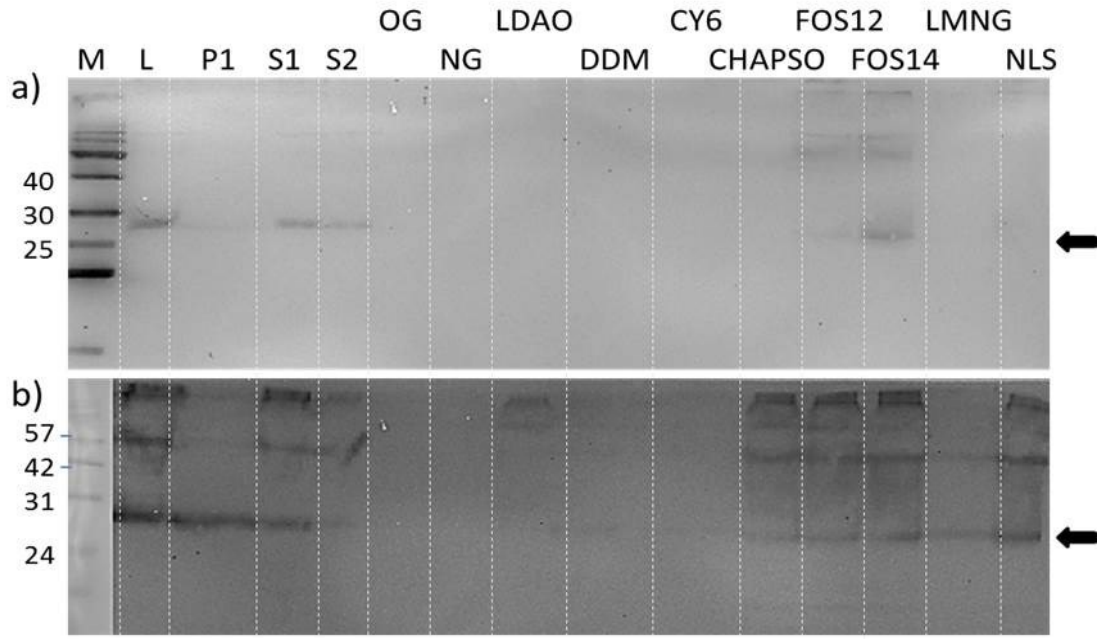

Figure 3.52 Detergent screen of insect expressed APH-1 protein.

a) Anti-His tag western blot. b) Anti-Rho tag western blot. L: lysate; P1 and S1: pellet and supernatant after 1000g centrifugation. S2: supernatant after a 100 000 g centrifugation. All the supernatants after solubilization were loaded equally to the gel. Arrows indicate the position of APH-1 monomer.

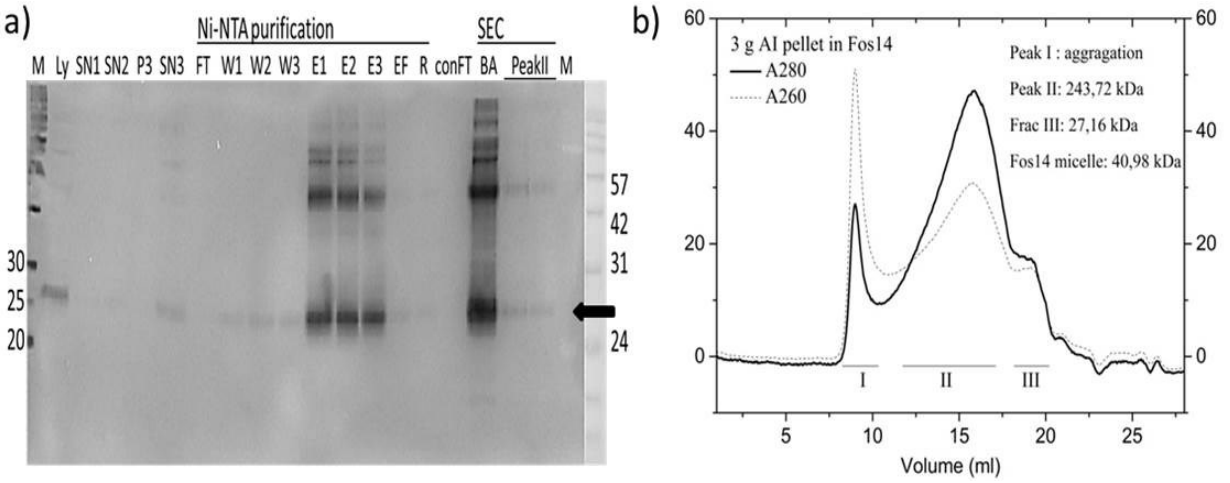

Figure 3.53 Ni-NTA affinity and SEC Purification of insect expressed APH-1 protein in FOS-14.

a) Anti-His western blot of Ni-NTA affinity purification of APH-1. Ly: lysate; SN1: supernatant after 3000 g centrifugation; SN2: supernatant after 100 000g centrifugation; P3 and SN3: pellet and supernatant after solubilization; EF: final elution fraction; R: resin after elution. b) SEC profile of APH-1 in FOS-14. Superose 6 10/300GL column was used in the experiment. SEC buffer: 20 mM HEPES, 200 mM NaCl, 10% Glycerol, 3 CMC FOS-14, 2 mM TCEP, pH 8. APH-1 monomer migrated at the molecular weight around 27 kDa on a 12% gel. Black arrow indicates APH-1 monomer.

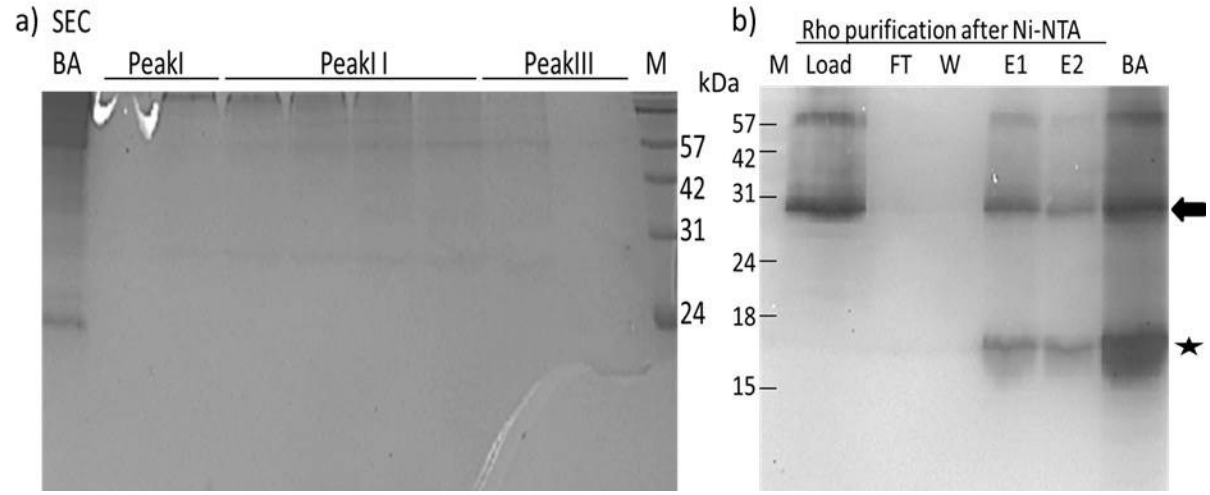

Figure 3.54 Purification of insect expressed APH-1 protein.

a) Blue stain of the SEC fractions of APH-1 after Ni-NTA affinity purification. b) Anti-His western blot of the second Rho affinity purification. The SEC fractions were pooled and bound with Rho1D4 resin in the cold room overnight. Degradation fragments (migrated between 15 kDa and 18kDa) were observed in the elution fractions from Rho affinity purification. The arrow indicates APH-1 monomer, the star indicates degradation fragment.

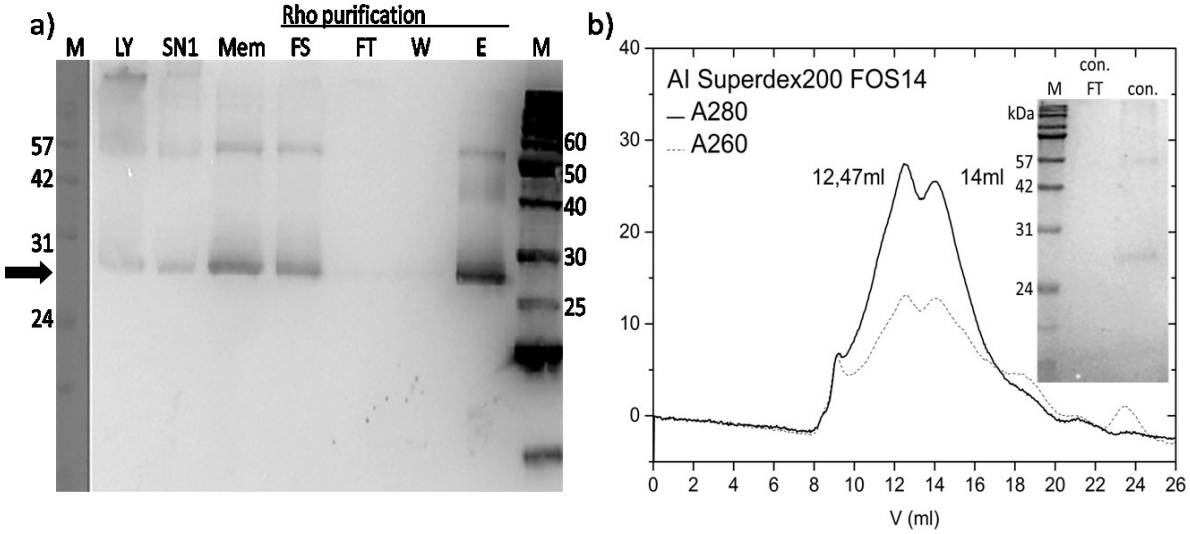

Figure 3.55 Rho1D4 purification of insect expressed APH-1protein.

a) Anti-His western blot of Rho affinity purification of APH-1. Ly: lysate; SN1: supernatant after 3000 g centrifugation; Mem: membrane fraction; FS: supernatant after solubilization. b) SEC profile of APH-1 in FOS-14. Proteins eluted from Rho resin were concentrated to 0.5 mL and load to a Superdex 200 10/300GL column. SEC buffer: 20 mM HEPES, 200 mM NaCl, 10% Glycerol, 3 CMC FOS-14, 2 mM TCEP, pH 8. Inner gel: Blue stain of concentrated peak fractions of APH-1. Black arrow indicates APH-1 monomer.

3.4 Biophysical characterization of different components of γ-secretase

Quality control of the purified proteins was carried out by circular dichroism (CD) and fluorescence measurements. Table 3.6 shows the expected and experimentally confirmed secondary structural contents of different components.

Table 3.6 Predicted and measured secondary structure contents of different components.

Protein	Secondary Structure	EM structure 5A63[40]	EM structure 5FN2[131]	Calculated Value*	Measured Value
Presenilin 1	Helical	**37%** (10 helices; 175 residues)	**48%** (11 helices; 226 residues)	**46.4%** (226 residues from 487 a.a.)	**41%**
	Beta sheet	**0%** (1 strands; 2 residues)	**0%** (1 strands; 2 residues)	**0%** (2 residues from 487 a.a.)	**13%** (FOS-14) or **14%** (FOS-16)
Nicastrin	Helical	**30%** (22 helices; 213 residues)	**28%** (21 helices; 199 residues)	**30.7%** (213 residues from 692a.a.)	**31%**
	Beta sheet	**17%** (32 strands;125 residues)	**14%** (29 strands; 102 residues)	**18%** (125 residues from 692 a.a.)	**20%**
PEN-2	Helical	**72%** (6 helices; 73 residues)	**67%** (5 helices; 68 residues)	**62.9%** (73 residues from 116a.a.)	**60%** (FOS-14) or **59%** (FOS-16)
	Beta sheet	**2%** (1 strands; 3 residues)	**2%** (1 strands; 3 residues)	**0%** (3 residues from 116 a.a.)	**7%** (FOS-14) or **5%** (FOS-16)
Aph-1	Helical	**73%** (8 helices; 196 residues)	**73%** (8 helices; 196 residues)	**65%** (196 residues from 298 a.a.)	n.a.
	Beta sheet		**0%** (1 strands; 1 residues)	**0%** (3 residues from 116 a.a.)	n.a.

*Calculated value is obtained from the calculation using EM structure corresponding residue number divided by the actual amino acids number in our constructs.

3.4.1 Nicastrin

FOS-14 purified nicastrin (Figure 3.56) exhibited the characteristic spectrum of α-helical proteins (minima at 208 and 222 nm) as shown in Figure 3.57 (left panel). Deconvolution of the far-UV CD data obtained at 4 °C yielded a secondary structural content of 32% α-helix, 23% β-sheet, 13% turns and 33% unordered structure (Table 3.7). The normalised root mean square difference (NRMSD) value of 0.02 defined a good fit between the calculated and the experimentally verified data. The calculated secondary structure content of nicastrin is broadly in agreement with the secondary structure obtained from the EM structure (5A63) [40] with a slightly higher proportion of β-sheet, 23% as opposed to 17%.

The far-UV CD and tryptophan fluorescence spectra of nicastrin were recorded over the

temperature range 4 °C to 100 °C to evaluate the thermal stability of the protein (Figure 3.57). In the far-UV CD spectra, a complete loss of the typical two minima helical negative peak occurred after 64 °C. The protein could partially recover its tertiary structure (ca. 90% of the initial intensity) upon cooling back from 100 °C to 4 °C (yellow curve in Figure 3.57, right panel). However, this partially recovery is accompanied by highly aggregated forms as an intensive 90°C light scattering peak was observed at 295 nm (yellow curve in Figure 3.57, right panel). The native nicastrin showed an emission maximum at 335 nm indicating most of the Trp residues were in a relatively hydrophobic microenvironment. A 4 nm red shift (from 335 nm to 339 nm) of the emission maximum was observed upon thermal denaturation suggesting the presence of solvent-exposed hydrophobic regions (Figure 3.57, right panel).

The thermal stability of NCT was analysed: A transition of α-helix to β-sheet was observed which was caused by the increasing temperature (Figure 3.58, left panel). The plot of maximum fluorescence signal against temperature did not show a two-state transition which might due to the protein aggregation. The formation of large aggregates after thermal denaturation was proved by SDS-PAGE (Figure 3.56). For both, far UV and near UV CD, spectra, the FOS-14 purified NCT exhibited a T_m value of ca. 59°C (Figure 3.58, right panel).

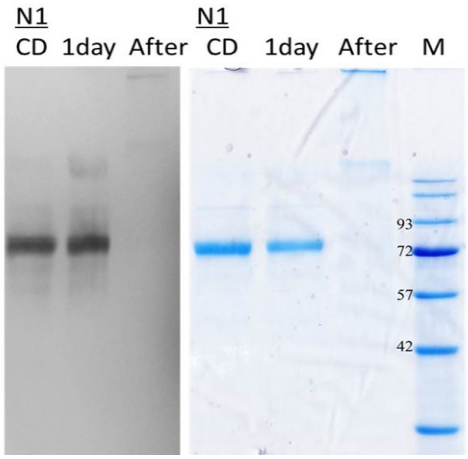

Figure 3.56 SDS-PAGE of nicastrin CD samples.
Left panel: anti-His western blot of nicastrin CD samples. Right panel: blue silver stained SDS-PAGE of nicastrin CD samples. SDS-resistant protein aggregates were observed on the top of the gel after thermal denaturation (marked as After).

Table 3.7 Deconvolution of CD data for nicastrin in FOS-14

Reference database	Helix 1	Helix 2	Strand 1	Strand 2	Turns	Unordered	Total	NRMSD
SMP180	0.15	0.16	0.13	0.09	0.13	0.33	0.99	0.020
Reference data set 4	0.18	0.13	0.12	0.08	0.19	0.29	0.99	0.019
Reference data set 7	0.19	0.14	0.12	0.08	0.17	0.30	1	0.016

Solutions from the CDSSTR method (DichrWeb) [180,181]

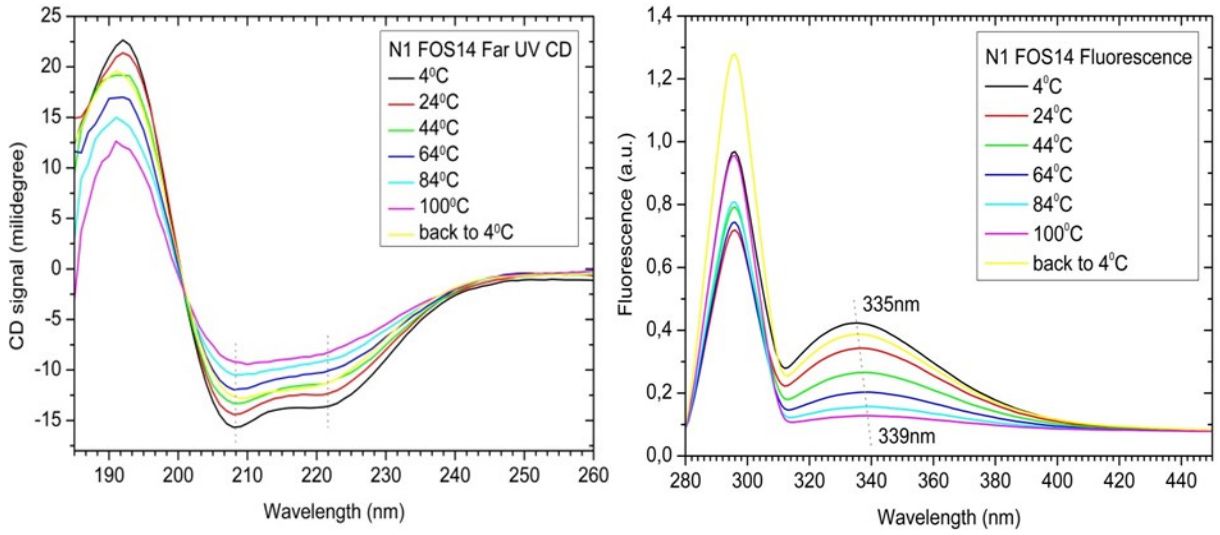

Figure 3.57 CD (Left) and fluorescence (Right) spectra of nicastrin.

Far UV circular dichroism and fluorescence were recorded for FOS-14 purified tetrameric NCT. Far-UV CD and fluorescence spectra were measured from 4 °C to 100 °C with every 20 °C intervals. An additional spectrum was measured after the samples cooled back to 4 °C (spectra shown in purple). Left panel: the CD spectra minima (208nm and 222nm) were marked with a dashed line. Right panel: A fluorescence peak maximum shift (dash line) was observed during the thermal denaturation.

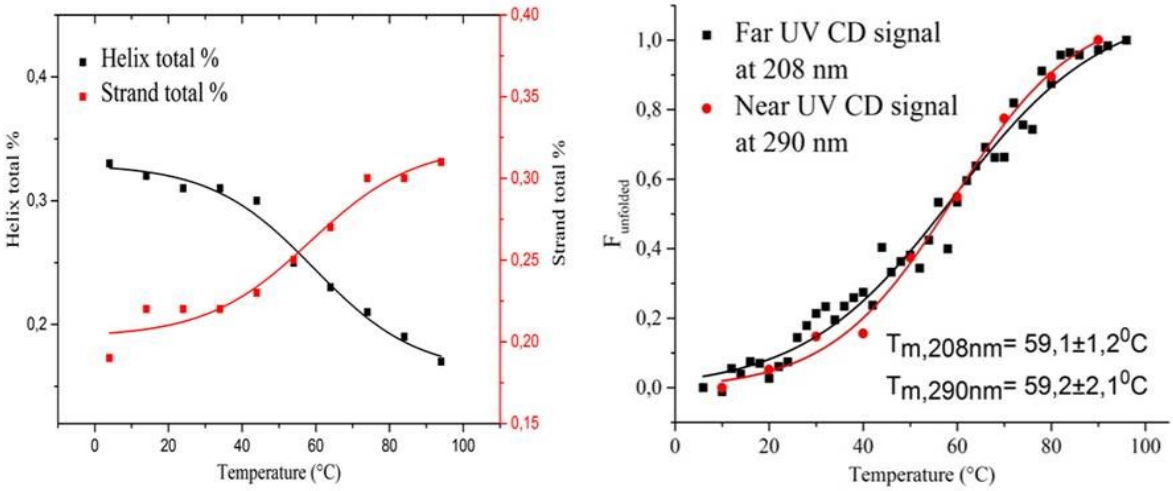

Figure 3.58 Thermal stability of FOS-14 purified nicastrin.

Left panel: Transition of the secondary structure of NCT from α-helix to β-sheet. Right panel: Temperature induced protein unfolding (calculated based on the far-UV CD signals at 208 nm and near UV CD signal at 290 nm).

3.4.2 PEN-2

The FOS-14 purified PEN-2 proteins were analysed by CD- and fluorescence spectroscopy. From far-UV CD spectra, FOS-14 purified PEN-2 exhibited a typical helical structure with a $\theta_{222/208}$ ratio of 1.11 (Figure 3.59 a). This value is usually used as an indicator of a coiled-coil interaction [182,183]. There was no observation of a shift of the fluorescence during the thermal denaturation indicating no significant changes in the tryptophan microenvironment (Figure 3.59

b). It was difficult to extract the melting temperature from either CD or fluorescence data using conventional methods (data not shown). Alternatively, a temperature-dependent α-helix to β-sheet transformation was observed when analysing the secondary structure content as a function of temperature (Figure 3.60a). The thermal denaturation process of PEN-2 displayed an intermediate state which formed between 64 to 74 °C suggesting a 3-state thermal unfolding of PEN-2.

It has been reported that during protein aggregation forming, light scattering will increase sharply when the particle size approaches the wavelength of the light [184]. The change of the 90° light scattering gives an indicator of protein aggregation. In the fluorescence experiment, the 90° light scattering was monitored at 300 nm. A heat-induced increase of the 90° light scattering was observed around 50 °C which reflected the formation of large particles (Figure 3.60b). This temperature is in agreement with the aggregation temperature obtained from DLS result (54.6 °C). This aggregation temperature reflected a combined property from both PEN-2 and FOS-14 detergent micelles.

The chemical induced denaturation of PEN-2 was investigated in a guanidine hydrochloride (GuHCl) titration experiment. The α-helical structure of PEN-2 appeared to be resistant to the denaturation additive. A dramatic decreasing of the CD signal monitored at 222 nm occurred at a concentration of GuHCl at 5.8 M (Figure 3.61).

PEN-2 is a protein rich in aromatic amino acids with 11 phenylalanine (9.5%), 6 tyrosine (5.2%) and 6 tryptophan residues (5.2%) within its 112 amino acids sequence. The near-UV CD spectrum of PEN-2 recorded in FOS-14 detergent showed a high peak with positive ellipticity at 290 nm which could be a combined contribution from Tyr and Trp residues (Figure 3.62). The flattened positive ellipticity between 255 to 270 nm was attributed to Phe. The high intensity of the near-UV CD spectra indicated a proper tertiary folding of the FOS-14 purified PEN-2.

PEN-2 protein purified in FOS-16 was subjected to a biophysical characterization as well. As shown in Figure 3.63, unlike in FOS-14, the far-UV CD spectra obtained from FOS-16 purified PEN-2 exhibited a lower 222/208 nm ratio of 0.96. Similar to the FOS-14 purified PEN-2, there was no shift of the fluorescence maximum from the thermal unfolding of PEN-2 in the presence of FOS-16 (Figure 3.63).

A temperature dependence of α-helix to β-sheet transition was obtained (Figure 3.64, a). Thermal stability of FOS-16 purified PEN-2 was further evaluated based on the temperature-dependent unfolding (Figure 3.64, b). The half-unfolded state of PEN-2 occurred at a

temperature of 66 °C. The same characterization was performed for the Rho-tagged PEN-2 and the C43 strain expressed PEN-2. Both of them exhibited a similar temperature for the half-unfolded state at around 56 °C in the presence of FOS-14 (Figure 3.65). The secondary structures of PEN-2 were compared (Table 3.8). There was not much difference in the secondary structure contents between the obtained PEN-2 proteins. All of them exhibited a helical structure of 59 - 60%.

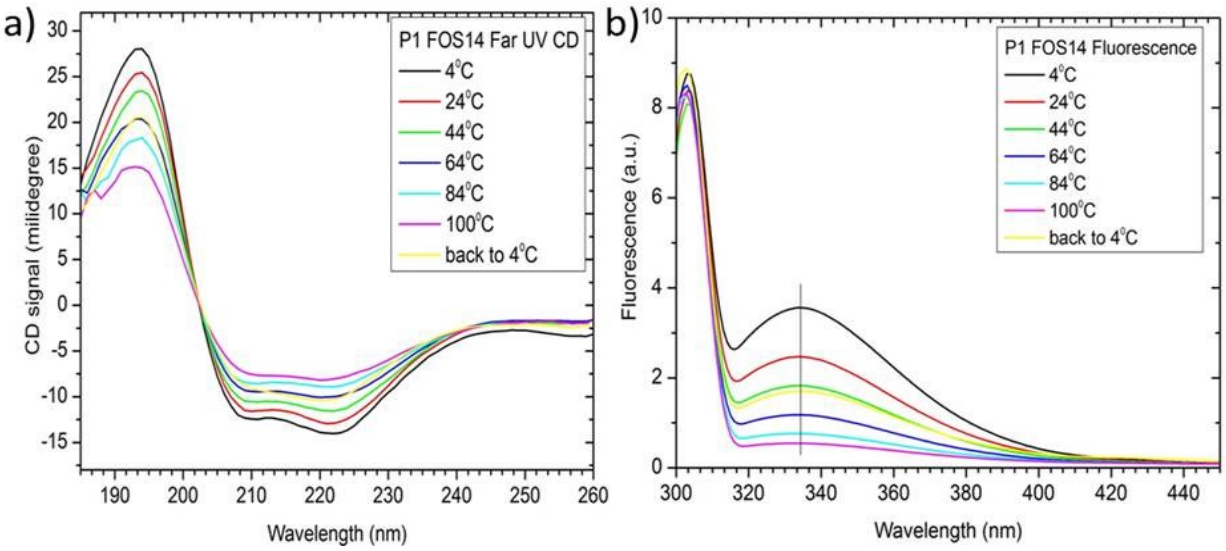

Figure 3.59 Far-UV CD and fluorescence spectra of PEN-2 in FOS-14.
Far UV circular dichroism and fluorescence signals were recorded for FOS-14 purified dimeric PEN-2 (from 4 °C to 100 °C with every 20 °C intervals). An additional spectrum was measured after the samples cooled back to 4 °C (spectra shown in yellow).

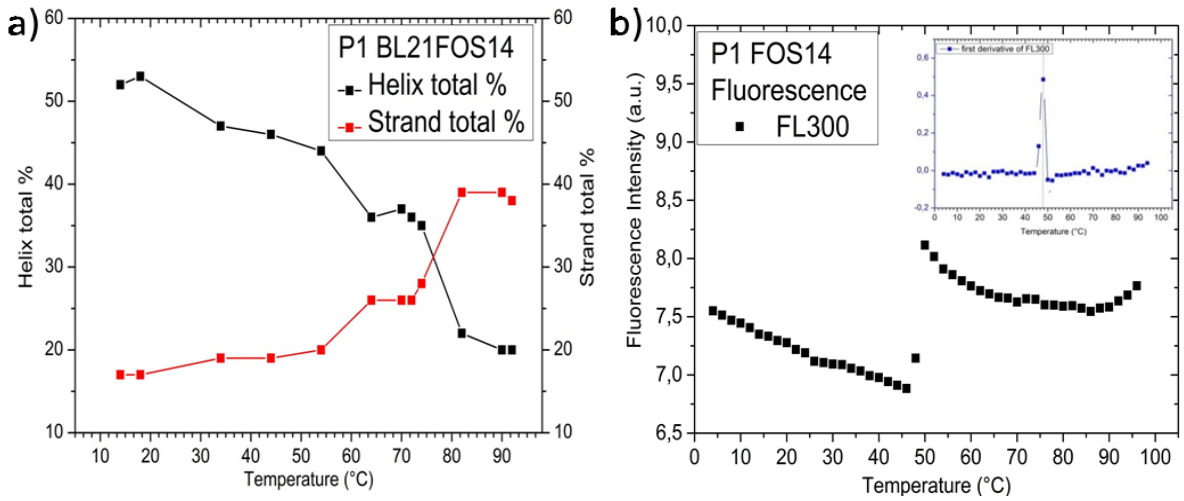

Figure 3.60 Thermal unfolding of PEN-2 in FOS-14.
(a) Plotting of secondary structure content against temperature showed a three-state transition. An intermediate plateau was observed at a temperature between 64 °C to 74 °C. (b) Fluorescence signals at

300 nm were plotted against temperature. Insert: first derivative plot of the fluorescence signal at 300 nm. A signal jump around 50 °C was observed.

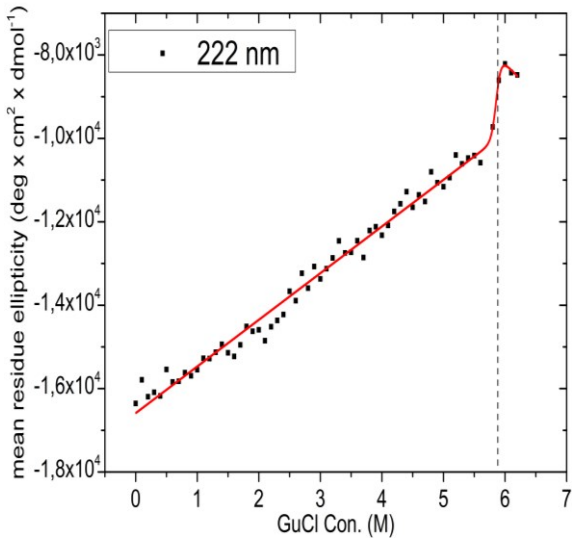

Figure 3.61 GuCl induced denaturation of PEN-2.

The chemical induced denaturation of PEN-2 was achieved by titration of guanidine hydrochloride (GuHCl). The α-helical structure of PEN-2 was partially resistant to the denaturation additive. The significant decrease of the CD signal monitored at 222 nm happened until the concentration of GuHCl reached 5.8 M.

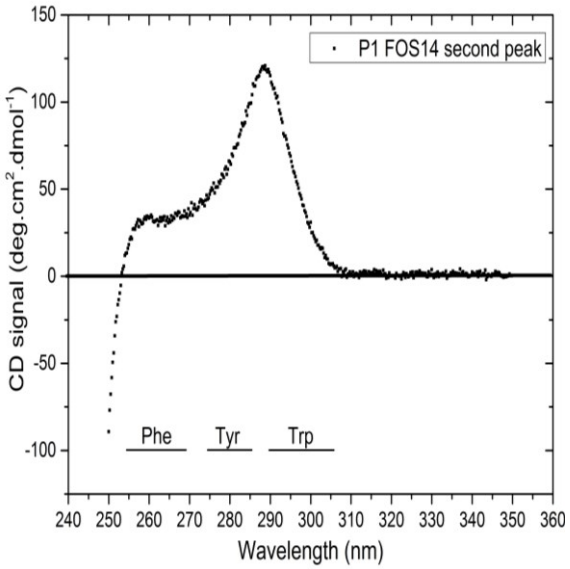

Figure 3.62 Near-UV CD spectra of PEN-2 in FOS-14.

The corresponding contribution region of each aromatic amino acid was marked in the spectrum. The high peak with positive ellipticity at 290 nm could be from a combined contribution from Tyr and Trp residues which indicated a proper tertiary folding of the FOS-14 purified PEN-2 protein.

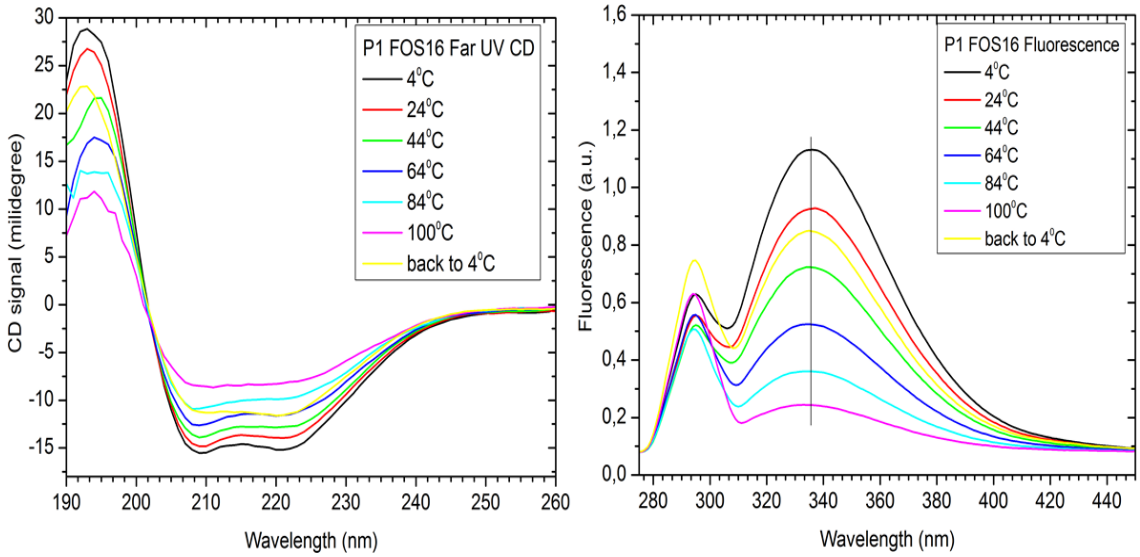

Figure 3.63 Far-UV CD (left) and Fluorescence spectra (right) of FOS-16 purified PEN-2.

Far UV circular dichroism and fluorescence signals were recorded for FOS-16 purified dimeric PEN-2 (from 4 °C to 100 °C with every 20 °C intervals). An additional spectrum was measured after the samples cooled back to 4 °C (spectra shown in yellow).

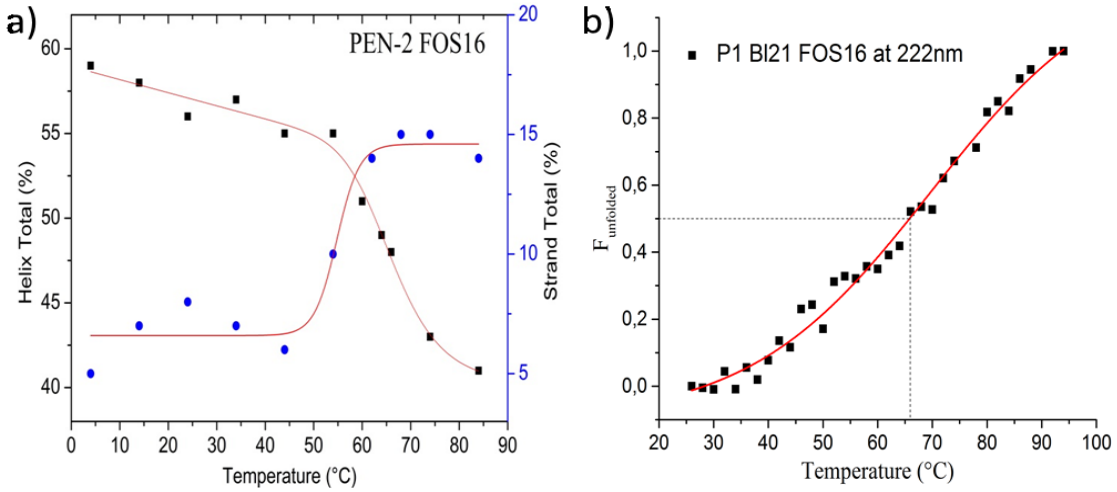

Figure 3.64 Thermal unfolding of PEN-2 in FOS-16

(a) Secondary structure content from FOS-16 purified PEN-2 showed a two-state transition upon thermal denaturation with a transition temperature around 55 °C. (b) Temperature dependence of the unfolded fraction of FOS-16 purified PEN-2. The temperature for the half-unfolded state of PEN-2 was indicated by dashed lines.

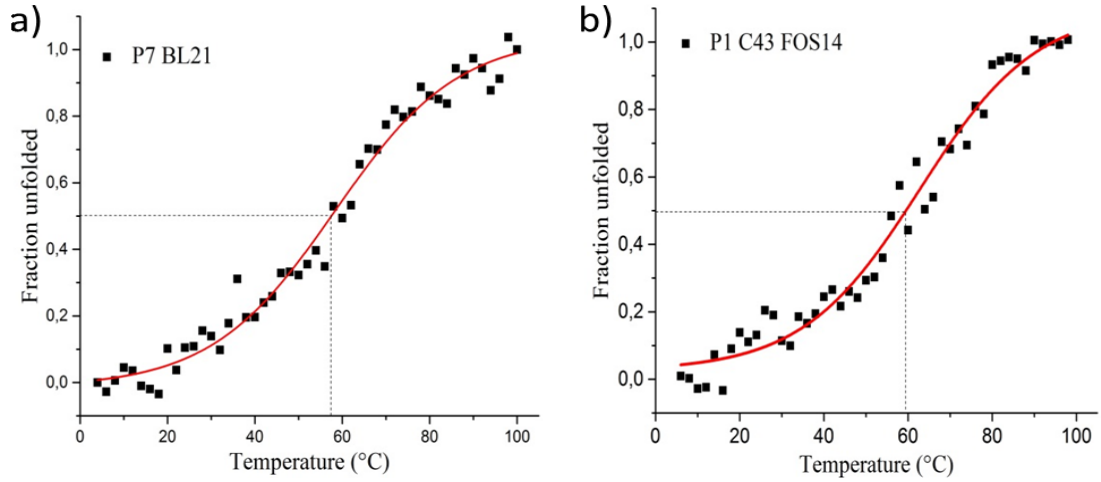

Figure 3.65 Thermal unfolding of different PEN-2 proteins.

Fraction unfolded was calculated based on the CD signals of (**a**) FOS-14 purified Rho tagged PEN-2 (P7) and (b) FOS-14 purified PEN-2 (from *E.coli* C43 strain expression). The temperature for the half-unfolded state of PEN-2 was indicated by dashed lines.

Table 3.8 Deconvolution of CD data for PEN-2 proteins.

Protein	Helix 1	Helix 2	Strand 1	Strand 2	Turns	Unordered	Total	NRMSD
P1 BL21 FOS-14	0.42	0.18	0.04	0.03	0.09	0.23	0.99	0.014
P1 BL21 FOS-16	0.39	0.20	0.02	0.03	0.11	0.24	0.99	0.024
P1 C43 FOS-14	0.46	0.15	0.11	0.03	0.08	0.16	0.99	0.009
P7 BL21 FOS-14	0.41	0.18	0.03	0.03	0.10	0.26	1.01	0.016

Solutions from the CDSSTR method using reference dataset SMP180 (DichrWeb)[180]

3.4.3 Presenilin 1

The secondary, tertiary structure and thermal stability of wild-type full-length Presenilin 1 and its mutation were characterised as described below.

3.4.3.1 H1

As described in section 3.2.3.3.1, two oligomeric species of Presenilin 1 full-length protein were obtained from SEC (hexamer and trimer). There are five cysteine residues in the Presenilin 1 protein sequence. The odd number of cysteine allows forming different disulphide bonds between two or more closely enough molecules. Different reducing reagents (TCEP, DTT and β-ME) were introduced in the purification steps. Biophysical characterization of the hexametric Presenilin 1 full-length protein in TCEP and DTT (or monomeric in β-ME) was carried out.

As shown in Figure 3.66 (right panel), the highest intensity of the fluorescence signal was obtained from the hexametric Presenilin 1 in the presence of TCEP, which indicated a better folded tertiary structure.

High concentrations of reducing reagents showed significant influence on the far-UV CD signal in the lower wavelength range. Therefore, protein buffers were exchanged to a CD compatible buffer containing 1mM reducing reagent before performing CD measurements. Slight differences were observed for the proteins with different reducing environment (Figure 3.66, left panel). In contrast to the fluorescence results, the hexametric Presenilin 1 measured in the CD buffer supplemented with 1mM DTT exhibited the highest helical content of 44%, while the hexameric proteins purified with 1mM TCEP contained only 37% helical structure (Table 3.9). Nevertheless, more degradation fragments were observed for the DTT sample (Figure 3.67). A possible explanation for the higher secondary structure content of DTT sample was that the fragments (between 31 to 42 kDa) existed in the DTT purified Presenilin 1 proteins contributed to the overall far-UV CD data (Figure 3.67). Although no significant change was detected from the SDS-PAGE, a slight loss of helical structure upon overnight storage was observed for the hexameric Presenilin 1 protein indicating a low stability. Despite the high yield and purity of the β-ME samples on the SDS-PAGE, it was speculated that the monomer peak of Presenilin 1 full-length protein obtained in β-ME might be partially denatured. This speculation was confirmed by both fluorescence intensity and far-UV CD data (with the lowest content of helical structural elements).

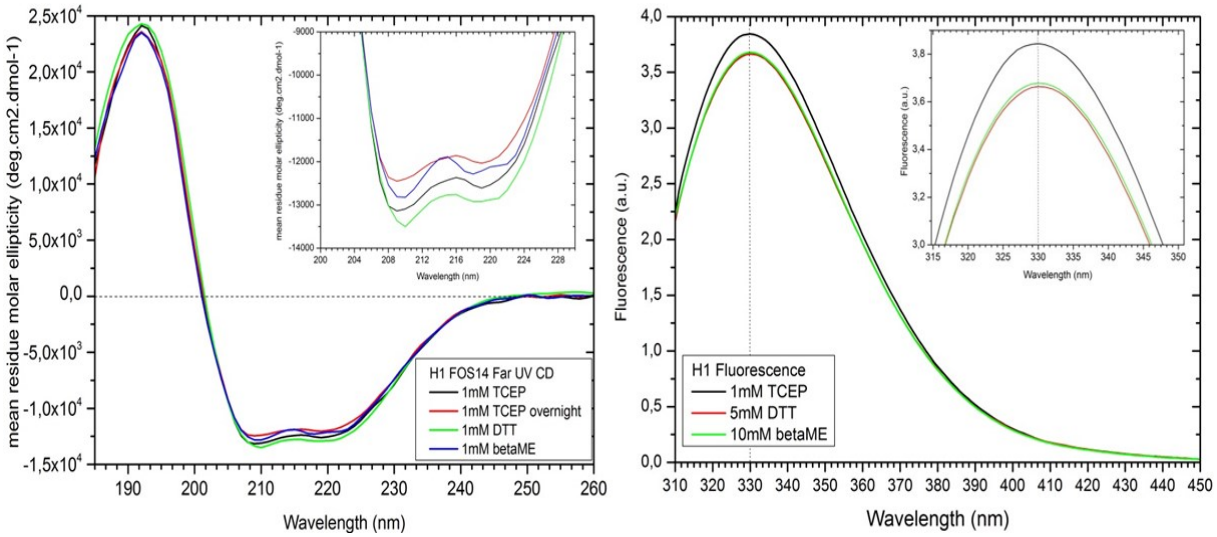

Figure 3.66 Effect of reducing reagent on hexametric Presenilin 1.

Left panel: CD spectra of PS1 in the present of different reducing reagents (measured at 4 ºC); Right panel: fluorescence spectra of PS1 in the original SEC buffer supplied with different reducing reagent (excitation wavelength: 295 nm).

Table 3.9 Deconvolution of CD data for Presenilin 1 supplemented with different reducing reagents.

Protein	Helix 1	Helix 2	Strand 1	Strand 2	Turns	Unordered	Total
H1 FOS-14+1mM TCEP	0.21	0.16	0.12	0.08	0.12	0.31	1
H1 FOS-14+1mM TCEP overnight	0.20	0.16	0.14	0.08	0.12	0.31	1.01
H1 FOS-14+1mM DTT	0.26	0.17	0.08	0.06	0.12	0.30	0.99
H1 FOS-14+1mM β-ME	0.19	0.15	0.14	0.08	0.12	0.31	0.99

Deconvolution by CDSSTR using reference data set SMP180 (DichroWeb)

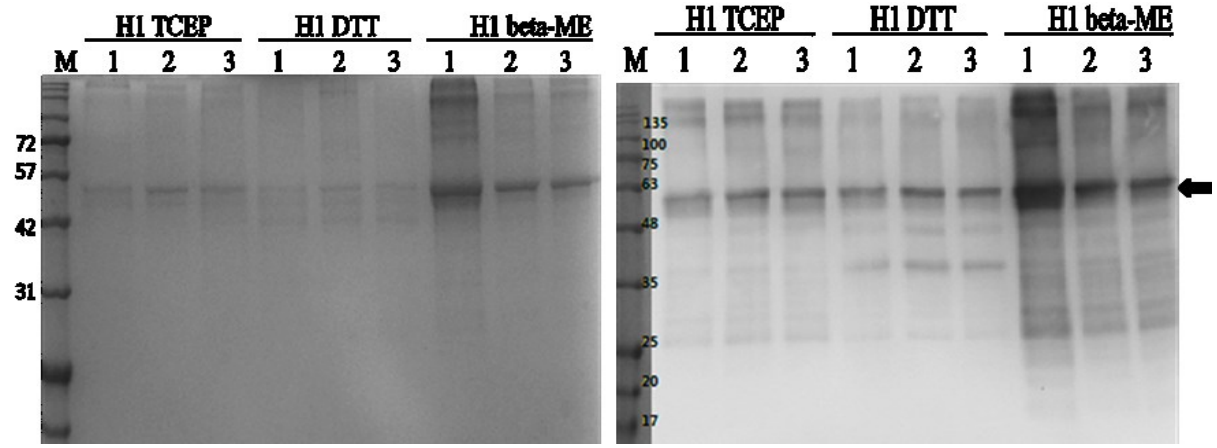

Figure 3.67 SDS-PAGE of hexameric Presenilin 1 purified using different reducing reagent.

1: protein samples in the purification buffer. 2: protein samples in the CD buffer; 3: protein samples in the CD buffer after overnight storage. Left panel: Blue stained SDS-PAGE; Right panel: Western blotting against His-tag.

Figure 3.68a shows the far-UV CD spectra of the FOS-14 purified trimeric Presenilin 1 full-length protein at different temperatures. The purity of the protein was validated from silver-blue stained SDS-PAGE (Figure 3.76). The upper band, which appeared in the range between 100 kDa to 125 kDa, was proved to be the SDS-resistant oligomers of Presenilin 1 by western blot. Plots of the CD signals at 208 nm and 221 nm *versus* temperature gave a melting temperature of 47.8 °C and 46.8 °C, respectively (Figure 3.68b). The intrinsic tryptophan fluorescence emission maximum of the native state (at 4°C) FOS-14 purified Presenilin 1 was at 330 nm (Figure 3.69, right panel). A gradual quenching of the fluorescence signal accompanying with a red shift (to 332 nm) was observed upon heating indicating an exposure of tryptophan side chains to a more polar microenvironment. There is 23 phenylalanine (4.7%), 19 tyrosine (3.9%) and 8 tryptophan residues (1.6%) in the 487 amino acids sequence of the full-length Presenilin 1. The near-UV CD spectra of hexametric and trimeric Presenilin 1 were overlaid in Figure 3.69 (left panel). Both of them showed two distinct peaks from phenylalanine between 250 to 270 nm. The differences in the intensity of the Phe peaks and the shapes of tyrosine and tryptophan peaks indicated distinctive conformations were adopted in these two oligomers surrounding the aromatic amino acid residues.

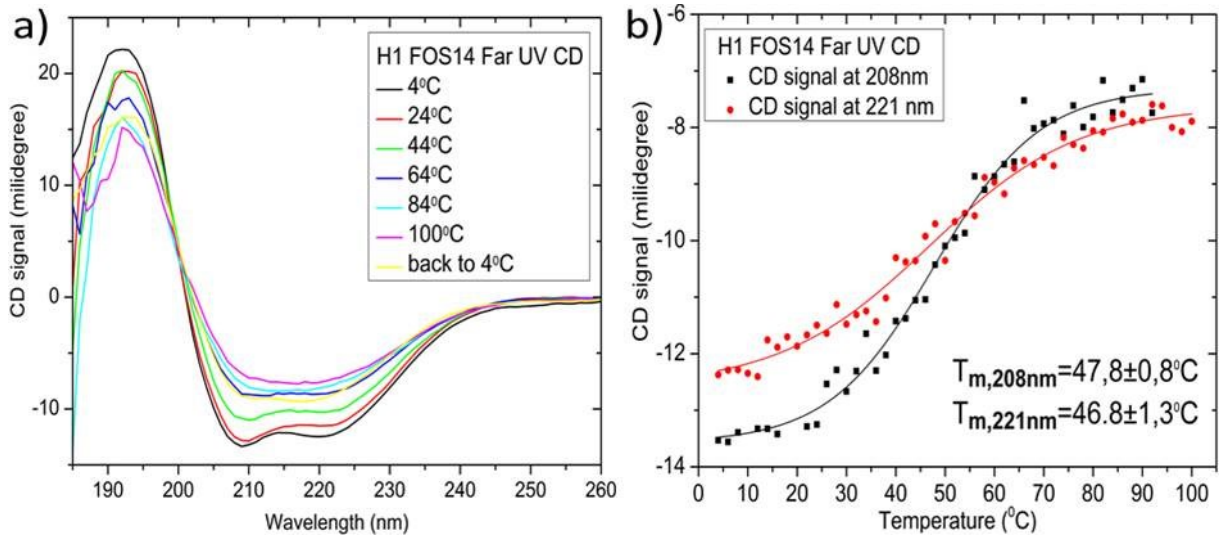

Figure 3.68 Far-UV CD spectra and thermal stability of FOS-14 purified Presenilin 1.
(a) Far UV circular dichroism signals were recorded for FOS-14 purified trimeric PS1 from 4 °C to 100 °C with every 20 °C intervals. An additional spectrum was measured after the samples cooled back to 4 °C (yellow). (b) T_m obtained based on CD signals at 208 nm and 222 nm.

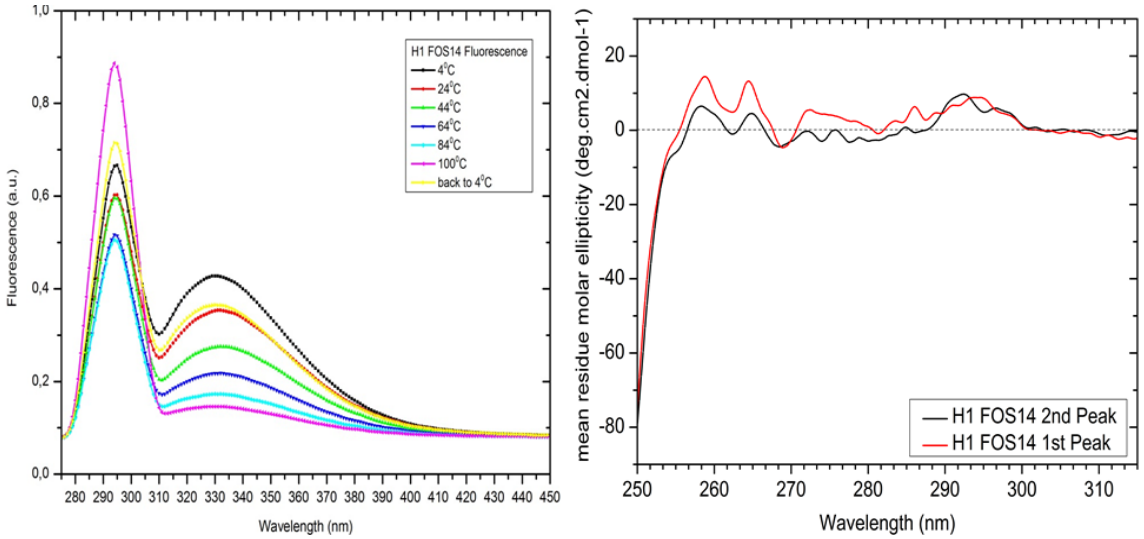

Figure 3.69 Fluorescence and near-UV CD spectra of FOS-14 purified Presenilin 1.
Left panel: fluorescence spectra were recorded for FOS-14 purified trimeric PS1 from 4 °C to 100 °C with every 20 °C intervals. An additional spectrum was measured after the samples cooled back to 4 °C (yellow). Right panel: near UV CD spectra of hexametric and trimeric PS1. Both of them exhibited a folded tertiary structure.

The CD and fluorescence spectra measured for FOS-16 purified trimeric Presenilin 1 were shown in Figure 3.70. It was an irreversible process of the thermal unfolding as well. Although there is a 92% recovery of the fluorescence intensity when cooling the sample back to 4 °C after temperature experiment, the high intensity of the scattering peak (at 295 nm) indicated a larger aggregation formation in the solution. The SDS-resistant aggregates were observed on the top of the SDS-PAGE after thermal unfolding (Figure 3.76). Analysis of CD signals at 208 and 221 nm as a function of temperature showed the melting points at 58 °C and 55.3 °C, respectively (Figure 3.71, right panel). The considerable difference in the thermal stability between the FOS-14 and FOS-16 purified Presenilin 1 is shown in Figure 3.71 (left panel). The FOS-16 purified presenilin 1 showed a higher thermal stability comparing to the FOS-14 purified protein.

From the deconvolution results of the far-UV CD data obtained at 4 °C, both FOS-14 and FOS-16 purified trimeric presenilin 1 proteins showed the same α-helical content of 41% with a slight difference of the β-strand content, 13% in FOS-14 versus 16% in FOS-16 (Table 3.10). These secondary structural contents were still 5% lower than the calculated value from the EM structure [131] (Table 3.6). Comparison of the tertiary structures of Presenilin 1 protein in different detergent environments was shown in Figure 3.75. Observations of the changes in the peak shape and intensity confirmed a detergent-induced alteration of the tertiary structure of Presenilin 1. The factors which are responsible for the shape and magnitude of near-UV CD spectrum of a protein include the number of aromatic amino acid residues, interaction among

the neighbouring aromatic amino acid residues, protein rigidity, hydrogen bond, polarizability, etc. [144,185]. FOS-14 and FOS-16 share the same chemical head group, but they have different carbon chain length, therefore the have different aggregation numbers and micelle sizes in the solution. The coverage (or interaction) of the detergents to the membrane protein hydrophobic regions could be then different which resulted in the change in the three-dimensional structure of Presenilin 1 in the presence of detergent of varied chain length. The difference in the secondary structure melting temperature indicated that the FOS-16 purified Presenilin 1 exhibited a better thermal stability comparing to the FOS-14 purified protein.

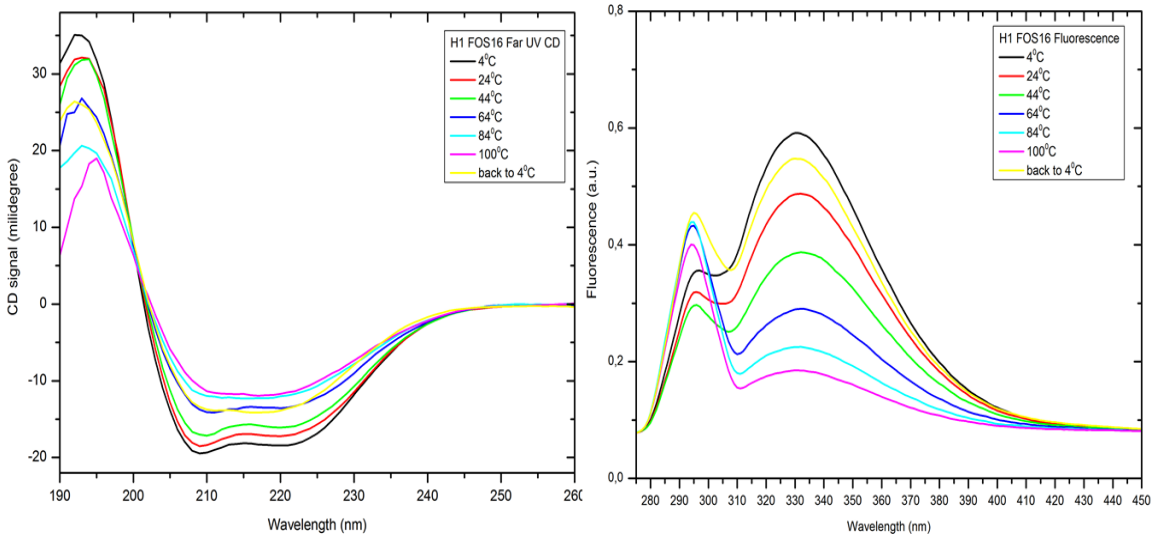

Figure 3.70 Far-UV CD (left) and fluorescence (right) spectra of FOS-16 purified Presenilin 1.

Far UV circular dichroism and fluorescence signals were recorded for FOS-16 purified trimeric PS1. Far-UV CD and fluorescence spectra were shown from 4 °C to 100 °C with every 20 °C intervals. An additional spectrum was measured after the samples cooled back to 4 °C (yellow).

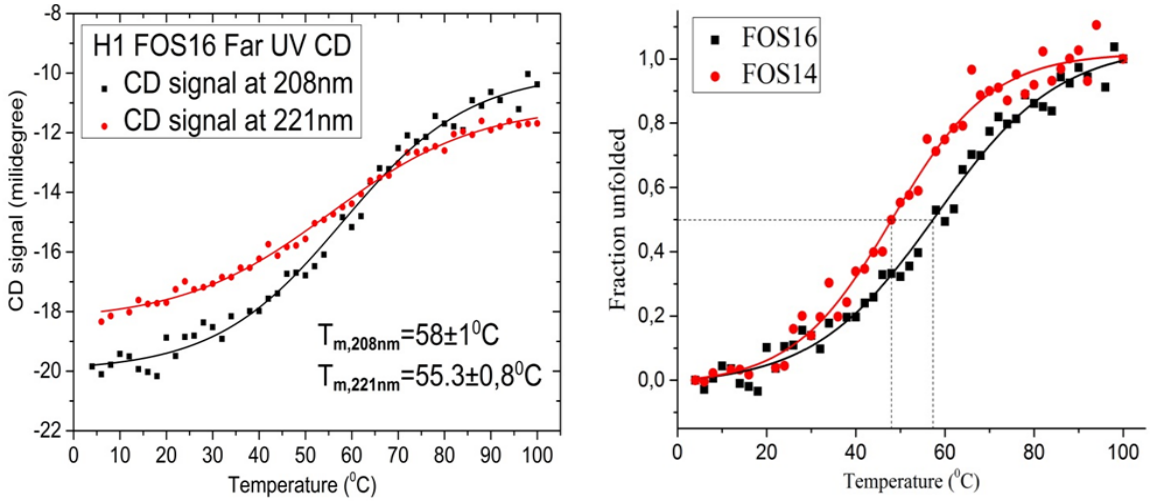

Figure 3.71 Thermal stability of Presenilin 1.

(a) T_m obtained from far-UV CD signals at 208 nm and 222 nm of FOS-16 purified presenilin 1. (b) Comparison of temperature-dependent fraction unfolding of FOS-14 and FOS-16 purified presenilin 1.

3.4.3.2 DelE9

Presenilin 1 DelE9 was designed with a deletion of the sequence in the exon E9 region. The far-UV CD spectrum of Presenilin 1 DelE9 trimeric protein acquired at 4 °C exhibited a predominantly α-helical protein with minima at 209 and 221 nm (Figure 3.72, left panel). However, the deconvolution result showed a 35% helical and 22% β-sheet content (Table 3.10). The blue-silver stained SDS-PAGE of CD samples showed a smear band with one dominate upper edge and one weaker lower edge between 40-50 kDa (Figure 3.74, left panel). Western blot confirmed positive signals for both edges (Figure 3.74, right panel). This diffuse band might reflect the structural heterogeneity of protein-detergent complexes, which bound a varied amount of SDS molecules. The unfolded fraction was calculated based on the CD signal at 209 nm and was compared for FOS-14 and FOS-16 purified DelE9 protein (Figure 3.72). Unlike the full-length protein, there was no observation of a significant difference in thermal stability for DelE9 in the presence of different detergents; both showed a half-unfolded state at 56 °C.

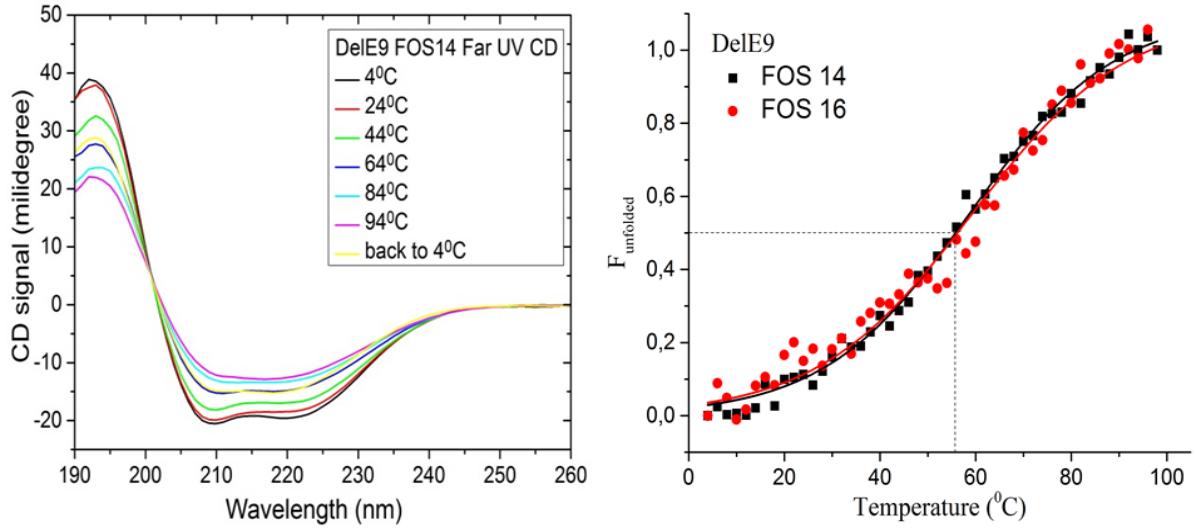

Figure 3.72 Far-UV CD spectra and thermal stability of DelE9.
(a) Far UV circular dichroism signals for FOS-14 purified trimeric DelE9 mutation from 4 °C to 100 °C with every 20 °C intervals. An additional spectrum was measured after the samples cooled back to 4 °C (yellow). (b) Comparison of unfolded fractions between FOS-14 and FOS-16 purified DelE9 proteins.

Different from the Presenilin wildtype protein, DelE9 showed a constant fluorescence emission maximum at 333 nm through the temperature experiment (Figure 3.73, left panel). Fluorescence emission intensity at 333 nm recovered to ca. 76% of the initial value when cooling the protein sample back to 4 °C after thermal denaturation (yellow curve in Figure 3.73,

left panel).This recovery indicated a dynamic stability of the detergent purified DelE9 protein. DelE9 Presenilin 1 construct has 23 phenylalanine (5%), 18 tyrosine (3.9%) and 7 tryptophan residues (1.5%). From the near-UV CD spectra, the trimeric DelE9 protein showed a higher intensity of the Trp peak than the hexameric protein (Figure 3.73, right panel). Although one Tyr and one Trp residues were deleted from the wild-type construct, the near-UV spectra of FOS-14 purified DelE9 exhibited similar magnitude in the Trp peak region compared to the wildtype Presenilin 1 near-UV CD spectra (Figure 3.75). Different peak shapes were observed mainly in the wavelength range typical for Tyr.

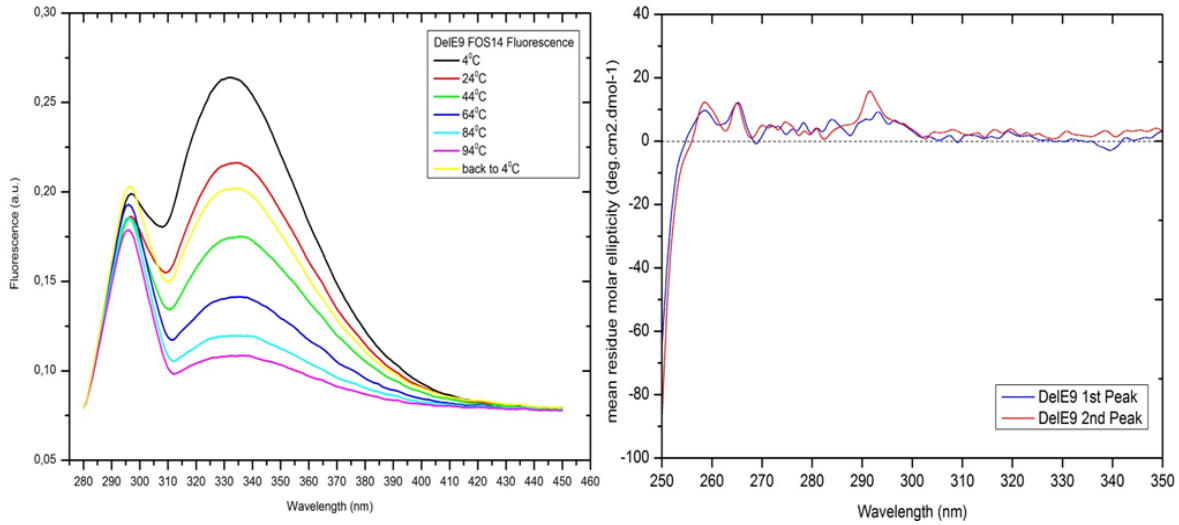

Figure 3.73 Fluorescence and near-UV CD spectra of FOS-14 purified DelE9.
Left panel: Fluorescence spectra for FOS-14 purified trimeric DelE9 from 4 °C to 100 °C. An additional spectrum was measured after the samples were cooled back to 4 °C (yellow). Right panel: near UV CD spectra of hexametric and trimeric DelE9. The trimeric DelE9 protein showed higher signal intensity in the tryptophan emission region (290-300 nm).

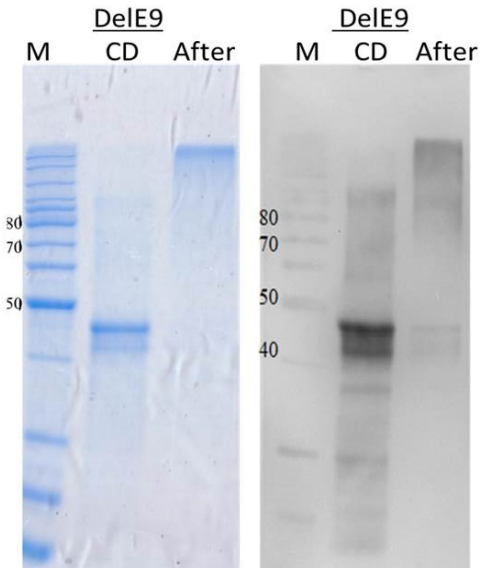

Figure 3.74 SDS-PAGE of DelE9 far-UV CD measurement samples.
Left panel: blue-silver stained SDS-PAGE of Presenilin DelE9 mutation protein CD samples. Right panel: anti-His western blot of Presenilin DelE9 mutation protein CD samples. SDS-resistant protein aggregates were observed on the top of the gel after thermal denaturation (marked as After).

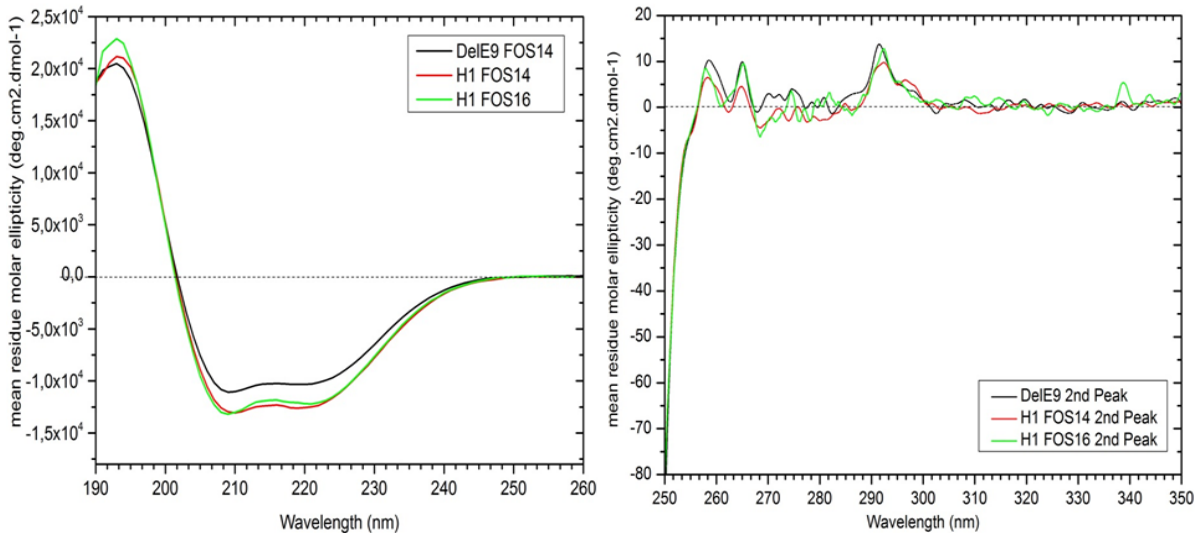

Figure 3.75 Comparison of Presenilin 1 proteins CD spectra.

Left panel: far-UV CD spectra of FOS-14 purified Presenilin DelE9 mutation (black), FOS-14 purified PS1 (red) and FOS-16 purified PS1 (green). Right panel: near UV CD spectra of FOS-14 purified Presenilin DelE9 mutation (black), FOS-14 purified PS1 (red) and FOS-16 purified PS1 (green).

Table 3.10 Deconvolution of CD data for Presenilin 1 constructs.

Protein	Helix 1	Helix 2	Strand 1	Strand 2	Turns	Unordered	Total	NRMSD
H1 FOS-14	0.23	0.18	0.07	0.06	0.13	0.32	0.99	0.021
H1 FOS-16	0.23	0.18	0.09	0.07	0.13	0.30	1	0.028
DelE9 FOS-14	0.18	0.17	0.13	0.08	0.13	0.32	1.01	0.012
DelE9 FOS-16	0.17	0.16	0.16	0.08	0.12	0.31	1	0.017

Deconvolution by CDSSTR using reference data set SMP180 (DichrWeb)

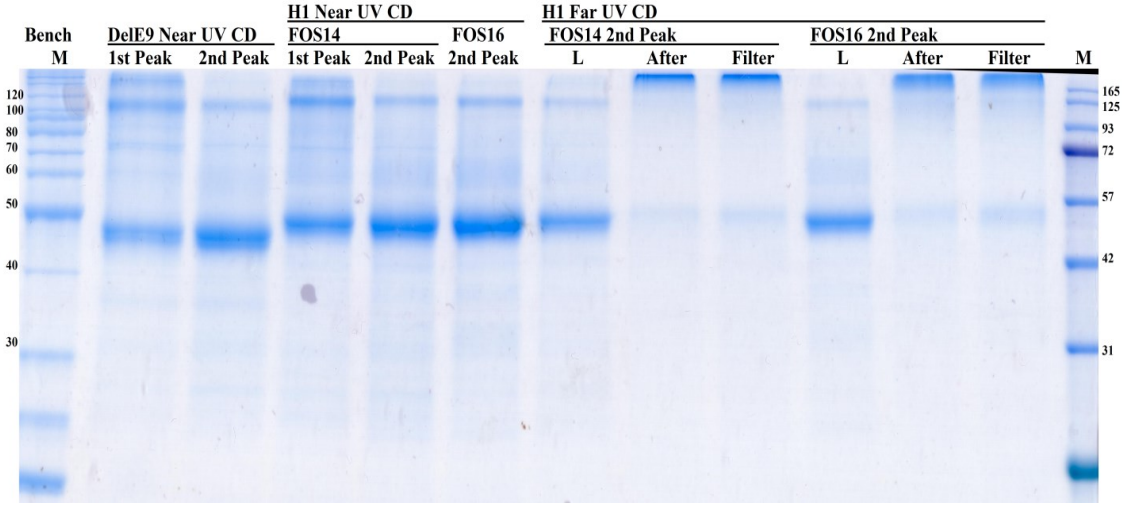

Figure 3.76 SDS-PAGE analysis of Presenilin 1 CD spectroscopy samples.

3.5 Crystallisation of different components

Crystallisation screens were performed for each individually purified protein. Apart from this, as presenilin and PEN-2 were supposed to form sub-complex in the γ-secretase, these two detergent purified proteins were directly mixed together with monoolein for crystallisation trials using the lipid cubic phase (LCP) method. The same method was applied to nicastrin and APPC100, as physically interactions of these two proteins were observed in the pull-down assays.

For nicastrin alone, since it has only one short C-terminal transmembrane domain (21 amino acids out of 692 amino acids), the detergent-purified protein was screened using conventional vapour diffusion crystallisation method as well. The crystallisation condition for nicastrin was optimised by varying the dilution factor of the reservoir (evaporation rate). After optimisation, crystals were obtained in 1.5 M $LiSO_4$, 0.1 M HEPES 7.5 from 1 to 1 dilution of 15 mg/mL protein with the reservoir.

PEN-2 protein was screened with monoolein (using the LCP method as well as the monoolein pre-coated MRC plates) and the normal vapour diffusion method. Small crystals were firstly observed under the condition with CAPS 10.5 and 30% PEG400 using a concentration of 5mg/mL protein mixing with 1/6 diluted reservoir (Figure 3.77). PEG screens and pH screens were performed to optimise the condition. Considering the evidence that PEN-2 interact with ferritin light chain[103], $FeCl_3$ was also added to the purified PEN-2 protein before crystallisation. In addition to detergent and LCP crystallisation, the crystallisation experiment for PEN-2 was also performed using the bicelle crystallisation method. In these experiments, different molar ratios of DMPC: CHAPSO were tested, but no protein crystals appeared so far. Apart from the condition mentioned above, PEN-2 crystals also appeared in 0.2 M $MgCl_2$, 0.1 M Imidazole pH 8 with 15% ethanol while using a 1 to 1 ratio of 15 mg/mL protein with the reservoir.

Obtained crystals were sent to ESRF (Grenoble) and Petra beam line (DESY, Hamburg). However, no diffraction was detected. The non-diffractive crystals were checked by western blotting to confirm the existence of the target proteins (Figure 3.78).

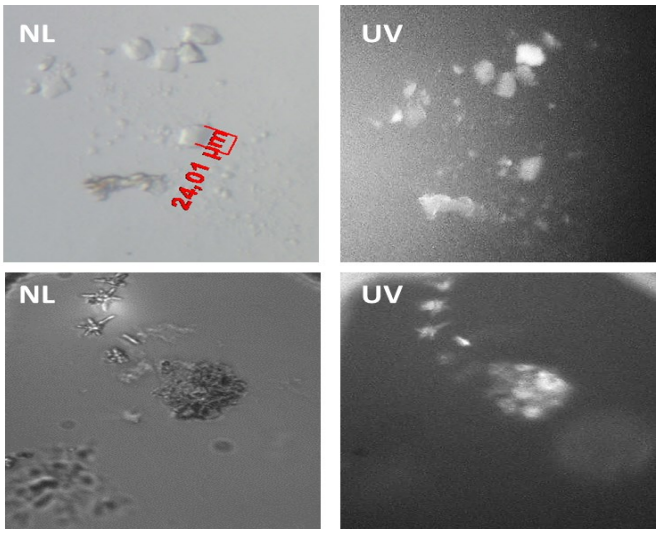

Figure 3.77 Crystals of PEN-2 and NCT.
NL: observation under normal light; UV: observation under UV. Upper panel: PEN-2 crystals observed after 1-month incubation at 18 °C. Lower panel: NCT crystals after optimisation.

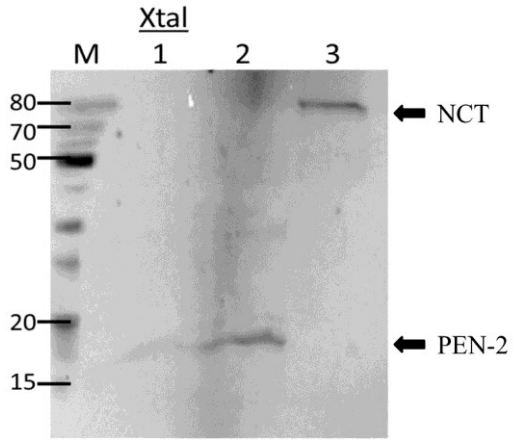

Figure 3.78 Western blot of the crystals of PEN-2 and nicastrin.
Lane 1: PEN-2 crystal sample (0.1 M CAPS pH10.5, 30% PEG400, with 1 µL 5 mg/mL protein + 1 µL 1/6 dilution reservoir). Lane 2: PEN-2 crystal sample (0.2 M $MgCl_2$, 0.1 M Imidazole pH 8, 15% Ethanol, with 1 µL 15 mg/mL protein + 1 µL reservoir). Lane 3: nicastrin crystal sample (1.5 M $LiSO_4$, 0.1 M HEPES 7.5, with 1 µL 15 mg/mL protein + 1 µL reservoir).

3.6 Reconstitution of γ-secretase sub-complexes

Presenilin (PS) is known to be the catalytic subunit of the γ-secretase complex. It is cleaved into an N-terminal and a C-terminal fragment upon activation. The complex of these two fragments will function as the active enzyme. PEN-2 is the Presenilin enhancer which is suggested to trigger the self-cleavage of presenilin protein. There is evidence showed that the sub-complex of these two components is catalytically active as γ-secretase [47]. The reconstitution and co-expression of the active sub-complex (Presenilin and PEN-2) were performed.

3.6.1 Direct assembly in detergent

The formation of Presenilin and PEN-2 sub-complex was firstly investigated by direct incorporation of detergent purified proteins. Detergent purified Presenilin and PEN-2 showed distinct peaks on a Superdex 200 column. The peak from the protein mixture of these two overlaid perfectly with the SEC profiles obtained from the respective protein (Figure 3.79)

which indicated no sub-complex formation under this condition. This was at least partially due to the homo-oligomers or the presence of detergent covering the interacting regions.

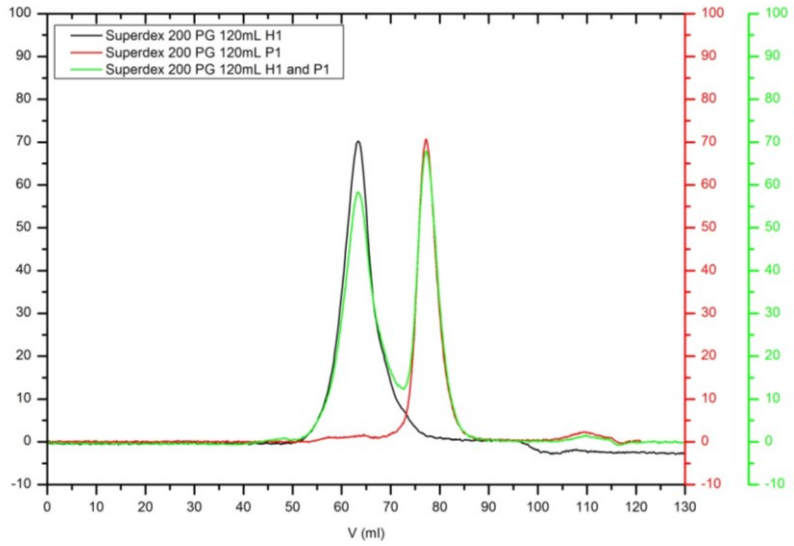

Figure 3.79 SEC profiles of Presenilin 1, PEN-2 and a mixture of these two proteins.
Detergent purified dimeric PEN-2 (red), trimetric PS1 (black) and the mixture of two proteins (green) were applied to SEC separately. The Absorption is given in units of mAu. There is no observation of a complex formation upon directly mixing the individually purified proteins.

3.6.2 Co-expression of Presenilin and PEN-2

Co-expression promotes protein interaction directly after the expression, which might give a higher chance to form sub-complex. The polyhistidine-tagged presenilin constructs and Rho-tagged PEN-2 constructs were co-transformed to investigate the sub-complex formation. Two plasmids were transformed together into either *E. coli* BL21 (DE3) or C43 strain. The expression of two proteins was cross-checked by western blotting against different tags. Both of the proteins were expressed by BL21 (DE3) strain, and no signal was detected from C43 strains (Figure 3.80). Several distinctive degradation bands were observed in the harvested cell samples (Figure 3.80).

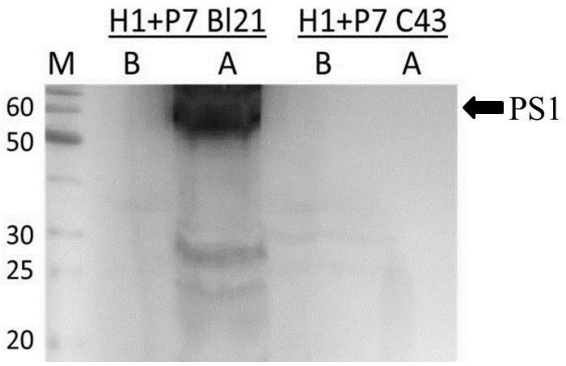

Figure 3.80 Co-expression of Presenilin 1 and PEN-2 in different *E. coli* strains.
Co-expression cells were collected and opened before and after induction. B: Cell samples took before induction; A: Cell samples were taken after induction. No target protein was expressed in the *E. coli* C43 strain.

Similar to the individual proteins, FOS-Choline detergents showed the best solubility in the

detergent screen for the co-expressed Presenlin1 and PEN-2 proteins. Mild detergents, like CHAPSO, could poorly solubilize the target proteins (data not shown). The affinity purification of co-expressed Presenilin 1 and PEN-2 was performed using Ni-NTA resin (Figure 3.81). Apart from the full-length protein signal, four more distinctive bands were detected in the elution fractions with different binding affinity to the affinity resin. From the SEC performed in FOS-14, two major peaks were partially separated with an intermediate species (Figure 3.82). According to the calibration, the three species had an apparent molecular mass of 189 kDa (I), 95 kDa (II) and 47.5 kDa (III), respectively. The apparent molecular weight of the sub-complex in the detergent micelle is expected to be ca. 110 kDa. Based on the size and the higher 260 to 280 ratio, the third peak contained mainly detergent micelles.

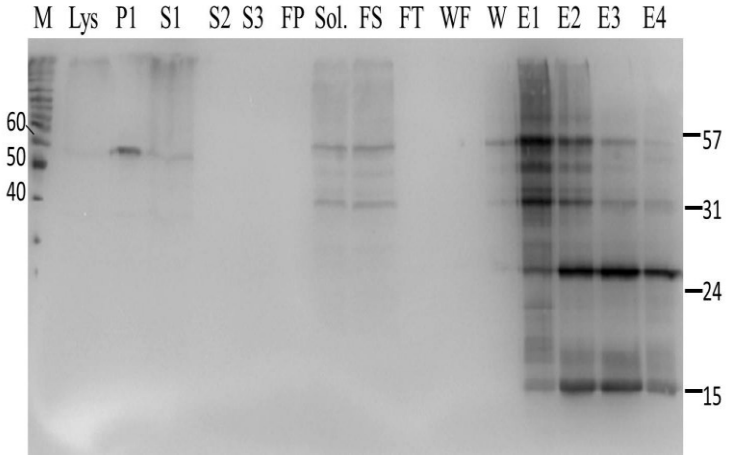

Figure 3.81 Ni-NTA affinity purification of co-expressed Presenilin 1 and PEN-2.
P1 and S1: pellet and supernatant after 900 g centrifugation; S2 and S3: supernatant after 9000 g and 100 000 g; FS and FP: supernatant and pellet after FOS-14 solubilization; WF and W: the last and total wash sample; Monoclonal anti-polyhistidine-HRP antibody (sigma) was used to probe presenilin. Markers are given in the unit of kDa.

The existence of both proteins in the SEC elution fractions was confirmed by western blotting (Figure 3.83). Both proteins were distributed over all three peaks from the SEC. The most intensive signals from both the His-tagged Presenilin 1 and Rho-tagged PEN-2 were coming from the species II. Compared to the individually purified Presenilin 1, band 1 and 2 showed the same migration behaviour as the full-length protein, while band 3 to 5 appeared to be more distinct in the co-expressed samples (Figure 3.83 b). Band 3 from the western blot has an apparent molecular weight between 31 kDa and 42 kDa, which corresponds to the size of Presenilin 1 N-terminal fragment. Surprisingly, all five western blotting positive bands of Presenilin 1 had their corresponding bands on the anti-Rho western blot for PEN-2 (Figure 3.83). It has been reported that PEN-2 (TM 1) interacts with Presenilin NTF (TM 3 and 4) and could form a detergent (1% DDM) resistant sub-complex [40,85]. On our PAGE, the Rho-tagged PEN-2 proteins were migrated to the same level of His-tagged Presenilin 1 or *vice versa*. A

possible explanation for this behaviour was that the two proteins or one protein with the other fragment formed some SDS-resistant interactions.

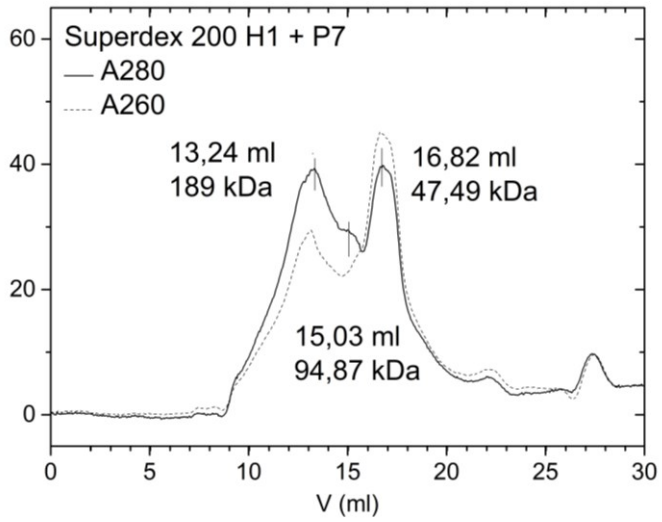

Figure 3.82 SEC profile of co-expression of Presenilin 1 and PEN-2. Superdex 200 10/300GL column was used in the experiment. SEC buffer : 2 CMC FOS-14, 200 mM NaCl, 20 mM HEPES pH 7.4, 1 mM TCEP, 10% Glycerol. The Absorption is given in units of mAu.

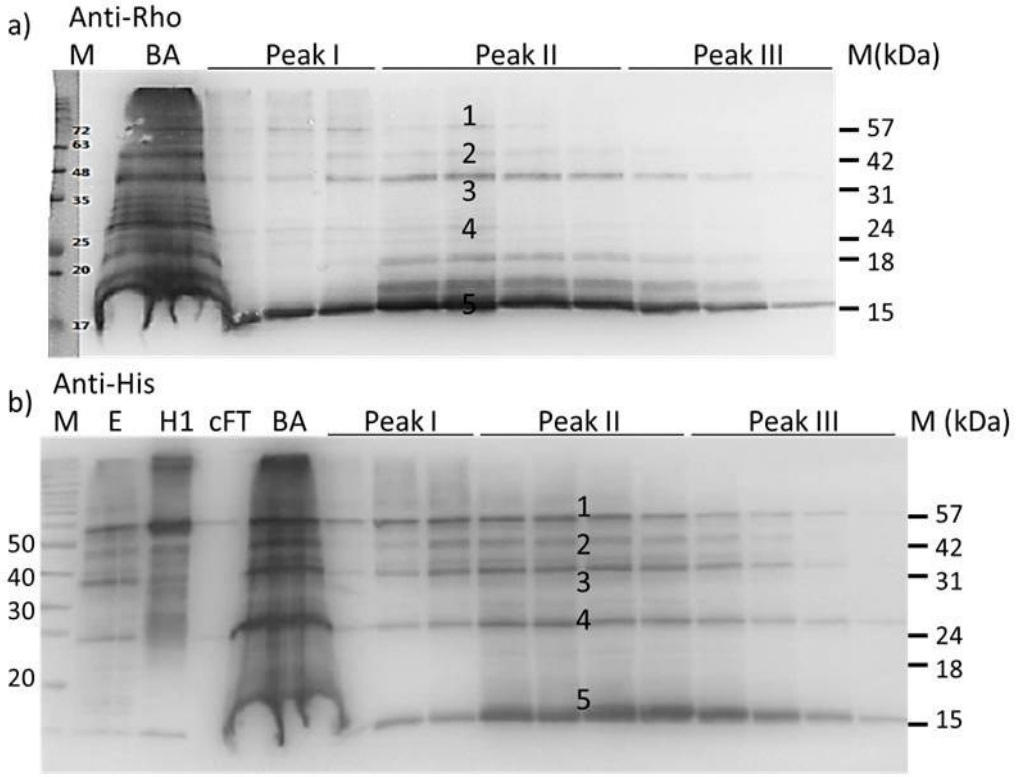

Figure 3.83 Western blot of co-expressed Presenilin 1 and PEN-2 SEC fractions. a) Ani-Rho tag western blot; b) Anti-His tag western blot. E: elution fraction from Ni-NTA purification; H1: control sample of single expressed Presenilin 1 protein; cFT: flow through sample during concentration. BA: concentrated protein samples taken before loading to SEC. Numbers in both PAGE indicating the corresponding position of identical bands.

3.6.3 Liposome-mediate reconstitution

Assembly of the γ-secretase sub-complex was further carried out via reconstitution of Presenilin and PEN-2 into liposomes. To remove the excess amount of detergents, Biobeads SM-2 was used to achieve a step-wise absorption of detergents during the reconstitution. Preliminary experiments were performed to investigation the effect of Biobeads SM-2 on the detergent removal from PEN-2 (Figure 3.84). PEN-2 remained in the supernatant after 3 hours incubation with Biobeads at 4 °C. And after 16 hours absorption, the FOS-14 detergents were completely removed from the protein, as a result, almost all PEN-2 proteins precipitated.

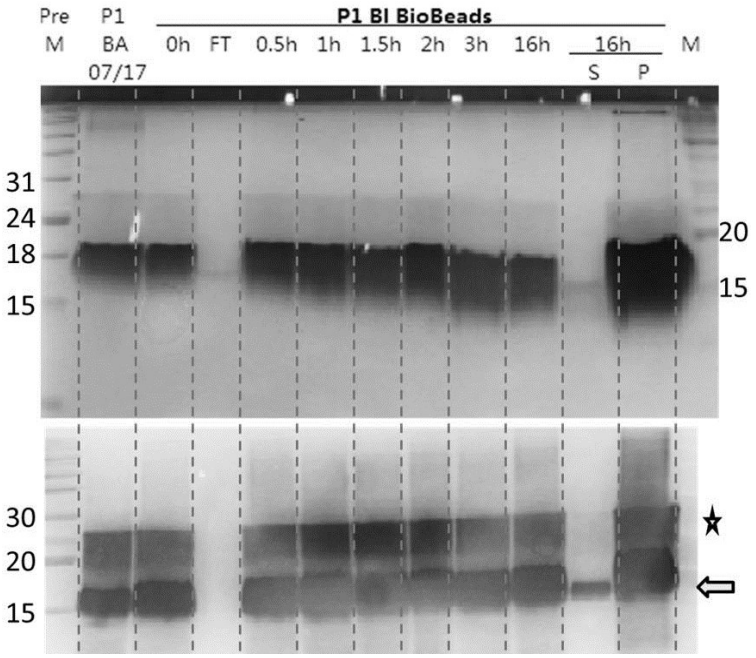

Figure 3.84 Biobeads absorption test of PEN-2. Upper panel: blue stained SDS-PAGE; Lower panel: anti-his tag western blotting. Supernatants at different time points were loaded. Both supernatant and pellet samples were loaded after 16 hours incubation. 0.2g/mL biobeads SM2 was added to the protein-detergent mixture, incubation was performed at 4°C with gentle agitation. Arrow: PEN-2 monomer, star: dimer.

It has been reported that for most membrane proteins, reconstitution is more efficient at a detergent concentration slightly in excess of the detergent-liposome saturation point [162]. From the titration curves of the prepared liposomes with CHAPSO (Figure 3.85), the detergent to liposome ratios at which the vesicles-to-micelles transition initiated and ended were estimated to be 0.17 and 0.69 (mol/mol) for liposomes composed of POPC to PE in a ratio of 4:1; and 0.06 and 0.38 (mol/mol) for the ratio of 9:1 liposomes, respectively. Thus, a detergent to lipid ratio of 0.4 (w/w, for the 4:1 liposome) and 0.28 (w/w, for the 9:1 liposomes) were selected for the reconstitution experiments.

The reconstitution process was monitored by western blot of the samples taken at different steps (Figure 3.86). There was no observation of significant loss of the target proteins during the detergent removal. A slight tendency of aggregation was observed during the DelE9

reconstitution. Over 90% proteins were recovered in the proteoliposome fractions. The reconstituted proteoliposomes could be harvested in the pellet after ultracentrifugation (Figure 3.87 b). Further purification of the obtained proteoliposomes was achieved by the sucrose gradient centrifugation (sucrose floating experiment). As expected, the reconstituted proteoliposomes were floating to the top of the sucrose gradient (Figure 3.87 a) and the impurities or denatured proteins were retained at different layers of the gradients (Figure 3.87 c, yellow arrow). A 50% sample volume increase was observed after dialysis experiments. The success of the insertion of the target proteins into liposomes was confirmed by western blot (Figure 3.88). A decrease of the signal intensity on the western blot of PEN-2 to Presenilin 1 ratio is observed in the samples after dialysis.

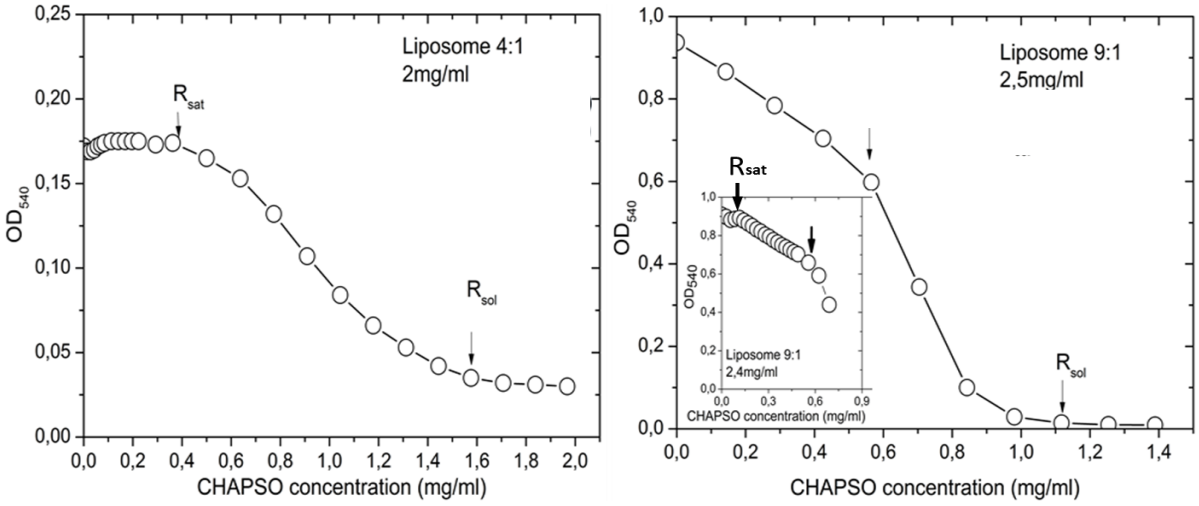

Figure 3.85 Titration curve of performed liposomes with CHAPSO.
Liposomes composed of POPC: PE lipids in a ratio of 4:1 (left) or 9:1 (right) (wt/wt) were titrated with CHAPSO. The physical states of the liposomes were probed by measuring the optical density at 540nm of the suspension. R_{sat} : the detergent concentration where the liposomes were saturated; R_{sol} : the point where the liposomes were solubilized. The middle arrow indicates the point at which concentration of CHAPSO was used for reconstitution. Inset: Titration curve of the right panel at a slower increasing step of the detergent concentration. POPC (16:0-18:1 PC): 1-palmitoyl-2-oleoyl-sn-glycero-3-phosphocholine from Avanti; PE: 3-sn-Phosphatidylethanolamine from Santa Cruz Biotechnology.

To evaluate the success of the sub-complex formation inside the reconstituted proteoliposome, efforts were made to re-solubilize the reconstituted proteoliposome using detergents. Mild detergents, as CHAPSO or DDM, which were reported to maintain the γ-secretase activity [85] and the successful solubilizers used before, the FOS-Choline group detergents were investigated here. Conventional amounts of CHAPSO or DDM could not extract the reconstituted proteins out of the lipids (data not shown). Re-solubilization was achieved in 1%

CHAPSO solubilization buffer by using a large excess of CHAPSO to lipids with a weight ratio of 25:1 (Figure 3.89). The SEC profiles of the re-solubilized proteins were found to be identical with two distinctive peaks (Figure 3.90). The species eluted from the first peak had a calculated molecular weight over 1000 kDa indicating the formation of large aggregates. The second peak showed a higher absorption of 260 nm over 280 nm indicating a lipid-rich species in this peak. The estimated molecular weight of this species is 43.5 kDa. The existence of the Presenilin 1 proteins in the elution fractions from SEC was confirmed by western blot (Figure 3.90). However, less than 20% of the initial input proteins were recovered after the SEC purification. The signal from PEN-2 was missing in the SEC elution fractions. This might be due to a low signal intensity which was below the detection limit. However, both the species recovered from SEC did not match the expected sub-complex size (70 kDa). The formation of large aggregates and the low recovery from the SEC indicated a poor stability of Presenilins in the presence of CHAPSO.

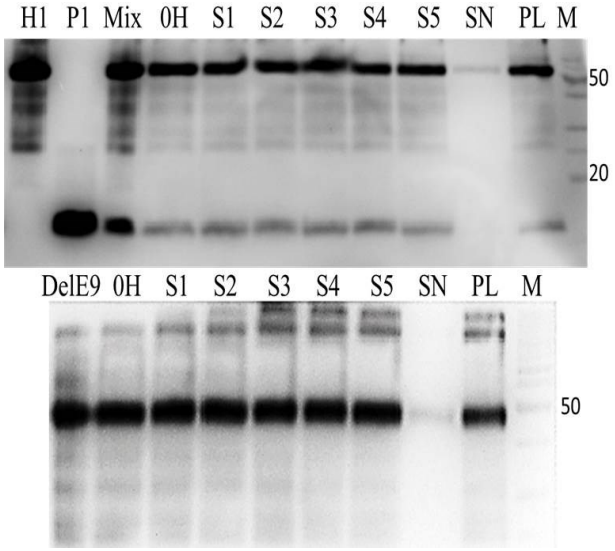

Figure 3.86 Western blot of reconstitution samples from different steps.
H1, P1 and DelE9: detergent purified PS 1, PEN-2 and the deletion form of PS 1. Mix: protein mixture of PS 1 and PEN-2; 0H and S1: samples taken immediately and 1 hour after adding the proteins to liposomes; S2 to S4: samples taken after different addition of biobeads into the protein-liposomes mixture; S5: the flow through collected after biobeads absorption; SN and PL: supernatant and reconstituted proteoliposomes after centrifugation.

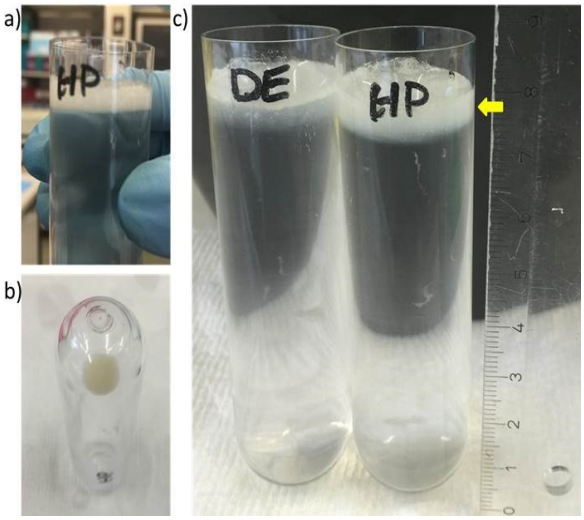

Figure 3.87 Sucrose floating analysis (a, c) and centrifugation (b) of reconstituted proteoliposomes.
A layer of proteoliposomes (semi-transparent, a and c, yellow arrow) was observed floating on the top of the sucrose gradient after ultracentrifugation. b) The White pellet of the proteoliposome after reconstitution.

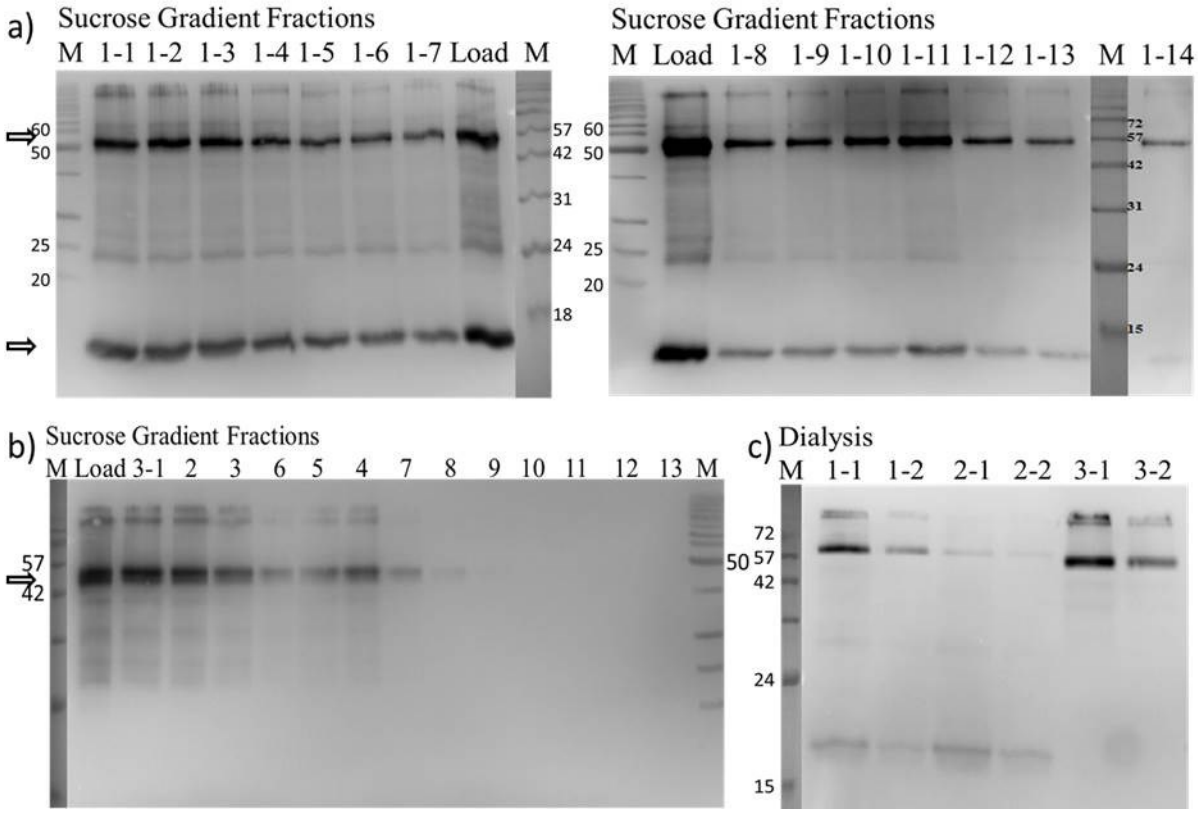

Figure 3.88 Western blot of the sucrose gradient (a, b) and dialysis samples (c).

a) Western blot of sucrose gradient fractions collected from Presenilin 1 and PEN-2 reconstituted proteoliposomes, fraction 1-1 to 1-14 were collected in 0.5 mL. b) Western blot of sucrose gradient fractions collected from DelE9 reconstituted proteoliposomes fraction 3-1 to 3-8 were collected in 1 mL each fraction, fraction 3-9 to 3-13 were collected in 5 mL. c) Western blot of samples after dialysis. 1-1 and 1-2 are reconstituted proteoliposomes using FOS-14 purified Presenilin 1 and PEN-2; 2-1 and 2-2 are reconstituted proteoliposomes using FOS-14-Cholesterol purified Presenilin 1 and PEN-2; 3-1 and 3-2 are reconstituted proteoliposomes using FOS-14 purified DelE9.

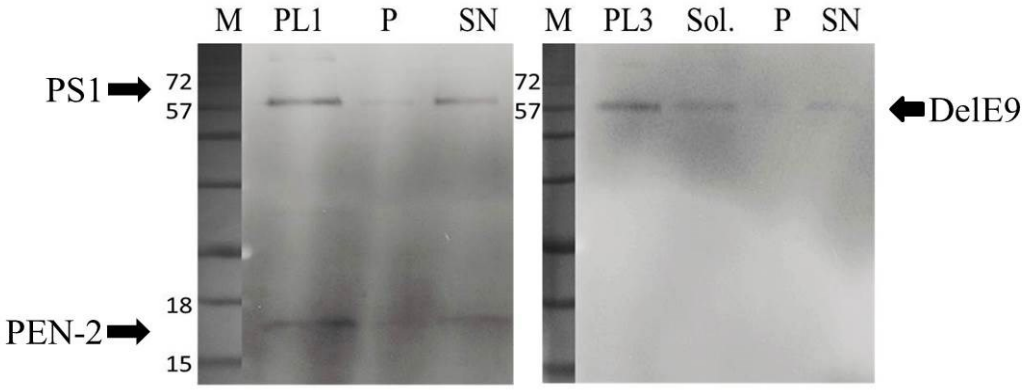

Figure 3.89 Western blot of CHAPSO re-solubilization of proteoliposomes.

PL1: reconstituted proteoliposome with Presenilin 1 and PEN-2; PL3: reconstituted proteoliposome with DelE9; Sol.: solubilization suspension; P and SN: pellet and supernatant after solubilization.

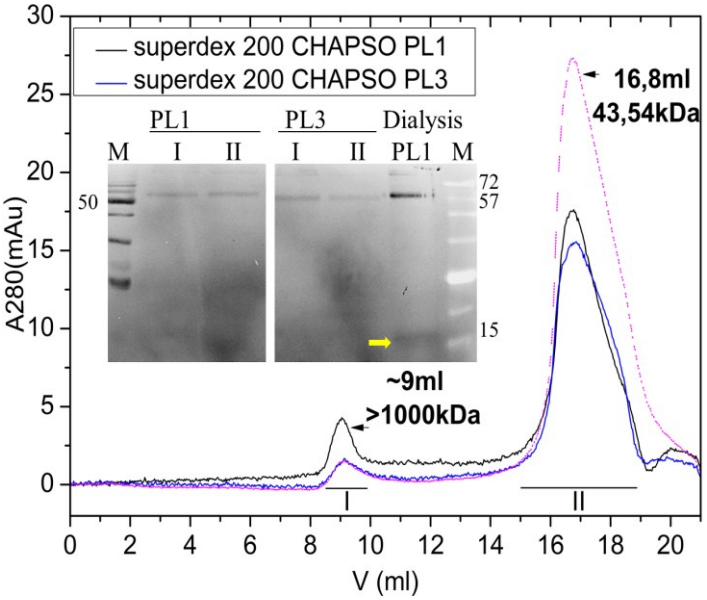

Figure 3.90 SEC and western blot of re-solubilized proteoliposomes in CHAPSO.
Superdex 200 10/300GL column was used in the experiment. SEC buffer : 2CMC CHAPSO, 200mM NaCl, 20mM HEPES pH7.4, 1mM TCEP, 10% Glycerol. Pink dot curve is the A260 absorption spectrum of PL3. Inner gel: western blot of concentrated peak fractions from SEC. PL1: reconstituted proteoliposome with Presenilin 1 and PEN-2; PL3: reconstituted proteoliposome with DelE9

3.6.4 Activity assay of Presenilin and PEN-2

3.6.4.1 Establishment of γ-secretase activity assay

To establish a γ-secretase activity assay, γ-secretase complex purified from mammalian cells and APPC100 proteins were acquired from Prof. Fraering's group at EPFL as a positive control. As shown in Figure 3.91, activities were observed for the control γ-secretase with the control substrate following their protocol[98,186]. Comparing the intensity of western blotting signals, a higher yield of the products was observed for the reaction in the presence of lipids than in the presence of liposomes. As suggested, a higher reaction temperature at 42°C and an increasing PC lipids concentration to 0.2% improved the productivity of the substrates (Figure 3.93, left panel lane 2).

3.6.4.2 The γ-secretase sub-complexes activity assays.

Γ-secretase activity assays were carried out using different materials obtained as described above, including the SEC fractions from the co-expression of Presenilin 1 and PEN-2 (Figure 3.83) and the reconstituted proteoliposomes obtained at different steps (Figure 3.86 and Figure 3.88). A difference in the signal patterns of the FOS-14 and Triton X-100 purified APPC100 comparing to the substrates obtained from EPFL was observed (Figure 3.93). A higher purity of APPC100 was achieved by changing detergent to NP-40 (Figure 3.92). Similar oligomeric state of the NP-40 purified APPC100 and C100F from EPFL was obtained. Considering detergents might inhibit the activity of the purified components, membrane pellets after lysis would be an alternative for activity assay [47,173]. Membrane fractions from Presenilin 1, DelE9 and co-expression of Presenilin 1 with PEN-2, Presenilin 2 with PEN-2 were applied for the activity

assays. The amount of additives such as brain polar lipids, cholesterol and CHAPSO were varied. Different reaction pHs from 4 to 9 was also screened. However, there was no product signal detected from the western blots under the tested experimental conditions (Figure 3.93).

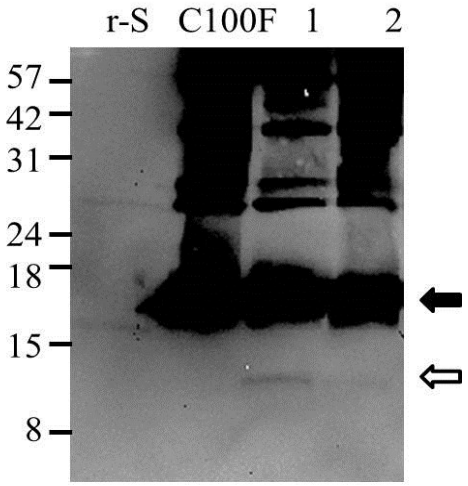

Figure 3.91 Γ-secretase activity assay positive control.
Western blot against Flag-tag. r-S: γ-secretase complex; C100F: APPC100; 1: reaction with raw lipids mixture; 2: reaction with extruded liposomes. Both proteins and substrates used here were acquired from EPFL. Black arrow indicates APPC100 monomer, the product is indicated in open arrow.

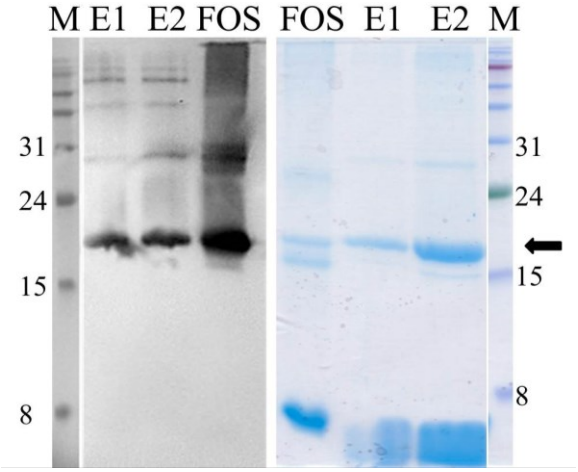

Figure 3.92 SDS-PAGE of APPC100.
Left: western blot against Flag-tag. Right: blue silver stain SDS-PAGE. E1 and E2: elution fractions of APPC100 from affinity purification performed in NP-40; FOS: FOS-14 purified APPC100. Black arrow indicates APPC100 monomer.

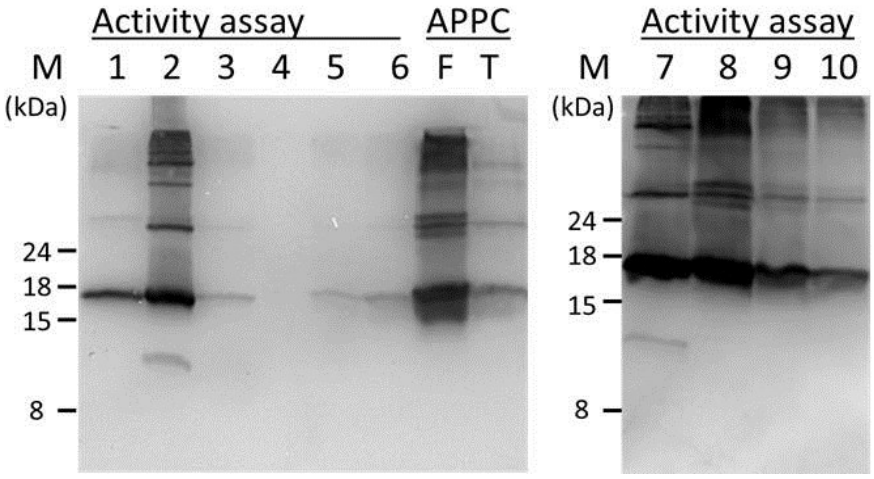

Figure 3.93 Western blot of γ-Secretase sub-complex activity assay
Anti-flag tag western blot. 1 and 8: reactions performed with γ-secretase complex and purified APPC100; 2 and 7: reactions performed with γ-secretase complex and C100F. 3-6: reactions performed using co-expressed membrane fractions with purified APPC100; 9-10: reactions performed using reconstituted proteoliposomes with home purified APPC100. F: FOS-14 purified APPC100; T: Triton X-100 purified APPC100.

3.6.5 Interaction between NCT and APPC100

Nicastrin has been proposed to be the substrate recognizer in the γ-secretase complex [70,166,167]. The interaction between NCT and APPC100 was observed in the *in-vitro* co-expression of NCT and APPC100 (Figure 3.19). To determine whether detergent purified NCT also physically associates with APPC100, the N-terminal His-tagged NCT and the C-terminal Flag-tagged APPC100 were subjected to pull-down assays using Flag resin or Ni-NTA agarose.

As shown in Figure 3.94 (a and c), the FOS-14 purified NCT was captured by and co-eluted with APPC100 which was bound to the Flag resin. There was no observation of the retention of NCT on the Flag resin without APPC100 (Figure 3.94 b). In the reverse experiment, Ni-NTA agarose pulled down His-tagged NCT together with APPC100 from the mixture of separately expressed and detergent purified proteins (Figure 3.94 d). To exclude the possibility that these observed interactions were mediated by unspecific binding of the hydrophobic regions of these two membrane proteins, a control membrane protein was used for the pull-down assay with APPC100 on the Flag resin. There was no observation of the control protein binding to the APPC on the resin (data not shown).

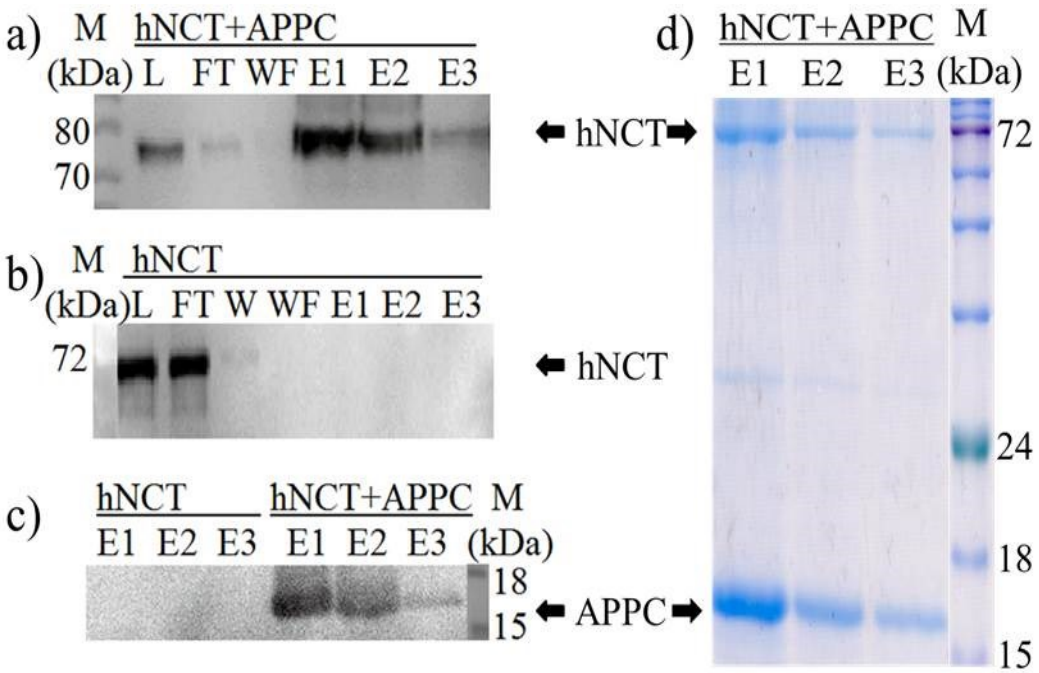

Figure 3.94 Pull-down assay of NCT and APPC100

Pull-down assays of NCT (hNCT) and APPC100 using Flag resin (a, b and c) or Ni-NTA agarose (d). FOS-14 purified hNCT was incubated with APPC100 pre-coated Flag resin (a) or empty Flag resin (b). L and FT indicate loaded sample and flow through sample. W and WF indicate wash samples taken at first and final washing step. E1 to E3 indicate three elution fractions. (a) and (b) anti-His western blots. (c) anti-Flag western blot. (d) blue silver staining of the elution fractions from Ni-NTA agarose pull-down assay (15% SDS-PAGE). The presence of hNCT and APPC100 is indicated by black arrows

A more detailed assessment of the interaction was provided by microscale thermophoresis (MST). Both proteins were labelled by NT647-NHS dye (NanoTemper Technologies GmbH). A serial titration of the unlabelled protein to a constant amount of labelled protein was performed. NT647-hNCT was kept at a constant concentration of 20 nM when titrated with unlabelled APPC100. The MST data at concentrations of APPC100 up to 20 µM gave an apparent dissociation constant (K_d) in the range of 1-2 µM (Figure 3.95 a, black curve). Heat denatured NCT were used as a reference (Figure 3.95, red). Consistent with the thermal denaturation results, NCT remained partial folded at the temperature of 46 °C. It showed a much lower binding affinity. The titration of hNCT to NT647-APPC100 (40 nM) yielded a hill shape MST signal indicating a biphasic event (Figure 3.95 d). Fitting the first 12 data points yielded an apparent K_d in the range of 0.1-0.2 µM, while the second low-affinity binding event happened with apparent K_d over 1 µM. However, these two estimated apparent K_d values were determined with less accuracy. Therefore, the importance of this reverse experiment was to provide additional information of the existence of the second binding event.

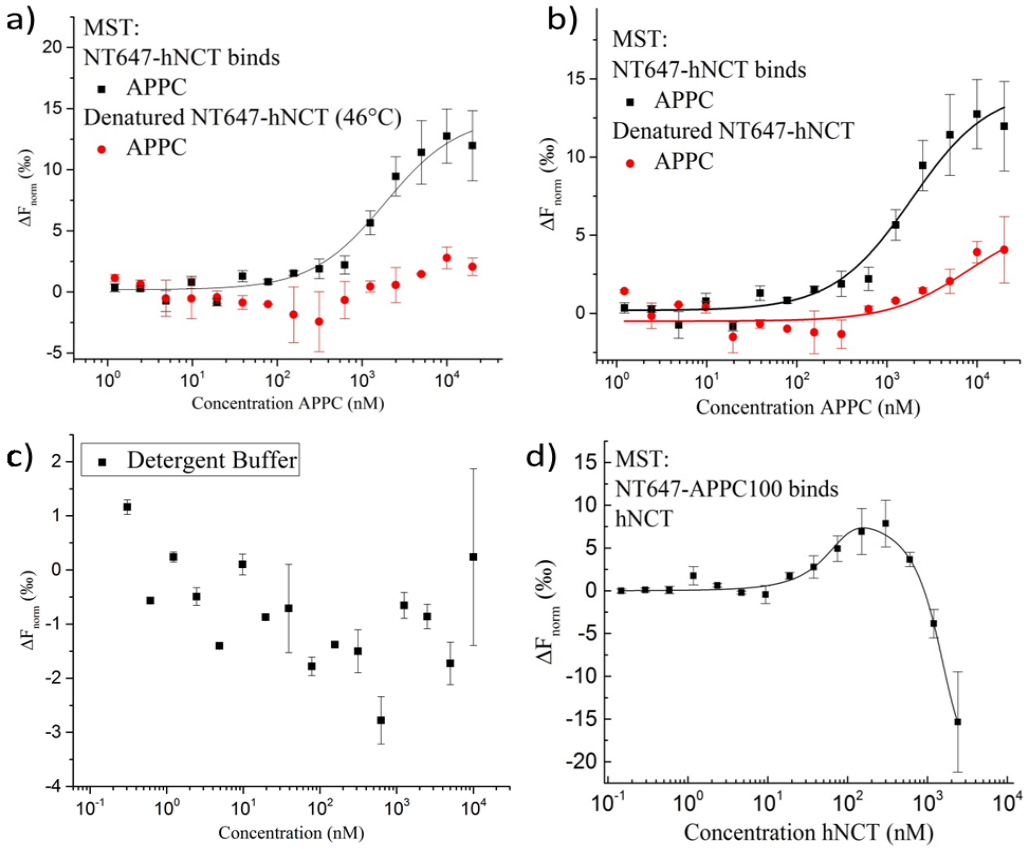

Figure 3.95 MST results of NCT and APPC100.

Data were plotted as normalised signal change as a function of ligand-protein concentration. Upper panel: titration of APPC100 to a constant amount of NT647-NHS labelled NCT. Native in black. a) 46°C denatured in red. b) 95°C denatured in red. c) Titration of detergent buffers to a constant amount of NT647-NHS dye. d) Titration of hNCT to a constant amount of NT647-NHS labelled APPC100.

4 Discussion

4.1 Expression and purification of APH-1

APH-1 is a 7 transmembrane protein which is known as the γ-secretase stabiliser [79,83]. Three variants of APH-1 have been identified in the human brain: APH-1aL, APH-1aS and APH-1b [81,82]. Here, APH1aL isoform was employed for the investigation due to its relatively high abundance in the γ-secretase complex. It has been reported that APH-1 was stable in the absence of any other γ-secretase component in mammalian cells [88]. In this study, however, APH-1 showed severe degradation for both proteins obtained from the *E.coli in vitro* expression system and the *in vivo* insect cell expression system. The degradation of *E.coli in-vitro* system expressed APH-1 occurred already during the expression at a slightly higher temperature at 30 °C (Figure 3.10). Far-UV CD spectra suggested an unfolded state of the purified APH-1 expressed at even a low temperature (20 °C) (Figure 3.13 and Figure 3.14). Furthermore, the conventional *in vivo E.coli* expression system failed to express APH-1 (detected by western blot). These results suggested that for this multiple transmembrane protein, a eukaryotic expression system might be necessary to maintain a correct folding and post-translational modification of the recombinant protein. Therefore, the expression of APH-1 in insect cell was carried out. Intriguingly, a signal peptide which has been reported to facilitate the insertion and function in type III b membrane proteins [179] showed significant improvement of APH-1 expression and stability in the insect cell expression system. Consistent with the cryo-EM structure, APH-1 falls into this group of membrane proteins with the amino terminus of the membrane protein located on the extracellular side of the membrane. The difficulty in extracting APH-1 from Sf9 insect cell membrane was unexpected. Only the long-chain zwitterionic FOS-cholines were able to solubilize the protein. This group of detergents was well-known as lipids mimics [187]. They share the same head groups as phospholipids but have only one single hydrophobic tail. The unique ability of FOS-choline detergents to solubilize APH-1 from the insect cell membrane might be explained by the potentially strong interaction between the protein and the membrane lipids. Detergent purified APH-1 showed tetrameric conformation in SEC (Figure 3.55). An SDS-resistant dimer band was observed on the SDS-PAGE which was reported in the previous study as well [85]. It is likely that the minimal subunit of this insect expressed APH-1 could be a dimer in the presence of detergents. As observed in Figure 3.54, APH-1 produced by this method also experienced a severe degradation upon long-term purification indicating that other unknown factors might be needed for proper folding and stabilising of APH-1. With a combination of Rho-tag affinity purification and SEC, a final

yield of 80 μg purified APH-1 per gram insect cell pellet was achieved.

4.2 Purification and characterization of full-length nicastrin

With the improvement in the knowledge of spatial folding of nicastrin based on the 1.95 Å homologue structure of ECD and the EM structure of γ-secretase [40,76], a large lobe and a small lobe structure was revealed with a lid structure which covers the putative substrate binding cave in the built model. Rotation of the large and small lobes and moving away the lid were proposed to be necessary for the substrate binding [40,74,75]. However, deletion of the lid domain did not show the expected regulating effect on the γ-secretase substrate processing [188]. The lid function might be better studied in the investigation of its regulating effect on the processing of ectodomain of APPC or Notch substrates (i.e., the length). The contrary results from human nicastrin make it more urgent to raise a more detailed, structure-based view of the protein. To elucidate the structural and functional properties of nicastrin, here we established an efficient protocol to produce the full-length human nicastrin from *E.coli* recombinant expression system.

As the largest component of γ-secretase, nicastrin has 709 amino acid residues among which 669 residues belong to the ECD. A topology of nicastrin TM domain and C-terminus suggested V696-A700 were solvent protected and may interact with micelles/membranes [132]. Intriguingly, this large protein was observed to be tightly anchored to the *E. coli* cell membrane by a short 20 residues transmembrane domain (Figure 3.26). Purification and biophysical characterization of the full-length nicastrin were carried out in FOS-14. Other detergents, such as CHAPSO or DDM led to either poor solubility or poor purity of the target protein. These two detergents were discussed here because CHAPSO which is also a zwitterionic detergent has been wildly utilised in the γ-secretase purification and activity assay, and DDM is one of the commonly used detergents for the structural and functional studies. However, the presence of both detergents severely distorted the conformation of the target protein, which is revealed by the aggregation formation. The preference of nicastrin for the FOS-choline group detergents might be due to the lipid-mimicking effect from these detergents which assist in retaining a proper folding of the transmembrane domain of NCT. FOS-14 purified nicastrin showed tetrameric oligomer from the SEC, while the uncharacterized homo-oligomerization of nicastrin has been reported previously in the mammalian cell line [189]. The value for secondary structure content obtained is in agreement with the EM structure as well as secondary structure prediction. The thermal stability assay showed a melting temperature around 59 °C indicating a stable conformation of nicastrin was obtained in FOS-14. The successful applications of the FOS-

choline group detergents were proved for GPCRs [141,190,191] and ABC transporters [192,193]. Although several cases showed that FOS-cholines interrupted the enzymatic activity or disrupted the protein folding [194,195], for γ-secretase purification and activity assays compatibility of FOS-choline has been reported [173,196]. The protocol described here is the first report of the full-length human nicastrin expression and purification which yields >1 mg homogeneous purified protein per liter cell culture.

The exact role which nicastrin plays in the γ-secretase complex is still controversial. Whether it conducts an active residue-based identification and recruitment of the substrate or it acts just as a steric block to keep the substrates with larger ectodomain out of the enzyme is still unclear[40,70,78]. In this study, co-IP of APPC100 with nicastrin was observed in the cell-free expression system (Figure 3.19), which suggested the formation of a detergent-resistant sub-complex between APPC100 and nicastrin during the co-expression. This interaction was further confirmed by pull-down assays using detergent purified nicastrin and APPC100 (Figure 3.94). An apparent dissociation constant in the range of 1-2 μM between NCT and APPC100 were obtained from MST experiments. The biphasic signal of the titration of NCT to APPC100 was possibly caused by binding induced fluorescence quenching. Nevertheless, APPC100 is known to form oligomers [197,198]. Another possibility of the biphasic event might be due to a dissociation of the oligomerized APPC100 upon the increasing concentration of NCT, which yielding free APPC100-NCT sub-complexes. It has been reported a mid-nM range K_d values of mammalian cell expressed γ-secretase complex to its native Notch substrate which was estimated based on densitometry [78]. The K_d value obtained here in the low μM range is consistent with the idea that this interaction contributes to an initial substrate docking. Other contacts of docking partners (e.g. PEN-2 [199]) or the enzymatic center within the γ-secretase complex (Presenilin NTF and CTF [199]) are likely contributed additionally to the binding affinity obtained of detergent purified proteins measured *in vitro*.

4.3 Biophysical characterization of detergent purified PEN-2

PEN-2 is the smallest component of γ-secretase. It interacts with both presenilin and nicastrin through the transmembrane region and the extracellular domain, respectively (as shown in Figure 4.1) [40]. The interaction interface between PEN-2 and presenilin was mapped to the TM 4 in the PS1 NTF [93], which is partially consistent with the EM structure. Additionally, although several previous studies predicted a commonly acceptable, double TM topology of PEN-2, a recent topology study and the EM structure revealed a novel three transmembrane-domain

conformation of PEN-2 in the γ-secretase complex [40,200]. Controversial opinions were also raised from investigations of the role of PEN-2 in the presenilin endoproteolysis process [98–100]. These conflicting results might need to be further analysed based on more detailed structural and functional studies of PEN-2 or PEN-2 and presenilin subcomplex.

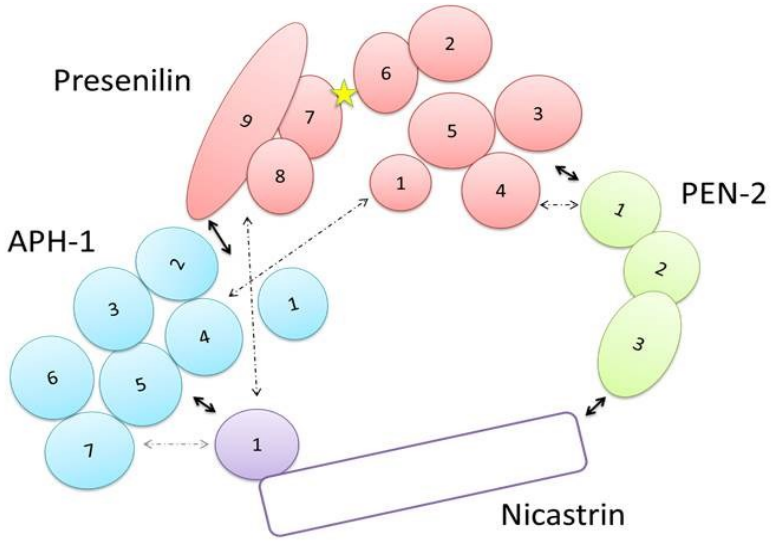

Figure 4.1 Intermolecular interactions in the γ-secretase.
The intermolecular interactions (solid black arrow) and the TM locations in the γ-secretase were illustrated based on the EM structure. The ECD of nicastrin is drawn in the empty rectangle. The previously predicted interactions are indicated as dash arrow.

In this study, a recombinant His-tagged human PEN-2 was expressed from the *E.coli* expression system. The recombinant PEN-2 protein was purified under a two-step fast purification protocol with a high yield of more than 4 mg pure protein per liter cell culture. It has been shown that an MBP-tagged PEN-2 integrated efficiently into the γ-secretase resulted in an enzymatic functional complex [201]. Furthermore, a polyhistidine-tagged PEN-2 has been reported to successfully rescue the γ-secretase function in the PEN-$2^{-/-}$ cell lines [95]. Therefore, the likelihood of this recombinant PEN-2 serving as a functional candidate of active γ-secretase complex is high. Although this small protein could be solubilized by several detergents, still FOS-choline group detergents gave the best yield and homogeneity. The calculated oligomeric state of detergent purified PEN-2 corresponded to a dimer. This dimer was stable in the presence of detergents with high solubilization capacity (through their long aliphatic chain). This indicates a strong inter-molecular interaction within the homodimer. The secondary structure deconvolution revealed a 60% helical content which was close to the value from the EM structure, further proved a proper folding of this detergent purified protein. Intriguingly, a

value of 1.11 was obtained from the CD signal $\theta_{222/208}$ ratio measured for FOS-14 purified PEN-2 and this ratio stayed above 1 during the thermal unfolding (Figure 3.59a). The ratio between the intensities of 222 and 208nm has been practically used as a scale for the presence of a coiled-coil conformation [182,183]. From the EM structure, PEN-2 contains three TMs with two half-spanning membrane helixes (TM 1 and TM 2) and a long helix of TM 3 [130]. It has been reported the coiled-coil interactions could form between the α-helical domains inside one protein molecule [202]. However, here is unlikely the case. There are no substantial coiled-coil segments predicted from the PEN-2 protein sequence (using COILS web server from Expasy). Only a low probability with a value of 0.244 was assigned to the residues Glu3 to Lys16 in which the residues N_7EEKLNLCRK$_{16}$ are located in the N-terminal half of TM 1. Thus, it is more likely this $\theta_{222/208}$ ratio obtained here is due to the helix oligomerization between two protein molecules which is consistent with the observation of dimer formation from the SEC. Similar cases were reported regarding the dimerization of the transmembrane peptides in the presence of lipids vesicles [203,204]. Surprisingly, the SEC (Figure 3.42) still suggested a dimeric state for PEN-2 in the FOS-16 complex although the $\theta_{222/208}$ ratio obtained from CD measurements showed a lower value of 0.96, and this value decreased further upon heating (Figure 3.63). It appears likely that the longer aliphatic chain of FOS-16 interrupted the original helix-helix intermolecular interactions present in FOS-14 and thereby captured another dimerization conformation.

The changes of maximum fluorescence intensities and characteristic minima of CD intensities are commonly investigated as a function of temperature to give a transition midpoint for analysing the protein stability. However, it was not possible to evaluate the data with a two-state model for PEN-2. There are six tryptophan residues (5.2%) in the PEN-2 primary sequence. The EM structure [40] shows that (i) Trp 30 is buried between the TM 1 and TM 2; (ii) Trp 58 and Trp 85 which located in the TMD 3 are pointing to the membrane bilayer; and (iii) the other three (Trp 36 in TMD 1 and Trp 67, Trp 74 in TMD 3) might be involved in the interaction with presenilin 1. In the detergent purified PEN-2 we must presume that there are 2 to 3 tryptophan residues exposed to the detergent environment, though it is unclear which of the residues, since the dimerization interface is unknown. Furthermore, there are 11 phenylalanine (9.5%) and 6 tyrosine (5.2%) residues within the 112 amino acids sequence of PEN-2. The failure to obtain the melting temperature of detergent purified PEN-2 through fluorescence might be due to the heating induced structural fluctuations of this small protein and the constant quenching of fluorescence emissions from the multi-aromatic-residues. For the thermal unfolding monitored by CD, continually decreasing CD intensity at 222 nm was observed for

both FOS-14 and FOS-16 purified PEN-2. Different denaturation processes might occur for these two different detergents-proteins complexes as illustrated in Figure 4.2. For the FOS-16 purified PEN-2, the thermal aggregation is closely correlated to the unfolding of the native structure with a sequential α to β secondary structure transition. It reached a half-unfolded state at the temperature of 60 °C. In contrast to FOS-16, the FOS-14 purified PEN-2 undergoes a 2-step denaturation in which an intermediate was stable between 64-74 °C (Figure 4.2 a). This intermediate existed in an aggregation form, which still exhibited 36% helical content. Further heating caused a dramatically changing from α-helical to β-sheet structure and eventually, the β-sheet dominated PEN-2 formed large aggregates and precipitated while the temperature rising above 90 °C.

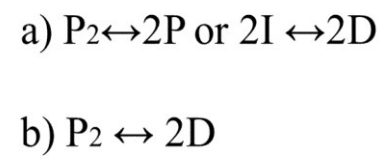

Figure 4.2 Different processes of heating induced protein dimer denaturation (Adapt from [205]).

P_2 indicates the protein dimer; 2P indicates two protein monomers; I indicates an intermediate state; 2D indicates two denatured molecules.

4.4 Purification and biophysical characterization of Presenilins

The full-length presenilins serve as a zymogen from which a cytosolic loop needs to be cleaved to produce catalytically active NTF and CTF heterodimers. The presenilin holoproteins exist in an intermediate subcomplex with APH-1 and NCT which exhibited a relatively shorter half-life than the PEN-2 stabilised NTF and CTF heterodimers [45,95]. Intriguingly, among many FAD-related mutations in presenilins, PS1 Exon 9 (ΔE9) and PS1 or PS2 $M_{292}D$ mutations have been reported to be stable and enzymatically active in the absence of endoproteolysis [98,206]. The mechanism behind this is unclear. The presenilin archaeal homologue structure, the 3.4 Å γ-secretase complex cryo-EM structure and the DAPT bound structure shed light to the understanding of the function and structure relationship of presenilins. Nonetheless, the flexibilities of TM 2 and TM 6 and the functionally related mechanism behind these leave a compelling call for more detailed information about presenilins. Here, the investigations of full-length presenilin 1 protein, N- and C-terminal fragments, as well as its ΔE9 mutation were aimed to gain better knowledge about these proteins properties and further their γ-secretase dependent or independent functions.

The attempt to express and purify a large amount of the C-terminal fragment failed due to the low expression level and instability of the protein. Interestingly, these results put into question the relevance of the NMR-structure of PS1 CTF obtained with SDS-solubilisation of *in-vitro* produced protein. The *E.coli* expressed C-terminal fragments were distributed in the supernatant after ultracentrifugation, which indicating either an incorrect folding of the proteins or a failed insertion of the proteins into the cell membrane due to low hydrophobicity. A possible reason is that the natural presenilin C-terminal fragments are generated by endoproteolysis from the full-length presenilins inside the membrane and interacted with its partners, whereas in the case of fragment expression the fragment has to insert into the membrane. The *E.coli* expressed CTF of presenilin lacks the membrane translocating signal sequence and undergoes degradation due to the absence of interaction partners.

The N-terminal fragment of presenilin 1 showed an expression yield as high as found for the full-length presenilin protein in *E.coli* and could be harvested from the membrane fraction. However, multiple oligomer states were observed for the protein which results in a poor homogeneity (Figure 3.48). The cryo-EM structure showed that TM 2 and TM 6 of presenilin were highly flexible, certain conformational changes of the protein were observed upon substrate or inhibitor binding [131]. These highly flexible regions in the NTF of presenilin might cause the differentiation in the intermediate states which could explain the different homo-oligomers observed in this study.

The detergent purified His-tagged presenilin 1 full-length protein runs at 50 kDa in the SDS-PAGE which is different from the predicted molecular weight (55 kDa) (Figure 3.76). This anomalous SDS-PAGE migration is common for membrane proteins which could be explained by the detergent binding effect [207]. The presenilin 1 full-length protein was purified as trimers in the detergents indicating at least two interaction interfaces needs to be covered which consists with its biophysical circumstance inside the γ-secretase complex: PS1-NTF interacts with PEN-2 and PS1-CTF interacts with APH-1 [40]. For trimeric presenilins, the molecular weight calculation based on SEC indicated a more compact conformation might be adopted in FOS-16. Consistent with this interpretation, the thermal denaturation revealed a more stable detergent-presenilin complex with FOS-16 than FOS-14. This stability difference is possibly not caused by the secondary structural elements but the protein spatial packing and protein-detergent interactions, since both FOS-14 and FOS-16 purified presenilin share an identical helical content. Although the secondary structural content of detergent purified presenilin 1 (41% helix and 13% strands) is in agreement with the predicted value (41.48% helix, 10.88% strands

from www. predictprotein.org), it still showed 5% less in the α-helix content and more β-strands compared to the calculated value from EM structures with 46% helix and 0% beta-sheet. The difference appears to be due to the two different states: cleaved enzymatically active Presenilin 1 compared to un-cleaved. Unexpectedly, a further decreased level of α-helical contents was observed in the detergent purified presenilin ΔE9 mutation which showed a difference of more than 10% from the calculated value. We cannot exclude that the observed difference might be due to primary-sequence dependent difference among the proteins (full-length wild-type presenilin, ΔE9 truncated presenilin and NTF-CTF heterodimer). However, there are also other possible explanations, such as oligomerization induced α-helix to β-strand transition since both proteins were isolated in a trimeric form; or the intrinsic conformational difference between ΔE9 and wild-type presenilins.

4.5 Γ-secretase sub-complex formation and activity assay

The reconstitutions of γ-secretase functional sub-complexes, namely PS NTF and CTF or presenilin and PEN-2 were carried out in this study under different ways. Intriguingly, although the pull-down experiments failed for *in vitro* expressed NTF and CTF in the presence of Brij 35, the nanodiscs rescued the interaction between *in vitro* co-expressed NTF and CTF (Figure 3.20 and Figure 3.22). Similar results were observed for presenilins and PEN-2: since the direct integration of FOS-14 purified presenilin 1 and PEN-2 did not show any co-elution from SEC, the full-length presenilin 1 or PS2 were found to be co-immunoprecipitated with PEN-2 in the presence of nanodiscs (Figure 3.21 and Figure 3.79). Although it is unclear whether the two proteins remain in the nanodiscs as a complex or as separate components, there is a higher incidence for both proteins to insert into the same nanodiscs as a complex than separately.

Like nanodiscs, liposomes are used in functional studies of membrane proteins (also γ-secretase) by providing a native-like environment with variable lipids composition [98,208,209]. The lipid-mediated reconstitution confirmed a successful insertion of PEN-2 with presenilin into liposomes. Unexpectedly, no specific fragmentations of presenilin were observed during the whole reconstitution period indicating the reconstituted presenilins did not undergo the endoproteolysis. In this setup, the completeness of the detergent to lipids exchange could not be verified. Detergents with relatively low CMCs like FOS-14 are usually difficult to be removed. It is possible that their presence might have impaired the native structure and/or function of the purified proteins which prevent the endoproteolysis upon reconstitution. However, previous studies have shown success in the functional reconstitution of the γ-secretase complex from

FOS-choline detergent into liposomes [173,196]. If this is the case, the detergents may not be the dominant cause for the deficit of activity.

Another possibility is that the detergent-purified proteins formed homo-oligomers before they encountered each other which would prevent the formation of the 1:1 presenilin-PEN-2 subcomplex. The interaction interface between presenilin and PEN-2 is located at both N-terminus of presenilin and PEN-2. There is a high probability that the trimeric presenilin and the dimeric PEN-2 are oligomerizing through the N-terminal interfaces which would prevent the formation of the functional heteromeric-subcomplex. The co-expression results further support this conclusion. In the presence of the same detergent FOS-14, fragmentation of presenilin was observed when it was co-expressed and purified with PEN-2. Although instability and degradation of presenilin 1 were detected during the individual protein purification as well, distinguishable fragmentation bands of presenilin were observed which were distinct from the smear pattern of unspecific degradation when PS was expressed alone (Figure 3.81 and Figure 3.83). Additionally, the migration pattern of PEN-2 from the co-expression also changed on the SDS-PAGE and SEC which indicated a detergent-resistance interaction between PEN-2 and presenilin. These results suggested that rather than detergent interference of the sub-complex formation, it is more likely that the oligomerization states of the individually purified components are blocking the heterodimer interaction interface.

Nevertheless, consistent with previous reports, detergents do impair the activity. Weaker signals were detected from the reactions of γ-secretase (positive control) with substrates which were purified in the presence of FOS-14. And no activity was detected from the FOS-14 purified co-expression components which suggested that it is necessary to reconstitute the co-expressed materials into liposomes to rescue the activity. Another factor not to be overlooked is the potential effect of lipids on the activity assay. The importance of lipids in the γ-secretase activities has been high lightened in past decades [170,173,208–210]. A proper ratio of different lipids components and a careful handling of the unsaturated lipids might be pivotal to improve the outcome of γ-secretase activity assay.

Hence, lacking of the γ-secretase catalytic activity from the *E.coli* expressed subunits in this study could fall in one or a combination of the following reasons: 1) the blocked interaction sites by the homo-oligomerization of individually purified components preventing the formation of a functional subcomplex; 2) the FOS-choline detergent interruption of the enzymatic activity; 3) the missing of essential phospholipids or other co-factors which down regulates the activity level.

Summary

The γ-secretase complex is a unique integral membrane protease which carries out the regulated intramembrane proteolysis of over 90 substrates. The structural and functional studies of the γ-secretase complex have been extensively implemented during the past decades. Four major components are well-known to be responsible for the native γ-secretase activity: presenilin, the catalytic core protein; PEN-2, a potential promoter for the presenilin endoproteolysis and a stabiliser for the active presenilin fragments; APH-1, a scaffold protein for the whole γ-secretase complex; and nicastrin, a substrate recognizer.

In this study, the four components of γ-secretase were expressed recombinantly from *E.coli* or insect cell expression system. All four components could be expressed separately and purified successfully *in vitro*. The cell-free expression system was employed to gain the general information about the properties of each component, as well as the intermolecular interactions. Large-scale protein production was achieved by *in vivo* cell expression. Optimised expression conditions, solubilization and purification protocols were developed for each individual protein. Three of the four components (presenilin, PEN-2 and nicastrin) were produced using the *E.coli* cells and purified in FOS-choline detergents with good yields (1-4 mg purified protein per liter cell culture) and high qualities which are suitable for downstream crystallisation application. Expression of APH-1 was achieved from insect cells with a yield of 80 μg purified protein per gram cell pellet. The identity and completeness of the target proteins were verified by both western blotting against the specific affinity tag and mass spectrometry (LS-MS/MS). The oligomer state of each detergent purified protein was characterised to be a dimeric state of PEN-2, a trimer of presenilin, a trimer of APH-1 and tetramer of nicastrin, respectively.

Further biophysical characterisation of nicastrin, PEN-2 and presenilin were conducted by CD and fluorescence spectroscopy. All three proteins exhibited a characteristic α-helix dominated secondary structure. Temperature dependent denaturation of the proteins showed a transition from α-helix to β-strand upon heating. The FOS-14 purified nicastrin exhibited 31% helical structure and 23% β-sheet which are in agreement with the secondary structure obtained from the EM structure. The melting temperature obtained from CD measurements suggested a relative heating resistant nicastrin with a T_m of 59 °C in FOS-14. Different FOS-choline detergents did not show much influence on the secondary structure content for PEN-2 and presenilin but altered the thermal stability of both proteins. PEN-2 undergoes a three-step denaturation process in the presence of FOS-14 with an intermediate state between 64-74 °C, and a two-state transition in the presence of FOS-16 with a half-unfolded state at 65 °C.

Presenilin 1 protein purified from FOS-14 exhibited a T_m of 47 °C; while FOS-16 purified proteins showed a T_m around 57 °C indicating differences in stability of presenilin 1 in the presence of different detergents. A truncated form of full-length presenilin 1 without the Exon 9 region between TM 6 and TM 7 was designed (DelE9). The thermal stability of DelE9 did not show differences in the presence of different detergents with a T_m value of 56 °C, suggesting the loop regions influence the stability of the presenilin 1-detergent complex.

Furthermore, the obtained proteins were subjected to crystallisation trials. Crystallisation conditions were optimised for the first crystals of PEN-2 and nicastrin. The protein crystals were confirmed to contain the respective target proteins by the western blot.

Individually expressed and purified presenilin 1 and PEN-2 were reconstituted into liposomes to investigate the *in vitro* assembly of γ-secretase. The successful insertion of the presenilin 1 and PEN-2 was confirmed by sucrose floating assay as well as re-solubilization in CHAPSO. Co-expression of presenilin and PEN-2 was also achieved using the *E.coli* BL21 (DE3) strain. Although the enzymatic activity was not obtained from the detergent purified subunits, specific fragmentation of presenilin 1 was observed by co-expressing the two proteins of the catalytic subcomplex, which indicates an activation of the endoproteolytic process of presenilin in the presence of PEN-2. Additionally, the physical interaction between nicastrin and the substrate of γ-secretase, APPC100, was proved by pull-down assays in the presence of detergent, which proves the formation of a substrate binding initiation complex. An apparent dissociation constant in the range of 1-2 μM was determined by microscale thermophoresis. This binding of NCT and APPC100 supports strongly the concept that nicastrin functions as an initial substrate receptor in the γ-secretase complex.

Zusammenfassung

Der γ-Sekretase Komplex repräsentiert ein besondere, Membran integrierte Protease, die innerhalb der Membran eine regulierte Proteolyse von über 90 Substraten katalysiert. Während der letzten Dekade wurden extensive Studien zu strukturellen und funktionellen Eigenschaften dieses Komplexes durchgeführt. Vier Proteine sind für die native γ-Sekretase Aktivität verantwortlich: Presenilin, die katalytische Komponente, PEN-2, der wahrscheinliche Promotor der endoproteolytischen Aktivierung, und Stabilisator der aktiven Presenilinfragmente, APH-1, das Gerüstprotein des Gesamtkomplexes, uns Nicastrin, welches für die Substraterkennung verantwortlich ist.

In dieser Arbeit wurden die vier Komponenten des γ-Sekretase Komplex rekombinant exprimiert. Alle vier Komponenten wurden separat exprimiert und erfolgreich gereinigt. . Durch Zellfreie Expression wurde allgemeine Information über die Eigenschaften der Komponenten erhalten, sowie über ihre molekulare Interaktion. Proteinproduktion im größeren Maßstab wurde durch in vivi Expression erreicht. Optimierung der Expressionsbedingungen, Solubilisierung und Reinigungsprotokolle wurden für jedes einzelne Protein separat durchgeführt. Drei der vier Proteine (Presenilin, Pen-2, Nicastrin) wurden in E. coli produziert und in Fos-Cholin mit guter Ausbeute (1-4 mg/L Kultur) und hoher Qualität produziert, welche hinreichend für die Durführung von Kristallisationsexperimenten war. Die Expression von APH-1 wurde in Insektenzellen mit einer Ausbeute von 80 µg gereinigtem Protein pro G Zellen erreicht. Die Identität und Vollständigkeit der Zielproteine wurde durch Western Blot gegen terminale Tags und Massenspektrometry (LS-MS/MS) nachgewiesen. Der Oligomerisierungsstatus der in Detergenz gereinigten Proteine wurde charakterisiert als Dimer für PEN-2, Timer für APH-1 und Presenilin, Tetramer für Nicastrin.

Die weitere Charakterisierung der Proteine of Nicastrin, PEN-2 und Presenilin wurde mit Hilfe von CD- und Fluoreszenz-Spektroskopie durchgeführt. Alle drei Proteine weiden eine von Helices dominierte Sekundärstruktur auf. Die Untersuchung der thermischen Denaturierung zeigte einen Temperatur-abhängigen Übergang von α-helix zu B-Struktur. In FOS-14 solubilisiertes Nicastrin zeigte übereinstimmend mit Daten aus der Elektronrnmikroskopie 31% helikale und 23% β-Faltblattstruktur. In Denaturierungsexperimenten erwies sich Nicastrin al sein relative stabiles Protein mit einer Schmelztemperatur von 59 °C für die Sekundärstruktur. Der Einfluss des Detergenz auf die Sekundärstruktur war schwach für PEN-2 und Presenilin, beeinflusste aber die Stabilität der beiden Proteine. PEN-2 durchlief eine 2-Schrittentfaltung mit einer intermediären Struktur zwischen 64-74 °C in FOS-14. In FOS-16 trat dagen eine

typische Entfaltung mit zwei Zuständen und einer Schmelztemperatur von 65 °C auf. Presenilin-1 in FOS-14 wies eine Tm von 47 °C auf, in FOS-16 dagen 57 °C, und zeigte damit einen deutlichen Einfluss des Detergenz auf die Stabilität. Eine trunkierte Form von Presenilin-1 (DelE9) ohne die durch Exon 9 kodierte Region zwischen den Helices TM6 und TM7 zeigte eine Tm von 56 °C für beide Detergenzien. Offenbar verursacht das deletierte Strukturelement eine Beeinflussbarkeit der Stabilität des Proteins.

Mit den gereinigten Proteinen wurden Kristallisationsexperimente durchgeführt und Bedingungen optimiert für die erhaltenen Kristalle von Nicastrin und PEN-2. Durch Western Blot konnte bestätigt werden, dass die Kristalle aus dem jeweiligen Protein bestanden.

Die separat exprimierten und gereinigten Proteine Presenlin-1 und PEN-2 wurden in Liposomen rekonstituiert, um die in-vitro Assemblierung der γ-Sekretase zu untersuchen. Die erfolgreiche Insertion konnte durch ein Zentrifugationsexperiment und Resolubilisierung in CHAPSO bestätigt werden. In E. coli coexprimiertes Presenilin-1 und PEN-2 zeigte nach Solubilisierung keine proteolytische Aktivität, obwohl bei der Expression das Auftreten spezifische Fragmentierung von Presenilin-1 beobachtet wurde, welches die Bildung des autokatalytischen Sub-Komplexes der Sekretase bewies. Weiterhin wurde die physische Interaktion von Nicastrin und dem Substrat APPC-100 in Gegenwart von Detergenz durch eine pull-down Experiment gezeigt, welches die Bildung eines Substrat-bindenden Initiationskomplexes beweist. Die apparente Dissotiationskonstante wurde durch microscale thermophoresis zu 1-2 μM bestimmt. Diese Bindung unterstützt stark das Konzept von Nicastrin als initialen Substratrezeptor im γ-Sekretase Komplex

Abbreviations

AD	Alzheimer's disease
AICD	APP intracellular domain
APH-1	Anterior pharynx-defective 1
APOE	Apolipoprotein E
APP	Amyloid precursor protein
ATP	Adenosinetriphosphate
Aβ	beta-amyloid
CD	Circular Dichroism
CTF	Carboxyl-terminal fragment
CV	Column volume
DLS	Dynamic light scattering
DNA	Deoxyribonucleic acid
DTT	Dithiothreitol
EDTA	Ethylendiethyltetraacetic acid
EOAD or LOAD	Early- or late-onset AD
ER	Endoplasmic reticulum
FAD	Familial AD
GuHCl	Guanidine hydrochloride
IEX	Ion Exchange Chromatography
IMAC	Immobilized metal affinity chromatography
IPTG	Isopropyl β-D-1-thiogalactopyranoside
MO	Monoolein
M_w	Molecular weight
MRE	Mean Residue Ellipticity
MRW	Molar residual weight
MS	Mass spectrometry
MS/MS	Tandem MS
NCT	Nicastrin

NLS	N-Lauroylsarcosine sodium salt
NFTs	Neurofibrillary tangles
NTF	Amino-terminal fragment
OD	Optical density
PAGE	Polyacrylamide gel electrophoresis
PCR	Polymerase chain reaction
PEN-2	Presenilin enhancer 2
PHF	Paired helical filament
PMSF	Phenylmethanesulfonyl fluoride
PS1	Presenilin1 protein
PS2	Presenilin2 protein
sAPPα or β	Soluble fragment of APP after α- or β-secretases cleavage
SDS	Sodium dodecyl sulfate
SEC	Size exclusion chromatography
TCEP	Tris (2-chlorethyl) phosphine
TEMED	Tetramethylethylenediamine
TM	Transmembrane
Tris	Tris (hydroxymethyl) aminomethane
UV	Ultraviolet
β-ME	β-Mercaptoethanol

Bibliography

1. Berchtold, N. C. & Cotman, C. W. Evolution in the Conceptualization of Dementia and Alzheimer's Disease: Greco-Roman Period to the 1960s. *Neurobiol. Aging* **19,** 173–189 (1998).
2. WHO | Dementia. *Fact sheet N°362* (2015). Available at: http://www.who.int/mediacentre/factsheets/fs362/en/. (Accessed: 11th February 2016)
3. Brookmeyer, R., Johnson, E., Ziegler-Graham, K. & Arrighi, H. M. Forecasting the global burden of Alzheimer's disease. *Alzheimer's Dement.* **3,** 186–191 (2007).
4. Strobel, G. What Is Early Onset Familial Alzheimer Disease (eFAD)? | ALZFORUM. Available at: http://www.alzforum.org/early-onset-familial-ad/overview/what-early-onset-familial-alzheimer-disease-efad. (Accessed: 10th May 2016)
5. Campion, D. *et al.* Early-onset autosomal dominant Alzheimer disease: prevalence, genetic heterogeneity, and mutation spectrum. *Am. J. Hum. Genet.* **65,** 664–70 (1999).
6. Bertram, L. & Tanzi, R. E. Thirty years of Alzheimer's disease genetics: the implications of systematic meta-analyses. *Nat. Rev. Neurosci.* **9,** 768–78 (2008).
7. Maccioni, R. B., Farías, G., Morales, I. & Navarrete, L. The Revitalized Tau Hypothesis on Alzheimer's Disease. *Arch. Med. Res.* **41,** 226–231 (2010).
8. Weingarten, M. D., Lockwood, A. H., Hwo, S. Y. & Kirschner, M. W. A protein factor essential for microtubule assembly. *Proc. Natl. Acad. Sci. U. S. A.* **72,** 1858–62 (1975).
9. Goedert, M., Spillantini, M. G., Jakes, R., Rutherford, D. & Crowther, R. A. Multiple isoforms of human microtubule-associated protein tau: sequences and localization in neurofibrillary tangles of Alzheimer's disease. *Neuron* **3,** 519–526 (1989).
10. Buée, L., Bussière, T., Buée-Scherrer, V., Delacourte, A. & Hof, P. R. Tau protein isoforms, phosphorylation and role in neurodegenerative disorders11These authors contributed equally to this work. *Brain Res. Rev.* **33,** 95–130 (2000).
11. Mandelkow, E.-M. & Mandelkow, E. Biochemistry and cell biology of tau protein in neurofibrillary degeneration. *Cold Spring Harb. Perspect. Med.* **2,** a006247 (2012).
12. Wang, Y. & Mandelkow, E. Tau in physiology and pathology. *Nat. Rev. Neurosci.* **17,** 22–35 (2015).
13. Raskin, J., Cummings, J., Hardy, J., Schuh, K. & Dean, R. A. Neurobiology of Alzheimer's Disease: Integrated Molecular, Physiological, Anatomical, Biomarker, and Cognitive Dimensions. *Curr. Alzheimer Res.* **12,** 712–722 (2015).
14. Passer, B. *et al.* Generation of an apoptotic intracellular peptide by gamma-secretase cleavage of Alzheimer's amyloid beta protein precursor. *J. Alzheimers. Dis.* **2,** 289–301 (2000).
15. Hardy, J. A. & Higgins, G. A. Alzheimer's disease: the amyloid cascade hypothesis. *Science* **256,** 184–5 (1992).
16. Selkoe, D. J. & Hardy, J. The amyloid hypothesis of Alzheimer's disease at 25 years. *EMBO Mol. Med.* e201606210 (2016). doi:10.15252/emmm.201606210
17. Roberson, E. D. *et al.* Reducing endogenous tau ameliorates amyloid beta-induced deficits in an Alzheimer's disease mouse model. *Science* **316,** 750–4 (2007).
18. Rapoport, M., Dawson, H. N., Binder, L. I., Vitek, M. P. & Ferreira, A. Tau is essential to beta -amyloid-induced neurotoxicity. *Proc. Natl. Acad. Sci. U. S. A.* **99,** 6364–6369 (2002).
19. Olsson, F. *et al.* Characterization of intermediate steps in amyloid beta (Aβ) production under near-native conditions. *J. Biol. Chem.* **289,** 1540–50 (2014).
20. Chow, V. W., Mattson, M. P., Wong, P. C. & Gleichmann, M. An Overview of APP Processing Enzymes and Products. *NeuroMolecular Med.* 1–12 (2009). doi:10.1007/s12017-009-8104-z
21. Kitaguchi, N., Takahashi, Y., Tokushima, Y., Shiojiri, S. & Ito, H. Novel Precursor of Alzheimer's Disease Amyloid Protein Shows Protease Inhibitory Activity. *Nature* **331,** 530–532 (1988).
22. Tanzi, R. E. *et al.* Protease Inhibitor Domain Encoded by an Amyloid Protein Precursor mRNA Associated with Alzheimer's Disease. *Nature* **331,** 528–530 (1988).

23. Kang, J. *et al.* The precursor of Alzheimer's disease amyloid A4 protein resembles a cell-surface receptor. *Nature* **325,** 733–736 (1987).

24. Fukuchi, K., Martin, G. M. & Deeb, S. S. Sequence of the protease inhibitor domain of the A4 amyloid protein precursor of Mus domesticus. *Nucleic Acids Res.* **17,** 5396 (1989).

25. Greenfield, J. P. *et al.* Endoplasmic reticulum and trans-Golgi network generate distinct populations of Alzheimer beta -amyloid peptides. *Proc. Natl. Acad. Sci.* **96,** 742–747 (1999).

26. Weidemann, A. *et al.* A Novel ε-Cleavage within the Transmembrane Domain of the Alzheimer Amyloid Precursor Protein Demonstrates Homology with Notch Processing †. *Biochemistry* **41,** 2825–2835 (2002).

27. Xu, X. Gamma-secretase catalyzes sequential cleavages of the AbetaPP transmembrane domain. *J. Alzheimers. Dis.* **16,** 211–24 (2009).

28. Jonsson, T. *et al.* A mutation in APP protects against Alzheimer's disease and age-related cognitive decline. *Nature* **488,** 96–9 (2012).

29. Vingtdeux, V., Sergeant, N. & Buée, L. Potential contribution of exosomes to the prion-like propagation of lesions in Alzheimer's disease. *Front. Physiol.* **3,** 229 (2012).

30. Haapasalo, A. & Kovacs, D. M. The many substrates of presenilin/γ-secretase. *J. Alzheimers. Dis.* **25,** 3–28 (2011).

31. De Strooper, B. *et al.* A presenilin-1-dependent gamma-secretase-like protease mediates release of Notch intracellular domain. *Nature* **398,** 518–22 (1999).

32. Arumugam, T. V. *et al.* Evidence that gamma-Secretase-Mediated Notch Signaling Induces Neuronal Cell Death via the Nuclear Factor-kB-Bcl-2-Interacting Mediator of Cell Death Pathway in Ischemic Stroke. *Mol. Pharmacol.* **80,** 23–31 (2011).

33. Ni, C. Y., Murphy, M. P., Golde, T. E. & Carpenter, G. gamma -Secretase cleavage and nuclear localization of ErbB-4 receptor tyrosine kinase. *Science* **294,** 2179–81 (2001).

34. Marambaud, P. *et al.* A presenilin-1/gamma-secretase cleavage releases the E-cadherin intracellular domain and regulates disassembly of adherens junctions. *EMBO J.* **21,** 1948–56 (2002).

35. Lammich, S. Presenilin-dependent Intramembrane Proteolysis of CD44 Leads to the Liberation of Its Intracellular Domain and the Secretion of an Abeta -like Peptide. *J. Biol. Chem.* **277,** 44754–44759 (2002).

36. De Strooper, B. Aph-1, Pen-2, and Nicastrin with Presenilin generate an active ??-Secretase complex. *Neuron* **38,** 9–12 (2003).

37. Kaether, C., Haass, C. & Steiner, H. Assembly, Trafficking and Function of gamma-Secretase. *Neurodegener. Dis.* **3,** 275–283 (2006).

38. Edbauer, D. *et al.* Reconstitution of gamma-secretase activity. *Nat. Cell Biol.* **5,** 486–8 (2003).

39. Laudon, H. *et al.* A Nine-transmembrane Domain Topology for Presenilin 1. *J. Biol. Chem.* **280,** 35352–35360 (2005).

40. Bai, X. *et al.* An atomic structure of human γ-secretase. *Nature* **525,** 212–217 (2015).

41. Sherrington, R. *et al.* Cloning of a gene bearing missense mutations in early-onset familial Alzheimer's disease. *Nature* **375,** 754–60 (1995).

42. Levy-Lahad, E. *et al.* Candidate gene for the chromosome 1 familial Alzheimer's disease locus. *Science (80-.).* **269,** 973–977 (1995).

43. Rogaev, E. I. *et al.* Familial Alzheimer's disease in kindreds with missense mutations in a gene on chromosome 1 related to the Alzheimer's disease type 3 gene. *Nature* **376,** 775–8 (1995).

44. Podlisny, M. B. *et al.* Presenilin Proteins Undergo Heterogeneous Endoproteolysis between Thr291and Ala299and Occur as Stable N- and C-Terminal Fragments in Normal and Alzheimer Brain Tissue. *Neurobiol. Dis.* **3,** 325–337 (1997).

45. Ratovitski, T. *et al.* Endoproteolytic processing and stabilization of wild-type and mutant presenilin. *J. Biol. Chem.* **272,** 24536–24541 (1997).

46. Capell, A. The Proteolytic Fragments of the Alzheimer's Disease-associated Presenilin-1 Form Heterodimers and Occur as a 100-150-kDa Molecular Mass Complex. *J. Biol. Chem.* **273,** 3205–3211 (1998).

47. Li, Y. *et al.* Presenilin 1 is linked with gamma -secretase activity in the detergent solubilized state. *Proc. Natl. Acad. Sci.* **97,** 6138–6143 (2000).

48. De Strooper, B. *et al.* Deficiency of presenilin-1 inhibits the normal cleavage of amyloid precursor protein. *Nature* **391,** 387–90 (1998).

49. Naruse, S. *et al.* Effects of PS1 Deficiency on Membrane Protein Trafficking in Neurons. *Neuron* **21,** 1213–1221 (1998).

50. Zhang, Z. *et al.* Presenilins are required for gamma-secretase cleavage of beta-APP and transmembrane cleavage of Notch-1. *Nat. Cell Biol.* **2,** 463–5 (2000).

51. Herreman, A. *et al.* Total inactivation of gamma-secretase activity in presenilin-deficient embryonic stem cells. *Nat. Cell Biol.* **2,** 461–2 (2000).

52. Wolfe, M. S. *et al.* Two transmembrane aspartates in presenilin-1 required for presenilin endoproteolysis and gamma-secretase activity. *Nature* **398,** 513–7 (1999).

53. Steiner, H. *et al.* A Loss of Function Mutation of Presenilin-2 Interferes with Amyloid -Peptide Production and Notch Signaling. *J. Biol. Chem.* **274,** 28669–28673 (1999).

54. Esler, W. P. *et al.* Transition-state analogue inhibitors of gamma-secretase bind directly to presenilin-1. *Nat. Cell Biol.* **2,** 428–34 (2000).

55. Li, Y. *et al.* Photoactivated gamma-secretase inhibitors directed to the active site covalently label presenilin 1. *Nature* **405,** 689–94 (2000).

56. Laudon, H. *et al.* Co-expressed presenilin 1 NTF and CTF form functional γ-secretase complexes in cells devoid of full-length protein. *J. Neurochem.* **89,** 44–53 (2004).

57. Steiner, H. & Haass, C. Intramembrane proteolysis by presenilins. *Nat. Rev. Mol. Cell Biol.* **1,** 217–24 (2000).

58. Cacquevel, M., Aeschbach, L., Houacine, J. & Fraering, P. C. Alzheimer's disease-linked mutations in presenilin-1 result in a drastic loss of activity in purified γ-secretase complexes. *PLoS One* **7,** e35133 (2012).

59. Sarasija, S. & Norman, K. R. A gamma-Secretase Independent Role for Presenilin in Calcium Homeostasis Impacts Mitochondrial Function and Morphology in Caenorhabditis elegans. *Genetics* **201,** 1453–1466 (2015).

60. Tu, H. *et al.* Presenilins Form ER Ca2+ Leak Channels, a Function Disrupted by Familial Alzheimer's Disease-Linked Mutations. *Cell* **126,** 981–993 (2006).

61. Bezprozvanny, I. Presenilins: a novel link between intracellular calcium signaling and lysosomal function? *J. Cell Biol.* **198,** 7–10 (2012).

62. Yu, G. *et al.* Nicastrin modulates presenilin-mediated notch/glp-1 signal transduction and betaAPP processing. *Nature* **407,** 48–54 (2000).

63. Morais, V. A. *et al.* The Transmembrane Domain Region of Nicastrin Mediates Direct Interactions with APH-1 and the γ-Secretase Complex. *J. Biol. Chem.* **278,** 43284–43291 (2003).

64. Schedin-Weiss, S., Winblad, B. & Tjernberg, L. O. The role of protein glycosylation in Alzheimer disease. *FEBS J.* **281,** 46–62 (2014).

65. Shirotani, K. *et al.* Gamma-secretase activity is associated with a conformational change of nicastrin. *J. Biol. Chem.* **278,** 16474–7 (2003).

66. Kimberly, W. T. *et al.* Complex N-linked Glycosylated Nicastrin Associates with Active -Secretase and Undergoes Tight Cellular Regulation. *J. Biol. Chem.* **277,** 35113–35117 (2002).

67. Herreman, a. gamma-Secretase activity requires the presenilin-dependent trafficking of nicastrin through the Golgi apparatus but not its complex glycosylation. *J. Cell Sci.* **116,** 1127–1136 (2003).

68. Zhang, X. *et al.* Identification of a tetratricopeptide repeat-like domain in the nicastrin subunit of γ-secretase using synthetic antibodies. *Proc. Natl. Acad. Sci. U. S. A.* **109,** 8534–9 (2012).

69. Esler, W. P. *et al.* Activity-dependent isolation of the presenilin- gamma-secretase complex reveals nicastrin and a gamma substrate. *Proc. Natl. Acad. Sci.* **99,** 2720–2725 (2002).

70. Shah, S. *et al.* Nicastrin Functions as a γ-Secretase-Substrate Receptor. *Cell* **122,** 435–447 (2005).

71. Dries, D. R. *et al.* Glu-333 of Nicastrin Directly Participates in -Secretase Activity. *J. Biol. Chem.* **284,** 29714–29724 (2009).

72. Hayashi, I. *et al.* Single Chain Variable Fragment against Nicastrin Inhibits the -Secretase Activity. *J. Biol. Chem.* **284,** 27838–27847 (2009).

73. Hayashi, I. *et al.* Neutralization of the γ-secretase activity by monoclonal antibody against extracellular domain of nicastrin. *Oncogene* **31,** 787–98 (2012).

74. Li, Y. *et al.* Structural Interactions between Inhibitor and Substrate Docking Sites Give Insight into Mechanisms of Human PS1 Complexes. *Structure* **22,** 125–135 (2014).

75. Elad, N. *et al.* The dynamic conformational landscape of gamma-secretase. *J. Cell Sci.* **128,** 589–598 (2015).

76. Xie, T. *et al.* Crystal structure of the γ-secretase component nicastrin. *Proc. Natl. Acad. Sci.* **111,** 13349–13354 (2014).

77. Chávez-Gutiérrez, L. *et al.* Glu332 in the nicastrin ectodomain is essential for γ-secretase complex maturation but not for its activity. *J. Biol. Chem.* **283,** 20096–20105 (2008).

78. Bolduc, D. M., Montagna, D. R., Gu, Y., Selkoe, D. J. & Wolfe, M. S. Nicastrin functions to sterically hinder γ-secretase–substrate interactions driven by substrate transmembrane domain. *Proc. Natl. Acad. Sci.* **113,** E509–E518 (2016).

79. Goutte, C., Tsunozaki, M., Hale, V. a & Priess, J. R. APH-1 is a multipass membrane protein essential for the Notch signaling pathway in Caenorhabditis elegans embryos. *Proc. Natl. Acad. Sci. U. S. A.* **99,** 775–9 (2002).

80. Francis, R. *et al.* aph-1 and pen-2 Are Required for Notch Pathway Signaling, γ-Secretase Cleavage of βAPP, and Presenilin Protein Accumulation. *Dev. Cell* **3,** 85–97 (2002).

81. Gu, Y. *et al.* APH-1 interacts with mature and immature forms of presenilins and nicastrin and may play a role in maturation of presenilin.nicastrin complexes. *J. Biol. Chem.* **278,** 7374–80 (2003).

82. Shirotani, K., Edbauer, D., Prokop, S., Haass, C. & Steiner, H. Identification of Distinct gamma-Secretase Complexes with Different APH-1 Variants. *J. Biol. Chem.* **279,** 41340–41345 (2004).

83. Takasugi, N. *et al.* The role of presenilin cofactors in the gamma-secretase complex. *Nature* **422,** 438–41 (2003).

84. LaVoie, M. J. *et al.* Assembly of the gamma-secretase complex involves early formation of an intermediate subcomplex of Aph-1 and nicastrin. *J. Biol. Chem.* **278,** 37213–22 (2003).

85. Fraering, P. C. *et al.* Detergent-Dependent Dissociation of Active γ-Secretase Reveals an Interaction between Pen-2 and PS1-NTF and Offers a Model for Subunit Organization within the Complex †. *Biochemistry* **43,** 323–333 (2004).

86. Lee, S.-F. *et al.* A conserved GXXXG motif in APH-1 is critical for assembly and activity of the gamma-secretase complex. *J. Biol. Chem.* **279,** 4144–52 (2004).

87. Edbauer, D., Kaether, C., Steiner, H. & Haass, C. Co-expression of nicastrin and presenilin rescues a loss of function mutant of APH-1. *J. Biol. Chem.* **279,** 37311–37315 (2004).

88. Niimura, M. *et al.* Aph-1 Contributes to the Stabilization and Trafficking of the gamma-Secretase Complex through Mechanisms Involving Intermolecular and Intramolecular Interactions. *J. Biol. Chem.* **280,** 12967–12975 (2005).

89. Pardossi-Piquard, R. *et al.* APH1 polar transmembrane residues regulate the assembly and activity of presenilin complexes. *J. Biol. Chem.* **284,** 16298–307 (2009).

90. Chen, A. C., Guo, L. Y., Ostaszewski, B. L., Selkoe, D. J. & LaVoie, M. J. Aph-1 Associates Directly with Full-length and C-terminal Fragments of -Secretase Substrates. *J. Biol. Chem.* **285,** 11378–11391 (2010).

91. Hu, C. *et al.* Nicastrin is required for amyloid precursor protein (APP) but not Notch processing, while anterior pharynx-defective 1 is dispensable for processing of both APP and Notch. *J. Neurochem.* **136,** 1246–1258 (2016).

92. Steiner, H. *et al.* PEN-2 Is an Integral Component of the gamma-Secretase Complex Required for Coordinated Expression of Presenilin and Nicastrin. *J. Biol. Chem.* **277,** 39062–39065 (2002).

93. Watanabe, N. *et al.* Pen-2 Is Incorporated into the -Secretase Complex through Binding to Transmembrane

Domain 4 of Presenilin 1. *J. Biol. Chem.* **280,** 41967–41975 (2005).

94. Luo, W. -j. PEN-2 and APH-1 Coordinately Regulate Proteolytic Processing of Presenilin 1. *J. Biol. Chem.* **278,** 7850–7854 (2003).

95. Prokop, S., Shirotani, K., Edbauer, D., Haass, C. & Steiner, H. Requirement of PEN-2 for Stabilization of the Presenilin N-/C-terminal Fragment Heterodimer within the -Secretase Complex. *J. Biol. Chem.* **279,** 23255–23261 (2004).

96. Prokop, S., Haass, C. & Steiner, H. Length and overall sequence of the PEN-2 C-terminal domain determines its function in the stabilization of presenilin fragments. *J. Neurochem.* **94,** 57–62 (2005).

97. Kim, S. H. & Sisodia, S. S. A sequence within the first transmembrane domain of PEN-2 is critical for PEN-2-mediated endoproteolysis of presenilin 1. *J. Biol. Chem.* **280,** 1992–2001 (2005).

98. Ahn, K. *et al.* Activation and intrinsic gamma-secretase activity of presenilin 1. *Proc. Natl. Acad. Sci. U. S. A.* **107,** 21435–40 (2010).

99. Mao, G., Cui, M.-Z., Li, T., Jin, Y. & Xu, X. Pen-2 is dispensable for endoproteolysis of presenilin 1, and nicastrin-Aph subcomplex is important for both γ-secretase assembly and substrate recruitment. *J. Neurochem.* **123,** 837–844 (2012).

100. Holmes, O., Paturi, S., Selkoe, D. J. & Wolfe, M. S. Pen-2 Is Essential for γ-Secretase Complex Stability and Trafficking but Partially Dispensable for Endoproteolysis. *Biochemistry* **53,** 4393–4406 (2014).

101. Bammens, L., Chavez-Gutierrez, L., Tolia, A., Zwijsen, A. & De Strooper, B. Functional and Topological Analysis of Pen-2, the Fourth Subunit of the -Secretase Complex. *J. Biol. Chem.* **286,** 12271–12282 (2011).

102. Shiraishi, H. *et al.* PEN-2 enhances gamma-cleavage after presenilin heterodimer formation. *J. Neurochem.* **90,** 1402–1413 (2004).

103. Li, X. *et al.* Ferritin light chain interacts with PEN-2 and affects γ-secretase activity. *Neurosci. Lett.* **548,** 90–4 (2013).

104. Hasegawa, H. *et al.* Both the sequence and length of the C terminus of PEN-2 are critical for intermolecular interactions and function of presenilin complexes. *J. Biol. Chem.* **279,** 46455–63 (2004).

105. Shirotani, K., Edbauer, D., Kostka, M., Steiner, H. & Haass, C. Immature nicastrin stabilizes APH-1 independent of PEN-2 and presenilin: identification of nicastrin mutants that selectively interact with APH-1. *J. Neurochem.* **89,** 1520–7 (2004).

106. Spasic, D. & Annaert, W. Building γ-secretase - the bits and pieces. *J. Cell Sci.* **121,** 413–420 (2008).

107. Hu, Y. & Fortini, M. E. Different cofactor activities in gamma-secretase assembly: evidence for a nicastrin-Aph-1 subcomplex. *J. Cell Biol.* **161,** 685–90 (2003).

108. Periz, G. & Fortini, M. E. Functional reconstitution of gamma-secretase through coordinated expression of presenilin, nicastrin, Aph-1, and Pen-2. *J. Neurosci. Res.* **77,** 309–322 (2004).

109. Verdile, G., Gandy, S. E. & Martins, R. N. The role of presenilin and its interacting proteins in the biogenesis of Alzheimer's beta amyloid. *Neurochem. Res.* **32,** 609–23 (2007).

110. Wolfe, M. S. Toward the structure of presenilin/γ-secretase and presenilin homologs. *Biochim. Biophys. Acta - Biomembr.* **1828,** 2886–2897 (2013).

111. Schroeter, E. H. *et al.* A presenilin dimer at the core of the gamma-secretase enzyme: insights from parallel analysis of Notch 1 and APP proteolysis. *Proc. Natl. Acad. Sci. U. S. A.* **100,** 13075–80 (2003).

112. Cervantes, S., Gonzàlez-Duarte, R. & Marfany, G. Homodimerization of presenilin N-terminal fragments is affected by mutations linked to Alzheimer's disease. *FEBS Lett.* **505,** 81–86 (2001).

113. Kornilova, A. Y., Bihel, F., Das, C. & Wolfe, M. S. The initial substrate-binding site of gamma-secretase is located on presenilin near the active site. *Proc. Natl. Acad. Sci. U. S. A.* **102,** 3230–5 (2005).

114. Kaether, C. *et al.* The presenilin C-terminus is required for ER-retention, nicastrin-binding and gamma-secretase activity. *EMBO J.* **23,** 4738–48 (2004).

115. Wang, J. *et al.* C-terminal PAL motif of presenilin and presenilin homologues required for normal active site conformation. *J. Neurochem.* **96,** 218–27 (2006).

116. Wang, J., Brunkan, A. L., Hecimovic, S., Walker, E. & Goate, A. Conserved 'PAL' sequence in presenilins is essential for γ-secretase activity, but not required for formation or stabilization of γ-secretase

complexes. *Neurobiol. Dis.* **15,** 654–666 (2004).

117. Sato, C., Morohashi, Y., Tomita, T. & Iwatsubo, T. Structure of the catalytic pore of gamma-secretase probed by the accessibility of substituted cysteines. *J. Neurosci.* **26,** 12081–8 (2006).

118. Sato, C., Takagi, S., Tomita, T. & Iwatsubo, T. The C-terminal PAL motif and transmembrane domain 9 of presenilin 1 are involved in the formation of the catalytic pore of the gamma-secretase. *J. Neurosci.* **28,** 6264–71 (2008).

119. Tolia, A., Chávez-Gutiérrez, L. & De Strooper, B. Contribution of presenilin transmembrane domains 6 and 7 to a water-containing cavity in the gamma-secretase complex. *J. Biol. Chem.* **281,** 27633–42 (2006).

120. Takagi, S., Tominaga, a., Sato, C., Tomita, T. & Iwatsubo, T. Participation of Transmembrane Domain 1 of Presenilin 1 in the Catalytic Pore Structure of the -Secretase. *J. Neurosci.* **30,** 15943–15950 (2010).

121. Lazarov, V. K. *et al.* Electron microscopic structure of purified, active gamma-secretase reveals an aqueous intramembrane chamber and two pores. *Proc. Natl. Acad. Sci. U. S. A.* **103,** 6889–6894 (2006).

122. Ogura, T. *et al.* Three-dimensional structure of the γ-secretase complex. *Biochem. Biophys. Res. Commun.* **343,** 525–534 (2006).

123. Osenkowski, P. *et al.* Cryoelectron Microscopy Structure of Purified γ-Secretase at 12 Å Resolution. *J. Mol. Biol.* **385,** 642–652 (2009).

124. Renzi, F. *et al.* Structure of -Secretase and Its Trimeric Pre-activation Intermediate by Single-particle Electron Microscopy. *J. Biol. Chem.* **286,** 21440–21449 (2011).

125. Sobhanifar, S. *et al.* Structural investigation of the C-terminal catalytic fragment of presenilin 1. *Proc. Natl. Acad. Sci.* **107,** 9644–9649 (2010).

126. Li, X. *et al.* Structure of a presenilin family intramembrane aspartate protease. *Nature* **493,** 56–61 (2013).

127. Dang, S. *et al.* Cleavage of amyloid precursor protein by an archaeal presenilin homologue PSH. *Proc. Natl. Acad. Sci.* **112,** 3344–3349 (2015).

128. Torres-Arancivia, C. *et al.* Identification of an archaeal presenilin-like intramembrane protease. *PLoS One* **5,** (2010).

129. Lu, P. *et al.* Three-dimensional structure of human γ-secretase. *Nature* **512,** 166–170 (2014).

130. Sun, L. *et al.* Structural basis of human γ-secretase assembly. *Proc. Natl. Acad. Sci.* **112,** 6003–6008 (2015).

131. Bai, X., Rajendra, E., Yang, G., Shi, Y. & Scheres, S. H. Sampling the conformational space of the catalytic subunit of human γ-secretase. *Elife* **4,** 1–42 (2015).

132. Li, Y., Liew, L. S. Y., Li, Q. & Kang, C. Structure of the transmembrane domain of human nicastrin-a component of γ-secretase. *Sci. Rep.* **6,** 19522 (2016).

133. Miles, J. S. & Wolf, C. R. Principles of DNA cloning. *BMJ* **299,** 1019–22 (1989).

134. Schwarz, D., Dötsch, V. & Bernhard, F. Production of membrane proteins using cell-free expression systems. *Proteomics* **8,** 3933–3946 (2008).

135. Schwarz, D. *et al.* Preparative scale cell-free expression systems: New tools for the large scale preparation of integral membrane proteins for functional and structural studies. *Methods* **41,** 355–369 (2007).

136. Klammt, C. *et al.* Evaluation of detergents for the soluble expression of α-helical and β-barrel-type integral membrane proteins by a preparative scale individual cell-free expression system. *FEBS J.* **272,** 6024–6038 (2005).

137. Yang, J.-P., Cirico, T., Katzen, F., Peterson, T. C. & Kudlicki, W. Cell-free synthesis of a functional G protein-coupled receptor complexed with nanometer scale bilayer discs. *BMC Biotechnol.* **11,** 57 (2011).

138. Bayburt, T. H. & Sligar, S. G. Membrane protein assembly into Nanodiscs. *FEBS Lett.* **584,** 1721–7 (2010).

139. Hodges, R. S., Heaton, R. J., Parker, J. M. R., Molday, L. & Molday, R. S. Antigen-antibody interaction. Synthetic peptides define linear antigenic determinants recognized by monoclonal antibodies directed to the cytoplasmic carboxyl terminus of rhodopsin. *J. Biol. Chem.* **263,** 11768–11775 (1988).

140. Takayama, H., Chelikani, P., Reeves, P. J., Zhang, S. & Khorana, H. G. High-level expression, single-step immunoaffinity purification and characterization of human tetraspanin membrane protein CD81. *PLoS*

One **3,** e2314 (2008).

141. Wang, X., Corin, K., Rich, C. & Zhang, S. Study of two G-protein coupled receptor variants of human trace amine-associated receptor 5. *Sci. Rep.* **1,** 102 (2011).

142. Einhauer, A. & Jungbauer, A. The FLAG^{TM} peptide, a versatile fusion tag for the purification of recombinant proteins. *J. Biochem. Biophys. Methods* **49,** 455–465 (2001).

143. Field, J. *et al.* Purification of a RAS-responsive adenylyl cyclase complex from Saccharomyces cerevisiae by use of an epitope addition method. *Mol. Cell. Biol.* **8,** 2159–65 (1988).

144. Kelly, S. M., Jess, T. J. & Price, N. C. How to study proteins by circular dichroism. *Biochim. Biophys. Acta - Proteins Proteomics* **1751,** 119–139 (2005).

145. Kelly, S. & Price, N. The Use of Circular Dichroism in the Investigation of Protein Structure and Function. *Curr. Protein Pept. Sci.* **1,** 349–384 (2000).

146. Greenfield, N. J. Using circular dichroism spectra to estimate protein secondary structure. *Nat. Protoc.* **1,** 2876–90 (2006).

147. Navarro, S. & Ventura, S. Fluorescent dye ProteoStat to detect and discriminate intracellular amyloid-like aggregates in Escherichia coli. *Biotechnol. J.* **9,** 1259–1266 (2014).

148. Vollrath, F., Hawkins, N., Porter, D., Holland, C. & Boulet-Audet, M. Differential Scanning Fluorimetry provides high throughput data on silk protein transitions. *Sci. Rep.* **4,** 5625 (2014).

149. Fluorescence wikipedia. Available at: https://en.wikipedia.org/wiki/Fluorescence.

150. Lakowicz, J. R. & Masters, B. R. *Principles of Fluorescence Spectroscopy, Third Edition*. *Journal of Biomedical Optics* **13,** (2008).

151. Seidel, S. A. I. *et al.* Microscale thermophoresis quantifies biomolecular interactions under previously challenging conditions. *Methods* **59,** 301–315 (2013).

152. Wienken, C. J. *et al.* Protein-binding assays in biological liquids using microscale thermophoresis. *Nat. Commun.* **1,** 100 (2010).

153. Jerabek-Willemsen, M. *et al.* MicroScale Thermophoresis: Interaction analysis and beyond. *J. Mol. Struct.* **1077,** 101–113 (2014).

154. Murphy, R. Static and dynamic light scattering of biological macromolecules: what can we learn? *Curr. Opin. Biotechnol.* **8,** 25–30 (1997).

155. Caffrey, M. & Cherezov, V. Crystallizing membrane proteins using lipidic mesophases. *Nat. Protoc.* **4,** 706–31 (2009).

156. Kubicek, J. *et al.* Controlled in meso phase crystallization - a method for the structural investigation of membrane proteins. *PLoS One* **7,** (2012).

157. Whiles, J. A., Deems, R., Vold, R. R. & Dennis, E. A. Bicelles in structure–function studies of membrane-associated proteins. *Bioorg. Chem.* **30,** 431–442 (2002).

158. Ujwal, R. & Bowie, J. U. Crystallizing membrane proteins using lipidic bicelles. *Methods* **55,** 337–341 (2011).

159. De Angelis, A. A. & Opella, S. J. Bicelle samples for solid-state NMR of membrane proteins. *Nat. Protoc.* **2,** 2332–2338 (2007).

160. Landau, E. M. & Rosenbusch, J. P. Lipidic cubic phases: a novel concept for the crystallization of membrane proteins. *Proc. Natl. Acad. Sci. U. S. A.* **93,** 14532–5 (1996).

161. Caffrey, M. Crystallizing membrane proteins for structure-function studies using lipidic mesophases. *Biochem. Soc. Trans.* **39,** 725–32 (2011).

162. Geertsma, E. R., Nik Mahmood, N. A. B., Schuurman-Wolters, G. K. & Poolman, B. Membrane reconstitution of ABC transporters and assays of translocator function. *Nat. Protoc.* **3,** 256–266 (2008).

163. Goddard, A. D., Dijkman, P. M., Adamson, R. J., dos Reis, R. I. & Watts, A. in *Methods in enzymology* **556,** 405–424 (2015).

164. Rigaud, J.-L., Pitard, B. & Levy, D. Reconstitution of membrane proteins into liposomes: application to energy-transducing membrane proteins. *Biochim. Biophys. Acta - Bioenerg.* **1231,** 223–246 (1995).

165. Simeonov, P., Werner, S., Haupt, C., Tanabe, M. & Bacia, K. Membrane protein reconstitution into liposomes guided by dual-color fluorescence cross-correlation spectroscopy. *Biophys. Chem.* **184,** 37–43 (2013).

166. Chávez-Gutiérrez, L. *et al.* Glu(332) in the Nicastrin ectodomain is essential for gamma-secretase complex maturation but not for its activity. *J. Biol. Chem.* **283,** 20096–105 (2008).

167. Bolduc, D. M. & Wolfe, M. S. Structure of nicastrin unveils secrets of γ-secretase. *Proc. Natl. Acad. Sci. U. S. A.* **111,** 14643–4 (2014).

168. Membrane Proteins of Known Structure. Available at: http://blanco.biomol.uci.edu/mpstruc/. (Accessed: 20th March 2016)

169. Raman, P., Cherezov, V. & Caffrey, M. The Membrane Protein Data Bank. *Cell. Mol. Life Sci.* **63,** 36–51 (2006).

170. Fraering, P. C. *et al.* Purification and Characterization of the Human γ-Secretase Complex †. *Biochemistry* **43,** 9774–9789 (2004).

171. Stempfle, D., Kanwar, R., Loewer, a., Fortini, M. E. & Merdes, G. In Vivo Reconstitution of -Secretase in Drosophila Results in Substrate Specificity. *Mol. Cell. Biol.* **30,** 3165–3175 (2010).

172. Wu, C. C. & Yates, J. R. The application of mass spectrometry to membrane proteomics. *Nat. Biotechnol.* **21,** 262–267 (2003).

173. Zhou, H., Zhou, S., Walian, P. J. & Jap, B. K. Dependency of γ-secretase complex activity on the structural integrity of the bilayer. *Biochem. Biophys. Res. Commun.* **402,** 291–296 (2010).

174. Barrett, P. J. *et al.* The Amyloid Precursor Protein Has a Flexible Transmembrane Domain and Binds Cholesterol. *Science (80-.).* **336,** 1168–1171 (2012).

175. Wahrle, S. *et al.* Cholesterol-Dependent γ-Secretase Activity in Buoyant Cholesterol-Rich Membrane Microdomains. *Neurobiol. Dis.* **9,** 11–23 (2002).

176. Matsumura, N. *et al.* -Secretase Associated with Lipid Rafts: MULTIPLE INTERACTIVE PATHWAYS IN THE STEPWISE PROCESSING OF -CARBOXYL-TERMINAL FRAGMENT. *J. Biol. Chem.* **289,** 5109–5121 (2014).

177. Vetrivel, K. S. *et al.* Association of γ-Secretase with Lipid Rafts in Post-Golgi and Endosome Membranes. *J. Biol. Chem.* **279,** 44945–44954 (2004).

178. Urano, Y. *et al.* Association of active gamma-secretase complex with lipid rafts. *J. Lipid Res.* **46,** 904–12 (2005).

179. Guan, X. M., Tong Sun Kobilka & Kobilka, B. K. Enhancement of membrane insertion and function in a type IIIb membrane protein following introduction of a cleavable signal peptide. *J. Biol. Chem.* **267,** 21995–21998 (1992).

180. Abdul-Gader, A., Miles, A. J. & Wallace, B. A. A reference dataset for the analyses of membrane protein secondary structures and transmembrane residues using circular dichroism spectroscopy. *Bioinformatics* **27,** 1630–6 (2011).

181. Sreerama, N. & Woody, R. W. Estimation of Protein Secondary Structure from Circular Dichroism Spectra: Comparison of CONTIN, SELCON, and CDSSTR Methods with an Expanded Reference Set. *Anal. Biochem.* **287,** 252–260 (2000).

182. Zhou, N. E., Kay, C. M. & Hodges, R. S. Synthetic model proteins. *J. Biol. Chem.* **267,** 2664–2670 (1992).

183. Lau, S. Y., Taneja, a K. & Hodges, R. S. Synthesis of a model protein of defined secondary and quaternary structure. Effect of chain length on the stabilization and formation of two-stranded alpha-helical coiled-coils. *J. Biol. Chem.* **259,** 13253–13261 (1984).

184. Benjwal, S., Verma, S., Röhm, K.-H. & Gursky, O. Monitoring protein aggregation during thermal unfolding in circular dichroism experiments. *Protein Sci.* **15,** 635–9 (2006).

185. Mandal, S. *et al.* A Surfactant-Induced Functional Modulation of a Global Virulence Regulator from Staphylococcus aureus. *PLoS One* **11,** e0151426 (2016).

186. Alattia, J.-R. *et al.* Highly efficient production of the Alzheimer's γ-Secretase integral membrane protease complex by a multi-gene stable integration approach. *Biotechnol. Bioeng.* **110,** 1995–2005 (2013).

187. Iwata, S. *Methods and Results in Crystallization of Membrane Proteins*. (Internat'l University Line, 2003).

188. Zhang, X. *et al.* Evidence That the 'Lid' Domain of Nicastrin Is Not Essential for Regulating γ-Secretase Activity. *J. Biol. Chem.* **291,** 6748–6753 (2016).

189. Walker, E. S., Martinez, M., Wang, J. & Goate, A. Conserved residues in juxtamembrane region of the extracellular domain of nicastrin are essential for gamma-secretase complex formation. *J. Neurochem.* **98,** 300–9 (2006).

190. Ren, H. *et al.* High-level production, solubilization and purification of synthetic human GPCR chemokine receptors CCR5, CCR3, CXCR4 and CX3CR1. *PLoS One* **4,** e4509 (2009).

191. Cook, B. L. *et al.* Large-scale production and study of a synthetic G protein-coupled receptor: Human olfactory receptor 17-4. *Proc. Natl. Acad. Sci.* **106,** 11925–11930 (2009).

192. Galián, C. *et al.* Optimized purification of a heterodimeric ABC transporter in a highly stable form amenable to 2-D crystallization. *PLoS One* **6,** e19677 (2011).

193. Infed, N., Hanekop, N., Driessen, A. J. M., Smits, S. H. J. & Schmitt, L. Influence of detergents on the activity of the ABC transporter LmrA. *Biochim. Biophys. Acta - Biomembr.* **1808,** 2313–2321 (2011).

194. Hirayama, H., Kimura, Y., Kioka, N., Matsuo, M. & Ueda, K. ATPase activity of human ABCG1 is stimulated by cholesterol and sphingomyelin. *J. Lipid Res.* **54,** 496–502 (2013).

195. Nguyen, T. A., Lieu, S. S. & Chang, G. An Escherichia coli -Based Cell-Free System for Large-Scale Production of Functional Mammalian Membrane Proteins Suitable for X-Ray Crystallography. *Mol. Microbiol.* 85–91 (2010). doi:10.1159/000283512

196. Zhou, S., Zhou, H., Walian, P. J. & Jap, B. K. CD147 is a regulatory subunit of the gamma-secretase complex in Alzheimer's disease amyloid beta-peptide production. *Proc. Natl. Acad. Sci. U. S. A.* **102,** 7499–7504 (2005).

197. Beel, A. J. *et al.* Nonspecificity of Binding of γ-Secretase Modulators to the Amyloid Precursor Protein. *Biochemistry* **48,** 11837–11839 (2009).

198. Botev, A. *et al.* The Amyloid Precursor Protein C-Terminal Fragment C100 Occurs in Monomeric and Dimeric Stable Conformations and Binds γ-Secretase Modulators. *Biochemistry* **50,** 828–835 (2011).

199. Fukumori, A. & Steiner, H. Substrate recruitment of -secretase and mechanism of clinical presenilin mutations revealed by photoaffinity mapping. *EMBO J.* (2016). doi:10.15252/embj.201694151

200. Zhang, X., Yu, C. J. & Sisodia, S. S. The topology of pen-2, a γ-secretase subunit, revisited: evidence for a reentrant loop and a single pass transmembrane domain. *Mol. Neurodegener.* **10,** 39 (2015).

201. Holmes, O., Paturi, S., Wolfe, M. S. & Selkoe, D. J. Functional analysis and purification of a Pen-2 fusion protein for gamma-secretase structural studies. *J. Neurochem.* (2014). doi:10.1111/jnc.12772

202. Koronakis, V., Sharff, A., Koronakis, E., Luisi, B. & Hughes, C. Crystal structure of the bacterial membrane protein TolC central to multidrug efflux and protein export. *Nature* **405,** 914–9 (2000).

203. Khemtémourian, L., Buchoux, S., Aussenac, F. & Dufourc, E. J. Dimerization of Neu/Erb2 transmembrane domain is controlled by membrane curvature. *Eur. Biophys. J.* **36,** 107–112 (2007).

204. Carlier, L. *et al.* Investigating the role of GXXXG motifs in helical folding and self-association of plasticins, Gly/Leu-rich antimicrobial peptides. *Biophys. Chem.* **196,** 40–52 (2015).

205. Neet, K. E. & Timm, D. E. Conformational stability of dimeric proteins: quantitative studies by equilibrium denaturation. *Protein Sci.* **3,** 2167–74 (1994).

206. Steiner, H. *et al.* The Biological and Pathological Function of the Presenilin-1 Exon 9 Mutation Is Independent of Its Defect to Undergo Proteolytic Processing. *J. Biol. Chem.* **274,** 7615–7618 (1999).

207. Rath, A., Glibowicka, M., Nadeau, V. G., Chen, G. & Deber, C. M. Detergent binding explains anomalous SDS-PAGE migration of membrane proteins. *Proc. Natl. Acad. Sci. U. S. A.* **106,** 1760–5 (2009).

208. Osenkowski, P., Ye, W., Wang, R., Wolfe, M. S. & Selkoe, D. J. Direct and Potent Regulation of -Secretase by Its Lipid Microenvironment. *J. Biol. Chem.* **283,** 22529–22540 (2008).

209. Ayciriex, S. *et al.* The lipidome associated with the -secretase complex is required for its integrity and activity. *Biochem. J.* **473,** 321–334 (2016).

210. Hoke, D. E. *et al.* In vitro gamma-secretase cleavage of the Alzheimer's amyloid precursor protein correlates to a subset of presenilin complexes and is inhibited by zinc. *FEBS J.* **272,** 5544–5557 (2005).

Appendix I: DNA and protein sequences

APH1

APH-1 DNA Sequence

CCG CA TATG CATCATCACCACCATCACCATCATCATCACGCAATTGAAGGTCGT
GGTGCAGCAGTTTTTTTTGGTTGTACCTTTGTTGCATTTGGTCCGGCATTTGCACTGTTTCTGATTACCGTTGCCGGTGATCCGCTG
CGTGTTATTATTCTGGTTGCGGGTGCATTTTTTTGGCTGGTTAGCCTGCTGCTGGCAAGCGTTGTTTGGTTTATCCTGGTTCATGTTA
CCGATCGTAGTGATGCACGTCTGCAGTATGGTCTGCTGATTTTTGGTGCAGCCGTTAGCGTTCTGCTGCAAGAAGTTTTTCGTTT
CGCATATTACAAACTGCTGAAAAAAGCAGATGAAGGTCTGGCAAGCCTGAGCGAAGATGGTCGTAGCCCGATTAGCATT
CGTCAGATGGCCTATGTTAGCGGTCTGAGCTTTGGTATTATTAGCGGTGTTTTTAGCGTGATTAACATTCTGGCAGATGCACTG
GGTCCGGGTGTTGTTGGTATTCATGGTGATAGCCCGTATTATTTCCTGACCAGCGCATTTCTGACCGCAGCAATTATCCTGCT
GCATACCTTTTGGGGTGTTGTGTTTTTTGATGCATGTGAACGTCGTCGTTATTGGGCACTGGGCCTGGTTGTGGGTAGCCATCT
GCTGACCAGTGGTCTGACCTTTCTGAATCCGTGGTATGAAGCAAGTCTGCTGCCGATTTATGCAGTTACCGTTAGCATGGGT
CTGTGGGCATTTATTACCGCAGGCGGTAGCCTGCGTAGCATTCAGCGTAGTCTGCTGTGTCGTCGTCAAGAGGATAGCCG
TGTTATGGTTTATAGCGCACTGCGTATTCCGCCTGAAGAT TAA C TCGAGGG

A1 Protein Sequence

MHHHHHHHHHHAIHGRGAAVFFGCTFVAFGPAFALFLITVAGDPLRVIILVAGAFFWLVSLLLASVVWFILVHVTDRSDARL
QYGLLIFGAAVSVLLQEVFRFAYYKLLKKADEGLASLSEDGRSPISIRQMAYVSGLSFGIISGVFSVINILADALGPGVVGIHG
DSPYYFLTSAFLTAAIILLHTFWGVVFFDACERRRYWALGLVVGSHLLTSGLTFLNPWYEASLLPIYAVTVSMGLWAFITAGGSL
RSIQRSLLCRRQEDSRVMVYSALRIPPED

A7 Protein Sequence

MGAAVFFGCTFVAFGPAFALFLITVAGDPLRVIILVAGAFFWLVSLLLASVVWFILVHVTDRSDARLQYGLLIFGAAVSVLLQ
EVFRFAYYKLLKKADEGLASLSEDGRSPISIRQMAYVSGLSFGIISGVFSVINILADALGPGVVGIHGDSPYYFLTSAFLTAAIILL
HTFWGVVFFDACERRRYWALGLVVGSHLLTSGLTFLNPWYEASLLPIYAVTVSMGLWAFITAGGSLRSIQRSLLCRRQEDSR
VMVYSALRIPPKDGSSGTETSQVAPA

AI Protein Sequence

MGAAVFFGCTFVAFGPAFALFLITVAGDPLRVIILVAGAFFWLVSLLLASVVWFILVHVTDRSDARLQYGLLIFGAAVSVLLQ
EVFRFAYYKLLKKADEGLASLSEDGRSPISIRQMAYVSGLSFGIISGVFSVINILADALGPGVVGIHGDSPYYFLTSAFLTAAIILL
HTFWGVVFFDACERRRYWALGLVVGSHLLTSGLTFLNPWYEASLLPIYAVTVSMGLWAFITAGGSLRSIQRSLLCRRQEDSR
VMVYSALR IPPEDLVPRG SHHHHHHLEV LFQGPGSSGT ETSQVAPA

NCT

NCT DNA Sequence

CCG CA TATG CATCATCACCACCATCACCATCATCATCACGCAATTGAAGGTCGT

AATAG CGTTGAACGC AAAATCTATA TTCCGCTGAA TAAAACCGCA CCGTGTGTTC GTCTGCTGAA TGCAACCCAT
CAGATTGGTT GTCAGAGCAG CATTAGCGGT GATACCGGTG TTATTCATGT TGTGGAAAAA GAAGAGGATC
TGCAGTGGGT TCTGACCGAT GGTCCGAATC CGCCTTATAT GGTTCTGCTG GAAAGCAAAC ATTTTACCCG
TGATCTGATG GAAAAACTGA AAGGTCGTAC CAGCCGTATTGCAGGTCTGG CAGTTAGCCT GACCAAACCG
AGTCCGGCAA GCGGTTTTAG CCCGAGCGTTCAGTGTCCGA ATGATGGTTT TGGTGTTTAT AGCAATAGCT
ACGGTCCGGA ATTTGCACATTGTCGTGAAA TTCAGTGGAA TAGCCTGGGT AATGGTCTGG CCTATGAAGA TTTTAGCTTT
CCGATTTTCC TGCTGGAAGA TGAGAATGAA ACCAAAGTGA TCAAACAGTG CTATCAGGAT CATAATCTGA
GCCAGAATGG TAGCGCACCG ACCTTTCCGC TGTGTGCAAT GCAGCTGTTT AGCCACATGC ATGCAGTTAT
TAGCACCGCA ACCTGTATGC GTCGTAGCAG CATTCAGAGC ACCTTTAGCA TTAATCCGGA AATGTTTGT
GATCCGCTGA GCGATTATAA TGTTTGGAGC ATGCTGAAAC CGATTAATAC CACCGGCACC CTGAAACCGG
ATGATCGTGT TGTTGTTGCA GCAACCCGTC TGGATAGCCG TAGCTTTTTT TGGAATGTTG CACCGGGTGC
AGAAAGCGCA GTTGCAAGCT TTGTTACCCA GCTGGCAGCA GCAGAAGCAC TGCAAAAAGC ACCGGATGTT
ACCACCCTGC CTCGTAATGT GATGTTTGTT TTTTTTCAGG GCGAAACCTT CGATTATATT GGTAGCAGCC GTATGGTGTA
CGATATGGAA AAAGGTAAAT TTCCGGTGCA GCTGGAAAAT GTTGATAGCT TTGTTGAACT GGGTCAGGTT
GCACTGCGTA CCAGTCTGGA ACTGTGGATG CATACCGATC CGGTTAGCCA GAAAAATGAA AGCGTTCGTA
ATCAGGTTGA AGATCTGCTG GCAACCCTGG AAAAAAGCGG TGCGGGTGTT CCGGCAGTTA TTCTGCGTCG
TCCGAATCAG AGCCAGCCGC TGCCTCCGAG CAGCCTGCAG CGTTTTCTGC GTGCACGTAA TATTAGTGGT
GTTGTTCTGG CAGATCATAG CGGTGCATTT CACAATAAAT ACTACCAGAG CATCTATGAC ACCGCAGAAA
ATATCAATGT TAGCTATCCG GAATGGCTGA GTCCGGAAGA AGATCTGAAT TTTGTTACCG ATACCGCAAA
AGCACTGGCA GATGTTGCAA CCGTTCTGGG TCGTGCACTG TATGAACTGG CAGGCGGTAC AAATTTTAGC

GATACCGTTC AGGCAGATCC GCAGACCGTT ACCCGTCTGC TGTATGGTTT TCTGATTAAA GCAAATAACA
GCTGGTTCCA GAGCATTCTG CGCCAGGATC TGCGTAGCTA TCTGGGTGAT GGTCCGCTGC AGCACTATAT
TGCAGTTAGC AGCCCGACCA ATACCACCTA TGTTGTTCAG TATGCACTGG CAAATCTGAC CGGCACCGTT
GTTAATCTGA CCCGTGAACA GTGTCAGGAT CCGAGCAAAG TTCCGAGCGA AAATAAAGAT CTGTATGAGT
ATAGCTGGGT TCAGGGTCCT CTGCATAGCA ATGAAACGGA TCGTCTGCCT CGTTGTGTTC GTAGTACCGC
ACGTCTGGCA CGTGCGCTGT CACCGGCATT TGAACTGAGC CAGTGGTCAA GCACCGAATA TAGCACCTGG
ACCGAAAGCC GTTGGAAAGA TATTCGTGCC CGTATTTTTC TGATCGCAAG CAAAGAACTG GAACTGATTA
CCCTGACCGT GGGTTTTGGT ATTCTGATTT TTAGCCTGAT TGTGACCTAT TGCATTAACG CAAAAGCCGA TGTTCTGTTT
ATTGCACCGC GTGAACCGGG TGCCGTTAGC TATTAA C TCGAGGCT

N1 Protein Sequence

MHHHHHHHHHHAIEGRNSVERKIYIPLNKTAPCVRLLNATHQIGCQSSISGDTGVIHVVEKEEDLQWVLTDGPNPPYMVLLE
SKHFTRDLMEKLKGRTSRIAGLAVSLTKPSPASGFSPSVQCPNDGFGVYSNSYGPEFAHCREIQWNSLGNGLAYEDFSFPIFL
LEDENETKVIKQCYQDHNLSQNGSAPTFPLCAMQLFSHMHAVISTATCMRRSSIQSTFSINPEIVCDPLSDYNVWSMLKPINTT
GTLKPDDRVVVAATRLDSRSFFWNVAPGAESAVASFVTQLAAAEALQKAPDVTTLPRNVMFVFFQGETFDYIGSSRMVYD
MEKGKFPVQLENVDSFVELGQVALRTSLELWMHTDPVSQKNESVRNQVEDLLATLEKSGAGVPAVILRRPNQSQPLPPSSL
QRFLRARNISGVVLADHSGAFHNKYYQSIYDTAENINVSYPEWLSPEEDLNFVTDTAKALADVATVLGRALYELAGGTNFSD
TVQADPQTVTRLLYGFLIKANNSWFQSILRQDLRSYLGDGPLQHYIAVSSPTNTTYVVQYALANLTGTVVNLTREQCQDPSK
VPSENKDLYEYSWVQGPLHSNETDRLPRCVRSTARLARALSPAFELSQWSSTEYSTWTESRWKDIRARIFLIASKELELITLTVGFG
ILIFSLIVTYCINAKADVLFIAPREPGAVSY

PEN-2

PEN-2 DNA Sequence

CCGCATATG CATCATCACCACCATCACCATCATCATCACGCAATTGAAGGTCGT

AATCTGGAACGTGTTAGCAACGAAGAAAAACTGAATCTGTGCCGCAAATATTACCTGGGTGGTTTTGCATTTCTGCCGTTTCT
GTGGCTGGTTAACATCTTTTGGTTTTTTCGTGAAGCATTTCTGGTTCCGGCATATACCGAACAGAGCCAGATTAAAGGTTATGTTT
GGCGTAGCGCAGTTGGTTTTCTGTTTTGGGTTATTGTTCTGACCAGCTGGATTACCATCTTTCAGATTTATCGTCCGCGTTGGGGT
GCACTGGGTGATTATCTGAGCTTTACCATTCCGCTGGGCACCCCG TAA CTCGAGGG

P1 Protein Sequence

MHHHHHHHHHHAIEGRNLERVSNEEKLNLCRKYYLGGFAFLPFLWLVNIFWFFREAFLVPAYTEQSQIKGYVWRSAVGFLF
WVIVLTSWITIFQ IYRPRWGALGDYLSFTIPLGTP

P7 Protein Sequence

MNLERVSNEEKLNLCRKYYLGGFAFLPFLWLVNIFWFFREAFLVPAYTEQSQIKGYVWRSAVGFLFWVIVLTSWITIFQIYRPR
WGALGDYLSFTIPLGTPGSSGTETSQVAPA

Presinlin1

PSEN-1 DNA Sequence

CATATGACCGAACTGCCTGCACCGCTGAGCTATTTTCAGAATGCACAGATGAGCGAAGATAACCATCTGAGCAATACCG
TTCGTAGCCAGAATGATAATCGTGAACGTCAAGAACACAATGATCGTCGTAGCCTGGGTCATCCGGAACCGCTGAGTAAT
GGTCGTCCGCAGGGTAATAGCCGTCAGGTTGTTGAACAGGATGAAGAGGAAGATGAAGAACTGACCCTGAAATATGGT
GCCAAACATGTGATTATGCTGTTTGTTCCGGTTACCCTGTGTATGGTTGTTGTTGTGGCAACCATTAAAAGCGTGAGCTTTTATAC
CCGTAAAGATGGCCAGCTGATTTATACCCCGTTTACCGAAGATACCGAAACCGTTGGTCAGCGTGCACTGCATAGTATTCT
GAATGCAGCAATTATGATTAGCGTGATTGTGGTGATGACCATTCTGCTGGTTGTTCTGTATAAATACCGCTGCTATAAAGTGATT
CATGCCTGGCTGATTATTAGCAGCCTGCTGCTGCTGTTTTTCTTCAGCTTTATCTATCTGGGCGAAGTGTTCAAAACCTATAATGT
TGCCGTTGATTATATCACCGTTGCACTGCTGATTTGGAATTTTGGTGTTGTTGGCATGATTAGCATCCATTGGAAAGGTCCGCTG
CGTCTGCAGCAGGCATATCTGATTATGATTTCAGCACTGATGGCCCTGGTGTTCATCAAATATCTGCCGGAATGGACCGCAT
GGCTGATTCTGGCAGTTATTAGCGTTTATGATCTGGTTGCAGTTCTGTGTCCGAAAGGCCCTCTGCGTATGCTGGTTGAAACC
GCACAAGAACGTAATGAAACCCTGTTTCCGGCACTGATTTATTCAAGCACCATGGTTTGGCTGGTTAATATGGCAGAAGGT
GATCCGGAAGCACAGCGTCGTGTTAGCAAAAATAGCAAATACAATGCAGAAAGCACCGAACGTGAAAGCCAGGATA
CCGTTGCAGAAAATGATGATGGTGGTTTTAGCGAAGAATGGGAAGCCCAGCGTGATAGCCATCTGGGTCCGCATCGTAG
CACACCGGAAAGCCGTGCAGCAGTTCAAGAACTGAGCAGCTCAATCCTGGCAGGCGAAGATCCTGAAGAACGTGGT
GTTAAACTGGGTCTGGGTGATTTTATCTTTTATAGCGTTCTGGTTGGTAAAGCAAGCGCAACCGCAAGCGGTGATTGGAATAC
CACCATTGCATGTTTTGTTGCCATTCTGATTGGTCTGTGTCTGACATTACTGCTGCTGGCCATTTTCAAAAAAGCACTGCCTGCC
CTGCCGATTAGCATTACCTTTGGTCTGGTTTTTTACTTCGCAACCGATTATCTGGTTCAGCCGTTTATGGATCAACTGGCATTTCA
CCAGTTTTACATCGAGAACCTGTATTTTCAGTCAGGTAGCAGCCATCATCACCATCACCATTAACTCGAG

H1 Protein Sequence

MGSSHHHHHHSSGLVPRGSHMTELPAPLSYFQNAQMSEDNHLSNTVRSQNDNRERQEHNDRRSLGHPEPLSNGRPQGN
SRQVVEQDEEEDEELTLKYGAKHVIMLFVPVTLCMVVVVATIKSVSFYTRKDGQLIYTPFTEDTETVGQRALHSILNAAIMISVI
VVMTILLVVLYKYRCYKVIHAWLIISSLLLLFFFSFIYLGEVFKTYNVAVDYITVALLIWNFGVVGMISIHWKGPLRLQQAYLIMISA
LMALVFIKYLPEWTAWLILAVISVYDLVAVLCPKGPLRMLVETAQERNETLFPALIYSSTMVWLVNMAEGDPEAQRRVSKNSK
YNAESTERESQDTVAENDDGGFSEEWEAQRDSHLGPHRSTPESRAAVQELSSSILAGEDPEERGVKLGLGDFIFYSVLVGKA
SATASGDWNTTIACFVAILIGLCLTLLLLAIFKKALPALPISITFGLVFYFATDYLVQPFMDQLAFHQFYI

Pesinlin1-NTF

PSEN-1 NTF DNA Sequence

ATGACCGAACTGCCTGCACCGCTGAGCTATTTTCAGAATGCACAGATGAGCGAAGATAACCATCTGAGCAATACCGTTC
GTAGCCAGAATGATAATCGTGAACGTCAAGAACACAATGATCGTCGTAGCCTGGGTCATCCGGAACCGCTGAGTAATGG
TCGTCCGCAGGGTAATAGCCGTCAGGTTGTTGAACAGGATGAAGAGGAAGATGAAGAACTGACCCTGAAATATGGTGC
CAAACATGTGATTATGCTGTTTGTTCCGGTTACCCTGTGTATGGTTGTTGTTGTGGCAACCATTAAAAGCGTGAGCTTTTATACCC
GTAAAGATGGCCAGCTGATTTATACCCCGTTTACCGAAGATACCGAAACCGTTGGTCAGCGTGCACTGCATAGTATTCTGA
ATGCAGCAATTATGATTAGCGTGATTGTGGTGATGACCATTCTGCTGGTTGTTCTGTATAAATACCGCTGCTATAAAGTGATTCAT
GCCTGGCTGATTATTAGCAGCCTGCTGCTGCTGTTTTTCTTCAGCTTTATCTATCTGGGCGAAGTGTTCAAAACCTATAATGTTGC
CGTTGATTATATCACCGTTGCACTGCTGATTTGGAATTTTGGTGTTGTTGGCATGATTAGCATCCATTGGAAAGGTCCGCTGCGT
CTGCAGCAGGCATATCTGATTATGATTTCAGCACTGATGGCCCTGGTGTTCATCAAATATCTGCCGGAATGGACCGCATGG
CTGATTCTGGCAGTTATTAGCGTTTATGATCTGGTTGCAGTTCTGTGTCCGAAAGGCCCTCTGCGTATGCTGGTTGAAACCGC
ACAAGAACGTAATGAAACCCTGTTTCCGGCACTGATTTATTCAAGCACC TAA C TCGAGGG

H1N Protein Sequence

MGSSHHHHHHSSGLVPRGSHMTELPAPLSYFQNAQMSEDNHLSNTVRSQNDNRERQEHNDRRSLGHPEPLSNGRPQGNSRQVVEQDEE
EDEELTLKYGAKHVIMLFVPVTLCMVVVVATIKSVSFYTRKDGQLIYTPFTEDTETVGQRALHSILNAAIMISVIVVMTILLVVLYKYRCYKVIHAW
LIISSLLLLFFFSFIYLGEVFKTYNVAVDYITVALLIWNFGVVGMISIHWKGPLRLQQAYLIMISALMALVFIKYLPEWTAWLILAVISVYDLVAVLCP
KGPLRMLVETAQERNETLFPALIYSST

1NR Protein Sequence

MLTFMASDSEEEVCDERTSLMSAESPTPRSCQEGRQGPEDGENTAQWRSQENEEDGEEDPDRYVCSGVPGRPPGLEEELTLKYGAKHVI
MLFVPVTLCMIVVVATIKSVRFYTEKNGQLIYTTFTEDTPSVGQRLLNSVLNTLIMISVIVVMTIFLVVLYKYRCYKFIHGWLIMSSLMLLFLFTYIYLG
EVLKTYNVAMDYPTLLLTVWNFGAVGMVCIHWKGPLVLQQAYLIMISALMALVFIKYLPEWSAWVILGAISVYDLVAVLCPKGPLRMLVET
AQERNEPIFPALIYSSAGSSGTETSQVAPA

Presinlin1-CTF

PSEN-1 CTF DNA Sequence

CATATGGTTTGGCTGGTTAATATGGCAGAAGGTGATCCGGAAGCACAGCGTCGTGTTAGCAAAAATAGCAAATACAATGC
AGAAAGCACCGAACGTGAAAGCCAGGATACCGTTGCAGAAAATGATGATGGTGGTTTTAGCGAAGAATGGGAAGCCC
AGCGTGATAGCCATCTGGGTCCGCATCGTAGCACACCGGAAAGCCGTGCAGCAGTTCAAGAACTGAGCAGCTCAATC
CTGGCAGGCGAAGATCCTGAAGAACGTGGTGTTAAACTGGGTCTGGGTGATTTTATCTTTTATAGCGTTCTGGTTGGTAAAGC
AAGCGCAACCGCAAGCGGTGATTGGAATACCACCATTGCATGTTTTGTTGCCATTCTGATTGGTCTGTGTCTGACATTACTGC
TGCTGGCCATTTTCAAAAAAGCACTGCCTGCCCTGCCGATTAGCATTACCTTTGGTCTGGTTTTTTACTTCGCAACCGATTATCT
GGTTCAGCCGTTTATGGATCAACTGGCATTTCACCAGTTTTACATCGAGAACCTGTATTTTCAGTCAGGTAGCAGCCATCATC
ACCATCACCATTAACTCGAG

1CR Protein Sequence

MVWLVNMAEGDPEAQRRVSKNSKYNAESTERESQDTVAENDDGGFSEEWEAQRDSHLGPHRSTPESRAAVQELSSSILAGEDPEERGVK
LGLGDFIFYSVLVGKASATASGDWNTTIACFVAILIGLCLTLLLLAIFKKALPALPISITFGLVFYFATDYLVQPFMDQLAFHQFYIGSSGTETSQV
APA

Appendix II: Primers

Table II.1 Primers for cloning

		nt	CG%	T_m °C
APH1_Nde1_new	GGAATTC catatg GGTGCAGCAGTTTT	27	44.4	72.5
APH_Xho_R	CCC TCG AGT TAA TCT TCA GGC G	22	54.5	68.1
APH1_Rho_Xho1	GGGCTCGAGaattCTATTAAGCTGGCGCCACCTGGGAAG TCTCGGTGCCGGAGGAGCC ATCTTCAGGCGGAATACGCAG	79	59.5	95
AHP1_insF opt	ccgctcgag ATG GGTGCTGCTGTGTT	26	61.5	79.6
AHP1_insR opt	cgc GGATCCTTAAGCGGGAGCCACTT	26	61.5	78.9
NCT_Nde1_new	GGAATTC catatg AATAGCGTTGAACGC	28	42.8	71.1
NCT_Xho_R	AGC TCG AGT TAA TAG CTA ACG G	22	45.4	60.9
PEN2_Nde1_new	GGAATTC catatg AATCTGGAACGTG	26	42.3	69
PEN2_Xho_R	CCC TCG AGT TAC GGG GTG C	19	68.4	69.3
PEN2_Nco1	CATG ccatgg gt AATCTGGAACGTG	25	52	73.6
PEN2_Rho_Xho1	GGGCTCGAGaattCTATTAAGCTGGCGCCACCTGGGAAG TCTCGGTGCCGGAGGAGCC CGGGGTGCCCAGCGGAATGGT	79	64.5	95
PS1_Nde1	GGAATTCCATATG ACCGAACTGCCTGCAC	29	51.7	76.6
PS1_Xho1	ccg ctcgag aattc tta GATGTAAAACTGGTGAAAT	36	38.9	74.2
PS1_22bR	ccg CTCGAG aattc TTA ATGGTGATGGTGAT	31	45.1	75.6
PS1N_Xho1	ccg ctcgag aattc tta GGTGCTTGAATAAAT	32	40.6	73
PS1N_Rho_Xho1	GGGCTCGAGCTATTAAGCTGGCGCCACCTGGGAAGTCT CGGTGCCGGAGGAGCC GGTGCTTGAATAAATCAGTG	74	59.4	95
PS1C_Nde1	GGAATTC CATATG GTTTGGCTGGTTAAT	28	39.2	70.2
PS2_Nde1_new	GGAATTC catatg CTGACCTTTATGGCGA	29	44.8	74.2
PS2_Xho1_no tta	CCG ctcgag AATATACAGCTGATG	24	50	67.9
PS2_Rho_Xho1	GGGCTCGAGCTATTAAGCTGGCGCCACCTGGGAAGTCT CGGTGCCGGAGGAGCC AATATACAGCTGATGGCTGG	74	60.8	95
PS2N_Rho_Xho1	GGGCTCGAGCTATTAAGCTGGCGCCACCTGGGAAGTCT CGGTGCCGGAGGAGCC TGCGCTAGAATAAATCAGCG	74	60.8	95
Deta E9 F	ACCGAACGTGAAAGCCAGGATACCGTT	27	51.8	75.4
Deta E9 R	GCTTGAATAAATCAGTGCCGGAAACAGGG	29	48.3	75.4

T_m values were calculated from Thermo Scientific Web Tools-T_m Calculator

Acknowledgements

I would like to thank the China scholarship council (CSC) program and Forschungszentrum Juelich for the financial support during my Ph.D. study.

I would like to express my sincere gratitude to my advisor Prof. Dr. Jörg Labahn for his continuous support and encouragement of my Ph.D. study and the related research, for his patient and guidance.

I sincerely thank Dr. Ge Yang for guiding me when I joined the group. I am truly grateful for his supervision over the four years, for every discussion we had and for all his help academically and personally.

I am thankful to my colleagues, Dr. Udaya K Tiruttani S and Daniel Worms, for their insightful comments on my project whenever necessary. It has been so nice to be lab mates with them. I will always remember the fun we had in our lab. Furthermore, I like to thank Sabrina Kress and Abhilasha Singh for their great support in our lab.

I also want to thank Dr. Jan Kubicek and Dr. Barbara Maertens from Cube Biotech for preparing the lipids and insect cell cultures. I would like to thank Prof. Patrick C. Fraering and his student Hermeto Gerber from EPFL for providing the substrates and enzymes as positive controls. I also would like to thank Maria Marta Garcia Alai, Ioana Maria Nemtanu, and Janina Hinrichs from SPC at EMBL, Hamburg for help with ThemalFluor and Nanotemper, and Dr. Sven Falke with DLS.

I wish to express my gratefulness to all my friends as well. Being with them makes the life abroad a really nice experience. And I appreciate all the beautiful moments we shared together.

Last but not the least, I would like to thank my family: my boyfriend for his love and patience, and my parents, who supported me spiritually throughout my Ph.D. study and my whole life.

Erklärung

Ich erkläre, dass ich die vorliegende Arbeit selbständig und ohne unerlaubte Hilfe verfasst habe. Die vorliegende Arbeit wurde weder in der jetzigen oder in ähnlicher Form bei einer anderen Institution eingereicht. Es wurden zuvor keine Promotionsversuche unternommen

Hamburg, _____

Kun Yu